

**Hydroxylation Reactions in Bioinorganic Models for
Copper Enzymes: A Density Functional Theory
Assessment**

Dissertation

Zur Erlangung des Doktorgrades
der Naturwissenschaften

vorgelegt beim
Fachbereich Biochemie, Chemie und Pharmazie der
Johann Wolfgang Goethe - Universität
in Frankfurt am Main

von

Puneet Gupta

aus
Kanpur (Indien)

Frankfurt 2016

D30

vom Fachbereich Biochemie, Chemie und Pharmazie der
Johann Wolfgang Goethe - Universität als Dissertation angenommen.

Dekan: Prof. Dr. Michael Karas

Gutachter: Prof. Dr. Max C. Holthausen

Prof. Dr. Siegfried Schindler

Datum der Disputation: 18.05.2016

To my wife

Acknowledgements

My special thank to my PhD supervisor, Prof. Max Holthausen, for being the most influential person during my doctoral study. His love and dedication in solving science problems, and his commitment to his students is a great source of inspiration to me. I appreciate the freedom and guidance given to me throughout my graduate years. I am also thankful to Prof. Matthias Wagner for his valuable suggestions and ideas during my research projects.

My deepest thank to my M.Sc. supervisor, Prof. Rabindranath Mukherjee, for showing me the right path to join Prof. Holthausen's group. He is the person who dragged my interest in science.

It is my immense pleasure to thank to all my collaborators from the groups of Prof. Matthias Wagner, Prof. Harald Schwalbe and Prof. Siegfried Schindler. I also sincerely thank all my colleagues from Prof. Holthausen's group for giving me a healthy and pleasant working environment. I specially thank Dr. Martin Diefenbach and Dr. Samat Tussupbayev for always being helpful in solving problems related to my PhD projects. I thank Dr. Guido Wagner for giving me helping hands for all kind of IT-related problems. I am also thankful to Mrs. Carolin Friedrich in helping me to tackle everyday issues. I am extremely grateful to Prof. Walter Thiel for his valuable suggestions to my thesis.

Summary of the thesis was translated in the German version (*Zusammenfassung*) by Julia I. Schweizer, Lioba Meyer, Dr. Martin Diefenbach, and Dr. Guido Wagner. I greatly appreciate their help in this regard. Financial support was provided by the Beilstein-Institut Frankfurt am Main within the research collaboration NanoBic. Quantum chemical calculations were performed at the Center for Scientific Computing (CSC) Frankfurt am Main on the Fuchs and LOEWE-CSC high performance computer clusters.

Last but not the least, I would like to thank my wonderful lovely family, Mom, Dad, my elder brother Navneet and my wife Manisha for their unconditional love and support and for being there for me always.

Puneet Gupta

Frankfurt am Main (Germany)

Contents

Abstract.....	11
1 Chapter 1: Introduction.....	14
1.1 Copper Proteins and Enzymes	14
1.2 Copper-dioxygen Reactivity in Enzymes.....	16
1.2.1 Selective Aliphatic C–H Hydroxylation	17
1.2.2 Selective Aromatic C–H Hydroxylation/Oxidation.....	19
1.3 Biomimetic Cu/O ₂ Chemistry: Structure and Reactivity	21
1.3.1 Mononuclear Cu-O ₂ Complexes and C–H Hydroxylations.....	22
1.3.2 Dinuclear Cu-O ₂ Complexes and C–H Hydroxylations	29
2 Chapter 2: Density Functional Theory Applications to Biomimetic Cu/O ₂ Chemistry	45
2.1 Mechanistic Studies of C–H Hydroxylation	45
2.2 Cu ₂ P ^S /Cu ₂ O ₂ Interconversion: A Torture Track for DFT	48
3 Chapter 3: Results and Discussion	51
3.1 DFT Benchmark.....	51
3.1.1 Experimental Reference Systems.....	51
3.1.2 Computational Details.....	52
3.1.3 DFT Model Systems	53
3.1.4 Results and Discussion.....	54
3.1.5 Conclusions	60
3.2 Reaction 1: An Aliphatic C–H Hydroxylation	61
3.2.1 Motivation.....	61
3.2.2 Computational Details.....	61
3.2.3 Choice of the Computational Molecular Model.....	62
3.2.4 Mechanistic Study.....	63
3.2.5 Conclusions	66
3.3 Reaction 2: An Aromatic C–H Hydroxylation	66
3.3.1 Motivation.....	66
3.3.2 Model System	68

3.3.3	Mechanistic Study.....	69
3.3.4	Conclusions.....	72
3.4	Reaction 3: Aliphatic vs Aromatic C–H Hydroxylations	72
3.4.1	Motivation.....	72
3.4.2	Model System and Mechanistic Study.....	73
3.4.3	Conclusions.....	76
4	Chapter 4: Conclusions.....	77
	Zusammenfassung.....	81
	Abbreviations.....	86
	References.....	88
	Appendices.....	98
	Curriculum Vitae	125

Abstract

The high selectivity of biological transformations taking place in Nature have long inspired synthetic chemists to develop analogous chemical processes. Similarly, transient intermediates identified in chemical transformations often provide a basis to understand biological processes. Therefore, new insights gained in biological studies are often useful for chemistry and vice versa.

Proteins, and catalytically active enzymes, are among the most essential units of living cells. Metalloproteins or -enzymes, i.e., proteins or enzymes that contain transition metal ions such as copper, nickel, iron or zinc are often involved in processes like (1) metal-ion storage and transport, (2) exchange of electrons with the environment in catalysis and electron transfer reactions, and (3) dioxygen storage, transport, and metabolization.

For decades, copper-mediated biological oxidations have spurred a great deal of interest among synthetic and catalytic chemists. Copper enzymes such as dopamine β -monooxygenase (D β M), peptidylglycine α -hydroxylating monooxygenase (PHM), particulate methane monooxygenase (pMMO) and tyrosinase activate molecular oxygen (O_2) and incorporate one of the oxygen atoms selectively into C–H bonds yielding hydroxylated organic substrates. Remarkable progress in bioinorganic research has led to the development of a large number of copper-based model systems supported by various nitrogen donor ligands that bind O_2 , cleave the O–O bond, and/or afford hydroxylation reactions similar to copper enzymes. These synthetic model systems have helped to understand the structure-activity relationships of their biological role models and supporting theoretical studies have contributed substantially to the development of the field. Specifically, several density functional theory (DFT) studies have provided detailed mechanistic insights into copper-mediated aliphatic and aromatic hydroxylation reactions. Until to date, however, pertinent quantum chemical research still suffers from severe problems as to identify sufficiently accurate and efficient methods for mechanistic studies, and conflicting literature reports have created confusions within the scientific community. Therefore, the first aim of this thesis is to identify a DFT method well suited to describe copper-mediated hydroxylation reactions.

With this method at hand a number of interesting hydroxylation reactions is investigated aiming at a detailed understanding of the underlying reaction mechanisms.

The thesis is divided into four chapters of which the first, the introductory chapter, is further divided into three sections (1) *copper proteins and enzymes*, (2) *copper-O₂ reactivity in enzymes* and (3) *biomimetic Cu/O₂ chemistry*. The first section gives a brief overview of a number of copper enzymes. The second section provides a concise introduction to the biochemical transformations brought about by those copper enzymes that perform aliphatic and aromatic hydroxylation reactions. It is shown that such copper enzymes carry different types of active sites which are responsible for their specific biological functions. These copper enzymes with their biological function are the role models for synthetic chemistry. In the third section, *biomimetic Cu/O₂ chemistry*, the insights gathered in the past 35 years of extensive research on copper-based synthetic model systems that mimic various aspects of copper-enzyme reactivity are reviewed. Various types of active copper sites have been realized in these synthetic model systems and a brief introduction to the respective reactivities towards C–H bonds is presented. We will specifically focus on isomerization processes of dinuclear active Cu₂O₂ sites and the specific reactivity aspects of these isomers, as these phenomena have been the subject of enormous research efforts aiming at the understanding of the function of the enzyme tyrosinase.

Theory has been integral part of this research and density functional theory (DFT) has effectively taken over the role as a working horse in most studies. Therefore, the second chapter is devoted to an exposition of earlier DFT applications in mechanistic studies of Cu/O₂ chemistry. We specifically highlight the problems related to the use of DFT in this field and illustrate the present state of knowledge.

The third chapter of this thesis provides results and discussion of (1) *DFT benchmark studies* and (2) *mechanistic studies*. In the first section, the results of a careful benchmark study on the performance of various DFT methods to study the μ - η^2 : η^2 -peroxo-dicopper(II)/bis(μ -oxo)dicopper(III) core isomerization and the C–H hydroxylation processes are compared with available experimental reference data. We provide an assessment of the effects of relativity, counteranions, and dispersion on the reference reactions. The most suitable DFT method evolving from this study, BLYP-D/def2-TZVP including solvent and relativistic corrections, is applied in the next sections to investigate the mechanistic scenario

underlying three copper-dioxygen mediated hydroxylation reactions of aliphatic and aromatic C–H bonds. Our mechanistic studies show that bis(μ -oxo)dicopper(III) complexes are capable of achieving selective aliphatic and aromatic C–H hydroxylations. The study of substituent effects in these reactions has further shown that the bis(μ -oxo)dicopper complex acts as an electrophile in hydroxylation.

The fourth chapter presents the conclusions of our investigations. Part of the work presented in this thesis has been published in a peer reviewed journal and enclosed in appendix 1. Further research work, not presented in chapters 1-4, was conducted during my PhD time. This has led to two publications which are added in the appendix.

Chapter 1

Introduction

In the first section we will present a number of copper enzymes with their active sites and biological function. In the second section we will put emphasis on those copper enzymes which catalyze the aliphatic and aromatic hydroxylation of organic substrates by O₂ from air. In the third section we will outline the key findings of numerous publications on copper-oxygen containing synthetic model systems that have been devised in the past 35 years to mimic the structure and function of their biological role models. We will focus in particular on studies on the binding of O₂ and on the selective hydroxylation of C–H bonds.

1.1. Copper Proteins and Enzymes

Copper is an essential element for almost all living organisms, although it usually occurs only in trace amounts. Here, copper ions are bound to proteins and enzymes, which are involved in a variety of biological functions including (1) electron transfer; (2) dioxygen storage, transport and metabolization; (3) catalysis.^[1] The different roles of the copper proteins or enzymes require different types of active sites. Classically, these active sites are divided into mainly three classes (type-1, type-2, type-3) based on their unique spectroscopic characteristics, specific coordination environment, and nuclearity (cf. Figure 1.1).^[1]

Type-1 (T1) active sites contain a single copper ion bound to the sulfur donor atom of a cysteinate (Cys) residue and the nitrogen donor-atoms of two histidine (His) residues in a trigonal pyramidal coordination environment. In most T1 sites, the copper ion is further weakly coordinated to methionine (Met) and/or glutamine (Glu) residues in an axial position. All T1 copper active sites share as a spectroscopic characteristic an intense absorption peak in the visible region at around 600 nm, which is why they are also called blue copper sites.^[2] The other important common characteristic of T1 sites is an extremely small hyperfine coupling constant in their electron paramagnetic resonance (EPR) spectra. T1 sites are

involved in electron-transfer processes and can be found in copper proteins such as plastocyanin^[3], azurin and amicyanin.^[4]

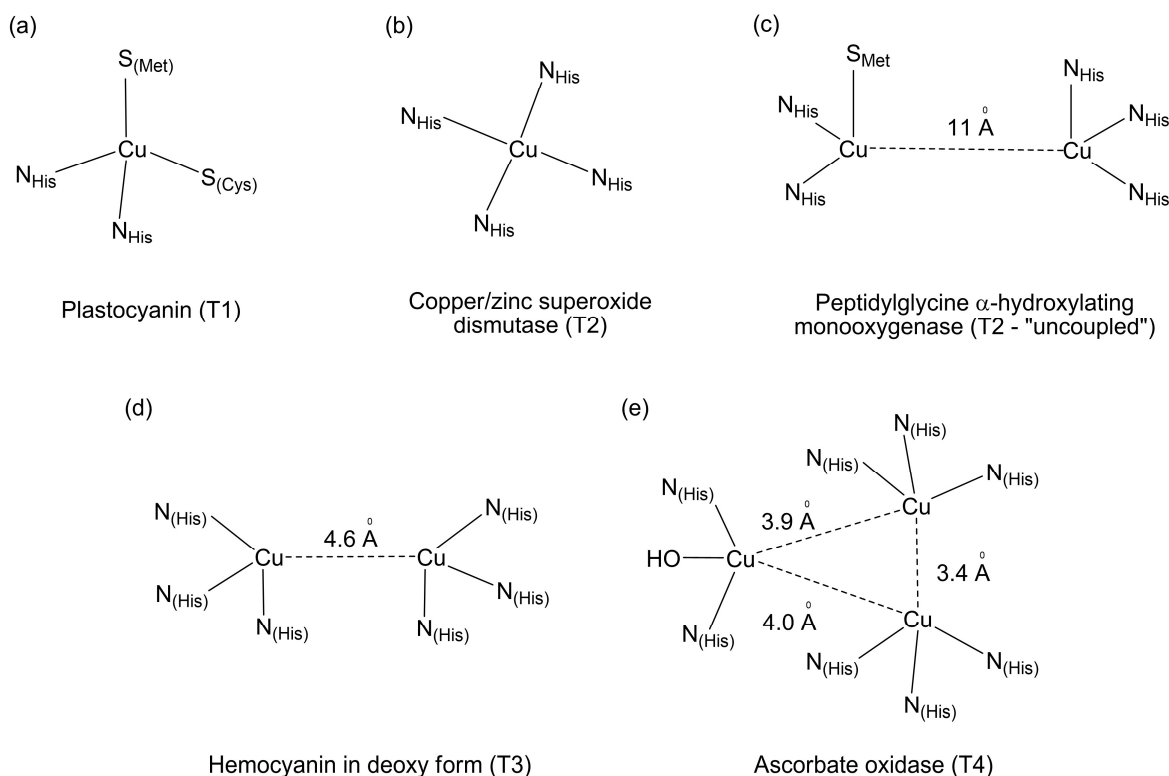


Figure 1.1. Schematic representations of the active sites of selected copper proteins: (a) plastocyanin^[3] (T1); (b) copper/zinc superoxide dismutase^[5] (T2); (c) peptidylglycine α -hydroxylating monooxygenase^[6] (two uncoupled T2 sites); (d) deoxyhemocyanin^[7] (T3); (e) ascorbate oxidase^[8] (T4).

Type-2 (T2) active sites are also mononuclear complexes of copper ions coordinated by N- or O-donor ligands in a square planar or distorted tetragonal geometry.^[9] T2 sites do not exhibit strong absorption bands in the visible region of their absorption spectra but their UV-vis and EPR spectra are comparable to those of regular square planar copper(II) compounds. Proteins containing T2 active sites are mostly involved in catalysis (such as the disproportionation of the $O_2^{\cdot -}$ superoxide anion and alcohol oxidation reactions), where the presence of vacant coordination sites allows the catalytic oxidation of substrate molecules. These active sites can be found in copper enzymes such as copper-zinc superoxide dismutase,^[5] amine oxidase,^[10] and galactose oxidase.^[11] Some dinuclear active sites comprised of two non-equivalent, spatially separated and magnetically uncoupled copper ions, also belong to the type-2 class. In such sites only one of the copper ions is directly

involved in catalytic transformations while the other acts as an electron source to support this function. Such dinuclear T2 active sites are found in enzymes such as peptidylglycine α -hydroxylating monooxygenase (PHM)^[6] and dopamine β -monooxygenase (D β M)^[12].

Type-3 (T3) active sites feature two copper ions located in close proximity, each coordinated to the protein environment by three histidine residues. The oxidized form of these active sites is EPR inactive owing to antiferromagnetic coupling of the unpaired spins of the Cu(II) ions. T3 active sites are involved in O₂ transport, activation, and metabolization in, e.g., the copper-protein hemocyanin^[7] or the copper-enzymes catechol oxidase^[13] and tyrosinase.^[14]

There also exist **type-4** (T4) active sites which are composed of a T2 and a T3 site forming together a trinuclear copper cluster. In some proteins, an additional T1 site also exists, located at some distance from the trinuclear copper cluster, and both sites interact through a Cys-His electron transfer pathway. Examples for enzymes incorporating T4 sites are laccase (polyphenol oxidase),^[15] ascorbate oxidase^[8] and ceruloplasmin^[16], which are involved in the catalytic oxidation of various organic substrates.

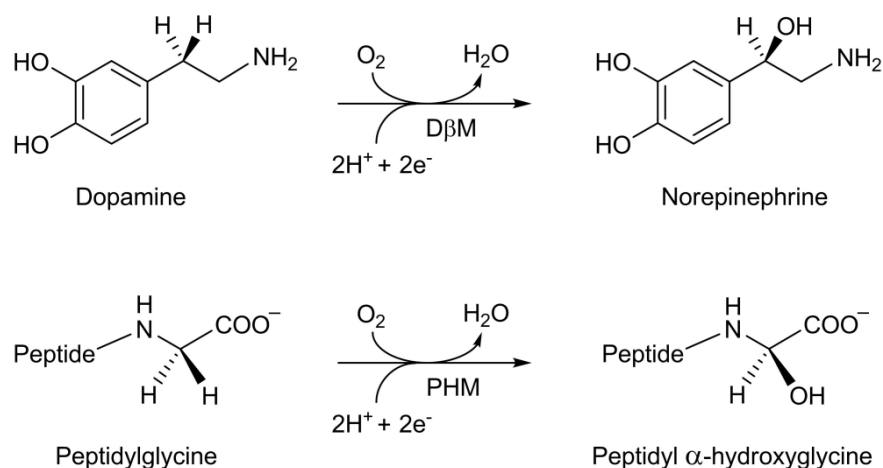
1.2. Copper-Dioxygen Reactivity in Enzymes

Dioxygen is one of the most essential elements required to sustain life. It plays vital roles in the metabolization of various substances such as amino acids, lipids, vitamins, hormones and sugars). However, due to its triplet electronic ground state, its reactions with singlet organic substrates are spin forbidden.^[17] In order to overcome the spin-forbiddenness of the metabolization of dioxygen, enzymes (e.g., oxygenases, oxidases, or peroxidases) often make use of metal cofactors. Oxygenases are those enzymes which catalyze the incorporation of oxygen atoms from O₂ into a substrate. They are divided into two subgroups, monooxygenases or dioxygenases, based on whether one or both oxygen atoms of O₂ are incorporated into the substrate. Monooxygenases play important roles in organic substrate hydroxylations by inserting a single oxygen atom into C–H bonds. Examples for some important monooxygenases are dopamine β -monooxygenase (D β M), peptidylglycine α -

hydroxylating monooxygenase (PHM), particulate methane monooxygenase (pMMO), and tyrosinase.

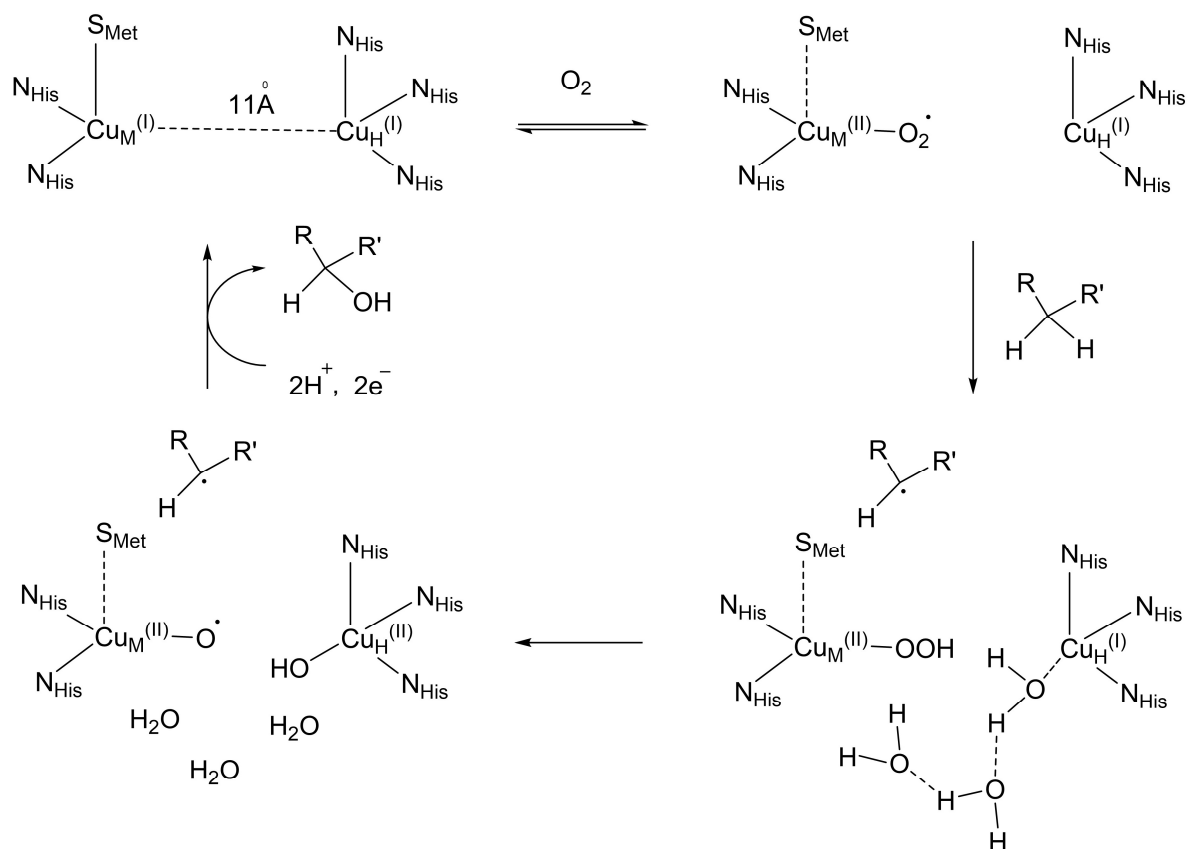
1.2.1. Selective Aliphatic C–H Hydroxylation

Copper monooxygenases containing binuclear type-2 active sites such as D β M and PHM mediate the selective hydroxylation of aliphatic C–H bonds utilizing molecular oxygen in higher eukaryotes.^[18] D β M catalyzes the hydroxylation of dopamine to produce norepinephrine (Scheme 1.1, top); both dopamine and norepinephrine are neurotransmitters in the sympathetic nervous system.^[19] PHM catalyzes the transformation of glycine-extended peptides to their α -hydroxylated products, which is the first step in the biosynthesis of important hormonal peptides (Scheme 1.1, bottom).^[20]



Scheme 1.1. Physiological function of the copper containing enzymes dopamine β -monooxygenase (D β M) and peptidylglycine α -hydroxylating monooxygenase (PHM).

Crystallographic studies of PHM revealed that its catalytic core is composed of two copper sites separated by 11 Å with no bridging ligand between them (Scheme 1.2).^[6] Both copper sites are also unique in their coordination environment as one copper site, designated Cu_H, is bound to three histidines residues whereas the other, designated Cu_M, is bound to two histidines and a methionine residue. Both copper sites are solvent exposed and a water-filled cleft has been identified at the solvent interface which links the two copper binding domains.^[6] While the structure of PHM has been crystallographically characterized, the crystal structure of D β M is unknown as of today.^[1]



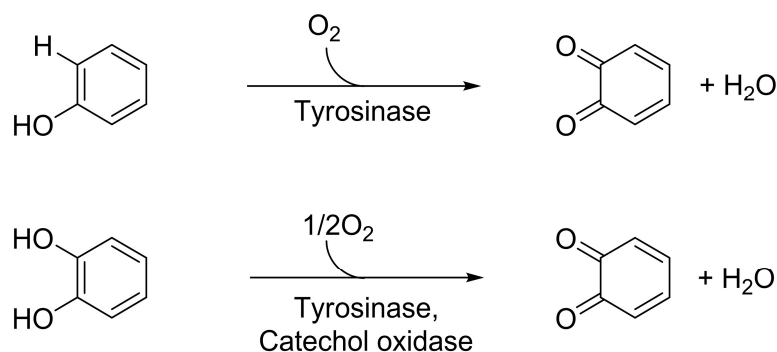
Scheme 1.2. Proposed mechanism for the biological function of DβM and PHM.^[12b]

Based on the structural information available for the PHM on the one hand and by comparison of spectroscopic and kinetic data available for both, PHM and DβM, on the other, a similar mechanism for the biological function of both enzymes has been proposed.^[12b, 18a] According to the suggested mechanistic scenario, the Cu_M site binds O₂ to form an EPR silent copper(II)-superoxide moiety, which subsequently abstracts a hydrogen atom from the substrate present in close proximity. The Cu_H site then supplies an electron to Cu_M, most likely through a water-mediated long range electron transfer. This electron transfer is believed to induce the heterolytic O–O cleavage of the Cu_M(II)–hydroperoxo intermediate, yielding water and a Cu_M(II)–oxo radical, which in turn recombines with the substrate radical to form the alcohol product.

Particulate methane monooxygenase (pMMO) is a copper enzyme found in methanotrophic bacteria, which catalyzes the selective hydroxylation of methane to methanol.^[21] The crystal structure of a pMMO enzyme showed that it contains two different (mononuclear and dinuclear) copper sites and a mononuclear zinc site.^[21]

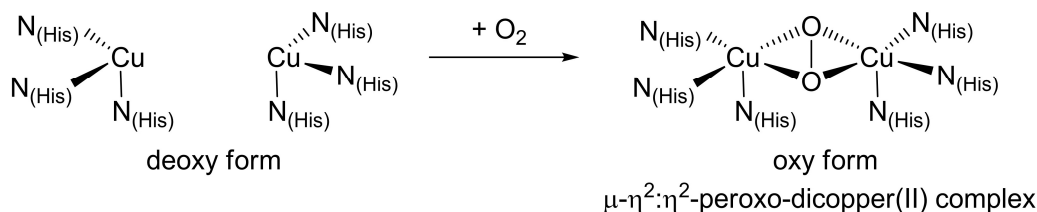
1.2.2. Selective Aromatic C–H Hydroxylation/Oxidation

Tyrosinase, a monooxygenase featuring a type-3 coupled binuclear copper (CBC) active site, is widely found in bacteria and eukaryotes and mediates O₂ metabolism to selectively form *ortho*-quinones from monophenols; it catalyses, e.g., the conversion of tyrosine to dopaquinone, the key precursor for the biosynthesis of the skin-pigment melanin (Scheme 1.3).



Scheme 1.3. Tyrosinase (Ty) mediated oxidation using O₂ (top). The second reaction is catalyzed by both Ty and catechol oxidase (CO).^[22]

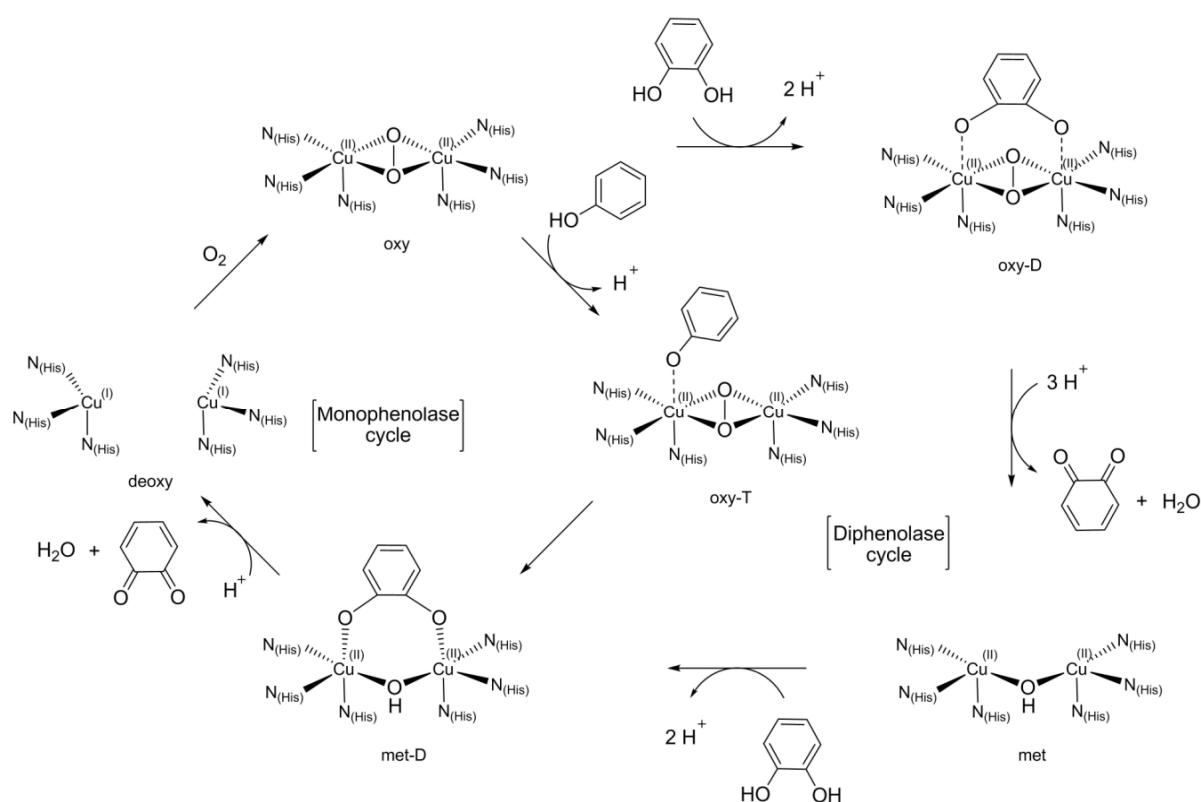
As mentioned earlier, the type-3 active sites are composed of a binuclear copper center with each Cu bound to three histidine imidazoles.^[14] Upon exposure to O₂, the deoxy form binds O₂ in a side-on bridging mode to form a μ - η^2 : η^2 -peroxo-dicopper(II) complex; this structural motif has been confirmed in a crystallographic study (Scheme 1.4).^[14]



Scheme 1.4. Dioxygen binding at the binuclear copper active sites of the CBC proteins and enzymes.

Solomon and coworkers proposed a catalytic mechanism for the biological function of tyrosinase with two interpenetrating cycles (monophenolase and diphenolase cycles, Scheme 1.5).^[9a, 23] The monophenolase cycle starts with the deoxy state of tyrosinase by binding of dioxygen to generate the oxy state. Next, the oxy state binds the monophenol substrate in the

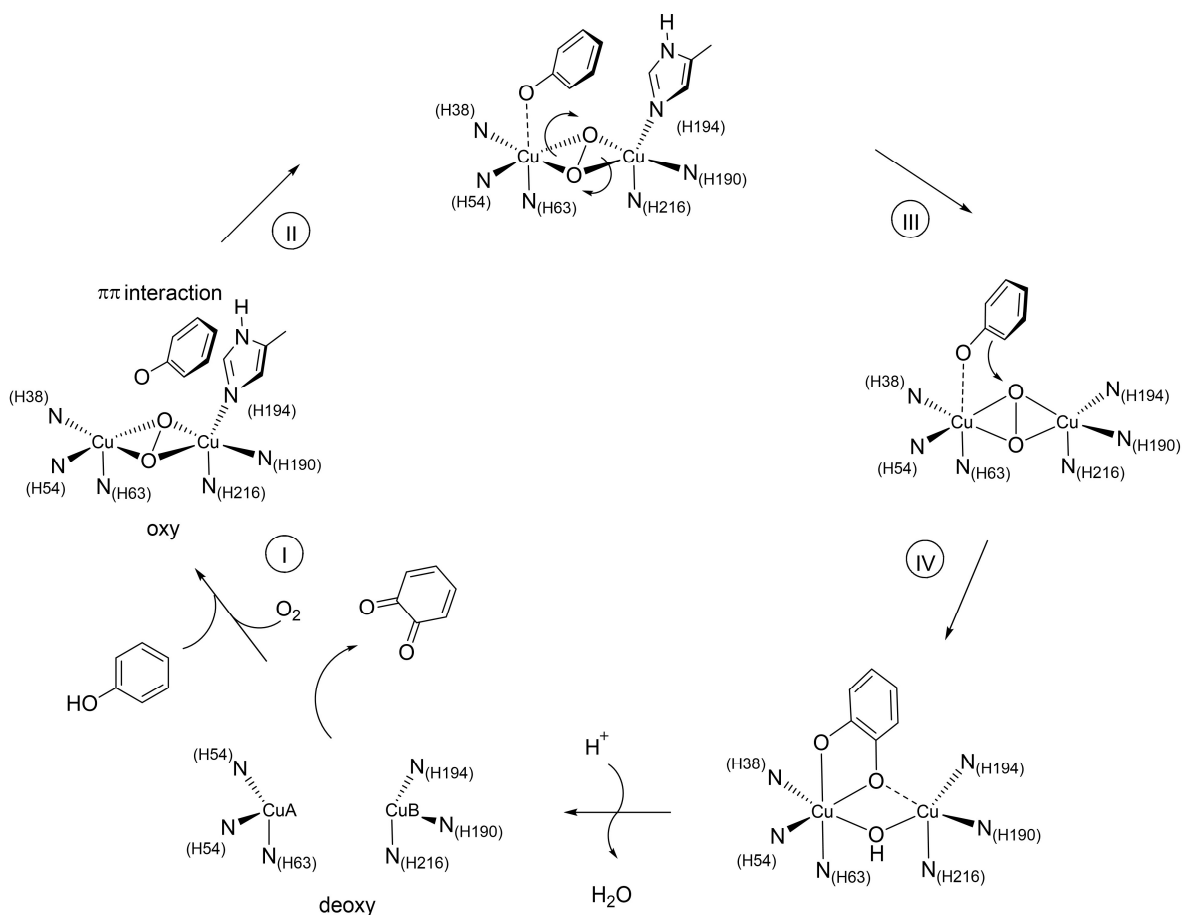
axial position of one of the copper centers to generate the oxygen-phenolate ternary complex oxy-T which subsequently converts into the met-D state consisting of an *o*-diphenolate attached to copper centers. The met-D state finally releases *o*-quinone, which leads back to the deoxy state and closes the monophenolase cycle. The diphenolase cycle starts from the oxy state by binding of the *o*-diphenol to both copper centers to generate the oxy-D state, which subsequently releases *o*-quinone and water to generate the met state. Binding of a second equivalent of the *o*-diphenol to the met complex leads to the met-D state at which point the diphenolase cycle funnels back into the monophenolase cycle.



Scheme 1.5. Monophenolase and diphenolase catalytic cycles of tyrosinase according to Solomon et al.^[9a, 23]

The report of the first tyrosinase crystal structure by Matoba and coworkers in 2006 represents a major breakthrough in biological sciences.^[14] Utilizing this information, Tucek and Decker rationalized the regioselectivity of the *ortho*-hydroxylation/oxidation of phenols by tyrosinase.^[24] In the first step, the deoxy form of tyrosinase binds molecular oxygen to convert into its oxy form, in which the phenolic substrate has π - π interactions with the His194 residue of tyrosinase (Scheme 1.6). In the oxy form the *ortho* position of the

monophenolic substrate is oriented towards the binuclear copper active site, which provides a rationale for the regioselectivity of the *ortho*-hydroxylation/oxidation. In the next step, the phenolic substrate binds directly to CuA (trans to His63) after making a slight shift from His194 to CuA. In the subsequent steps hydroxylation/oxidation of the aromatic ring occurs.



Scheme 1.6. Hydroxylation/oxidation of a monophenolic substrate by tyrosinase according to Tuczek and Decker.^[24]

1.3. Biomimetic Cu/O₂ Chemistry: Structure and Reactivity

As detailed in the previous section, several copper enzymes are capable of selectively incorporating oxygen from O₂ into C–H bonds under mild conditions and the particular constitution of their active sites enables the specific functionalization of aliphatic (DβM and PHM) or aromatic C–H bonds (tyrosinase).^[14] The biological functions of these active sites in C–H bond oxidation have attracted enormous interest among synthetic chemists due to

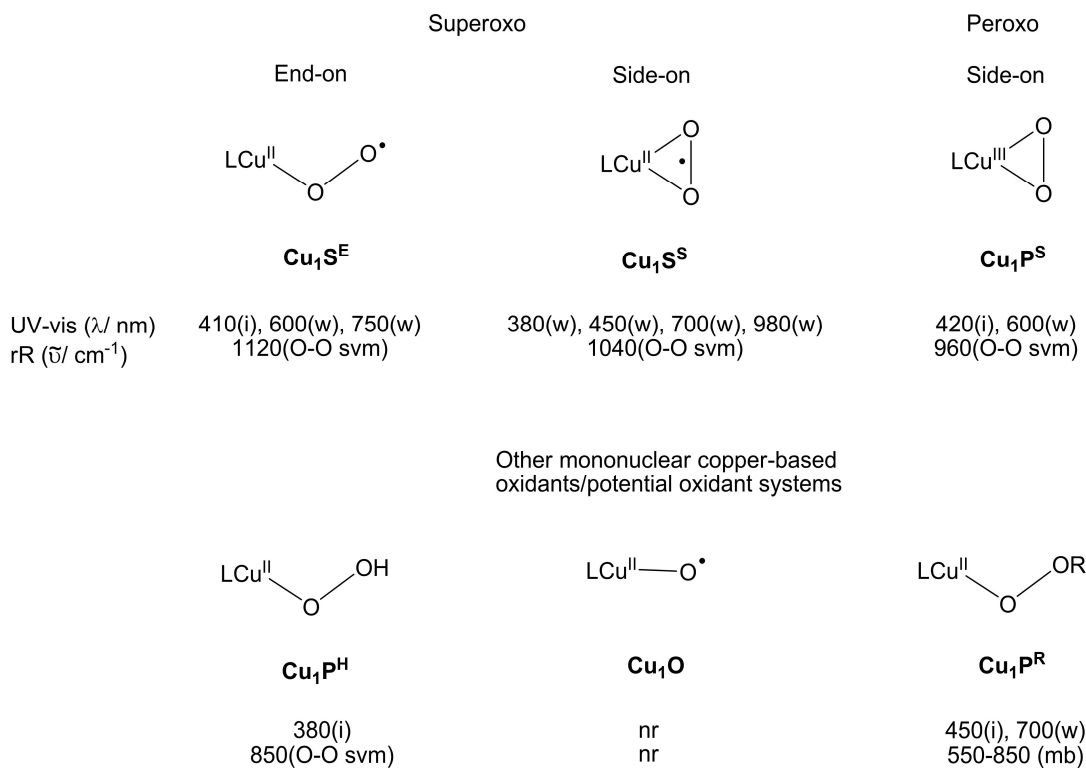
their potential relevance to synthetic oxidation catalysis.^[25] Therefore, in the realm of bioinorganic copper chemistry, the binding of O₂ to Cu complexes supported by simple donor ligands, and the subsequent oxidation reactivity of the Cu-O₂ species formed, have been an active area of research in the past three and a half decades. A number of such studies on small synthetic model systems has demonstrated the existence of various Cu_n-O₂ complexes, which served as relevant oxidant models in copper chemistry and biochemistry (Figure 1.2).^[25a-d] In the following, several examples of crystallographically and spectroscopically characterized Cu_n-O₂ complexes will be presented and their reactivity towards C–H bonds will be discussed.

1.3.1. Mononuclear Cu-O₂ Complexes and C–H Hydroxylations

Two types of mononuclear LCu-O₂ complexes have been characterized in bioinorganic studies: LCu(II)-superoxo(O₂[−]) and (2) LCu(III)-peroxo(O₂^{2−}) (Figure 1.2; L indicates supporting ligands).^[25a] While two binding modes have been identified for the former species (end-on η^1 and side-on η^2) only the side-on coordination has been found for the latter. Both, the end-on as well as the side-on Cu(II)-superoxo species result from formal transfer of one electron from the Cu(I) ion onto the O₂ molecule, whereas the Cu(III)-peroxo species results from formal transfer of two electrons from Cu(I). Both, the dioxygen coordination mode (end-on or side-on) and the oxidation state of the copper ion (+2 or +3) are controlled by the nature of supporting ligands (L), although, judging from the pertinent literature basis, the specific directing role of the ligands appears not well understood.^[26] While a number of mononuclear LCu₁-O₂ species have been characterized mostly by means of UV-vis and resonance Raman spectroscopy (cf. Figure 1.2, top),^[27] only a few were unambiguously structurally characterized by X-ray crystallographic analysis.^[27e, 27r-u, 28] In the following, these mononuclear LCu₁-O₂ species are denoted **Cu₁S^E**, **Cu₁S^S**, and **Cu₁P^S** for copper(II) end-on superoxo, copper(II) side-on superoxo, and copper(III) side-on peroxo species, respectively.^[25q]

In 1994, Kitajima and coworkers reported the first X-ray characterization of a mononuclear Cu(II) side-on superoxo complex (**1** in Figure 1.3). The complex was synthesized at −50°C by the addition of O₂ to the Cu(I) complex (supported by a sterically

Mononuclear



Dinuclear

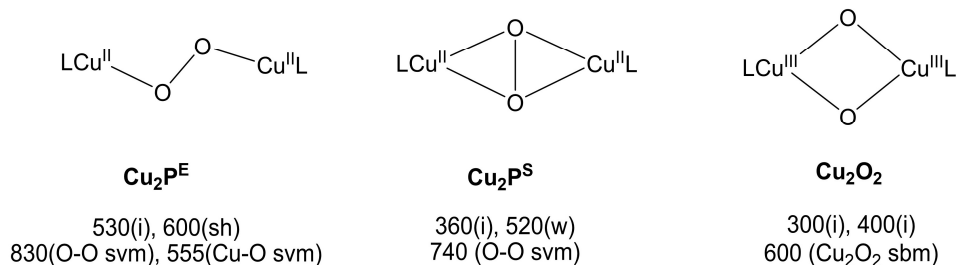


Figure 1.2. Copper/oxygen complexes suggested as reactive intermediates (L denotes supporting ligand) with typical UV-vis and resonance Raman (rR) characteristics. The nomenclature of copper complexes follows Karlin's work.^[25q] Abbreviations: i (intense), w (weak), mb (multiple bands), sh (shoulder), svm (stretching vibration mode), sbm (symmetric breathing mode), nr (not reported).

demanding monoanionic tridentate ligand $\text{HB}(3\text{-}t\text{-Bu-5-}i\text{-Pr-pz})_3^-$ bearing peripheral *t*-butyl and *i*-propyl substituents, pz = pyrazolyl; *t*-Bu = *tert*-butyl; *i*-Pr = isopropyl).^[27e] However, this complex was found stable only in the solid state and it transformed into a dinuclear species in solution. Chen and coworkers used the sterically more demanding ligand $\text{HB}(3\text{-Ad-5-}i\text{-Pr-pz})_3^-$ bearing adamantyl (Ad) substituents in the 3-position to synthesize the mononuclear Cu(II) end-on superoxo complex in solution (**2** in Figure 1.3).^[27h] This complex

is EPR-silent and exhibits a resonance Raman band at 1043 cm^{-1} similar to other well-characterized superoxide species.^[29] The complex is further characterized by very weak d–d transition bands at 383, 452, 699 and 980 nm. No experimental data is available for any chemical reactivity of $\text{Cu}_1\text{S}^{\text{S}}$ species.

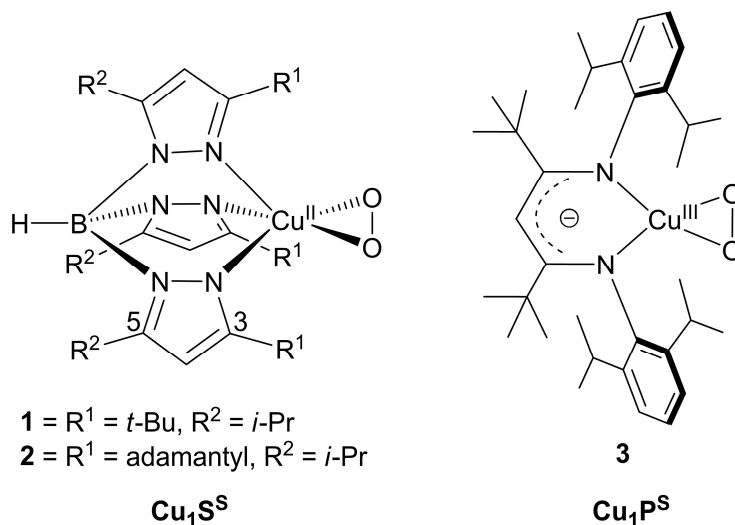
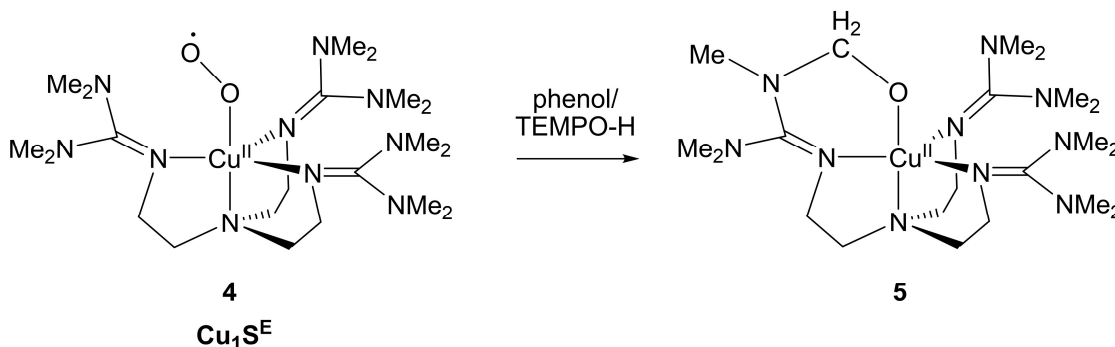


Figure 1.3. Mononuclear Cu(II) side-on superoxo complexes ($\text{Cu}_1\text{S}^{\text{S}}$) and Mononuclear Cu(III) side-on peroxo complex ($\text{Cu}_1\text{P}^{\text{S}}$).

In 2002, Tolman and coworkers structurally characterized a mononuclear Cu(III) side-on peroxo complex supported by a monoanionic β -diketiminato ligand (cf. **3** in Figure 1.3).^[27r, 27s] In this complex, the +3 oxidation state of copper is stabilized through the strong electron donating properties of the β -diketiminato ligand. X-ray crystal structure analysis of this EPR silent complex revealed an O–O bond length of 1.392 \AA and the O–O resonance Raman signature observed at 961 cm^{-1} indicates considerable peroxide (O_2^{2-}) character.^[27r, 30] No further examples for side-on mononuclear CuO_2 complexes have been reported and none of these complexes has shown any C–H bond activation reactivity.^[31]

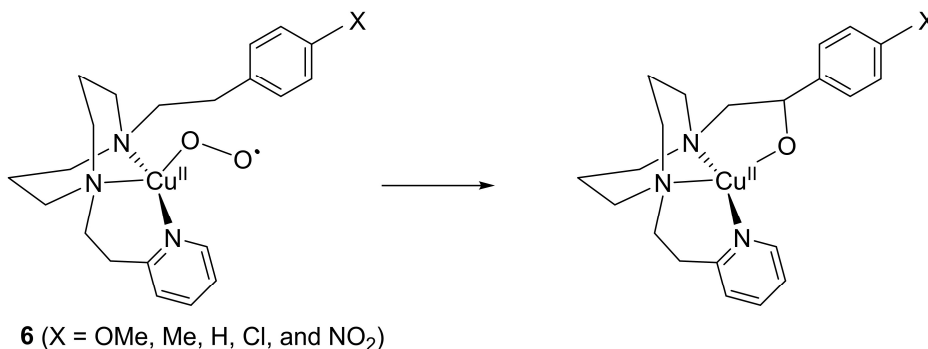
Employing a supporting TMG_3tren ligand [$\text{TMG}_3\text{tren} = \text{tris}(2\text{-}(N\text{-tetramethylguanidyl)ethyl})\text{-amine}$], Schindler and coworkers crystallized the first mononuclear Cu(II) end-on superoxo complex ($\text{Cu}_1\text{S}^{\text{E}}$) at low temperature (**4** in Scheme 1.7).^[27u] With an observed O–O bond length of 1.280 \AA in the crystal, the complex is further characterized by an intense absorption band at 447 nm, with two weaker features at 680 and 780 nm and a resonance Raman band at 1117 cm^{-1} .^[27m] In contrast to the $\text{Cu}_1\text{S}^{\text{S}}$ and $\text{Cu}_1\text{P}^{\text{S}}$ complexes, which were assigned singlet ground states, detailed investigations revealed a triplet electronic

ground state for this complex.^[27o] In the presence of hydrogen-atom donors such as phenols or TEMPO-H it decomposes at higher temperatures through intramolecular aliphatic ligand hydroxylation of an *N*-methyl group of the TMG₃tren ligand to yield a copper(II) alkoxide product **5** (Scheme 1.7).^[32]



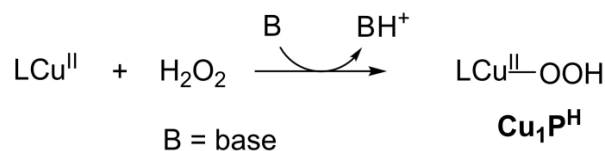
Scheme 1.7. Complex **4** as the mononuclear Cu(II) end-on superoxo species (**Cu₁S^E**), and its thermal decomposition in the presence of hydrogen-atom donors (e.g. phenols or TEMPO-H) resulting in intramolecular aliphatic ligand hydroxylation.

Itoh and coworkers later prepared a **Cu₁S^E** species **6**, which was, however, characterized only spectroscopically, and observed intramolecular aliphatic ligand hydroxylation of the activated benzylic C–H position, even without adding a hydrogen-atom donor (Scheme 1.8).^[27q] Kinetic investigation of this reaction (first order decay of the complex followed by NMR analysis, kinetic isotope effect (KIE) = 4.1 at –60°C) disclosed the intramolecular C–H bond cleavage as the rate-limiting step. A Hammett analysis ($\rho = -0.5$) revealed characteristics for an electrophilic attack of the Cu(II)–superoxo moiety in the course of the hydrogen-atom abstraction, similar to the proposal of Klinman for the aliphatic hydroxylation by the enzymes D β M and PHM.^[18a]



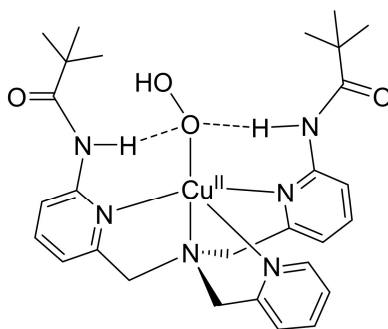
Scheme 1.8. Intramolecular aliphatic ligand hydroxylation in the **Cu₁S^E** species **6**.

The potential role of yet other copper/oxygen species as oxidants was investigated in further work. Mononuclear Cu(II) end-on hydroperoxo species ($\text{Cu}_1\text{P}^{\text{H}}$) can be generated by reaction of copper(II) complexes with H_2O_2 in the presence of an amine base, such as triethylamine, to deprotonate H_2O_2 (Scheme 1.9).^[28, 33] $\text{Cu}_1\text{P}^{\text{H}}$ complexes exhibit a resonance Raman band at $\sim 850\text{ cm}^{-1}$ and show an intense UV-vis absorption band at $\sim 380\text{ nm}$.



Scheme 1.9. Reaction of Cu(II) complexes with H_2O_2 and an amine base to generate Mononuclear Cu(II) end-on hydroperoxo species ($\text{Cu}_1\text{P}^{\text{H}}$).

The first crystal structure of a $\text{Cu}_1\text{P}^{\text{H}}$ complex, $[\text{Cu}^{\text{II}}(\text{bppa})(\text{OOH}^-)]^+$ (bppa = bis(6-pivalamide-2-pyridylmethyl)-(2-pyridylmethyl)amine) was reported by Masuda and co-workers (Figure 1.4).^[28] Their study revealed the presence of stabilizing hydrogen-bonding interactions between the proximal oxygen of the hydroperoxo group and N-H fragment of the bppa ligand.^[33h]

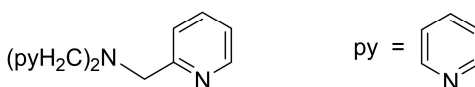


Hydrogen bonding: N-H ---- O

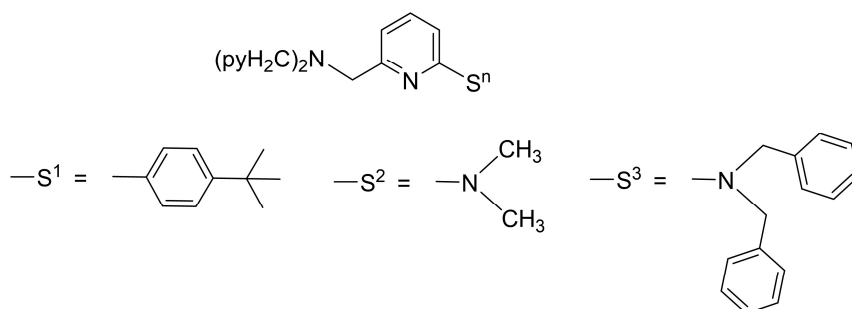
Figure 1.4. Mononuclear Cu(II) end-on hydroperoxo species ($\text{Cu}_1\text{P}^{\text{H}}$) species containing hydrogen bonding interactions.

Karlin and co-workers performed the aromatic ligand hydroxylation via a spectroscopically detected mononuclear $\text{Cu}_1\text{P}^{\text{H}}$ intermediate supported by the modified tris(2-pyridylmethyl)amine (TMPA) ligand (L-S^1) (Reaction-1 in Scheme 1.10).^[33m]

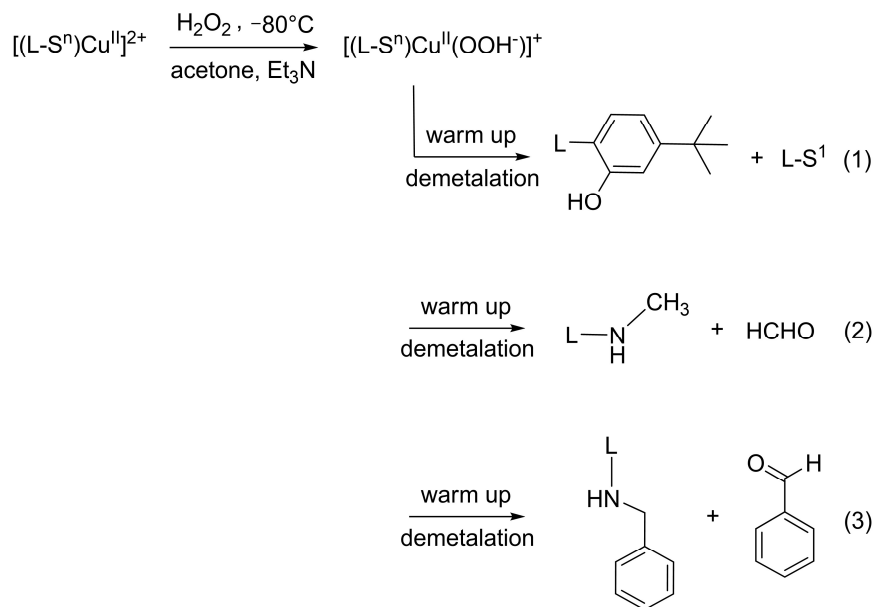
TMPA ligand (L)



Modified TMPA ligands (L-S^n)



Reactions (1-3)

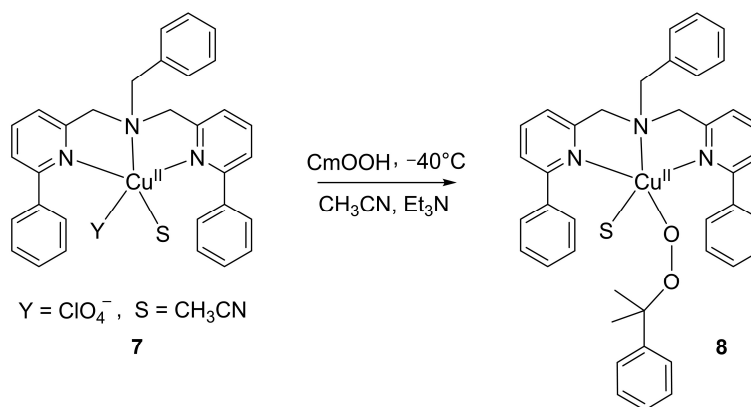


Scheme 1.10. Top: TMPA (tris[2-pyridyl]methyl)amine and modified TMPA ligands. Bottom: Aromatic ligand hydroxylation (1), and oxidative N-dealkylation (2 and 3).

In related work this group studied the influence of modified TMPA ligands carrying *N,N*-dimethylamino or *N,N*-diphenylamino groups (L-S^2 and L-S^3). With these ligands other mononuclear Cu(II)–hydroperoxo intermediates were detected spectroscopically and the formation of formaldehyde/benzaldehyde was observed resulting from oxidative *N*-

demethylation reactions (Reactions 2 and 3 in Scheme 1.10).^[33n, 33o] Dinuclear species generated with these ligands did not show the aromatic/oxidative N-demethylation reactions, which led the authors to conclude that either mononuclear copper(II) end-on hydroperoxo ($\text{Cu}^{\text{II}}\text{OOH}$) or high-valent copper-oxo species resulting from O–O bond homolysis of $\text{LCu}^{\text{II}}\text{OOH}$ are the reactive key intermediates in these reactions. Mononuclear copper-oxo species Cu_1O have also been postulated as a possible reactive intermediate in several other synthetic oxidation reactions.^[34] While such a species has never been isolated in synthetic work it has been detected in a combined mass-spectrometric/theoretical gas-phase study, in which its reactivity as oxidant was also reported.^[35]

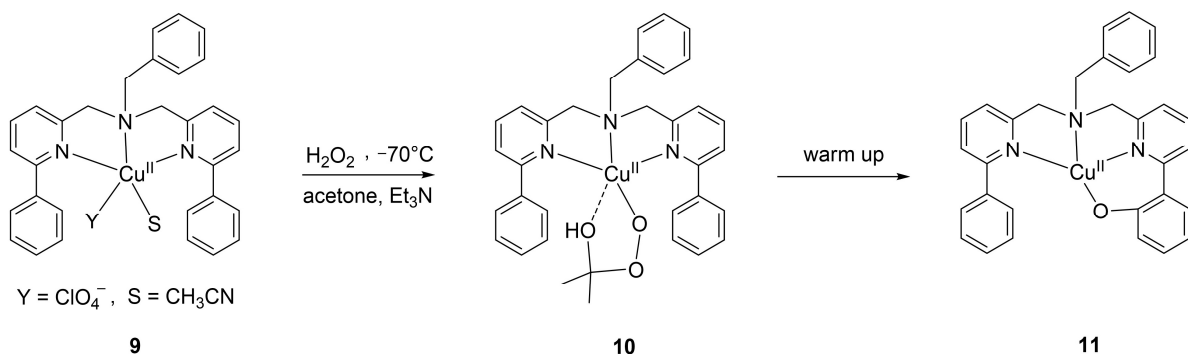
Similar to $\text{Cu}_1\text{P}^{\text{H}}$ complexes, mononuclear Cu(II) alkylperoxo complexes $\text{Cu}_1\text{P}^{\text{R}}$ have been prepared by reacting Cu(II) starting material with alkylhydroperoxide (ROOH) in the presence of a base.^[36] For example, Itoh and coworkers recently reported a new $\text{Cu}_1\text{P}^{\text{R}}$ complex (**7**) generated by reacting the Cu(II) complex (**8**) with cumene hydroperoxide in the presence of triethylamine at -40°C in acetonitrile (Scheme 1.11).^[36b] The resulting complex exhibits an intense absorption band at 465 nm and a weak UV-vis absorption at 725 nm (associated to a d-d transition). The resonance Raman spectrum of the complex is rather complicated exhibiting several isotope sensitive bands at $550\text{--}850\text{ cm}^{-1}$. This mononuclear Cu(II) alkylperoxo complex did not show any aromatic ligand hydroxylation.



Scheme 1.11. Generation of a mononuclear Cu(II) alkylperoxo complex ($\text{Cu}_1\text{P}^{\text{R}}$).

In other work Itoh and coworkers studied a $\text{Cu}_1\text{P}^{\text{R}}$ species supported by a tridentate bis(pyridylmethyl)amine ligand and observed the *ortho*-hydroxylation of one of the phenyl substituents attached to pyridine donor groups (Scheme 1.12).^[37] The alkylperoxo complex

10 was spectroscopically characterized in a reaction of **9** with H₂O₂ in the presence of triethylamine in acetone at low temperature. Upon warming of the solution, efficient aromatic ligand hydroxylation took place, yielding the phenolate complex **11**, which was characterized by single-crystal X-ray structural analysis. Based on detailed spectroscopic and kinetic analyses including Hammett analysis and kinetic deuterium labeling experiments (KIE = 1.0), an electrophilic aromatic substitution mechanism was suggested.



Scheme 1.12. Aromatic ligand hydroxylation observed in a Cu₁P^R species.^[37]

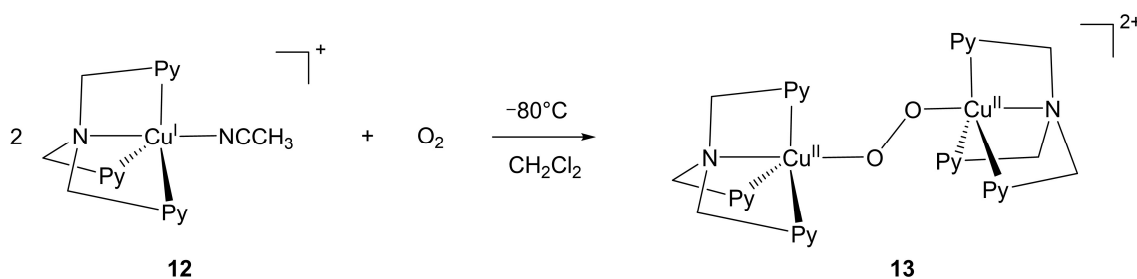
In summary, a number of mononuclear LCu₁-O₂ species (Cu₁S^S, Cu₁P^S, Cu₁S^E and Cu₁P^H) has been isolated and characterized by X-ray crystallography, whereas others were characterized by spectroscopic techniques such as UV-vis and resonance Raman (rR) only. Interestingly, all the mononuclear species produce unique signals in UV-vis and resonance Raman spectra (Figure 1.2). Cu₁S^E species are capable of mediating aliphatic hydroxylations, whereas Cu₁P^H and Cu₁P^R species have been found to be involved in aromatic hydroxylations.

1.3.2. Dinuclear Cu-O₂ Complexes and C-H Hydroxylations

Three kinds of dinuclear (LCu)₂-O₂ species have been discovered in the past decades, realizing three different O₂ coordination modes in trans-μ-1,2-peroxo-dicopper(II) cores (Cu₂P^E), μ-η²:η²-peroxo-dicopper(II) cores (Cu₂P^S), and bis(μ-oxo)dicopper(III) cores (Cu₂O₂) (Figure 1.2).^[25b-p, 38] In this section we discuss all three types of dinuclear (Cu₂O₂)L₂ species and their reactivity towards C-H bonds.

In 1988 Karlin and coworkers reported the first structural characterization of dinuclear Cu₂P^E species.^[39] The complex (**13** in Scheme 1.13) was synthesized by the addition of O₂ to

the TMPACu(I) complex **12** in CH₂Cl₂ at -80°C. Crystal structure analysis of **13** revealed an O–O bond length of 1.43 Å, indicative of a peroxo species.^[39] **13** is EPR-silent as a result of strong antiferromagnetic coupling between the two Cu(II) ions through the end-on peroxo bridge,^[39] and exhibits resonance Raman bands at 832 cm⁻¹ and 561 cm⁻¹ assigned to the O–O and Cu–O stretching vibrational modes, respectively.^[40] The solution of **13** exhibits UV-vis absorptions at 525 nm (intense), 590 nm (shoulder) and 1,035 nm (weak). The first two absorption bands were assigned to peroxo-to-Cu(II) charge transfer and the third band to a d-d transition.



Scheme 1.13. Generation of a Cu₂P^E complex (**13**) starting from [Cu^I(TMPA)(CH₃CN)]⁺ complex (**12**).

A number of Cu₂P^E complexes have been reported with similar structural and spectroscopic features.^[25g, 25h, 27l, 41] Schindler and co-workers discovered that TMPA or Me₆tren [tren = tris(2-aminoethyl)amine] supported Cu₂P^E complexes (**13** in Scheme 1.13 and Figure 1.5), which are extremely labile even at low temperatures, can be stabilized to exist at room temperature for long times if bulky counteranions such as tetraphenylborate (BPh₄⁻) are used instead of the commonly employed anions ClO₄⁻ or PF₆⁻.^[42] The same group also observed reactivity of the complex **13** towards aliphatic C–H bonds of external substrates; this complex was shown to afford the oxidation of a methyl C–H bond of toluene to produce benzaldehyde (major product) and benzyl alcohol (minor product).^[42]

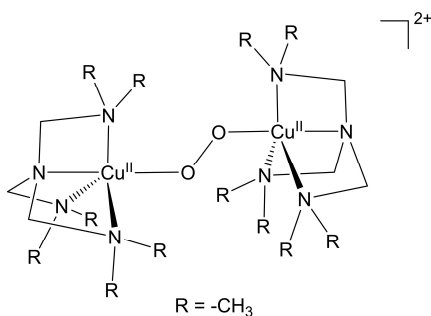
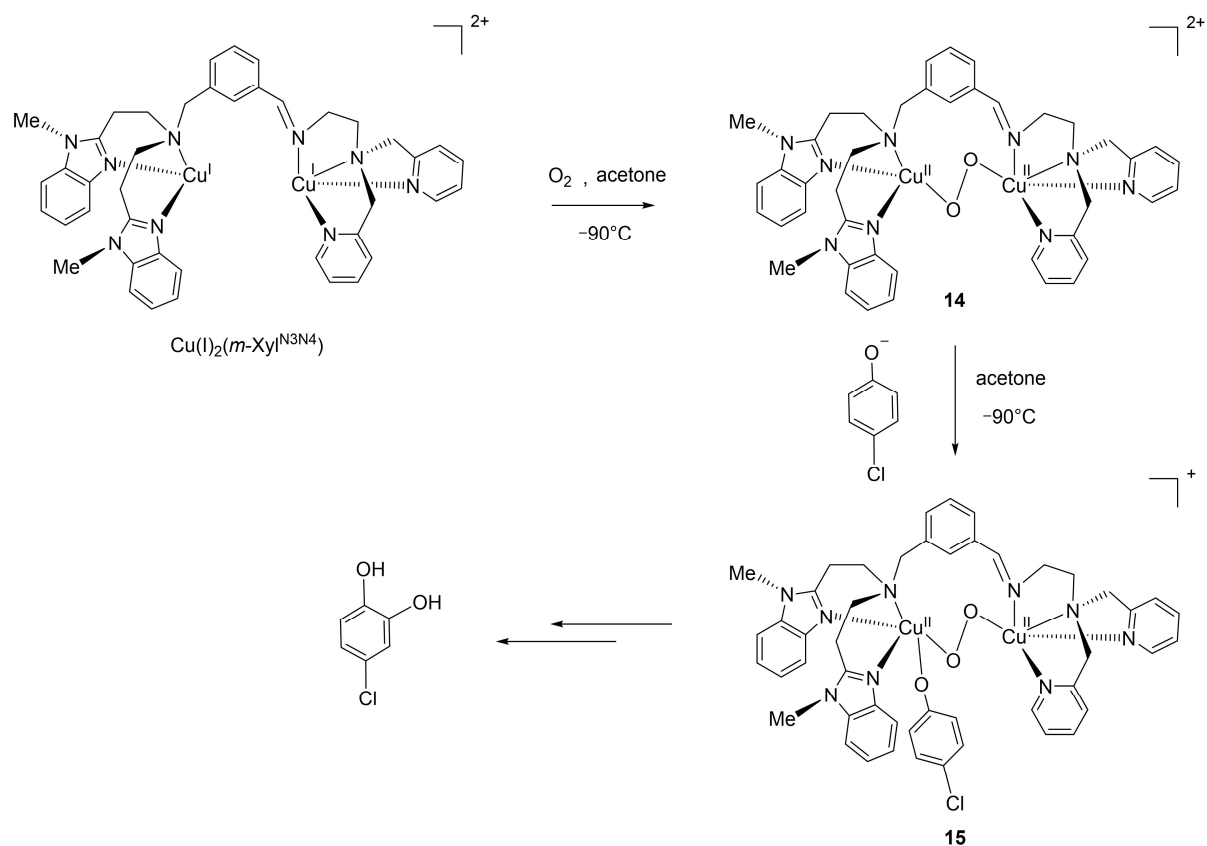


Figure 1.5. A Me₆tren supported trans-μ-1,2-peroxo-dicopper(II) species (Cu₂P^E).

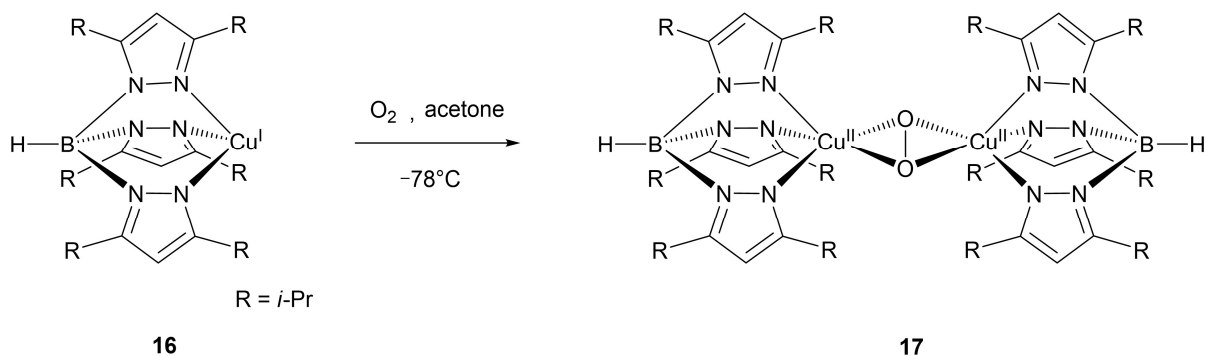
Garcia-Bosch et al. showed that $\text{Cu}_2\text{P}^{\text{E}}$ intermediates are also capable of hydroxylating aromatic C–H bonds: this group carried out a reaction of the asymmetric $\text{Cu}(\text{I})_2(m\text{-Xyl})^{\text{N}3\text{N}4}$ system with O_2 in acetone at -90°C (Scheme 1.14).^[43] The $\text{Cu}_2\text{P}^{\text{E}}$ intermediate **14** was characterized by UV-vis and resonance Raman spectroscopy in this study. Further, adding sodium *p*-chlorophenolate to the reaction mixture resulted in a (spectroscopically detected) $\text{Cu}_2\text{P}^{\text{E}}$ complex **15** with a bound *p*-chlorophenolate ion. Upon warming of the reaction mixture followed by acidic workup, *p*-chlorocatechol was obtained.



Scheme 1.14. Aromatic hydroxylation mediated by a $\text{Cu}_2\text{P}^{\text{E}}$ core established by Garcia-Bosch and coworkers.^[43]

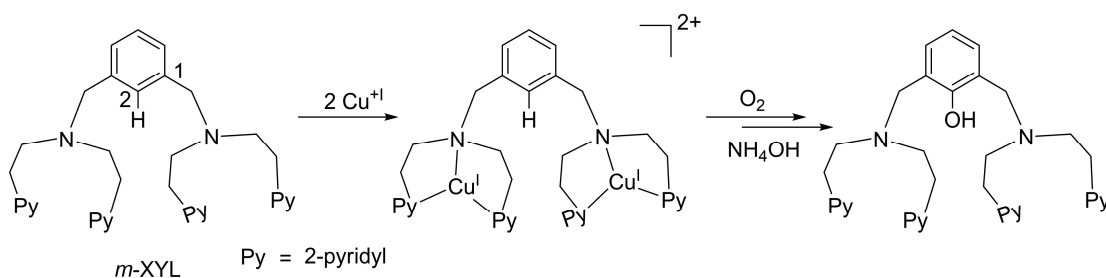
The first crystal structure of a $\mu\text{-}\eta^2\text{:}\eta^2\text{-peroxo-dicopper(II)}$ species ($\text{Cu}_2\text{P}^{\text{S}}$), obtained by the addition of O_2 to the $[\text{Cu}(\text{HB}(3,5\text{-}i\text{Pr}_2\text{pz})_3)]$ complex (**16**) in acetone at -78°C (Scheme 1.15), was reported by Kitajima and coworkers in 1989.^[44] The $\text{Cu}_2\text{P}^{\text{S}}$ complexes are the most extensively studied copper-dioxygen species in the literature due to their relevance to the oxy forms of type-3 copper proteins.^[38h] To date, a number of $\text{Cu}_2\text{P}^{\text{S}}$ crystal structures with different supporting ligands are known.^[44-45] $\text{Cu}_2\text{P}^{\text{S}}$ complexes typically exhibit UV-vis

intense peroxide-to-Cu(II) charge transfer absorption bands at 340–380 nm and weaker absorptions in the range 510–550 nm. These species also have isotope sensitive resonance Raman signatures at 730–760 cm^{-1} for the O–O bond stretching vibration of the side-on peroxide ligand.^[25g]



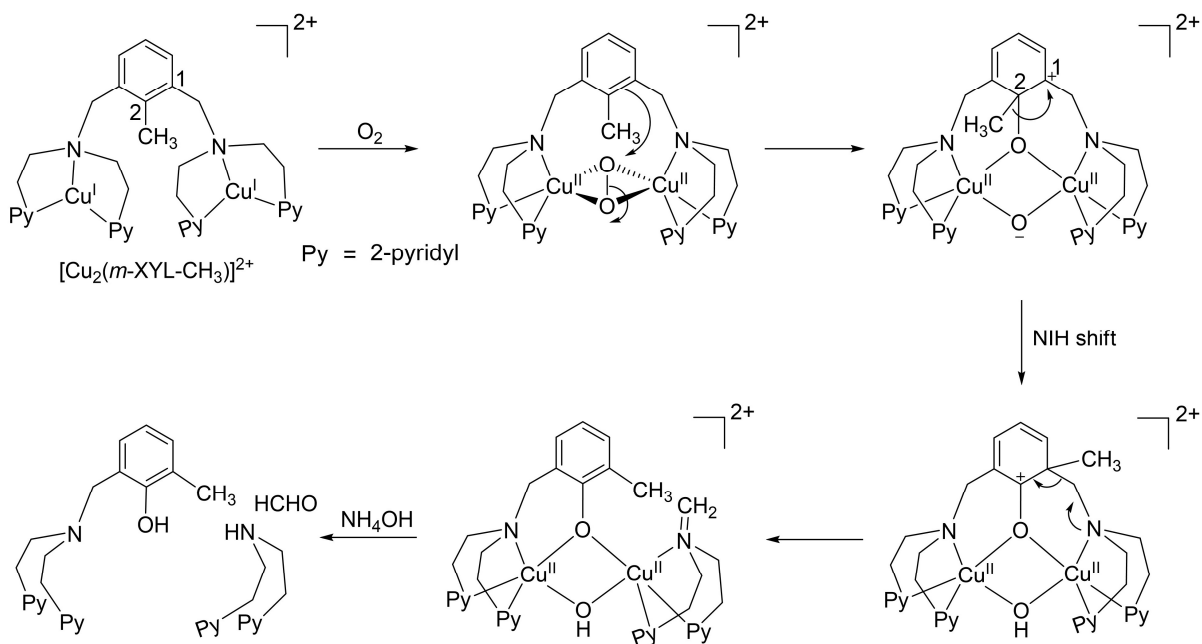
Scheme 1.15. Generation of a dinuclear $\text{Cu}_2\text{P}^{\text{S}}$ complex (17) starting from $[\text{Cu}(\text{HB}(3,5\text{-}i\text{Pr}_2\text{pz})_3)]$ complex (16).

Karlin and coworkers reported the first synthetic model for the tyrosinase-like aromatic hydroxylation. After passing O_2 into a solution of a dinucleating *m*-xylyl-bridged (2-pyridylethyl)ethylamine ligand (*m*-XYL) and a Cu(I) salt, selective hydroxylation of the 2-xylyl position was observed (Scheme 1.16).^[46] Kinetic studies carried out with copper complexes supported by various *p*-substituted *m*-XYL ligands revealed an increasing hydroxylation rate with increasing electron-donating power of the substituents in *para* position, whereas electron-withdrawing *p*-substituents lowered the hydroxylation rate.^[47] Moreover, the *p*- NO_2 substituted system showed no hydroxylation activity. Instead the reaction stopped after formation a $\text{Cu}_2\text{P}^{\text{S}}$ complex, which was detected spectroscopically. This led the authors to propose that the $\text{Cu}_2\text{P}^{\text{S}}$ intermediate represents the active species involved in the hydroxylation process.^[48]



Scheme 1.16. $\text{Cu}_2(\text{XYL})$ system of Karlin and coworkers serving as the first model for a tyrosinase-like aromatic hydroxylation.

In further mechanistic work the same group used a *m*-XYL dinucleating ligand methylated in the 2-position of the bridging arene ring (*m*-XYL-CH₃) in order to block this position from hydroxylation.^[49] However, in contrast to expectation, hydroxylation of the 2-xylyl position took place and analysis of the reaction products evidenced that the reaction involved a 1,2-migration of the methyl group on the aromatic ring was concluded to yield the hydroxylated products (Scheme 1.17). Reminiscent of the so-called “NIH shift”,^[50] this hydroxylation-induced migration of the methyl group led to the conclusion that the reaction involves an electrophilic attack on the aromatic ring of the *meta*-xylene spacer by the **Cu₂P^S** moiety. Analogous reactivity studies with numerous *m*-XYL-based dinucleating ligand systems were published in subsequent years by several research groups. Casella and coworkers modified Karlin's *m*-XYL ligand replacing the pyridyl by sterically more demanding benzimidazole groups.^[51] The corresponding complex was capable of hydroxylating an exogenous phenolate substrate with O₂. Similar to Karlin's results, their study also revealed the formation of a **Cu₂P^S** species in the course of the reaction.^[51b]



Scheme 1.17. Proposed mechanism for the hydroxylation of the 2-xylyl position in the $[\text{Cu}_2(m\text{-XYL-CH}_3)]^{2+}$ complex using O_2 .^[49]

Soon after Casella and coworkers reported on the monophenolase activity of the complex $[\text{Cu}_2(\text{LB5})]^{2+}$ (Figure 1.6).^[52] This system not only mediated the selective *o*-

hydroxylation of an external phenolate but also afforded hydroxylation of an external phenol substrate. The authors proposed that the reactivity differences are related to the presence of an additional non-coordinating N-donor arm in the ligand **LB5** acting as internal base to deprotonate phenols to phenolates. This role of an internal base has already been assumed for tyrosinase.^[14, 24]

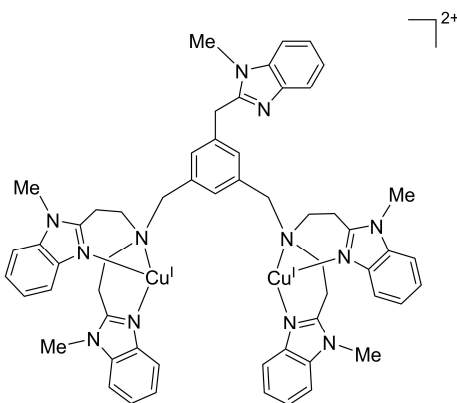


Figure 1.6. The $[\text{Cu}_2(\text{LB5})]^{2+}$ system.

Later, also stimulated by Karlin's successful work with *m*-xylene-bridged (2-pyridylethyl)ethylamine ligands (Schemes 1.16 and 1.17),^[46a, 46b, 49, 53] Itoh and coworkers devised the related unbridged ligand $\text{L}^{\text{Py}2}$ (Figure 1.7)^[54] and showed that oxygenation of the corresponding copper complex at $-94\text{ }^\circ\text{C}$ in acetone leads to the formation of a $\text{Cu}_2\text{P}^{\text{S}}$ intermediate. Reaction with several *p*-substituted phenolates gave the corresponding catechols in high yield. Also for this system, kinetic studies indicated that electrophilic attack of the $\text{Cu}_2\text{P}^{\text{S}}$ intermediate on the aryl ring of the substrate represents the rate-limiting step. A $\text{Cu}_2\text{P}^{\text{S}}$ intermediate was also detected in an independent study by Casella's group, employing the $\text{L}^{\text{bz}2}$ ligand (Figure 1.7), upon exposure of the corresponding mononuclear copper complex $[\text{Cu}(\text{L}^{\text{bz}2})]^+$ to O_2 at $-94\text{ }^\circ\text{C}$.^[55] Also this system afforded hydroxylation of an external phenolate substrate.

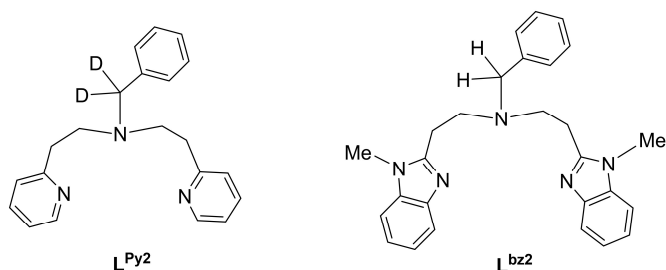
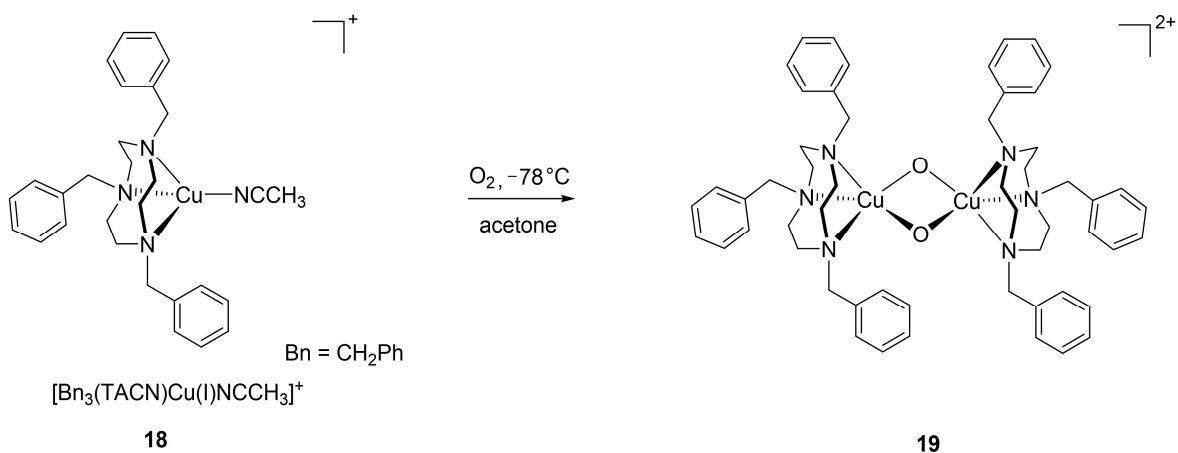


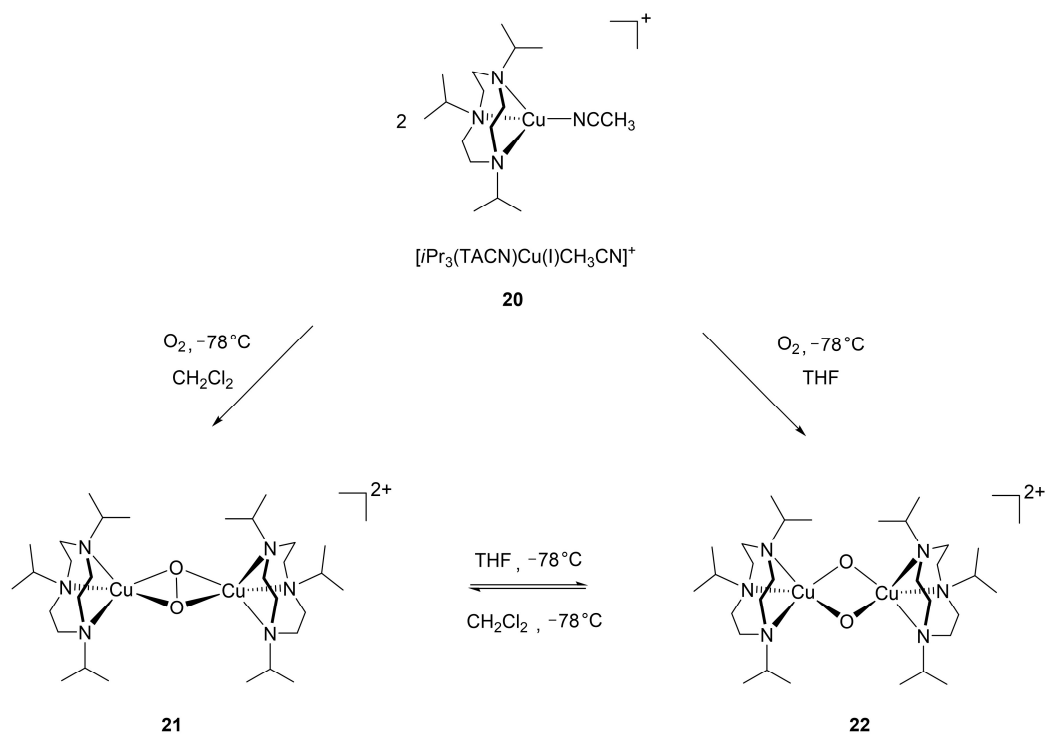
Figure 1.7. The ligand systems $\text{L}^{\text{Py}2}$ and $\text{L}^{\text{bz}2}$, employed in reactivity studies by Itoh^[54] and Casella^[55], respectively.

The first crystal structure of a species containing a bis(μ -oxo)dicopper core was reported by Tolman and coworkers in 1996.^[56] The complex was obtained by bubbling O_2 through the solution of the complex $[Bn_3(TACN)Cu(I)(CH_3CN)]^+$ (H_3TACN : 1,4,7-triazacyclononane) in acetone at $-78^\circ C$ (Scheme 1.18). Several crystal structures of Cu_2O_2 species have been reported in later work.^[27r, 56-57] Unlike Cu_2P^S , Cu_2O_2 species typically exhibit two ligand-to-metal charge transfer UV-vis absorption bands at ~ 300 and ~ 400 nm and a resonance Raman band at $\sim 600\text{ cm}^{-1}$ attributable to the symmetric Cu_2O_2 core vibration.^[25b, 38b, 56]



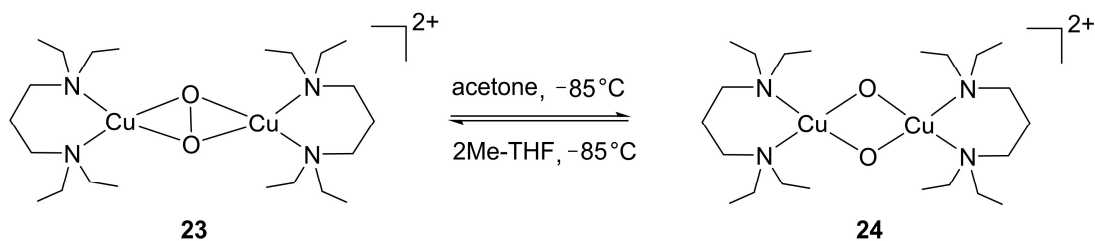
Scheme 1.18. Generation of a dinuclear Cu_2O_2 complex (**19**) starting from $[Bn_3(TACN)Cu(I)(CH_3CN)]^+$ (**18**).

Tolman and coworkers established that an equilibrium between the isomeric Cu_2P^S and Cu_2O_2 cores exists under certain conditions.^[56] This group reported that oxygenation of the complex $[iPr_3(TACN)Cu(I)CH_3CN](ClO_4)$ (**20**) in CH_2Cl_2 generates an intermediate (**21**), which shows UV-vis and resonance Raman features typical for Cu_2P^S species (Scheme 1.19), but when the oxygenation of $[iPr_3(TACN)Cu(I)CH_3CN](ClO_4)$ was carried out in tetrahydrofuran (THF), the UV-vis and resonance Raman signatures typical for a Cu_2O_2 species were observed. Most notably, **21** can thus interconvert to **22** upon solvent exchange, implying that the Cu_2P^S and Cu_2O_2 isomers exist in a balanced equilibrium. Only briefly later also Stack and coworkers reported Cu_2P^S/Cu_2O_2 equilibria sensitive to the choice of solvent and found by UV-vis spectroscopic observation a gradual shift towards the Cu_2P^S species with decreasing dielectric constant of the solvent (Scheme 1.20).^[25c] For example, use of the solvent 2-MeTHF with a moderate dielectric constant ($\epsilon = 6.97$) shifts the



Scheme 1.19. Synthesis and interconversion of **21** (a $\text{Cu}_2\text{P}^{\text{S}}$ species) and **22** (a Cu_2O_2 species).

equilibrium towards the $\text{Cu}_2\text{P}^{\text{S}}$ isomer, whereas acetone with a higher dielectric constant ($\epsilon = 20.7$) shifts the equilibrium towards the Cu_2O_2 isomer. A spectrum with superimposed signatures of both isomers was observed in THF ($\epsilon = 7.52$), which has a dielectric constant between that of acetone and 2-MeTHF. Akin to Tolman's interpretation detailed above, this result implied the existence of a balanced equilibrium under the specific conditions of the experiment.



Scheme 1.20. Interconversion between Cu_2O_2 species **23** ($\text{Cu}_2\text{P}^{\text{S}}$) and **24** (Cu_2O_2).

Stack's group also studied the influence of various bidentate N-donor ligands on this equilibrium and concluded that, quite generally, complexes supported by sterically demanding ligands prefer formation of the $\text{Cu}_2\text{P}^{\text{S}}$ isomer whereas strongly σ -donating

ligands shift the relative isomer stabilities towards the Cu_2O_2 core.^[25c] In addition, they found that an increase of the steric demand of the ligands leads to a decrease of the nuclearity of copper-dioxygen complexes (Figure 1.8).

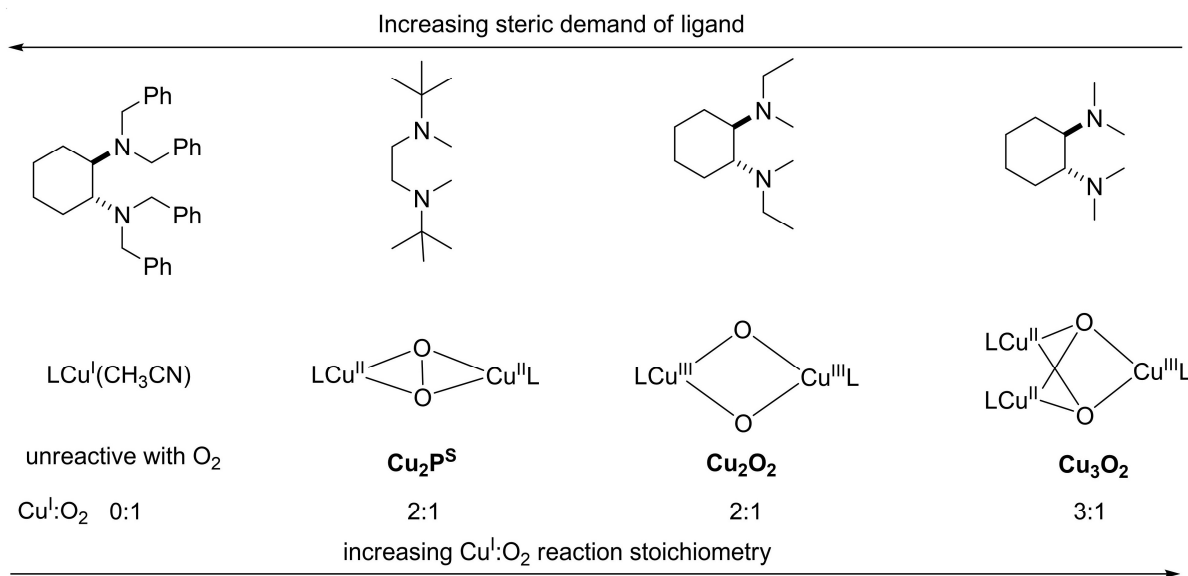


Figure 1.8. Decreasing the steric demand of ligands increases the $\text{Cu}^{\text{I}}\text{-L}:\text{O}_2$ reaction ratio in the complexes formed.

In related work the Stack group showed that also counteranions exert a bias on $\text{Cu}_2\text{P}^{\text{S}}/\text{Cu}_2\text{O}_2$ equilibria.^[58] Use of bidentate N-donor ligands with a more flexible propylene bridge ($^{\text{pd}}\text{L}^1$, $^{\text{pd}}\text{L}^2$) [$^{\text{pd}}\text{L}$: 1,3-diaminopropane)] led to the formation of spectroscopically detectable $\text{Cu}_2\text{P}^{\text{S}}/\text{Cu}_2\text{O}_2$ mixtures upon addition of dioxygen to the Cu(I) precursor complexes in THF with triflate (CF_3SO_3^-) counteranions (Figure 1.9).

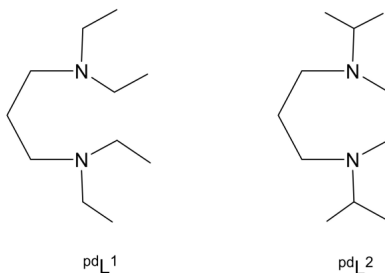


Figure 1.9. Bidentate N-donor ligands $^{\text{pd}}\text{L}^1$ and $^{\text{pd}}\text{L}^2$. ($^{\text{pd}}\text{L}$: 1,3-diaminopropane).

The relative stability of the two Cu_2O_2 isomers was further investigated using various counteranions in THF at -85°C . It was shown, for example, that in the presence of SbF_6^- UV-Vis features indicative of Cu_2O_2 species arise, whereas $\text{Cu}_2\text{P}^{\text{S}}$ species were detected in the presence of CH_3SO_3^- or CF_3CO_2^- ; use of CF_3SO_3^- led to a mixture of both isomers. Overall, the authors concluded that more strongly coordinating anions such as CH_3SO_3^- lead to a stabilization of $\text{Cu}_2\text{P}^{\text{S}}$ species, whereas more weakly coordinating anions such as SbF_6^- stabilize Cu_2O_2 species.

Reactivity studies employing various bidentate and tridentate ligands revealed that ligand structural and electronic effects dominantly control the relative stabilities of $\text{Cu}_2\text{P}^{\text{S}}$ and Cu_2O_2 cores.^[25g] Copper complexes of tridentate aromatic or mixed aromatic/aliphatic N-donor ligands generally form $\text{Cu}_2\text{P}^{\text{S}}$ species, whereas copper complexes with bi- or tridentate aliphatic amine ligands either lead to Cu_2O_2 species or equilibrating mixtures of $\text{Cu}_2\text{P}^{\text{S}}$ and Cu_2O_2 species (a list of representative ligands employed in such studies is given in Figure 1.10).

Hence, the relative stability of $\text{Cu}_2\text{P}^{\text{S}}$ and Cu_2O_2 species is sensitive to the nature of the supporting N-donor ligands, solvents and coordinating counteranions. Primarily, $\text{Cu}_2\text{P}^{\text{S}}/\text{Cu}_2\text{O}_2$ equilibria are influenced by structural and electronic effects of the supporting ligands: (1) Increasing steric demands within a family of ligands destabilizes Cu_2O_2 cores and biases the $\text{Cu}_2\text{P}^{\text{S}}/\text{Cu}_2\text{O}_2$ equilibrium toward $\text{Cu}_2\text{P}^{\text{S}}$. (2) Aromatic N-donor ligands stabilize $\text{Cu}_2\text{P}^{\text{S}}$ species, and aliphatic N-donor ligands stabilize either Cu_2O_2 complexes or induce $\text{Cu}_2\text{P}^{\text{S}}/\text{Cu}_2\text{O}_2$ equilibria. Further, the nature of solvents and counteranions exert secondary effects on $\text{Cu}_2\text{P}^{\text{S}}/\text{Cu}_2\text{O}_2$ equilibria: Generally, less polar solvents (CH_2Cl_2) shift the $\text{Cu}_2\text{P}^{\text{S}}/\text{Cu}_2\text{O}_2$ equilibrium towards $\text{Cu}_2\text{P}^{\text{S}}$ and more polar solvents (acetone) shift the equilibrium toward Cu_2O_2 . Weakly coordinating counteranions (SbF_6^-) bias the $\text{Cu}_2\text{P}^{\text{S}}/\text{Cu}_2\text{O}_2$ equilibrium toward Cu_2O_2 whereas strongly coordinating counteranions (CF_3SO_3^-) bias it towards $\text{Cu}_2\text{P}^{\text{S}}$.

The observation of $\text{Cu}_2\text{P}^{\text{S}}/\text{Cu}_2\text{O}_2$ equilibria raised the question whether bis(μ -oxo)dicopper cores might play a role as reactive intermediates in hydroxylation reactions. Tolman and coworkers performed the hydroxylation of aromatic C–H bonds in the 2-(diethylaminomethyl)-6-phenylpyridine (**L** in Scheme 1.21) supported dinuclear copper complex formed with O_2 in acetone at -70°C (Scheme 1.21).^[59] The resulting solution

exhibits absorption and resonance Raman signatures of a Cu_2O_2 species and the hydroxylated product was obtained after warming and aqueous workup with NH_3 .

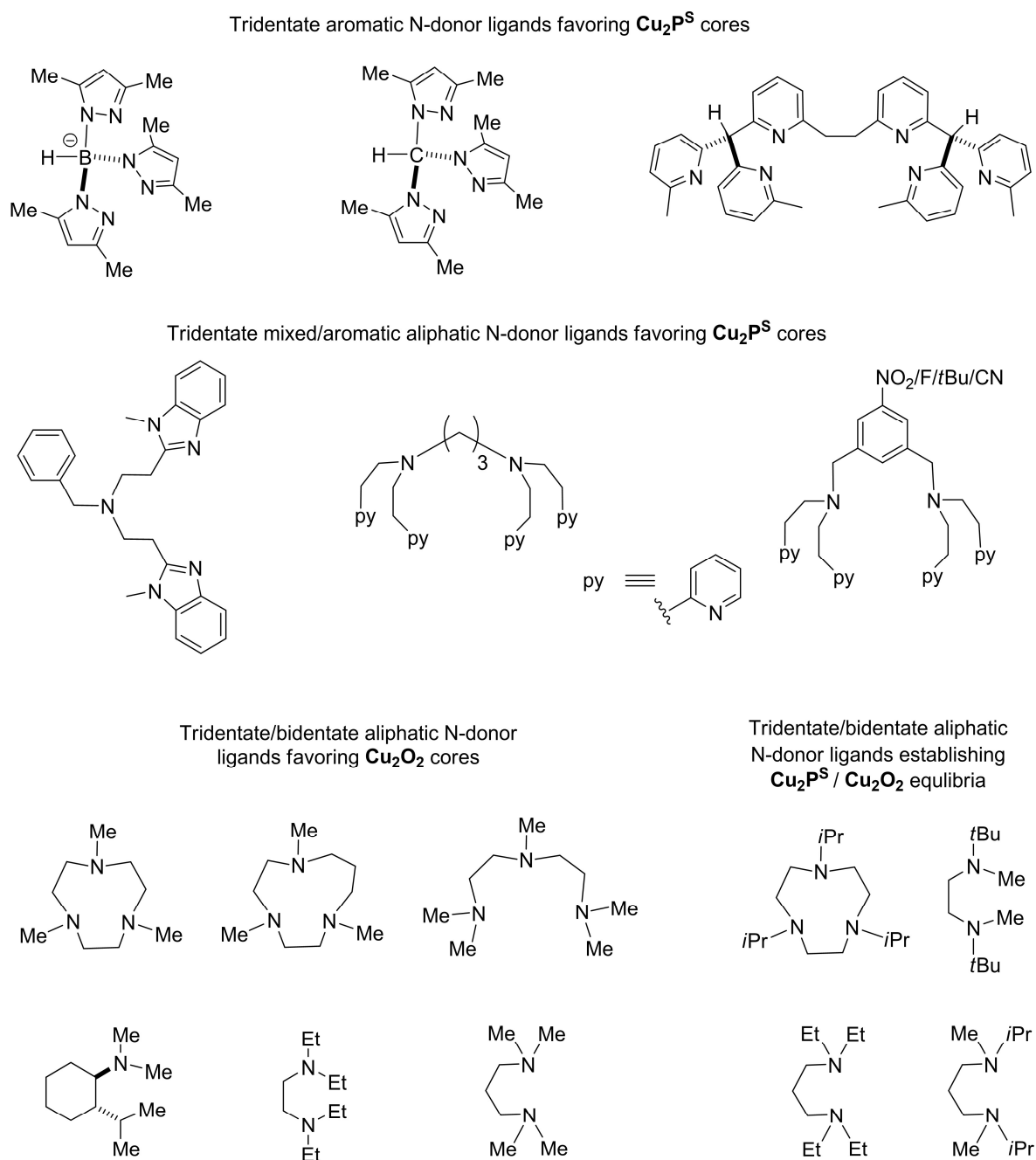
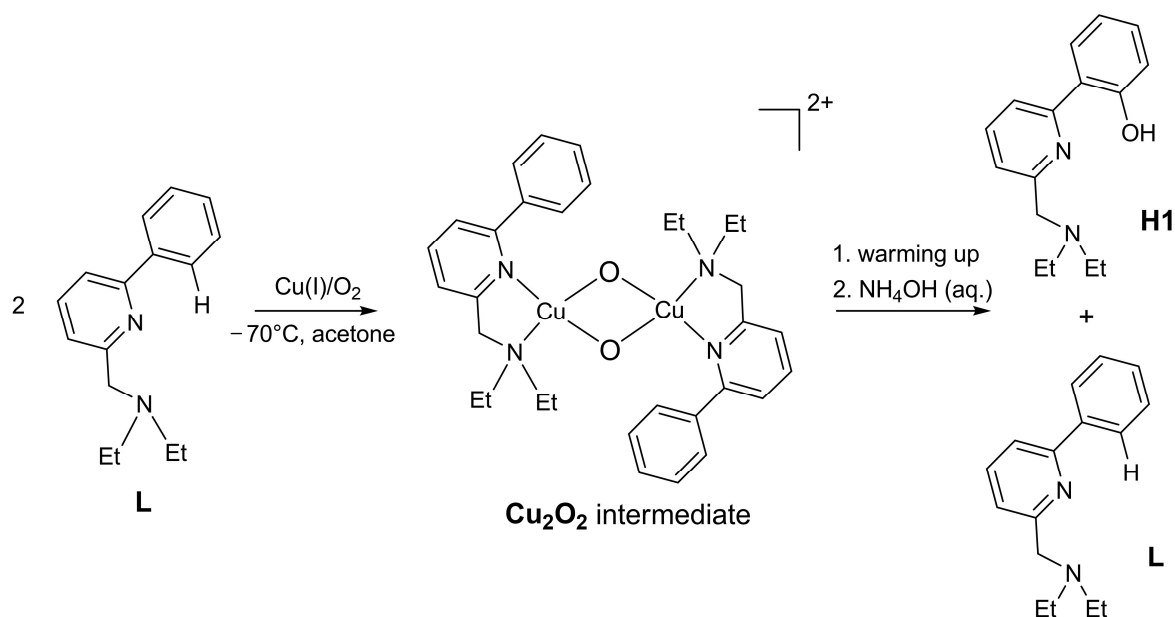


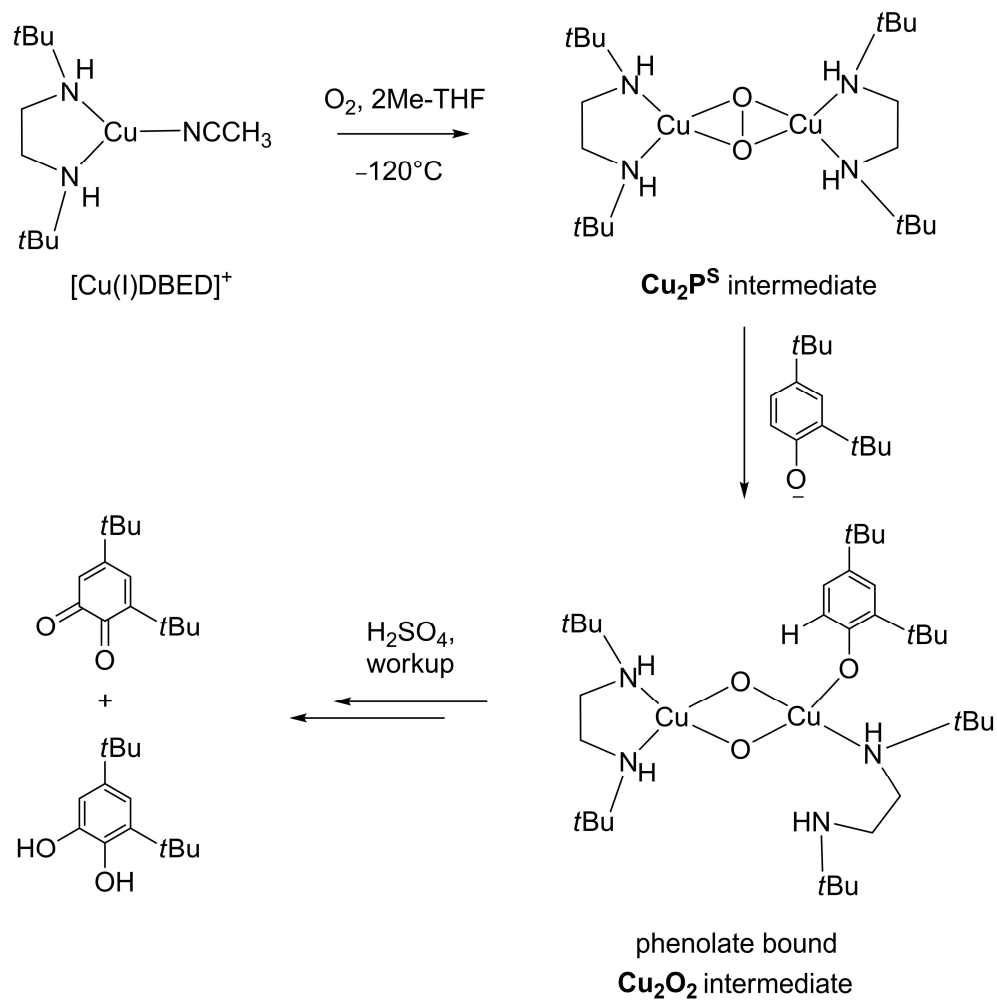
Figure 1.10. Tridentate and bidentate N-donor ligands.



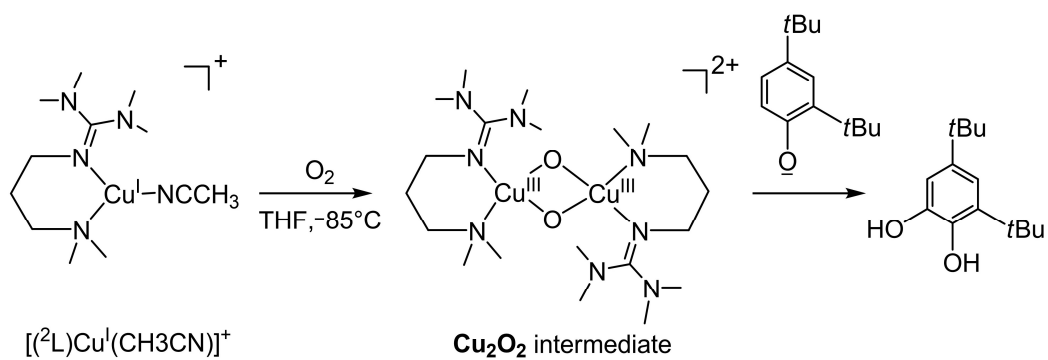
Scheme 1.21. Aromatic ligand hydroxylation by reacting a Cu(I) complex with the ligand 2-(diethylaminomethyl)-6-phenylpyridine (**L**) in presence of O₂ at -70°C in acetone.^[59]

Soon later, Stack and coworkers showed that monooxygenation of an external phenolate can be mediated by a **Cu₂O₂** species.^[60] Exposure of the [Cu(DBED)]⁺ complex (DBED = *N,N'*-di-*tert*-butyl-ethylenediamine; Scheme 1.22) to O₂ at -120°C in 2-MeTHF led to the formation of a spectroscopically detected **Cu₂P^S** species. Subsequent addition of 2,4-di-*tert*-butylphenolate at -120°C led to formation of a phenolate-bound **Cu₂O₂** complex (Scheme 1.22). After warming and acidic workup of the solution a 1:1 mixture of the corresponding catechol and *o*-quinone was found. Kinetic studies suggested that the hydroxylation step follows an electrophilic aromatic substitution pathway, similar to the monooxygenation via **Cu₂P^S** cores and the authors proposed a mechanistic scenario for the monooxygenase reactivity of **Cu₂O₂** species. In another example, Herres-Pawlis, Stack and coworkers first prepared the solution of a **Cu₂O₂** complex employing the hybrid permethylated amine/guanidine ligand ²L (Scheme 1.23).^[61] Subsequent addition of a 2,4-di-*tert*-butyl phenolate resulted in quantitative formation of the corresponding catechol.

Recently, Tuzek and coworkers were successful in developing various synthetic model systems employing mononuclear copper complexes which showed tyrosinase-like hydroxylation reactivity. It was not clear, however, whether the hydroxylations took place via dinuclear or mononuclear copper/dioxygen intermediates.^[62]

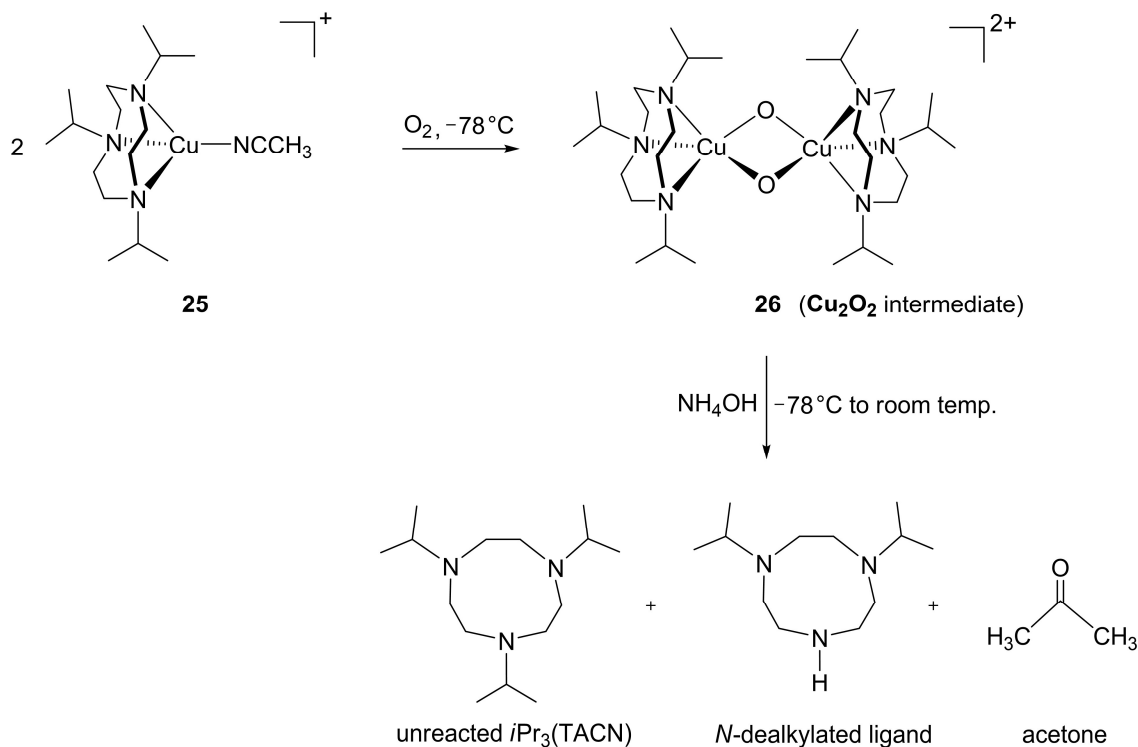


Scheme 1.22. Reactivity of $[\text{Cu(I)DBED}]^+$ towards O_2 and external phenolate.



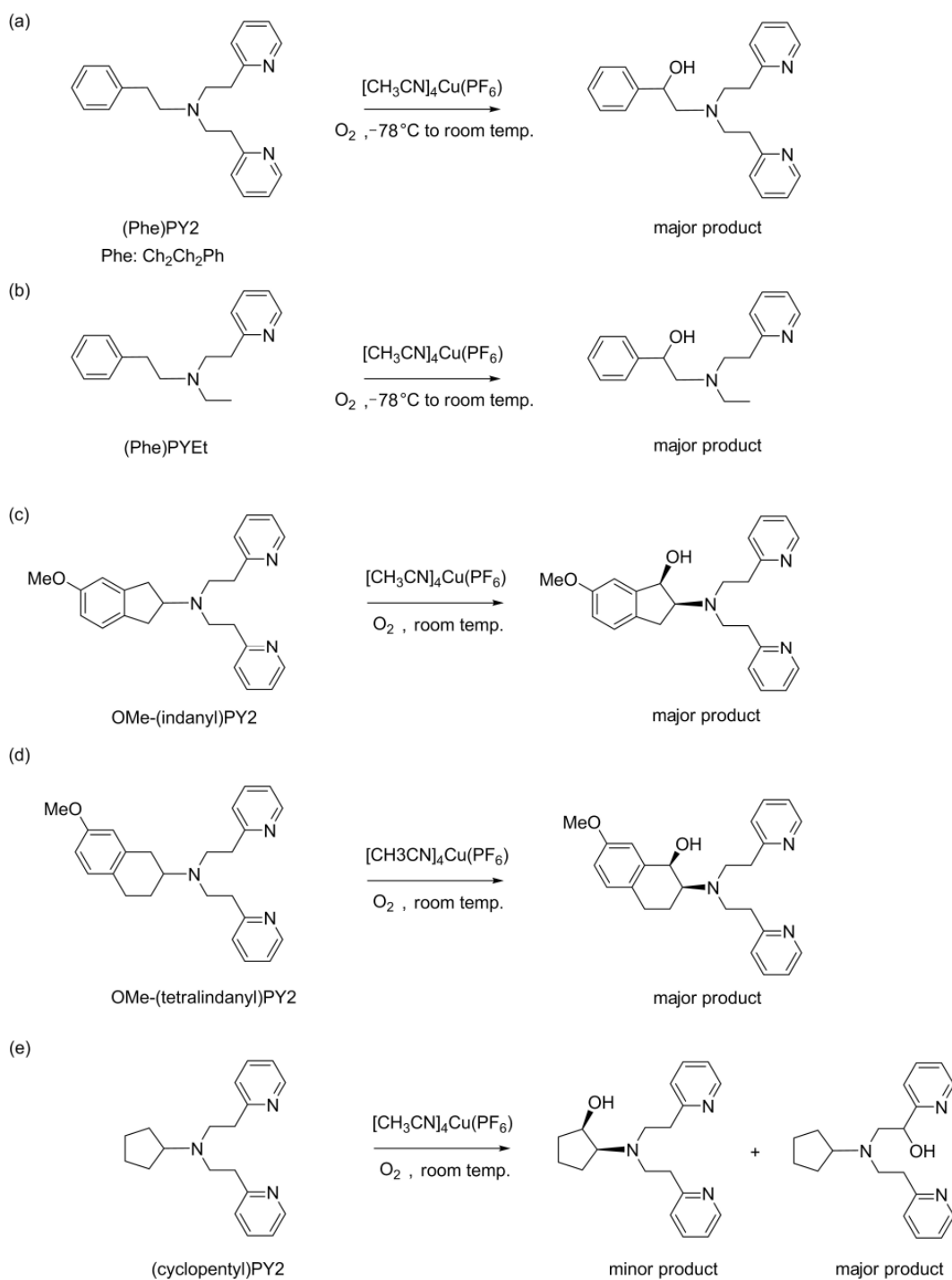
Scheme 1.23. Reactivity of the Cu_2O_2 intermediate supported by the ligand (^2L) .^[61]

Cu_2O_2 intermediates were not only found to be involved in aromatic hydroxylation reactions but also in aliphatic hydroxylation reactions. In the mid-1990s, Tolman and coworkers observed aliphatic C–H bond activation after passing O_2 into a THF solution of the copper complex **25** (Scheme 1.24).^[63] In this reaction, the occurrence of a Cu_2O_2 intermediate (**26**) was spectroscopically detected (UV-vis, EXAFS and resonance Raman), which points at the role of **26** as reactive intermediate in this reaction.



Scheme 1.24. Aliphatic C–H bond activation reported by Tolman and coworkers.^[63]

Later, Itoh and coworkers carried out investigations on the aliphatic C–H bond hydroxylation reactivity in copper complexes of the ligands (Phe)PY2 and (Phe)PYEt (Scheme 1.25, a and b).^[64] In these systems, the benzylic C–H bonds were selectively hydroxylated and rather stable product alcohols were obtained quantitatively. Thereby, this system represents the first biomimetic model for the hydroxylation function of monooxygenases like D β M and PHM. A Cu_2O_2 intermediate was identified by spectroscopic means and suggested as key reactive intermediate. Réglie and co-workers investigated the corresponding reactivity of tridentate ligands carrying indanyl,^[65] tetralinyl^[65] and cyclopentyl^[66] groups (Scheme 1.25, c-e) and found hydroxylations to occur with high regio-

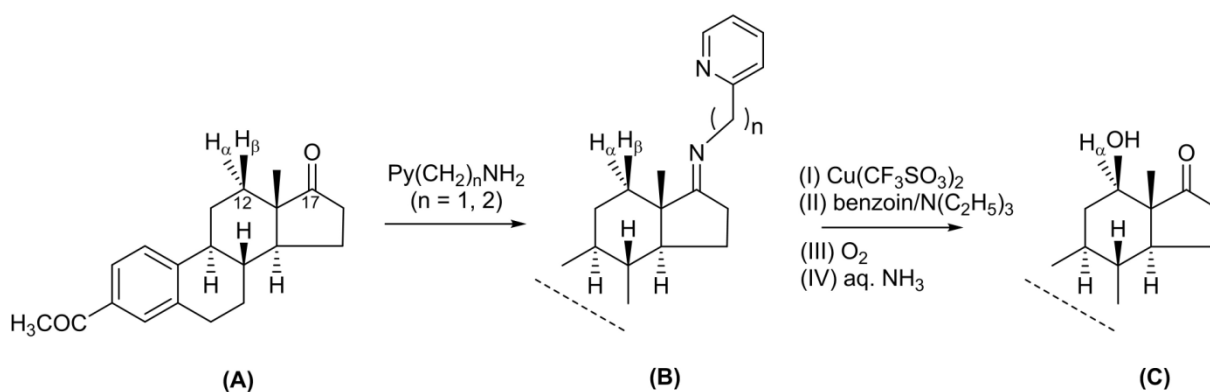


Scheme 1.25. (a, b) Regioselective aliphatic C–H activation reported by Itoh and co-workers.^[64] (c, d) Regio- and stereoselective aliphatic C–H activation reported by Réglier and co-workers.^[65] (e) Competing C–H bond hydroxylations in different positions.^[66]

and stereoselectivity in β -position to the N-donor atom. In the case of the cyclopentyl-substituted ligand, however, the expected hydroxylation of the cyclopentyl C–H bonds was

not the dominant reaction but the alcohol resulting from hydroxylation of the CH₂ group adjacent to one of the pyridine rings was obtained as the major product.

Various other studies reported efforts to insert an oxygen atom into non-activated C–H bonds using copper complexes,^[27a, 67] but truly remarkable success was reported by the Schönecker group in 2003.^[68] In their work, the non-activated and sterically protected C(sp³)–H bond of a steroid molecule was hydroxylated regio- and stereoselectively at ambient temperature and pressure. To this end the 17-keto form of steroid **A** was reacted with primary (2-pyridyl)alkylamines of the type Py(CH₂)_nNH₂ (*n* = 1, 2) in a condensation reaction to give a Schiff base (17-imine, **B** in Scheme 1.26), thereby augmenting the steroid framework with a bidentate N-donor site. Subsequently, a Cu(II) salt was added to a CH₂Cl₂ solution of **B** and benzoin/triethylamine, which was exposed to O₂ to initiate the oxidation. After workup in aqueous NH₃, the 12β-hydroxy-17-ketone (**C**) was isolated – thus a highly regio- and stereoselective hydroxylation of the otherwise inaccessible β-C–H bond was achieved. Recently, the Schönecker approach has successfully been used to accomplish a selective hydroxylation step as part of the synthetic protocol for the build-up of related steroidal skeletons.^[69] Even after more than a decade a complete mechanistic study on the Schönecker reaction is still due,^[70] however the reaction has been assumed to occur via a Cu₂O₂ intermediate.^[68c]



Scheme 1.26. Regio- and stereoselective C(sp³)–H_β bond hydroxylation reported by Schönecker.^[68]

Chapter 2

Density Functional Theory Applications to Biomimetic Copper/Dioxygen Chemistry

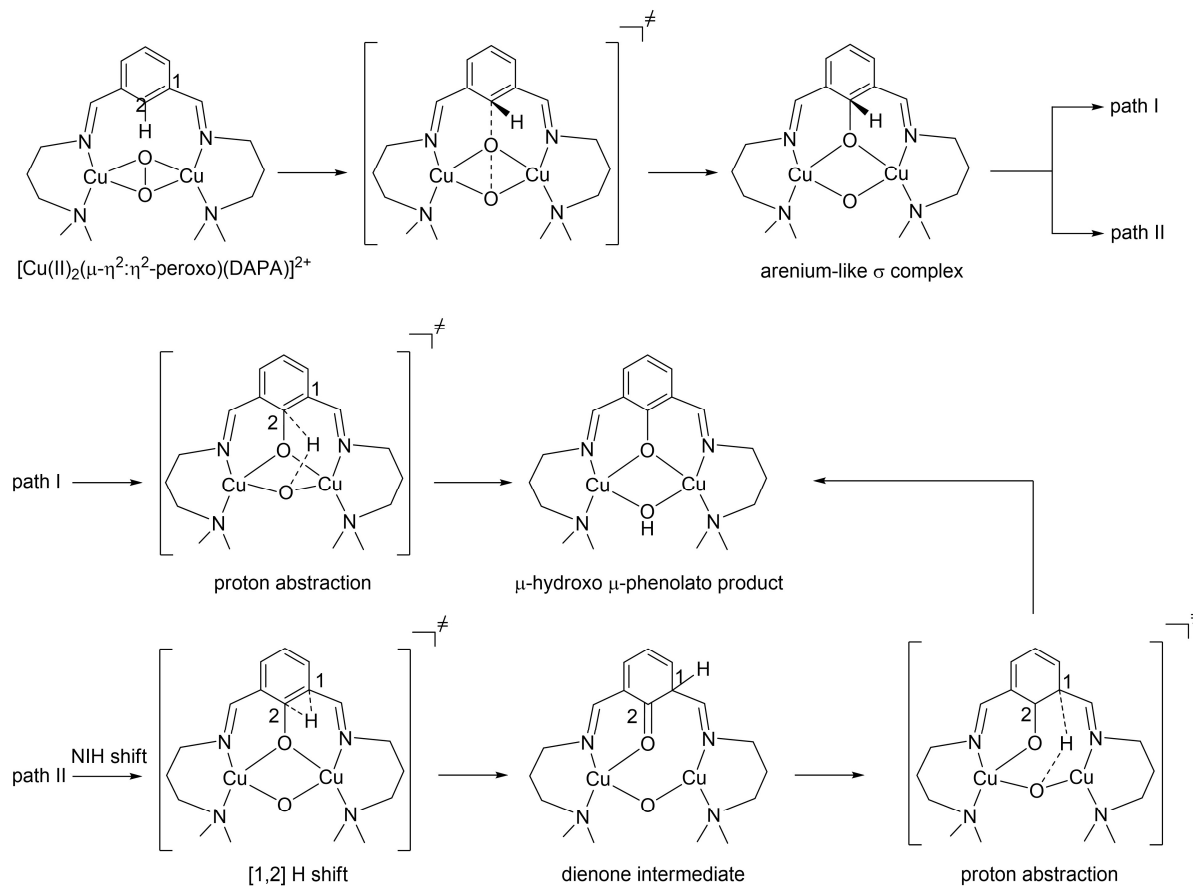
Density functional theory (DFT) has been applied widely to investigate reaction mechanisms underlying the aromatic and aliphatic C–H hydroxylation reactions mediated by various synthetic copper-dioxygen complexes. (For the detailed information on the foundation of DFT selected references are cited.^[71]) In the following, some exemplary DFT-based mechanistic studies for hydroxylation reactions are presented. Later, problems related to application of DFT in these systems are discussed.

2.1 Mechanistic Studies of C–H Hydroxylation

A DFT-based mechanistic study on the copper-mediated intramolecular aromatic ligand hydroxylation was carried out by Holthausen and coworkers (Scheme 2.1).^[72] In the experimental part of this study, formation of a dinuclear copper complex supported by the DAPA ligand (DAPA = 1,3-bis-[(3-(N-dimethyl)propyl)iminomethyl]benzene, a *m*-xylyl-based dinucleating ligand) is reported and hydroxylation in the *ortho*-position of the 2-xylyl position was observed upon exposure to O₂. The authors demonstrated that the μ - η^2 : η^2 -peroxo-dicopper(II) core attacks on the aromatic ring of the *m*-xylene spacer via a multicenter transition state (simultaneous O–O bond cleavage and C–O bond formation) to produce an arenium-like σ complex. Two competing low energy pathways leading to the final hydroxylated product were located.

Along the first pathway, the proton in 2-position of the aromatic ring present in the σ complex is directly abstracted by the bridging μ -oxo atom to generate the hydroxylated μ -hydroxo μ -phenolato product in a single step. Alternatively, the σ complex transforms into a μ -hydroxo μ -phenolato product in two steps: Initially, the σ complex rearranges into a dienone via a [1,2] H shift (analogous to Karlin's proposed NIH shift)^[49] across the phenyl ring. Subsequently, proton abstraction from the 1-position of the dienone intermediate by the

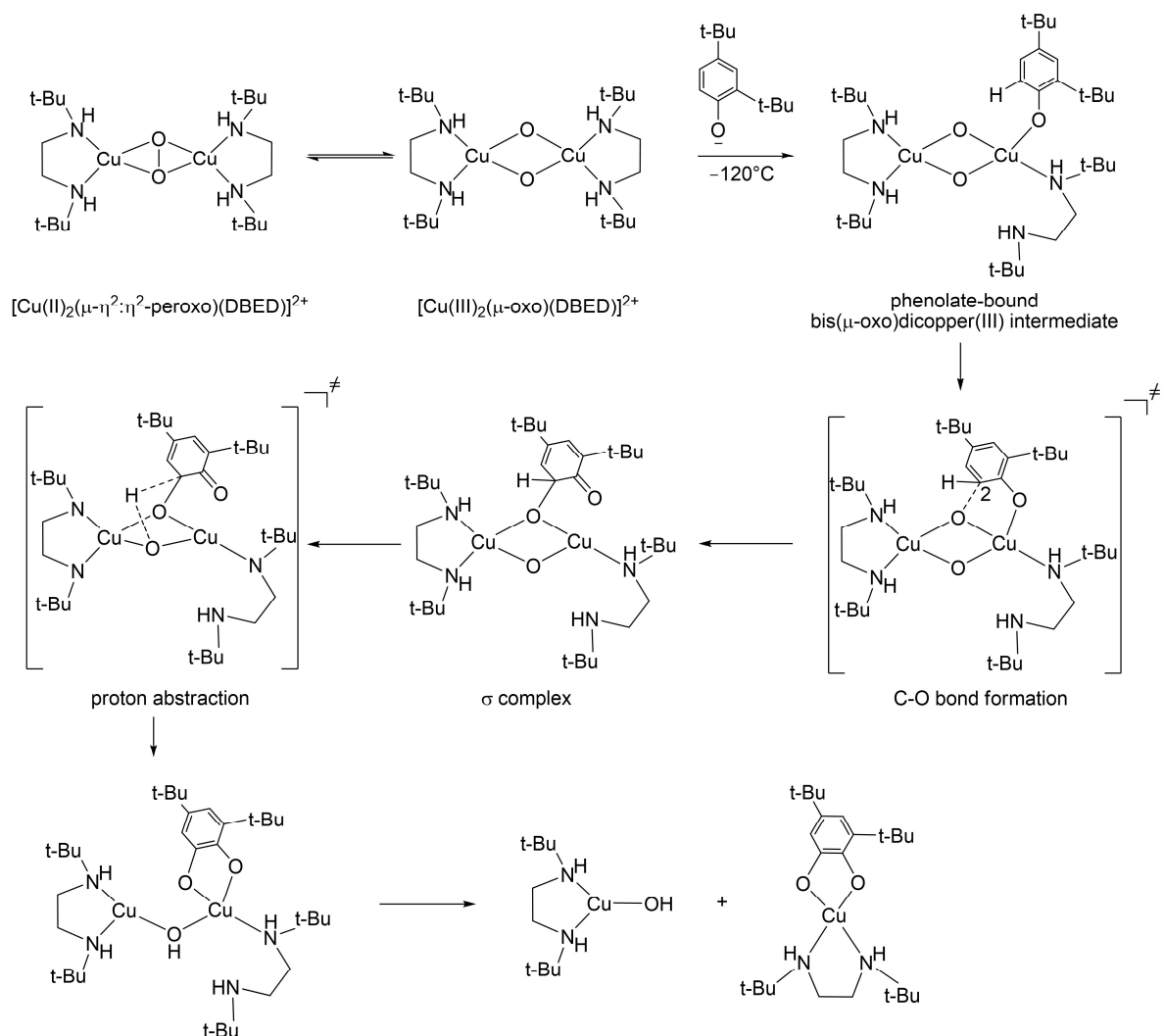
bridging μ -oxo atom takes place, which results in product formation. Conclusively, the direct involvement of the μ - $\eta^2:\eta^2$ -peroxo-dicopper(II) intermediate in the aromatic ligand hydroxylation was demonstrated. It was also demonstrated that in the O–O bond cleavage and the C–O bond formation steps take place in a concerted manner.



Scheme 2.1. Reaction pathways for the aromatic ligand hydroxylation starting from $[\text{Cu(II)}_2(\mu\text{-}\eta^2:\eta^2\text{-peroxo})(\text{DAPA})]^{2+}$ complex.^[72]

In another DFT-based mechanistic study Blomberg and coworkers investigated the aromatic hydroxylation of an external phenolate by Stack and coworkers studied experimentally (cf. Chapter 1, Scheme 1.22).^[73] The results confirmed an equilibrium between the bis(μ -oxo)dicopper(III) and μ - $\eta^2:\eta^2$ -peroxo-dicopper(II) isomers preceding the hydroxylation step (Scheme 2.2). Further, it was shown that after the addition of the phenolate substrate in the equilibrium mixture of the two $[\text{Cu}_2\text{O}_2]^{2+}$ isomers, the phenolate-bound bis(μ -oxo)dicopper(III) intermediate is more stable than its peroxo counterpart. Subsequently, the bis(μ -oxo)dicopper(III) moiety attacks the 2-position of the coordinated

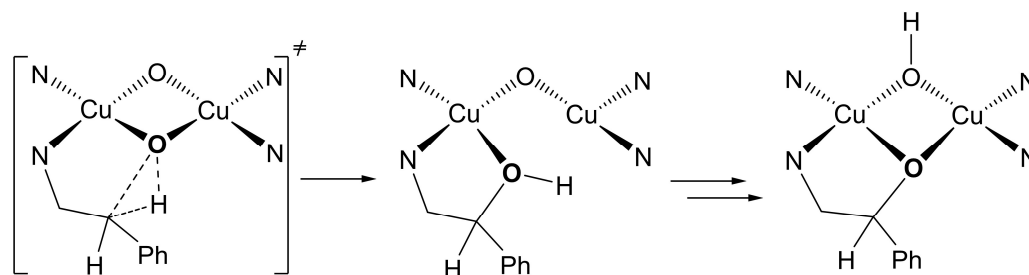
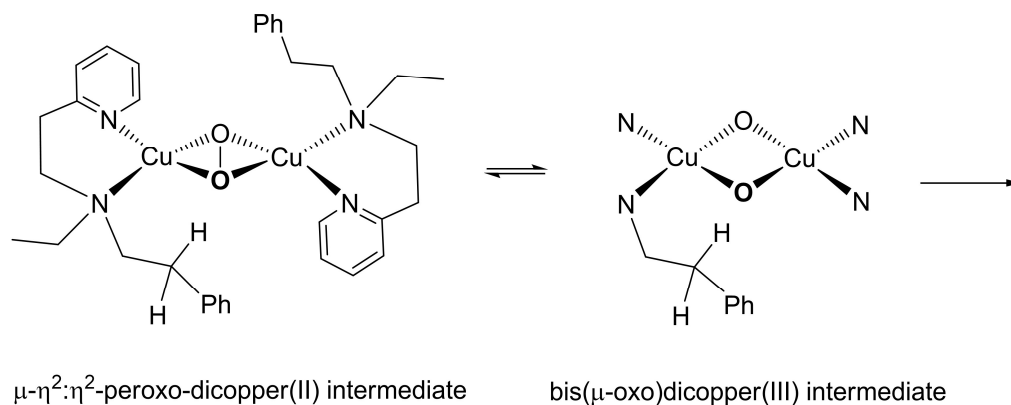
phenolate substrate which results in the formation of the C–O bond between one of the bridging oxygen atoms in the bis(μ -oxo)dicopper(III) moiety and the 2-position of the ring-carbon atom in the bound-phenolate substrate leading to a σ complex. Proton abstraction by the second bridging oxygen atom of the $[\text{Cu}_2\text{O}_2]^{2+}$ core then yields the final products. Hence, also this work demonstrates that a bis(μ -oxo)dicopper(III) intermediate is capable of mediating aromatic hydroxylation.



Scheme 2.2. Mechanistic scenario for the hydroxylation of an external phenolate substrate in the $[\text{Cu(III)}_2(\mu\text{-oxo})(\text{DBED})]^{2+}$ system.^[73]

In Chapter 1, Scheme 1.25b, the aliphatic hydroxylation investigated by Itoh and coworkers has been introduced, and in a DFT study by Spuhler and Holthausen a reaction mechanism was established for the $[\text{Cu}_2\text{O}_2]^{2+}$ complex supported by the bidentate ligand system (Scheme 2.3).^[74] The evolving mechanistic scenario features a $\mu\text{-}\eta^2\text{:}\eta^2\text{-peroxo-}$

dicopper(II)/bis(μ -oxo)dicopper(III) core isomerization with subsequent rate limiting C–H bond cleavage, followed directly by an OH rebound step, which leads to the formation of the product alcohol without occurrence of an intermediate.



Scheme 2.3. Concerted non-synchronous hydroxylation pathway for the aliphatic hydroxylation in Itoh's system established by DFT-based calculations.^[74]

2.2. $\text{Cu}_2\text{P}^{\text{S}}/\text{Cu}_2\text{O}_2$ Interconversion: A Torture Track for DFT

The $\text{Cu}_2\text{P}^{\text{S}}$ and Cu_2O_2 core isomerization has already caught enormous attention in synthetic chemistry as these isomers are involved in aromatic^[51b, 55, 59-61, 72-73, 75] and aliphatic^[63-64, 65, 68a, 76] C–H bond hydroxylation reactions. However, the study of this interconversion has been extremely painstaking experimentally since it is sensitive to solvents,^[77] temperature,^[77a, 78] and counteranions^[58]. At the same time quantum chemical studies on this interconversion were found to be extraordinarily demanding, as the relative energies of Cu_2O_2 and $\text{Cu}_2\text{P}^{\text{S}}$ species vary drastically with the method applied^[79] and are sensitive to dispersion,^[80] solvent^[79] and relativistic^[81] effects. Specifically, it was also an

open question whether or not to apply the broken-symmetry approach (BS) for the peroxo-isomer with its coupled copper(II) ions.^[82] The BS concept is an extremely useful tool for the prediction of exchange coupling constants in molecules with interacting paramagnetic centers.^[83] Below, we represent some previous DFT works on the $\text{Cu}_2\text{P}^{\text{S}}/\text{Cu}_2\text{O}_2$ isomerizations, to illustrate the particularly problematic choice of DFT approaches for the sufficiently accurate assessment of Cu_2O_2 core isomerizations.

Cramer and coworkers employed a small computational model system ($\text{Cu}_2\text{P}^{\text{S}}$ and Cu_2O_2 cores containing ammonia as ligands) for their DFT-based benchmark study. As reference these authors chose highly correlated *ab initio* multireference configuration interaction (MRCI)^[84] and renormalized coupled cluster [CR-CC-(2,3)]^[85] methods. Their study concluded that the BS-DFT approach failed dramatically, but pure density functionals (e.g. BLYP) used within the restricted Kohn-Sham (KS)-DFT approach were found in good agreement with the reference calculations.^[82] However, the significance of this study was limited owing to the use of rather small molecular models and the neglect of dispersion as well as relativistic effects.

More recently Neese and Liakos investigated a slightly larger computational model system, a $[\text{Cu}_2\text{O}_2]^{2+}$ core supported by ethylene diamine ligands;^[81] for reference calculations, they employed *ab initio* single reference local pair natural orbital coupled cluster (LPNO-CCSD)^[86] theory. In this study, the B3LYP density functional including dispersion and relativistic effects within the restricted KS approach was identified as the most accurate method.

Siegbahn and coworkers chose $[\text{Cu}_2\text{O}_2]^{2+}$ complexes supported by iPr_3TACN ligands, for which it was known from experimental studies that the corresponding Cu_2O_2 and $\text{Cu}_2\text{P}^{\text{S}}$ species are in equilibrium (see Chapter 1, Scheme 1.19).^[80] The authors used the experimentally estimated energy difference of the two isomers to benchmark DFT methods. The modified B3LYP* density functional^[87] (with 15% Fock exchange) including dispersion and relativistic effects within the BS-DFT approach was found in good agreement with experiments.

In summary, these selected examples illustrate the inconclusive situation as to the proper choice of methods for DFT studies in this field of research. Although $\text{Cu}_2\text{P}^{\text{S}}/\text{Cu}_2\text{O}_2$ isomerizations have been studied several times over the years by numerous research

groups,^[79-82, 88] the following two key questions remain open: (1) Is the BS-DFT approach to be applied for a $\text{Cu}_2\text{P}^{\text{S}}/\text{Cu}_2\text{O}_2$ isomerization? (2) How well does a method benchmarked for a $\text{Cu}_2\text{P}^{\text{S}}/\text{Cu}_2\text{O}_2$ isomerization work for the subsequent C–H bond activation reaction? Therefore, in the next chapter, we will work on these issues.

Chapter 3

Results and Discussion

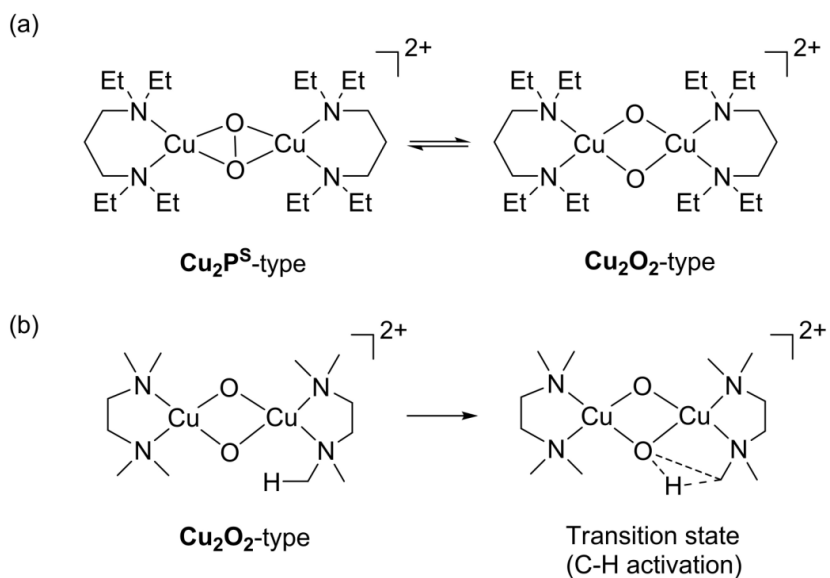
In the first section of this chapter, the results of a systematic DFT benchmark study are reported, which was carried out against available experimental references for a $\text{Cu}_2\text{P}^{\text{S}}/\text{Cu}_2\text{O}_2$ isomerization and a copper-dioxygen mediated C–H activation reaction. In the next sections the best benchmarked DFT method is applied in various aliphatic and aromatic hydroxylation reactions to unravel their reactivities.

3.1. DFT Benchmark

3.1.1. Experimental Reference Systems

As experimental references for the DFT-based benchmark study we chose two reactions from Stack's work. In the first reference reaction, a $\text{Cu}_2\text{P}^{\text{S}}/\text{Cu}_2\text{O}_2$ interconversion was experimentally studied based on $[\text{Cu}_2\text{O}_2]^{2+}$ complexes with TEPD ligands (TEPD = *N,N,N',N'*-tetraethylpropane-1,3-diamine) (Scheme 3.1a).^[58] In their study, a van't Hoff analysis yielded $\Delta H^\circ = -1.03(0.48)$ kcal/mol and $\Delta S^\circ = -5.73(0.48)$ cal/(mol K) for the isomerization in THF from which we derive the relative Gibbs free energy of the two isomers, $\Delta G_{188} = 0.05 \pm 0.14$ kcal/mol as the reference value. Furthermore, the extended X-ray absorption fine structure (EXAFS) analyses highlighted interactions of the individual copper cores with triflate counterions present in solution.

As a second reference reaction, the aliphatic C–H bond activation in a Cu_2O_2 isomer supported by TMED ligands (TMED = *N,N,N',N'*-tetramethylethylenediamine)^[76b] was investigated (Scheme 3.1b). The activation enthalpy $\Delta H^\ddagger = 15(1)$ kcal/mol and entropy $\Delta S^\ddagger = -15(2)$ cal/(mol K) of the aliphatic C–H bond cleavage was derived from an Eyring analysis in acetone from which we derive the Gibbs free energy of the activation barrier for the C–H bond activation, $\Delta G^\ddagger = 18.9(\pm 1.5)$ kcal/mol, at 263K as the reference value. Similar to the first reference reactions, the presence of triflate counteranions was considered here as well.



Scheme 3.1. (a) $\text{Cu}_2\text{P}^{\text{S}}/\text{Cu}_2\text{O}_2\text{-type}$ isomerization, (b) C–H bond activation via the $\text{Cu}_2\text{O}_2\text{-type}$ isomer.

3.1.2. Computational Details

Structures of the species involved in the experimental reference reactions were optimized at the density-functional level of theory (DFT) using the B3LYP-D2^[89] hybrid functional in conjunction with the LANL2DZ ECP/basis-set combination, i.e., the non-relativistic 10-electron effective core potential (ECP) and the corresponding basis set according to Hay and Wadt^[90] was used for Cu in combination with Dunning's non-polarized D95V basis set^[91] for all other atoms. A larger basis set was used for single point calculations to evaluate the influence of several other key factors (relativistic effects, dispersion, broken-symmetry wave functions). Geometry optimizations were performed employing restricted Kohn-Sham theory and, wherever required, open-shell singlet or triplet wave functions using the Gaussian09 program.^[92] Open-shell singlet/broken-symmetry (BS) optimizations were performed using "guess=mix" keyword as implemented in Gaussian09. Here, the closed-shell optimization is abbreviated as OPT^{CS} , whereas open-shell singlet and triplet as OPT^{BS} and OPT^{T} , respectively. Subsequently, benchmark calculations were performed on the optimized geometries by carrying out single point closed-shell or unrestricted open-shell singlet calculations employing a series of density-functionals together with various scalar relativistic approaches and basis sets with the program ORCA2.9.^[93] The series of dispersion (D3^[94]) corrected density functionals include pure GGA (BLYP,^[89a, 89b, 95] PBE,^[96] and revPBE^[97]),

meta GGA (TPSS,^[98]), hybrid GGA (B3LYP,^[89a-d] PBE0,^[99] revPBE0^[100]) and meta-hybrid GGA functionals (TPSSh,^[101] TPSS0,^[102]). Scalar relativistic effects were treated via three different approaches, i.e., employing either quasi-relativistic effective core potentials (ECPs),^[103] the zeroth-order regular approximation (ZORA) correction,^[104] or the second-order Douglas-Kroll-Hess (DKH) transformation.^[105] ECP-based closed-shell single points are abbreviated as SP1^{CS}, whereas ZORA- and DKH-based as SP2^{CS} and SP3^{CS}, respectively. Spin-projected singlet energies (E_{BS}) were obtained from BS-calculations employing the Yamaguchi formalism^[106] as implemented in ORCA2.9. ECP-based broken symmetry single points are abbreviated as SP1^{BS}, whereas ZORA- and DKH-based as SP2^{BS} and SP3^{BS}, respectively.

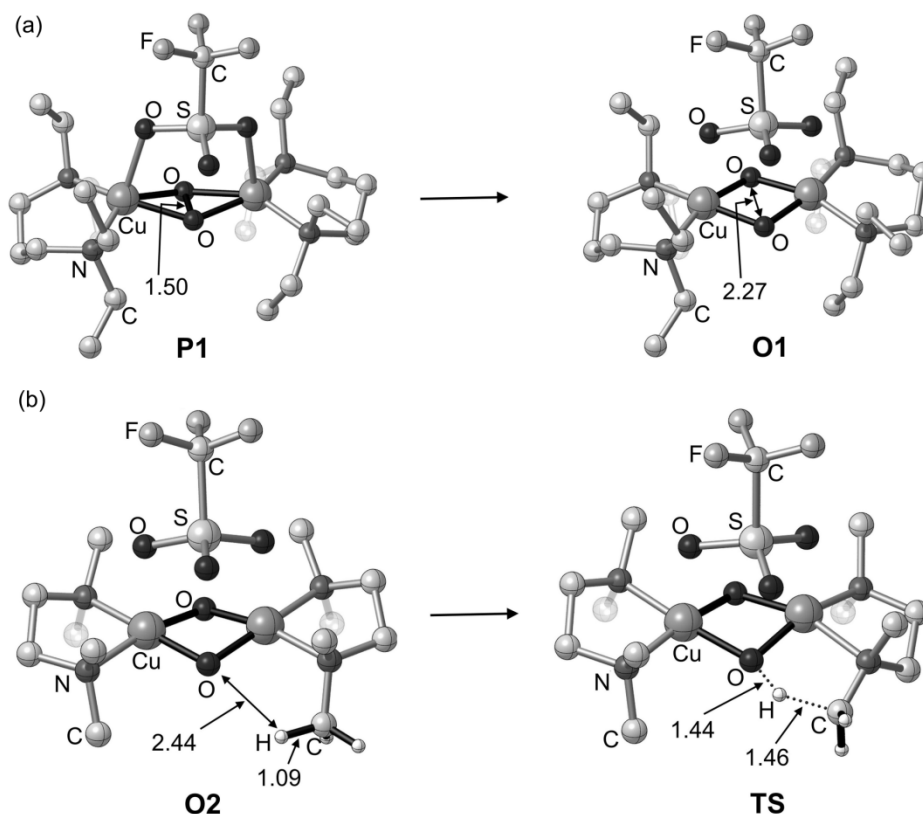
In ECP-based calculations, the def2-TZVP(SDD) basis set was used, which contains the def2-TZVP^[107] basis sets for C, H, N, O, F and S atoms, and the quasi-relativistic SDD-type^[103] ECP and the corresponding triple- ζ basis set^[103] for Cu. For ZORA- and DKH-based calculations, the corresponding segmented all-electron relativistically contracted (SARC) basis sets were used as implemented in the ORCA2.9 program.^[108] These basis sets are of TZVP quality with a segmented contraction. In order to accelerate calculations, the resolution-of-identity (RI)^[109] approximation for the pure functionals, and RI plus chain-of-spheres^[110] (RIJCOSX) approximation for the hybrid functionals were used employing the auxiliary def2-TZVP/J basis set.^[111]

To obtain Gibbs free energies, single point energies were corrected by unscaled zero point vibrational energies as well as thermal and entropic contributions obtained from Hessians computed at optimized gas-phase structures (see above). The "freqchk" utility implemented in Gaussian09 was used for this purpose. In the single point energy calculations, solvent effects were introduced using the conductor-like screening solvent model (COSMO^[112]), and dispersion corrections using either D2^[89e] or D3^[94] approach, as implemented in the ORCA2.9 program. Molecular pictures were drawn by means of the visualization software CYLview.^[113]

3.1.3. DFT Model Systems

The molecular models used for the benchmark studies are shown in Scheme 3.2. **P1** and **O1** correspond to $\text{Cu}_2\text{P}^{\text{S}}$ and Cu_2O_2 isomers, respectively, and a coordinating triflate

counteranion is explicitly considered. For the second reference reaction, **O2** and **TS** correspond to a Cu_2O_2 isomer and the transition state structure of the C–H activation.



Scheme 3.2. DFT-computed structures for (a) the **P1/O1** isomerization, (b) the C–H bond activation reaction. The triflate counteranion is coordinated at the Cu_2O_2 core in all the complexes. Selected interatomic distances given in Å.

3.1.4. Results and Discussion

The results of the benchmark study are shown in Figure 3.1, and Tables 3.1 and 3.2. If used in combination with the ECP, pure- and meta-GGA density functionals mostly perform better than their corresponding hybrid and meta-hybrid counterparts, respectively. For the isomer stabilities, however, inclusion of Fock-exchange in the hybrid functionals leads to a general stabilization of the **P1** isomer by about 1-8 kcal/mol. This is compensated by an opposite effect when using the ZORA or DKH approach instead of an ECP so that better agreement with experiment (Figure 3.1a and Table 3.1). The good agreement with experiment of hybrid methods combined with the ZORA or DKH approach does not carry over, however, to the computed activation barrier height (Figure 3.1b and Table 3.2). Clearly, the good

performance of the BLYP-D3/def2-TZVP(SDD)+COSMO approach stands out and gives the best agreement with the experimental data among all methods tested here for both model reactions.

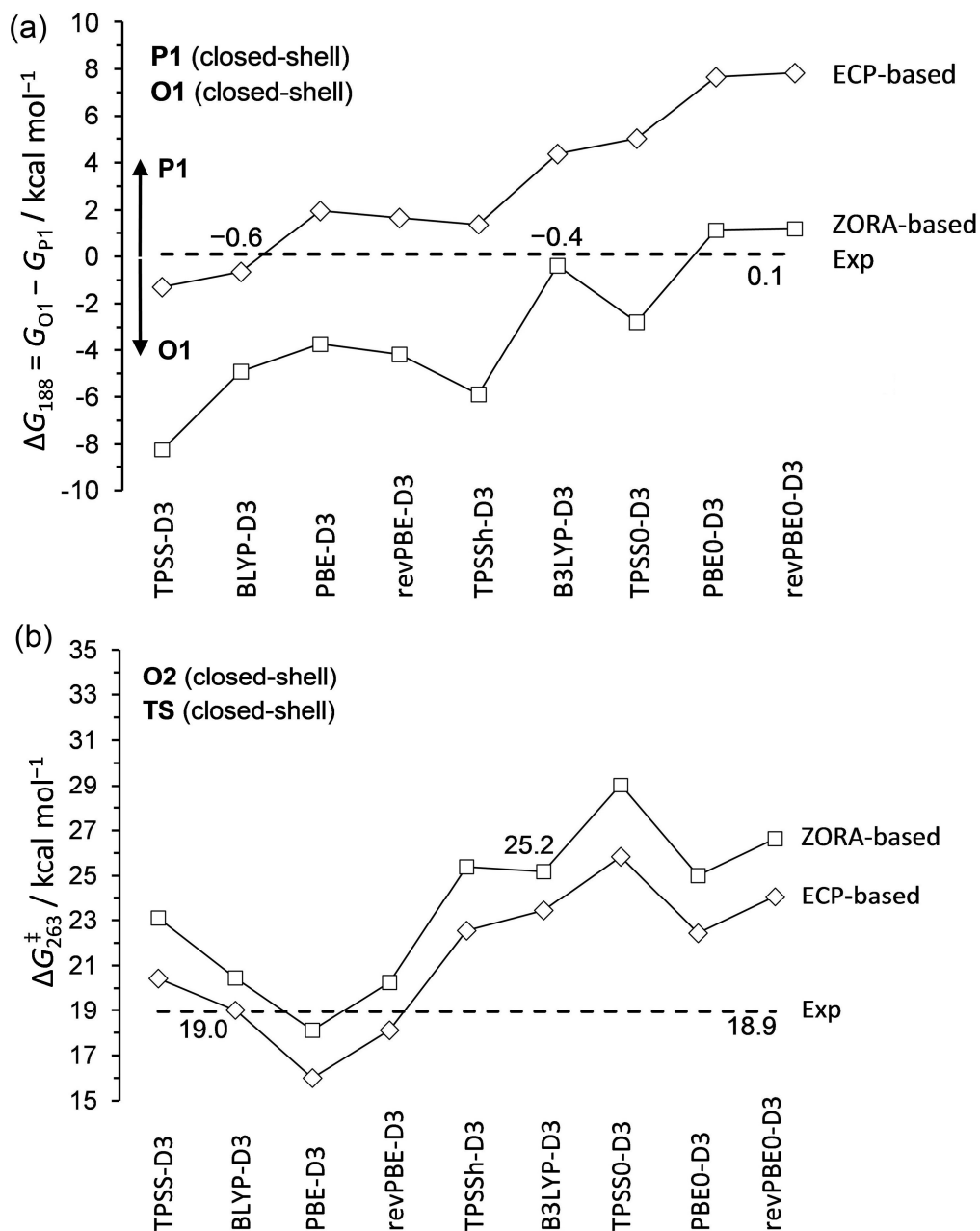


Figure 3.1. The experimental Gibbs free energies of (a) the **P1/O1** isomerization (ΔG in kcal/mol) and (b) the C–H bond activation reaction (ΔG^\ddagger in kcal/mol), are indicated by dashed lines and the DFT-based Gibbs free energies are shown as "ECP-based" and "ZORA-based" graphs. All computed data refers to closed-shell wave functions (cf. computational details).

Table 3.1. Relative Gibbs free energies (ΔG_{188} , in kcal/mol) computed for the **P1/O1** isomerization shown in Scheme 3.2a. The experimental reference is at 0.1 kcal/mol.^[58]

Functional ^[a]	ΔG_{188}		
	ECP ^[b]	ZORA ^[c]	DKH ^[d]
TPSS-D3 (0)	-1.3	-8.3	-8.0
BLYP-D3 (0)	-0.6	-4.9	-4.7
PBE-D3 (0)	2.0	-3.7	-3.5
revPBE-D3 (0)	1.7	-4.2	-4.0
TPSSh-D3 (10)	1.4	-5.9	-5.6
B3LYP-D3 (20)	4.4	-0.4	-0.1
TPSS0-D3 (25)	5.0	-2.8	-2.5
PBE0-D3 (25)	7.7	1.1	1.4
revPBE0-D3 (25)	7.8	1.2	1.4

[a] Amount of Fock-exchange (%) included in the functionals shown in parentheses.

[b] SP1^{CS}//OPT^{CS}, [c] SP2^{CS}//OPT^{CS}, [d] SP3^{CS}//OPT^{CS}, See computational details for abbreviations.

Table 3.2. Activation barriers (ΔG^\ddagger , in kcal/mol) computed for the C-H bond activation shown in Scheme 3.2b. The experimental reference is at 18.9 kcal/mol.^[76b]

Functional ^[a]	ΔG^\ddagger		
	ECP ^[b]	ZORA ^[c]	DKH ^[d]
TPSS-D3 (0)	20.4	23.1	23.0
BLYP-D3 (0)	19.0	20.5	20.4
PBE-D3 (0)	16.0	18.1	18.0
revPBE-D3 (0)	18.1	20.3	20.2
TPSSh-D3 (10)	22.5	25.4	25.3
B3LYP-D3 (20)	23.4	25.2	25.1
TPSS0-D3 (25)	25.8	29.0	28.9
PBE0-D3 (25)	22.4	25.0	24.9
revPBE0-D3 (25)	24.1	26.6	26.6

[a] Amount of Fock-exchange (%) included in the functionals shown in parentheses.

[b] SP1^{CS}//OPT^{CS}, [c] SP2^{CS}//OPT^{CS}, [d] SP3^{CS}//OPT^{CS}, See computational details for abbreviations.

The data compiled in Table 3.3 shows a significant influence of dispersion corrections on the isomer stabilities whereas only minor effects are seen for the computed barrier heights. The two dispersion corrected approaches, DFT-D2(BLYP-D2) and DFT-D3(BLYP-D3), give rather similar results (Table 3.3). Following Grimme's recommendations^[94], we thus prefer the latter in further calculations. In line with expectation we conclude that the addition of dispersion corrections favor **O1** over **P1** and **O2** over **TS**.

Table 3.3. Computed relative Gibbs free energies (with and without the inclusion of dispersion corrections) for the **P1/O1** isomerization (ΔG , in kcal/mol) and the C–H bond activation reaction (ΔG^\ddagger , in kcal/mol) shown in Scheme 3.2.

Functional ^[a]	$\Delta G^{[a]}$	$\Delta G^\ddagger^{[a]}$
BLYP	6.2	17.1
BLYP-D2	-1.8	18.7
BLYP-D3	-0.6	19.0

[a] <Functional>/def2-TZVP(SDD)+COSMO//B3LYP-D2/LANL2DZ

In the DFT work up to this point, we have treated the **P1** isomer applying closed-shell singlet wave functions. We investigated whether use of broken symmetry wave functions provides an improved description of the **P1** isomer. For this species, the closed- and open-shell singlet (BS) and triplet geometries are obtained using the DFT methods B3LYP-D2/LANL2DZ, (BS)UB3LYP-D2/LANL2DZ and UB3LYP-D2/LANL2DZ, respectively. On top of these geometries the ECP-, ZORA- and DKH-based broken symmetry single point calculations (U-BS) were carried employing the same set of density functionals (pure-GGAs, meta-GGAs, hybrids and meta-hybrids) and basis sets as used before. The **O1** isomer was still treated using closed-shell singlet wave functions. The ZORA-based results are shown in Figure 3.2 and Table 3.4. The ECP- and DKH-based results are documented in Table 3.5. Unrestricted calculations with the pure- and meta-GGAs density functionals do not converge to open-shell singlet (broken symmetry) solutions for **P1** even using properly constructed initial guess wave function with broken spin- and space symmetry but collapse to closed-shell singlet solutions. This tendency of pure- and meta-GGAs has already been documented in the literature.^[82] Proper BS wave functions were obtained only with hybrid and meta-hybrid density functionals.

In the ZORA-based BS single point calculations (Figure 3.2, Table 3.4), only the UTPSSh-D3 density functional performed well employing the open-shell singlet geometry of **P1** as shown in the plot "B" of Figure 3.2. Furthermore, the DKH-based results are very similar to ZORA-based results (Tables 3.4 and 3.5), but the ECP-based approach significantly overestimates the Gibbs free energy of the **P1/O1** isomerization (Table 3.5). Further analysis of Figure 3.2 illustrates that the stability of **P1** relative to **O1** increases significantly with the amount of Fock-exchange included in the density functionals (see, e.g.,

the results of the TPSSh-D3 and TPSS0-D3 functionals in Figure 3.2). A similar yet less pronounced trend was also seen in the Figure 3.1a.

For the C–H bond activation reaction, a broken-symmetry solution was not found for **TS** using the (BS)UTPSSh density functional, probably because the core of **TS** resembles an **O**-type isomer, for which as well only closed-shell solutions were obtained. Therefore, both **O2** and **TS** are closed-shell species and only pure- and meta-GGAs density functionals perform well; the TPSSh density functional overestimates the barrier height (Figure 3.1b). So, if considering both benchmark reactions, (BS)UTPSSh/SARC+ZORA+COSMO//OPT^{BS} is not the best choice.

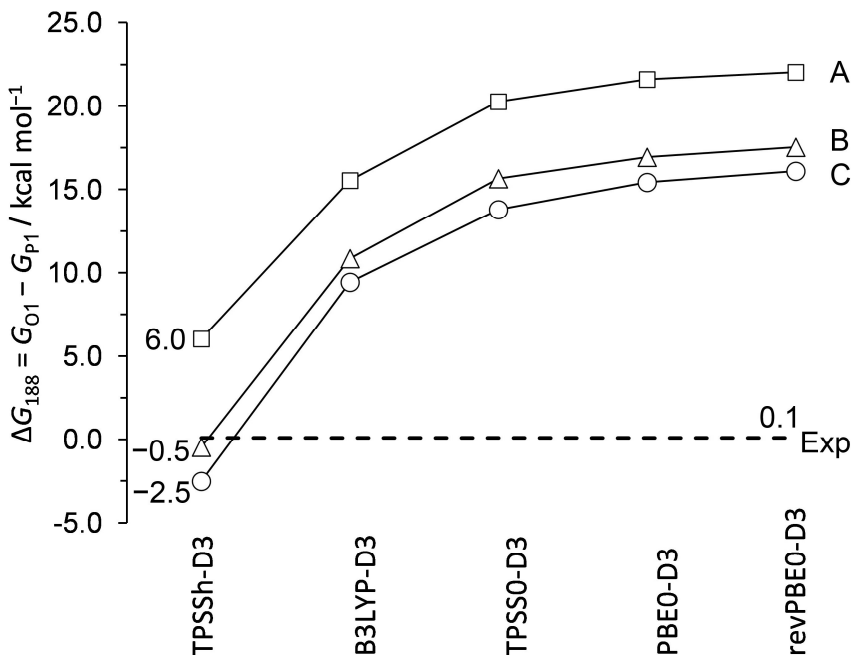


Figure 3.2. For the **P1/O1** isomerization, the experimental Gibbs free energy (ΔG , in kcal/mol) is shown by a dashed line, and the DFT-based Gibbs free energies (ΔG , in kcal/mol) are shown by the plots "A", "B" and "C". In all three plots **O1** was computed with SP2^{CS}//OPT^{CS}, but **P1** was computed in A with SP2^{BS}//OPT^{CS}, in B with SP2^{BS}//OPT^{BS} and in C with SP2^{BS}//OPT^T.

In summary we identified three suitable protocols for the **P1/O1** isomerization: SP1^{CS}(BLYP-D3)//OPT^{CS}, SP2^{CS}(B3LYP-D3)//OPT^{CS}, and SP2^{BS}(TPSSh)//OPT^{BS}. Instead, for the C–H bond activation only two protocols behaved well: SP1^{CS}(BLYP-D3)//OPT^{CS}, and SP2^{CS}(PBE-D3)//OPT^{CS}. Considering both the benchmarks, SP1^{CS}(BLYP-D3)//OPT^{CS} is best. Here, the optimization method "OPT^{CS}" includes B3LYP-D2 with a double- ζ basis set,

which was further improved to triple- ζ def2-TZVP(SDD) basis set by making use of auxiliary basis sets with BLYP-D2. On top of these structures, single point calculations were performed with BLYP-D3/def2-TZVP(SDD)+COSMO. Using this protocol, the relative Gibbs free energy for the **P1/O1** isomerization is -3.1 , and the barrier for the C–H bond activation is 19.0 kcal/mol. The results were found in good agreement with the experimental references.

Table 3.4. Computed Gibbs free energies (ΔG) for the **P1/O1** isomerization employing open-shell singlet (U-BS) wave-functions with various DFT methods using ZORA relativistic scheme. The reference is at 0.1 kcal/mol from the experimental studies.^[58]

Functional ^[a]	A ^[b]	$\Delta G_{188, \langle S^2 \rangle}$ B ^[c]	C ^[d]
TPSSh-D3 (10)	6.0, <0.7>	-0.5, <0.8>	-2.5, <0.9>
B3LYP-D3 (20)	15.5, <0.8>	10.8, <0.9>	9.4, <0.9>
TPSS0-D3 (25)	20.3, <0.9>	15.7, <0.9>	13.8, <1.0>
PBE0-D3 (25)	21.6, <0.8>	16.9, <0.9>	15.4, <1.0>
revPBE0-D3 (25)	22.0, <0.8>	17.5, <0.9>	16.1, <1.0>

[a] Amount of Fock-exchange (%) included in the functionals given in parentheses.

[b] **P1**: SP2^{BS}//OPT^{CS}, [c] **P1**: SP2^{BS}//OPT^{BS}, [d] **P1**: SP2^{BS}//OPT^T. In all three plots **O1** was computed with SP2^{CS}//OPT^{CS}. See computational details for abbreviations.

Table 3.5. Computed Gibbs free energies (ΔG , in kcal/mol) for the **P1/O1** isomerization employing broken symmetry wave-functions with various DFT methods using DKH or ECP schemes. The reference is at 0.1 kcal/mol from the experimental studies.^[58]

Functional ^[a]	DKH ^[b]	$\Delta G_{188, \langle S^2 \rangle}$	ECP ^[c]
TPSSh-D3 (10)	6.3, <0.7>		13.5, <0.7>
B3LYP-D3 (20)	15.8, <0.8>		21.6, <0.8>
TPSS0-D3 (25)	20.5, <0.9>		28.4, <0.9>
PBE0-D3 (25)	21.9, <0.8>		29.2, <0.9>
revPBE0-D3 (25)	22.3, <0.8>		28.8, <0.9>

[a] Amount of Fock-exchange (%) included in the functionals given in parentheses.

[b] **P1**: SP3^{BS}//OPT^{CS}, **O1**: SP3^{CS}//OPT^{CS}, [c] **P1**: SP1^{BS}//OPT^{CS}, **O1**: SP1^{CS}//OPT^{CS}. See computational details for abbreviations.

We considered the triflate counteranion in our model complexes. In order to extract the influence of the triflate counteranion on the Gibbs free energy of the **P1/O1** isomerization (ΔG_{188}) and the C–H bond activation reaction (ΔG^\ddagger), both reference reactions were studied

also in the absence of the triflate counteranion. The adopted DFT protocol computes ΔG_{188} and ΔG^\ddagger as -9.3 and 18.4 kcal/mol, respectively. This shows that ΔG_{188} is lowered noticeably from -3.1 kcal/mol (in the presence of triflate) to -9.3 kcal/mol (in the absence of triflate) indicating a significant stabilization of **P1** relative to **O1** due to the coordination of triflate counteranion at the axial positions of both the copper centers, whereas ΔG^\ddagger is influenced only slightly, i.e., 19.0 kcal/mol in the presence of triflate and 18.4 kcal/mol without. Similar conclusions were also reached in the experimental work of Stack and coworkers.^[58, 76f]

3.1.5. Conclusions

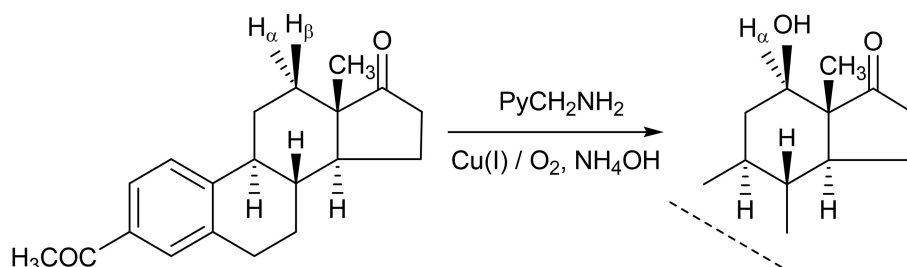
BLYP-D3/def2-TZVP(SDD)+COSMO//BLYP-D2/def2-TZVP(SDD) has been established as the best protocol from the DFT benchmark for both the reference reactions. In the benchmark study, we have found that the hybrid and meta-hybrid functionals tend to overestimate the relative stability of the **Cu₂P^S** core as well as the barrier height for the C–H bond activation. The extent of deviations depends upon the amount of Fock-exchange included within hybrid and meta-hybrid functionals. Dispersion corrections have been found important for the **Cu₂P^S/Cu₂O₂** isomerization but not for the C–H bond activation, regardless of the particular approach applied (D2 or D3). Dispersion corrections favor the **Cu₂O₂** isomer significantly over the **Cu₂P^S** isomer, however only slightly stabilize the **Cu₂O₂** isomer relative to the transition state.

Relativistic effects have been included via ECP-, ZORA- and DKH-based calculations. ZORA and DKH account for relativistic effects in a similar manner. Relativistic effects favor the **Cu₂O₂** isomer over its corresponding **Cu₂P^S** isomer and the C–H bond activation transition state. Coordination of the triflate counteranion has been found quite important in the **Cu₂P^S/Cu₂O₂** isomerization as its presence stabilizes the **Cu₂P^S** isomer substantially. For the computed barrier height of the C–H bond activation, however, no significant influence was seen.

3.2. Reaction 1: An Aliphatic C–H Hydroxylation

3.2.1. Motivation

In Chapter 1, Scheme 1.26, the regio- and stereoselective aliphatic hydroxylation investigated by Schönecker and coworkers was discussed. Here, the benchmarked DFT method will be applied to figure out the underlying reason for the high selectivity of the C–H hydroxylation (redrawn in Scheme 3.3).



Scheme 3.3. Regio- and stereoselective aliphatic hydroxylation.^[68]

3.2.2. Computational Details

Intermediates and transition states involved in the mechanistic study were optimized employing closed-shell singlet wave functions at the BLYP-D2/^[89a, 89b, 89e, 95]def2-TZVP(SDD) level using the Gaussian09^[92] program. The RI approximation was employed for improved numerical efficiency and the density fitting basis set corresponding to the def2-TZVP(SDD) basis set was generated automatically using the auto keyword as implemented in the Gaussian09 program.^[114] Default grid and convergence criteria were used throughout.

Subsequently, single point calculations were performed at the BLYP-D3^[89a, 89b, 94-95]/def2-TZVP(SDD) level including solvent (acetone) effects using the ORCA2.9 program.^[93] The solvent effects were introduced using the conductor-like screening solvent model (COSMO^[112]), as implemented in the ORCA program. In order to accelerate the calculations, the resolution-of-identity (RI)^[109] approximation was used employing the auxiliary def2-TZVP/J basis set.^[111]

To the energies obtained in single point calculations, thermal corrections were added to obtain Gibbs free energies. These thermal corrections have been obtained at 298.15 K from

gas-phase frequency calculations computed at the BLYP-D2/def2-TZVP(SDD)/auto level. Molecular pictures were drawn by means of the visualization software CYLview.^[113]

3.2.3. Choice of the Computational Molecular Model

We investigated this regio- and stereoselective hydroxylation reaction on the basis of the mechanistic scenario established previously for Itoh's regioselective aliphatic hydroxylation system.^[74] As in the reactive intermediate of Itoh's system, one of the two chelating ligands plays a spectator role so that the maximum efficiency of the reaction corresponds to 50% ligand hydroxylation. A similar observation was reported for Schönecker's system. Our model system consists of a $[\text{Cu}_2\text{O}_2]^{2+}$ core and two chelating ligands in equatorial positions. Two chelating N-donor model ligands (\mathbf{L}_1^1 and \mathbf{L}_2^2) were constructed from the actual ligand \mathbf{L}_2 (Figure 3.3). \mathbf{L}_1^1 represents the 'active' ligand subject to hydroxylation, whereas \mathbf{L}_2^2 plays a spectator role only. The active ligand consists of the steroid rings C and D only, because rings A and B are too remote from the $[\text{Cu}_2\text{O}_2]^{2+}$ active site to play any role in the course of the reaction observed. Similar to our benchmark reactions triflate counteranions have been used in Schönecker's experiment. Therefore, in our model system as well, a triflate counteranion was explicitly considered in the calculations. Model system **1** for the $\text{Cu}_2\text{P}^{\text{S}}$ -type species (Figure 3.4) serves as the starting point of our mechanistic investigation.

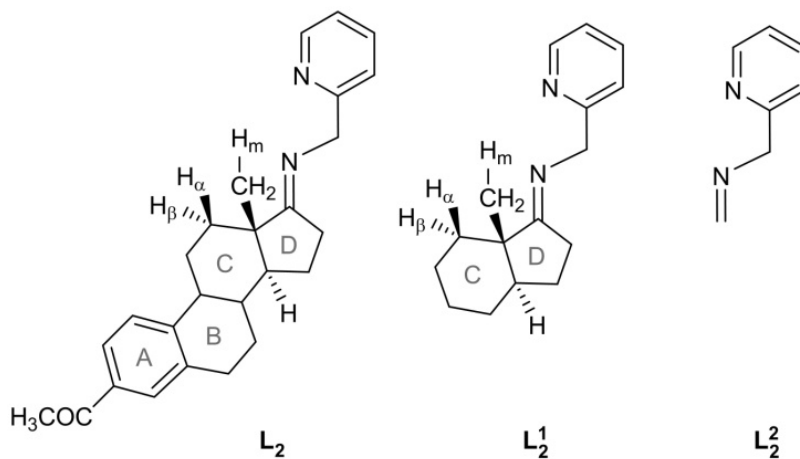


Figure 3.3. Actual ligand, \mathbf{L}_2 employed in the experiment, and model ligands used in our computational study.

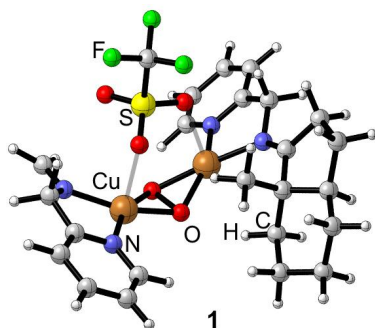
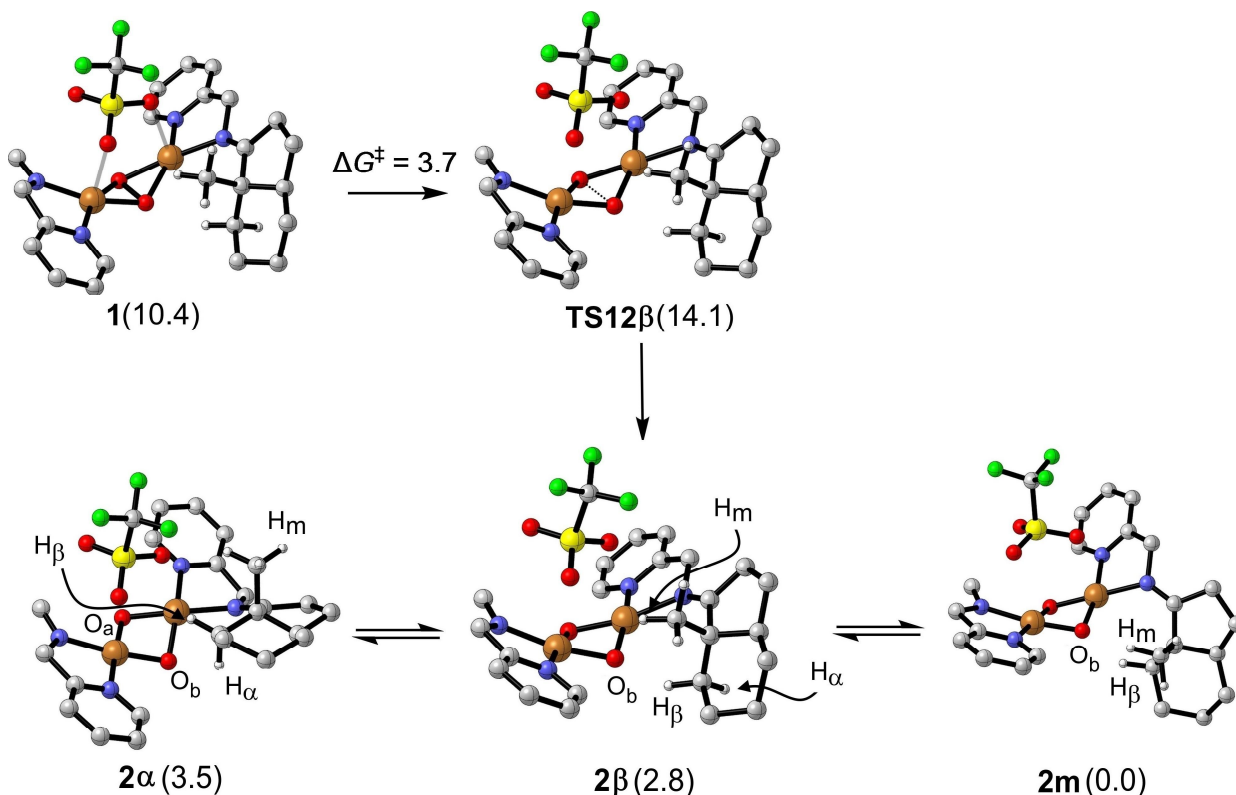


Figure 3.4. Model system **1** for the $\text{Cu}_2\text{P}^{\text{S}}$ species supported by the ligands L_2^1 and L_2^2 in the equatorial positions and coordinated by a triflate counteranion in the axial position.

3.2.4. Mechanistic Study

Commencing our discussion with the peroxo complex $[\text{Cu}_2(\text{II})\text{L}_2^1\text{L}_2^2(\mu\text{-}\eta^2\text{:}\eta^2\text{-O}_2)]^{2+}[\text{CF}_3\text{SO}_3]^-$ (**1**), the first elementary step along the reaction coordinate is the isomerization to form the bis(μ -oxo) isomer **2 β** (Scheme 3.4), which is 7.6 kcal/mol more stable than **1**. Both isomers are connected via **TS12 β** with a very small isomerization barrier of $\Delta G^\ddagger = 3.7$ kcal/mol.



Scheme 3.4. **1** and **2 β** intermediates with the interconnecting transition state **TS12 β** . The Gibbs free energies are relative to **2m**. The relative Gibbs free energies (ΔG_{298} in kcal/mol, 1 atm, CH_2Cl_2) are given in parentheses.

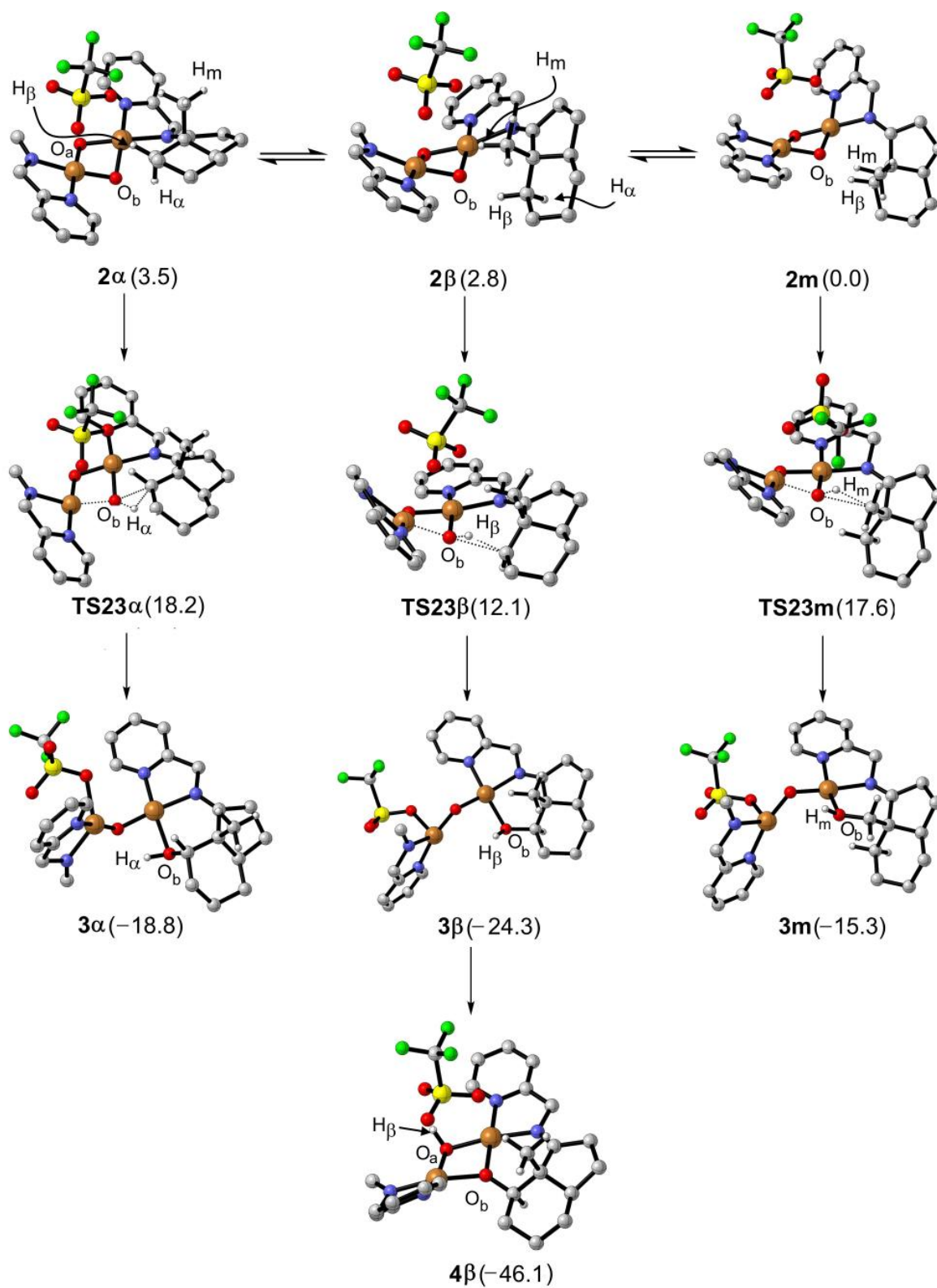
Two more conformations **2m** and **2a** next to **2β** were located (Scheme 3.4). The Gibbs free energies of **2β** and **2a** relative to **2m** are 2.8 and 3.5 kcal/mol, respectively. These conformations differ slightly in their orientation of the bicyclic rings (C and D in Figure 3.3) towards the Cu₂O₂ plane. In **2a**, **2β** and **2m**, the bicyclic rings are above, in, and below the Cu₂O₂ plane and the aliphatic C–H_α, C–H_β and C–H_m bonds activated in the subsequent step are in close proximity to the [Cu₂O₂]²⁺ cores, respectively. As shown in Scheme 3.4, these are the potential C–H bonds for activation in the respective [Cu₂O₂]²⁺ cores.

Cleavage of the C–H_m bond in **2m** via **TS23m** is associated with a barrier of 17.6 kcal/mol (Scheme 3.5). In a similar fashion the transition states **TS23β** and **TS23a** for the activation of the C–H_β and C–H_α bonds give rise to activation barriers of 12.1 and 18.2 kcal/mol in **2β** and **2a**, respectively. Formation of the corresponding hydroxylated product **3a/3β/3m** is strongly exergonic and the high reverse barriers render these steps irreversible.

Assuming that all three individual reactions follow the Curtin-Hammett principle^[115] (the rapidly interconverting intermediates **2a**, **2β** and **2m** form the products **3a**, **3β** and **3m** in irreversible steps), and excluding facile interconversion of the latter. The ratios of **3a/3β/3m** formed in the solution depend only on the relative Gibbs free energies of the transition states **TS23a/TS23β/TS23m**. The difference of the free energies ($\Delta\Delta G^\ddagger$) of **TS23a** and **TS23β** is 6.1 kcal/mol and of **TS23m** and **T23β** is 5.5 kcal/mol. Therefore, the ratios are:

$$\frac{c(\mathbf{3a})}{c(\mathbf{3β})} = e^{-\frac{\Delta\Delta G^\ddagger}{RT}} = 2.7 \times 10^{-5}, \quad \frac{c(\mathbf{3m})}{c(\mathbf{3β})} = 8.9 \times 10^{-5}$$

Hence, **3β** will be the dominant product formed. **3β** undergoes hydrogen atom transfer between the hydroxy group in **3β** and the residing bridging oxygen atom to generate a (μ -hydroxo)copper unit, which in the subsequent step rotates to yield the highly exergonic hydroxylated final product the μ -alkoxo(μ -hydroxo)copper complex **4β**. The barriers connecting **3β** to **4β** were not calculated in this work, however, such a reaction was found highly spontaneous in a similar study.^[74] These results are in excellent agreement with the experiments in terms of regio- and stereoselectivity of the C–H_β bond hydroxylation.



Scheme 3.5. Competitive C–H hydroxylation reactions via 2α , 2β and $2m$. Gibbs free energies relative to $2m$ in kcal/mol are shown in parentheses. Selected interatomic distances (Å) in 2α : $O_b\cdots H_\alpha = 2.4$, $O_b\cdots H_\beta = 2.6$; 2β : $O_b\cdots H_\beta = 1.9$, $O_b\cdots H_m = 2.3$; $2m$: $O_b\cdots H_\beta = 2.3$, $O_b\cdots H_m = 2.2$.

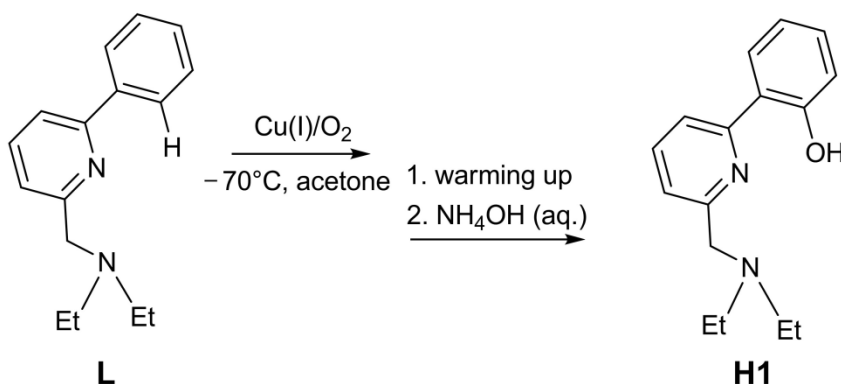
3.2.5. Conclusions

The benchmarked DFT method has been applied to assess the reaction paths underlying the regio- and stereoselectivity of the C–H hydroxylation in the Schöneck reaction. Three bis(μ -oxo) isomers close in energy (**2m**, **2 β** and **2 α**) were located that are more stable than the peroxo species. In each of these isomers, another aliphatic C–H bond is located in close proximity to the $[\text{Cu}_2\text{O}_2]^{2+}$ core. The barrier heights for the subsequent corresponding C–H $_{\beta}$, C–H $_{\text{m}}$ and C–H $_{\alpha}$ bonds activation steps are 12.1, 17.6 and 18.2 kcal/mol, respectively. Therefore, the barrier height for the C–H $_{\beta}$ bond activation is lowest, in line with the exclusive hydroxylation of this position observed in the experiment. The subsequent intermediates connecting to these transition states are highly exergonic and irreversible. Hence, the peroxo species **1 β** spontaneously converts to the bis(μ -oxo) isomer **2 β** , which subsequently involves in the regio- and stereoselective C–H $_{\beta}$ hydroxylation via a low barrier **TS23 β** to eventually yield the highly exergonic hydroxylated product.

3.3. Reaction 2: An Aromatic C–H Hydroxylation

3.3.1. Motivation

Employing the benchmarked DFT method, the aromatic regioselective C–H hydroxylation in the ligand 2-(diethylaminomethyl)-6-phenylpyridine (**L**) reported by Tolman and coworkers (Chapter 1, Scheme 1.21) was studied.^[59] This reaction is redrawn in Scheme 3.6.



Scheme 3.6. Aromatic ligand hydroxylation by reacting a Cu(I) complex with the ligand 2-(diethylaminomethyl)-6-phenylpyridine in the presence of O_2 at -70°C in acetone.

In order to observe the *para*-substituent effects on the hydroxylation process, the authors synthesized the OMe and NO₂ derivatives of the ligand **L** (**L-OMe** and **L-NO₂** in Figure 3.5). These ligands were further reacted with [Cu(NCCH₃)₄][SbF₆] in the presence of O₂ in acetone at -70°C. In case of **L-OMe**, a high yield from the rapid decay of the its corresponding bis(μ-oxo)dicopper intermediate was observed. For the system supported by the **L-NO₂** ligand, however, the yield of hydroxylated product was found to be negligible.

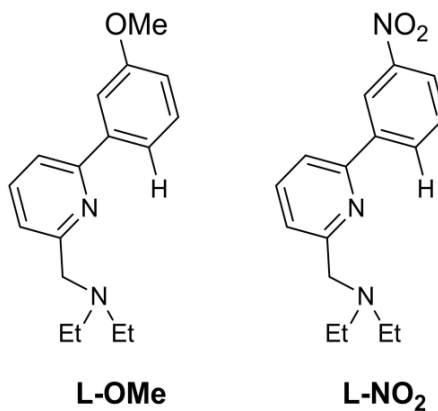
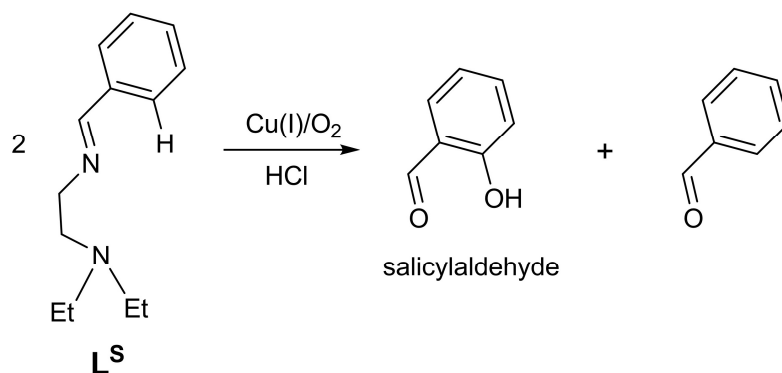


Figure 3.5. Ligands **L-OMe** and **L-NO₂**.

Very recently, Schindler and coworkers revisited the Tolman's aromatic hydroxylation for new synthetic applications.^[116] In place of the ligand **L**, this group used a ligand **L^s** to prepare a simple copper imine complex which afforded the selective *o*-hydroxylation of aromatic aldehyde by using O₂ as the oxidant to yield salicylaldehyde (Scheme 3.7).



Scheme 3.7. Oxidation of CuL^s complex with O₂.

3.3.2. Model System

The computational method used in this study was same as in the previous section 3.2. A slightly simplified model ligand **L1** was employed in our computational study by replacing ethyl by methyl groups (Figure 3.6). Further, employing these model ligands **L1**, a model **1** for the $\text{Cu}_2\text{P}^{\text{S}}$ -type isomer was built (Figure 3.7). Akin to earlier mechanistic studies on aromatic hydroxylation reactions,^[72-73] we assume initial formation of the $\mu\text{-}\eta^2\text{:}\eta^2\text{-peroxo}$ -dicopper(II) complex and we chose **1** as starting point for the exploration of reaction pathways.

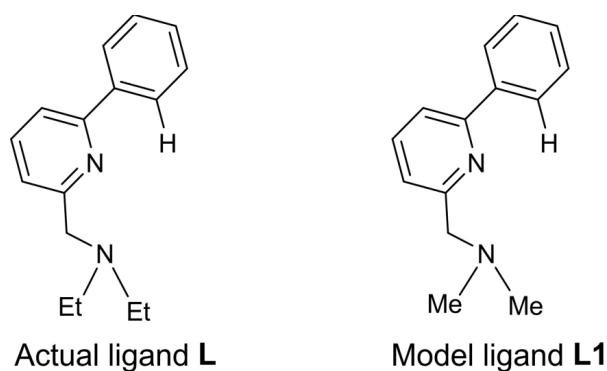


Figure 3.6. The actual ligand **L** and its DFT model **L1**.

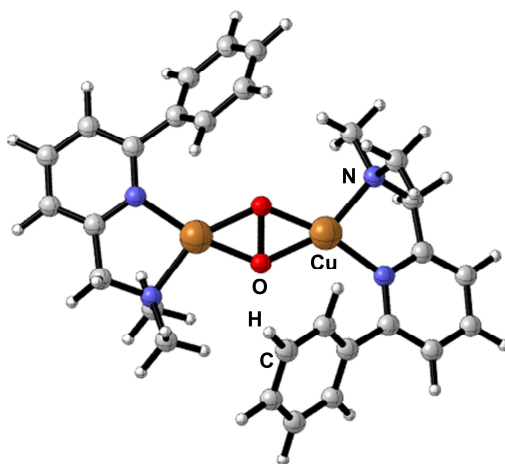
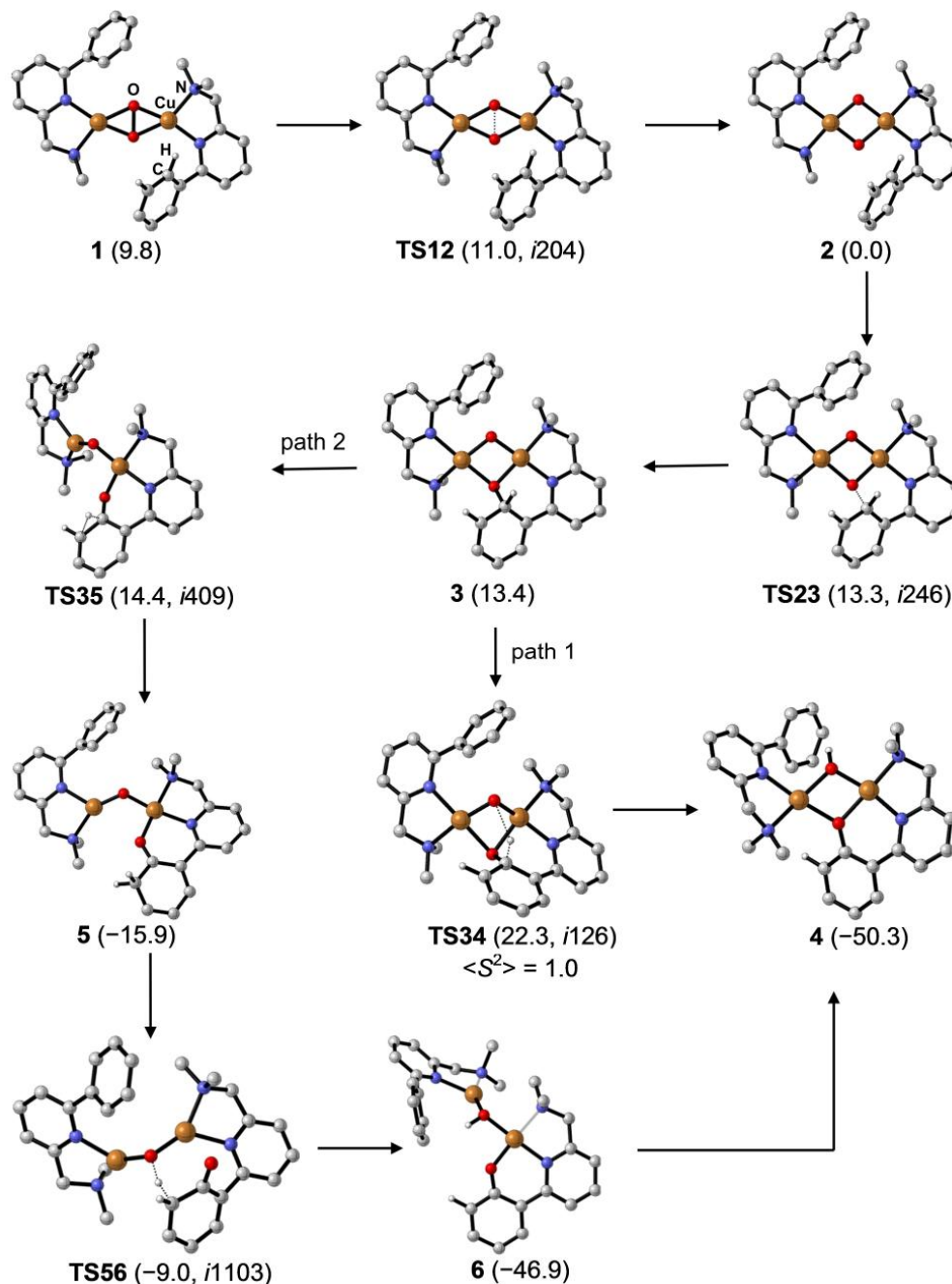


Figure 3.7. The DFT model system, **1**, supported by the ligands **L1**.

3.3.3. Mechanistic Study

1 is less stable than its bis(μ -oxo) isomer **2** by 10 kcal/mol and the core-isomerization process via **TS12** is connected with a minute activation barrier of merely 1 kcal/mol (Scheme 3.8).



Scheme 3.8. Computed reaction pathways for the intramolecular aromatic hydroxylation reaction starting from **1**. BLYP-D/TZVP(COSMO) results, relative Gibbs energies (-70 °C, solvent acetone) with reference to **2** in kcal/mol; imaginary wave numbers of transition state modes for the transition states; $\langle S^2 \rangle$ is the overlap integral between the magnetic orbitals in the broken-symmetry wave function of **TS34**; irrelevant H atoms are not shown.

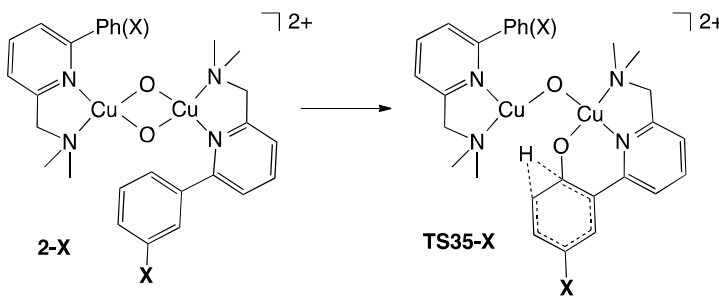
Thus, fully in line with experimental observation, we conclude that isomer **2** represents the dominant species in the initial phase of the reaction. In this minimum structure one of the μ -O atoms in the dicopper core is already located in close proximity (2.86 Å) to one of the *ortho*-carbon atoms of the phenyl group, which predetermines the position of the subsequent regioselective ligand hydroxylation commencing with a low-barrier C–O bond formation via **TS23** ($\Delta G^\ddagger = 13$ kcal/mol). The resulting σ -complex **3** is thermodynamically unstable and two pathways branch off at this point (Scheme 3.8).

Along path 1, **3** directly transforms into complex **4** via proton transfer onto the second μ -O atom. This highly exergonic step results in the formation of a (μ -OH)(μ -O)dicopper complex, which represents the final product of the reaction sequence studied here; from this proposed species the hydroxylated ligand is liberated in the experiments through aqueous workup at room temperature. With **TS34** giving rise to an effective activation barrier of $\Delta G^\ddagger = 22$ kcal/mol for the process leading from **2** to **4**, path 1 cannot kinetically compete with path 2: The latter involves exergonic, rate-limiting decay of **3** to the dienone intermediate **5** and subsequent proton abstraction via **TS56**, followed by a conformational transition, which leads to **4**. With an effective activation barrier of $\Delta G^\ddagger = 14$ kcal/mol associated with **TS35**, the sequence **2**→**5**→**4** represents the preferred route to product formation, and the emergence of a dienone intermediate is coherent with the mechanistic picture suggested in related theoretical work.^[72] The low barrier of merely 7 kcal/mol computed for the strongly exergonic decay of the dienone intermediate to form **6**, and subsequently **4**, implies that this species most likely escapes any attempts for an experimental characterization.

For further comparison with the earlier experimental results of Halfen et al., we also investigated the influence of activating and deactivating substituents introduced *para* to the activation site at the phenyl ring.^[63] The activation barriers resulting for the substituted systems compiled in Table 3.6 were computed as the Gibbs-energy difference at -70 °C between **2-X** and **TS35-X** assuming that the nature of the overall rate-limiting step in the course of the hydroxylation reaction (i.e., the 1,2-H shift for the dienone formation) is independent of the substitution. The resulting differences in computed barrier heights clearly follow the expected trend for substituent effects in electrophilic aromatic substitution reactions validating the view of the bis(μ -oxo)dicopper core as an electrophile.^[63] The high activation barrier obtained for the complex with the strongly deactivating NO₂ substituent

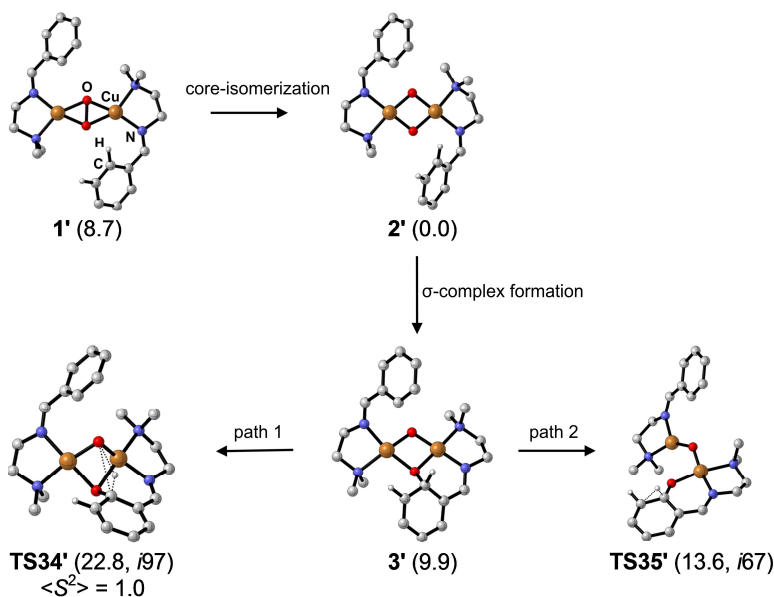
(20 kcal/mol) is in line with the fact that Tolman and coworkers did not observe formation of the hydroxylated PPN(NO₂) product in their low-temperature experiments.^[59, 117]

Table 3.6. Substituent effects on the overall rate-limiting step of the hydroxylation reaction.



X	ΔG^\ddagger (kcal/mol) at 203.15 K	Effect of X
OCH ₃	9.8	Strongly activating
OH	11.2	
CH ₃	12.7	
CH=CH ₂	13.6	
H	14.4	Reference
F	15.5	
CHO	18.7	
NO ₂	20.0	Strongly deactivating
CF ₃	20.5	

We further studied the reaction **CuL^s** complex with dioxygen. The reaction pathways and the nature of the rate-limiting step are still the same (Scheme 3.9). More on this reaction can be read in Appendix 1.



Scheme 3.9. Selected reaction steps computed for the aromatic hydroxylation reaction for the **L^s** ligand starting from **1'**. Gibbs free energies relative to **2'** in kcal/mol. BLYP-D/TZVP(COSMO) results, relative Gibbs energies (−70 °C, solvent acetone) are given in parenthesis together with the characteristic imaginary wave numbers of transition states. For all stationary points reported, closed shell singlet wavefunctions resulted in the computations, except **TS34'**, for which a broken-symmetry wave function was obtained. Irrelevant H atoms are not shown.

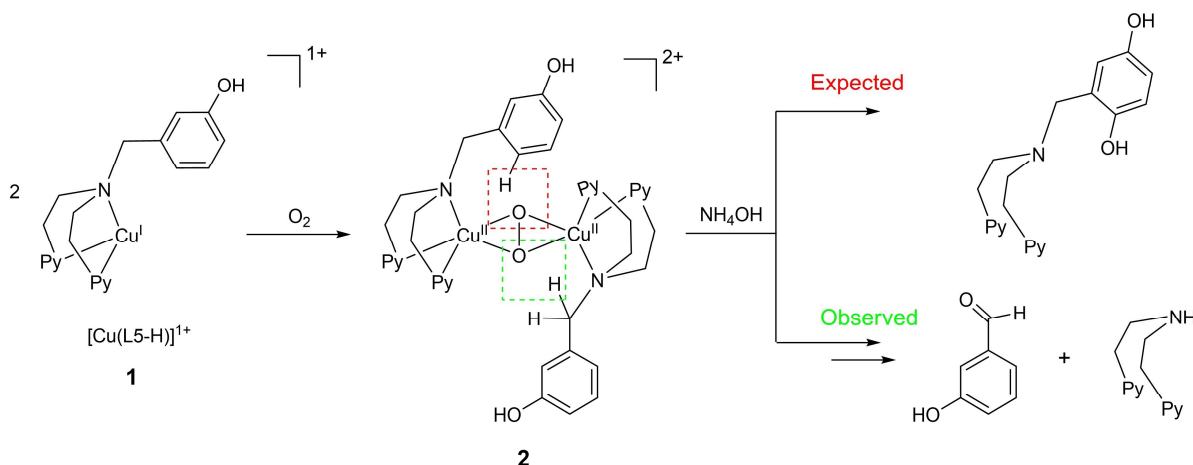
3.3.4. Conclusions

In this study, we have reported a DFT-based mechanistic study for a copper-dioxygen mediated aromatic ligand hydroxylation. We have shown that a bis(μ -oxo)dicopper(III) complex is capable of performing an aromatic ligand hydroxylation. In the mechanistic scenario, first one of the bridging oxygen atoms of the bis(μ -oxo)dicopper(III) core attacks the aromatic ring of the ligand system by forming an unstable σ -complex. From this species, two pathways branch off. Along the kinetically favored route, this intermediate decays into a rather stable dienone complex through a [1,2] proton shift. The newly formed C–H bond in the dienone intermediate is abstracted by the bridging oxygen atom which leads to formation of the hydroxylated product. The rate limiting step in this mechanism is the barrier connected with the formation of the dienone intermediate from the bis(μ -oxo)dicopper(III) complex. We have also investigated the effect of *para*-substituents on the rate limiting step. In case of electron donating substituents, the barrier for the rate limiting step is lowered. In case of electron withdrawing substituents, the barrier for the rate limiting step rises so that the hydroxylation is kinetically hindered at low temperatures. These results provide a straightforward rationalization for the experimental observations.

3.4. Reaction 3: Aliphatic vs Aromatic C–H Hydroxylations

3.4.1. Motivation

Tuczek and coworkers recently attempted an aromatic ligand hydroxylation of an appended phenol by reacting the copper(I) complex of the ligand [N-(3-hydroxyphenyl)methyl]bis[(2-pyrid-2-yl)ethyl]amine (L5-H) with O₂.^[76a] However, surprisingly, the expected aromatic ligand hydroxylation was not observed; aliphatic (benzylic) ligand hydroxylation took place instead, which resulted in the formation of *m*-hydroxy benzaldehyde as reaction product (Scheme 3.10). The reactivity of [Cu(L5-H)]¹⁺ with O₂ in acetone was followed in situ by UV-vis spectroscopy. The spectroscopic features indicated the presence of a μ - η^2 : η^2 -peroxo-dicopper(II) species (**2**).



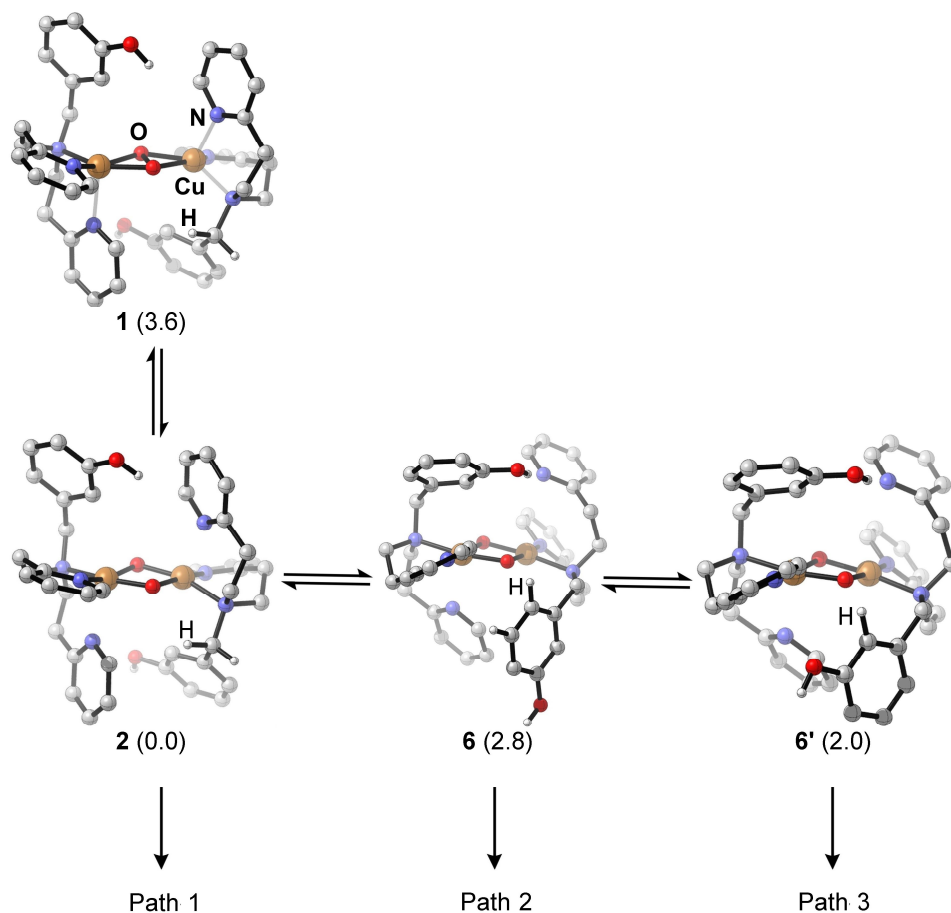
Scheme 3.10. Addition of $[\text{Cu}(\text{L5-H})]^{1+}$ complex with O_2 .

3.4.2. Model System and Mechanistic Study

The computational protocol used in this study was same as in section 3.2. DFT calculations were performed employing the full molecular model system for the $\mu\text{-}\eta^2\text{:}\eta^2\text{-peroxo}$ -dicopper(II) species **1** (Scheme 3.11). In the present study a counteranion is not added due to unavailability of a coordination site at both the copper centers.

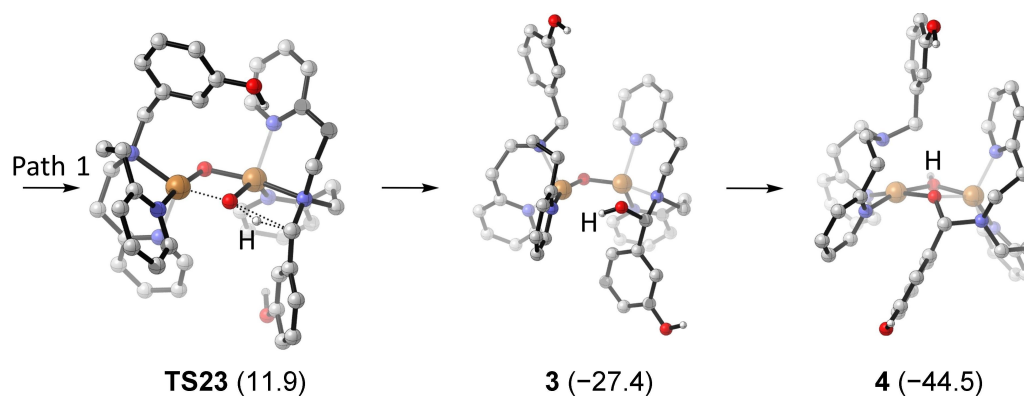
We already identified the most relevant mechanistic steps for aliphatic and aromatic hydroxylations in previous sections of this chapter. The key elementary steps arising from our earlier studies are transferred in the present study.

We started our study with an investigation of the $\mu\text{-}\eta^2\text{:}\eta^2\text{-peroxo}$ -dicopper(II)/bis($\mu\text{-oxo}$)dicopper(III) core isomerization (Scheme 3.11). The peroxo species **1** is around 4 kcal/mol less stable than its corresponding bis($\mu\text{-oxo}$) species **2**. In addition to the bis($\mu\text{-oxo}$) species **2** we identified two isomers **6** and **6'**, which differ in the orientation of the phenol group. **2** is relevant for the aliphatic hydroxylation because one of benzylic C–H bonds in **2** is preoriented favorably for direct activation by the Cu_2O_2 moiety. In **6** and **6'**, however, one of the phenol groups is exposed suitably for direct electrophilic attack by the Cu_2O_2 core. Commencing with the three bis($\mu\text{-oxo}$) isomers, we studied three C–H bond activation pathways giving rise to aliphatic (**2**) and aromatic hydroxylations (**6** and **6'**).



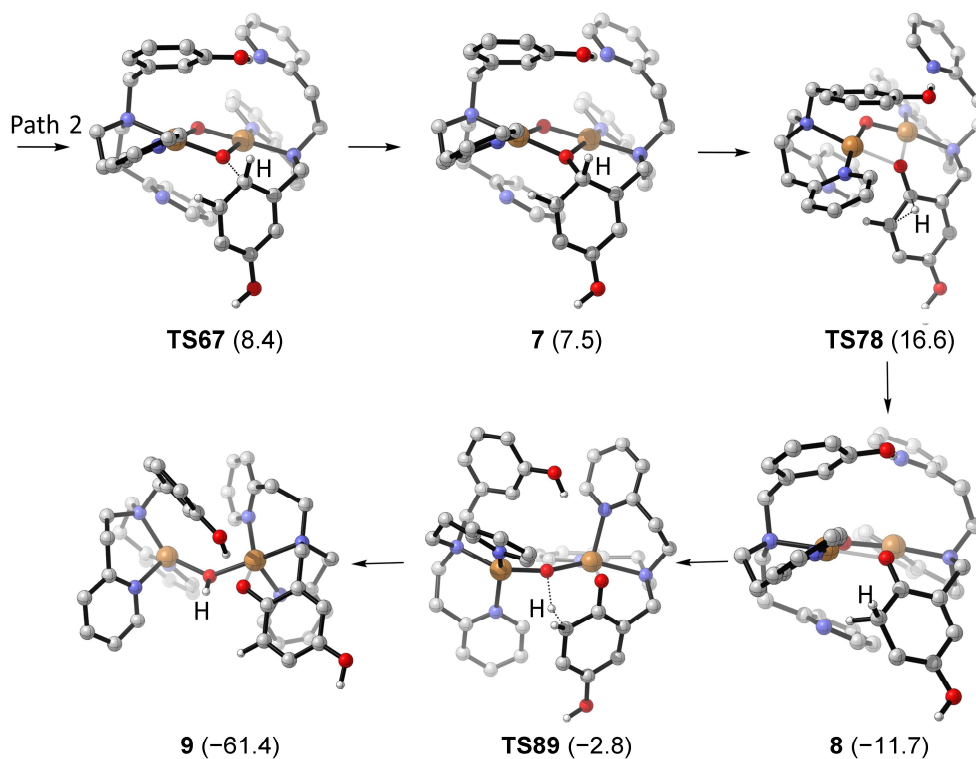
Scheme 3.11. $\mu\text{-}\eta^2\text{:}\eta^2\text{-peroxo-dicopper(II)/bis}(\mu\text{-oxo})\text{dicopper(III)}$ core isomerization between **1** and **2**. The three bis($\mu\text{-oxo}$)dicopper(III) species **2**, **6** and **6'**, which differ in their predisposed C–H bonds to bis($\mu\text{-oxo}$) moiety. In the drawing only the relevant C–H bonds are shown. All energies presented here are Gibbs free energies (kcal/mol) relative to **2** at 195K.

Path 1 (aliphatic hydroxylation): Aliphatic C–H bond activation in species **2** is initiated by **TS23**, which represents the transition state of a concerted C–H bond cleavage with concomitant C–O bond formation (Scheme 3.12). This step is very similar in nature to the previously reported work of Spuhler and Holthausen.^[74] The free energy barrier for this step is 11.9 kcal/mol (relative to **2**) and it leads to the highly exergonic formation of **3** without occurrence of further intermediates. **3** subsequently undergoes proton transfer to form **4** yet in another strongly exergonic step. The conversion from **3** to **4** should be associated with a small barrier as shown by the Holthausen group in a similar aliphatic hydroxylation study.^[74] Hence, **TS23** represents the rate-limiting barrier along pathway 1, and with 11.9 kcal/mol aliphatic hydroxylation represents a fast process even at low temperatures (-78°C).



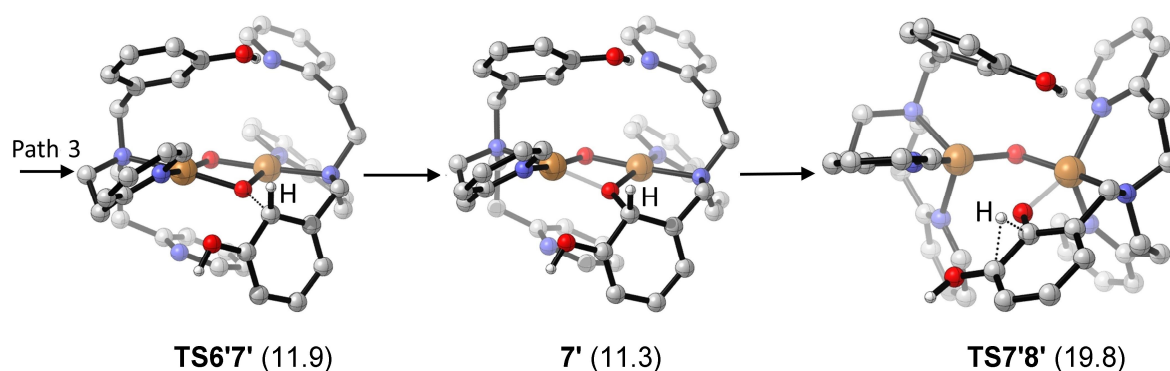
Scheme 3.12. Path 1 leading to the aliphatic hydroxylation. All energies presented here are Gibbs free energies (kcal/mol) relative to **2** at 195K.

Path 2 (Aromatic Hydroxylation): The bis(μ -oxo)dicopper(III) moiety in **6** attacks the ligand aromatic ring via transition state **TS67** ($\Delta G = 8.4$ kcal/mol, Scheme 3.13) and initiates the formation of the C–O bond yielding the unstable σ -complex **7** ($\Delta G = 7.5$ kcal/mol).



Scheme 3.13. Path 2 leading to the aromatic hydroxylation. All energies presented here are Gibbs free energies (kcal/mol) relative to **2** at 195K.

7 rearranges via hydrogen shift (**TS78**) to form the thermodynamically rather stable dienone intermediate **8** ($\Delta G = -11.7$ kcal/mol). **TS78** gives rise to a barrier of 16.6 kcal/mol relative to the species **2**. Subsequently, proton abstraction from **8** takes place via transition state **TS89** ($\Delta G = -2.8$ kcal/mol) leading to the highly exergonic formation of the product **9** ($\Delta G = -61.4$ kcal/mol). Hence, along pathway 2, the rate limiting step is the formation of the dienone intermediate **8** from the bis(μ -oxo)dicopper(III) species **2** with an overall barrier of 16.6 kcal/mol, which exceeds the barrier computed for the aliphatic hydroxylation along path 1 by 5 kcal/mol. Aromatic hydroxylation starting from **6'** (path 3, Scheme 3.14) involves the same elementary steps as path 2, but the computed activation barrier is yet 3 kcal/mol higher. Hence, we conclude that aliphatic hydroxylation via path 1 represents the kinetically favored process, while aromatic hydroxylation yields the thermodynamically favored product.



Scheme 3.14. Path 3 leading to the aromatic hydroxylation. All energies presented here are Gibbs free energies (kcal/mol) relative to **2** at 195K.

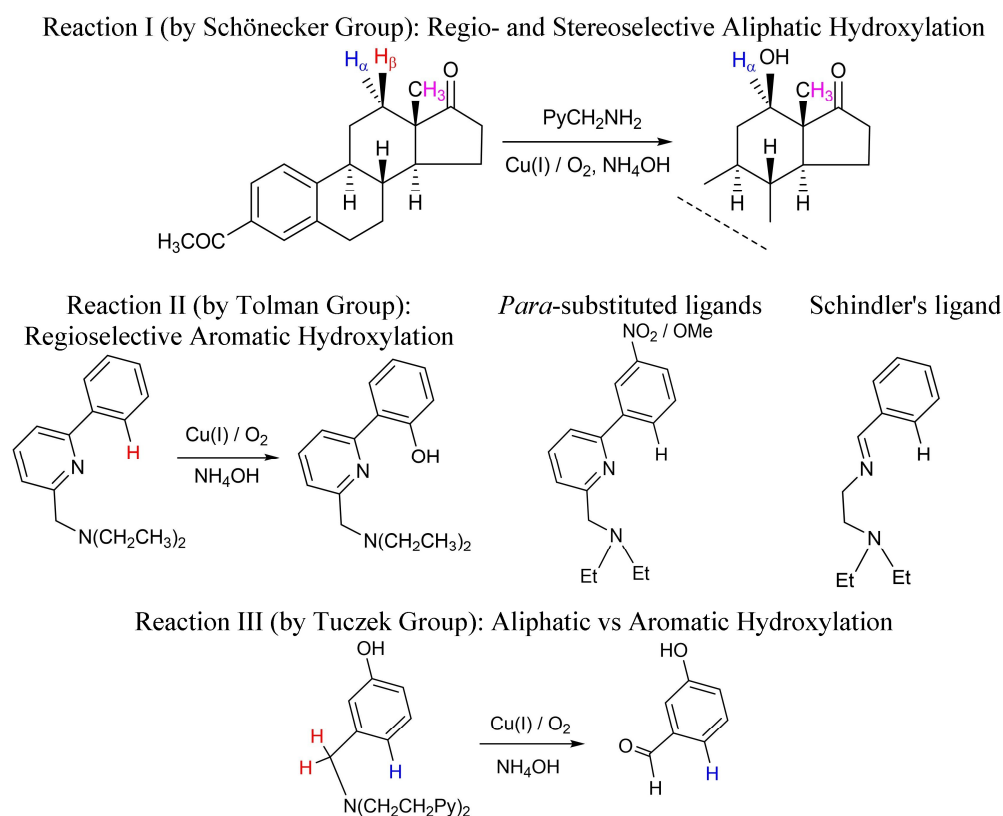
3.4.3. Conclusions

In this section, we have studied the competition between copper-dioxygen mediated aliphatic and aromatic C–H hydroxylations in a system investigated in an earlier experimental work of Tucek and coworkers. The barrier for the rate limiting step in the aliphatic hydroxylation has a barrier of 11.9 kcal/mol, whereas for the other two pathways for the aromatic hydroxylation, activation barriers of 16.6 and 19.8 kcal/mol occur. Therefore, our DFT study shows that the aliphatic hydroxylation is most favorable among the three pathways, in accordance with the experimental findings.

Chapter 4

Conclusions

The main aim of this thesis was to employ density functional theory (DFT) to study three experimentally observed copper-dioxygen mediated C–H hydroxylation reactions (Scheme 4.1). The first reaction (I) established experimentally by the group of Schönecker features a regio- and stereoselective aliphatic C–H hydroxylation. For this reaction, the task in this thesis was to employ DFT to find out the reason for observed regio- and stereoselectivity.



Scheme 4.1 The reactions studied in this thesis.

The second reaction (II) by the group of Tolman shows regioselective aromatic C–H hydroxylation, with pronounced effects of *p*-substituents such as NO₂ and OCH₃. In case of the *p*-NO₂ group, the authors did not observe any hydroxylated product. For this reaction, the first task was to employ DFT to find the reason for regioselectivity, and the second task was to investigate the effect of a series of *p*-substituents (OCH₃, OH, CH₃, CH=CH₂, H, CHO,

NO₂, and CF₃) on the hydroxylation process. We studied a very recent work of Schindler and coworkers who applied Tolman's reaction conditions to prepare salicylaldehyde using „simple“ copper-imine system. In the third reaction (III) experimentally studied by the group of Tuzek, aliphatic hydroxylation was observed instead of an expected tyrosinase-like aromatic hydroxylation. Therefore, for this reaction, the task was to employ DFT to unravel the reason for the preference of aliphatic over aromatic C–H hydroxylation.

As detailed in the exhaustive literature survey presented in chapters 1 and 2, previous experimental and theoretical studies on copper-dioxygen mediated C–H hydroxylation reactions reported that a **Cu₂P^S/Cu₂O₂** isomerization precedes C–H activation steps, which may take place from either of the two isomers. In the literature, partly opposing recommendations are found as to the choice of DFT methods for related studies. For **Cu₂P^S/Cu₂O₂** isomerizations, Cramer and coworkers have suggested to use the BLYP density functional including relativistic effects, whereas Siegbahn recommended the use of the B3LYP* density functional including dispersion, relativistic effects and solvent effects together with BS wavefunctions. More recently, Neese and coworkers found that B3LYP including dispersion, solvent and relativistic effects performs best for **Cu₂P^S/Cu₂O₂** isomerizations. For the **Cu₂P^S/Cu₂O₂**-mediated C–H activation step, no specific DFT benchmark study could be found in literature. However, some research groups have used the B3LYP and B3LYP* density functionals to study a copper-dioxygen mediated C–H bond activation processes.

In this thesis, DFT benchmarks have been undertaken against experimental reference data reported by Stack and coworkers for the **Cu₂P^S/Cu₂O₂** isomerization and the **Cu₂O₂**-mediated C–H bond activation. For the DFT benchmarks, a series of density functionals was chosen based on previous recommendations including dispersion, solvent and relativistic effects. The DFT protocol BLYP-D3/def2-TZVP(SDD)+COSMO//BLYP-D2/def2-TZVP(SDD) was found to work best for both benchmark reactions. This DFT protocol showed a deviation of 3 kcal/mol for the **Cu₂P^S/Cu₂O₂** isomerization and an error below 1 kcal/mol for the C–H activation barrier against the experimentally determined data.

In our DFT benchmark study, we found that the relative energies for the **Cu₂P^S** and **Cu₂O₂** isomers, and the barrier height for the **Cu₂O₂**-mediated C–H activation are particularly sensitive to the amount of Fock-exchange included in the density functionals, to

dispersion corrections and relativistic effect. For the $\text{Cu}_2\text{P}^{\text{S}}/\text{Cu}_2\text{O}_2$ core isomerization, inclusion of Fock-exchange destabilizes the Cu_2O_2 isomer whereas dispersion and relativistic effect stabilize the Cu_2O_2 isomer compared to the $\text{Cu}_2\text{P}^{\text{S}}$ isomer. For the C–H activation reaction, inclusion of Fock-exchange destabilizes the Cu_2O_2 isomer whereas dispersion and relativistic effect stabilize the Cu_2O_2 isomer relative to the transition state. In addition, the effect of triflate counteranions was also studied: Coordination of the counteranion destabilizes the Cu_2O_2 isomer whereas no prominent effect was noticed on the C–H activation barrier height.

The benchmarked DFT method was applied in subsequent mechanistic work to unravel the reason behind the observed regio- and stereoselectivity in the Cu_2O_2 -mediated aliphatic C–H hydroxylation in a steroid reported earlier experimental studies by Schönecker. In our DFT study the Cu_2O_2 isomer was found more stable than the $\text{Cu}_2\text{P}^{\text{S}}$ isomer in line with experimental observation. Subsequent C–H bond activation was identified as the rate limiting step of the overall hydroxylation reaction. For the three different C–H bond activation positions investigated, the lowest activation barrier was found for the C–H $_{\beta}$ position, perfectly in line with experimental observation.

Next, the benchmarked method was applied in a mechanistic study aiming at an evaluation of the reaction mechanism underlying the regioselective aromatic hydroxylation reported by Tolman and coworkers. Also for this system, and again in line with the experiment, the Cu_2O_2 isomer was found more stable than the $\text{Cu}_2\text{P}^{\text{S}}$ isomer. Subsequent electrophilic attack of the Cu_2O_2 core at the favorably oriented *ortho*-position of the phenyl group is followed by an overall rate limiting formation of a dienone intermediate. We also investigated the effect of *para*-substituents on this rate limiting step. Electron donating substituents attached in this position decrease the barrier height of the rate limiting step while electron withdrawing substituents increase the barrier height. For example: the barrier height for the rate limiting step for the *p*-NO₂-substituted ligand is 20 kcal/mol whereas for the *p*-OCH₃ substituted systems is 10 kcal/mol. A barrier height of 20 kcal/mol is too high for a reaction to take place at 203K, which provides a rationalization why Tolman and coworkers did not observe any hydroxylated product in this case.

For the reaction studied experimentally by Tuzcek and coworkers, both aliphatic and aromatic C–H hydroxylation pathways were studied. On one hand, the computed barrier

height for the rate-limiting step in the aliphatic C–H hydroxylation pathway is 12 kcal/mol whereas the computed barrier height for the aromatic C–H hydroxylation pathway is 17 kcal/mol. On the other hand, the hydroxylated product from the aromatic hydroxylation is thermodynamically more stable than the aliphatic hydroxylation. Therefore, the aliphatic C–H hydroxylation should be kinetically preferred over the aromatic C–H hydroxylation, whereas the aromatic hydroxylation is thermodynamically preferred. The computational findings are in accord with the experimental observations.

In this thesis, the DFT method BLYP-D3/def2-TZVP(SDD)+COSMO//BLYP-D2/def2-TZVP(SDD) has been proposed to study copper-dioxygen mediated aliphatic and aromatic hydroxylation reactions. It has been found in this work that prior to aliphatic or aromatic hydroxylation, a $\text{Cu}_2\text{P}^{\text{S}}/\text{Cu}_2\text{O}_2$ isomerization may take place. Unlike in $\text{Cu}_2\text{P}^{\text{S}}$ -promoted tyrosinase hydroxylation, Cu_2O_2 isomers in synthetic systems have also been shown to activate aliphatic as well as aromatic C–H bonds. Such reactions have been found electrophilic in nature.

Zusammenfassung

Die außerordentlich hohe Selektivität in der Natur vorkommender biologischer Prozesse inspiriert seit langem die Entwicklung analoger chemischer Prozesse in der synthetischen Chemie. Gleichzeitig bietet die Charakterisierung kurzlebiger Intermediate laborchemischer Umsetzungen Anhaltspunkte für ein tiefergehendes Verständnis biologischer Prozesse. Mithin können neue Erkenntnisse aus der biologischen Forschung grundsätzlich der Chemie von besonderem Nutzen sein und umgekehrt.

Proteine und katalytisch aktive Enzyme gehören zu den elementaren Bausteinen lebender Zellen. Metalloproteine oder -enzyme, deren aktives Zentrum Übergangsmetallionen wie Kupfer, Nickel, Eisen oder Zink enthält, sind beispielsweise in Prozessen involviert wie (1) Speicherung und Transport von Metallionen, (2) Übertragung von Elektronen in katalytischen bzw. Elektronentransfer-Prozessen, sowie (3) Speicherung, Transport und Verstoffwechslung von molekularem Sauerstoff. Seit Jahrzehnten erregt der Kupfer-vermittelte biologische Sauerstofftransfer enormes Interesse auf dem Gebiet der Katalyse in der synthetischen Chemie. Kupferenzyme wie Dopamin- β -Monooxygenase (D β M), Peptidylglycin- α -hydroxylierende Monooxygenase (PHM), partikuläre Methanmonooxygenase (pMMO) und Tyrosinase vermitteln die Aktivierung von molekularem Sauerstoff (O_2) und eine darauf folgende selektive Insertion eines Sauerstoffatoms in C-H-Bindungen zur Bildung hydroxylierter organischer Verbindungen. Diese Kupferenzyme lassen sich nach ihren aktiven Zentren in mononukleare, binukleare und trinukleare Systeme unterteilen, die für bestimmte spezifische biologische Funktionen verantwortlich sind. Beachtliche Fortschritte in der bioanorganischen Chemie haben eine Vielzahl an Kupfer-basierten, mit unterschiedlichen Stickstoffdonor-Liganden versehenen bioanorganischen Modellsystemen hervorgebracht, die molekularen Sauerstoff binden und die O-O-Bindung spalten können, sowie den Kupferenzymen nachempfundene Hydroxylierungsreaktionen ermöglichen. Im Fokus der vorliegenden Arbeit stehen Untersuchungen zum Isomerisierungsgleichgewicht des aktiven Zentrums der binuklearen Cu_2O_2 -Systeme und deren spezifische Reaktivitätsmuster, die Gegenstand aktueller

experimenteller Forschung sind und zum besseren Verständnis der Enzymaktivität der Tyrosinase beitragen können.

Quantenchemische Studien haben bereits substantielle Beiträge zum Verständnis der Kupfer-Sauerstoff-Chemie geleistet. Hierbei wurden größtenteils Berechnungen mittels Dichtefunktionaltheorie (DFT) herangezogen, die in besonderem Maße detaillierte Einblicke in den Mechanismus der Kupfer-vermittelten aliphatischen und aromatischen Hydroxylierung liefern konnten. Bis heute stellt jedoch die Wahl geeigneter quantenchemischer Methoden für mechanistische Studien eine enorme Herausforderung dar, die durch widersprüchliche Angaben in der Literatur noch verschärft wird. Folglich wird in dieser Arbeit zunächst eine zur Beschreibung der Kupfer-vermittelten Hydroxylierung geeignete DFT-Methode etabliert. Mit dieser Methode werden im Folgenden ausgewählte relevante Hydroxylierungsreaktionen mit dem Ziel untersucht, ein detailliertes Verständnis für den jeweiligen Reaktionsmechanismus zu entwickeln.

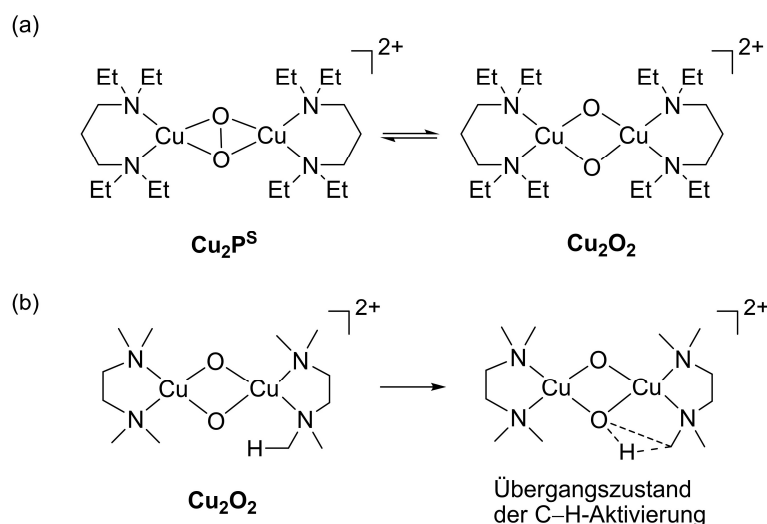
Frühere experimentelle und theoretische Studien an Kupferdisauerstoff-vermittelten C–H-Hydroxylierungsreaktionen berichteten, dass der C–H-Aktivierung ein $\text{Cu}_2\text{P}^{\text{S}}/\text{Cu}_2\text{O}_2$ -Isomerisierungsgleichgewicht vorausgeht (Schema 1). Folglich kann die nachfolgende Aktivierung der C–H-Bindung ausgehend von jedem der beiden Isomere ablaufen. In dieser



Schema 1. Isomerisierungsgleichgewicht zwischen $\text{Cu}_2\text{P}^{\text{S}}$ und Cu_2O_2 .

Arbeit wurden deshalb Benchmark-Rechnungen gegen experimentelle Referenzdaten durchgeführt, sowohl für die $\text{Cu}_2\text{P}^{\text{S}}/\text{Cu}_2\text{O}_2$ -Isomerisierung als auch für die Cu_2O_2 -vermittelte Aktivierung der C–H-Bindung (Schema 2). Hierbei zeigt das BLYP-D/def2-TZVP-Niveau unter Berücksichtigung von Solvenseffekten und relativistischen Korrekturen mit einer Abweichung von 3 kcal/mol für die $\text{Cu}_2\text{P}^{\text{S}}/\text{Cu}_2\text{O}_2$ -Isomerisierung und einem Fehler von weniger als 1 kcal/mol für die Barriere der C–H-Aktivierung die beste Übereinstimmung mit den experimentellen Daten. Besonders ausgeprägt ist dabei der

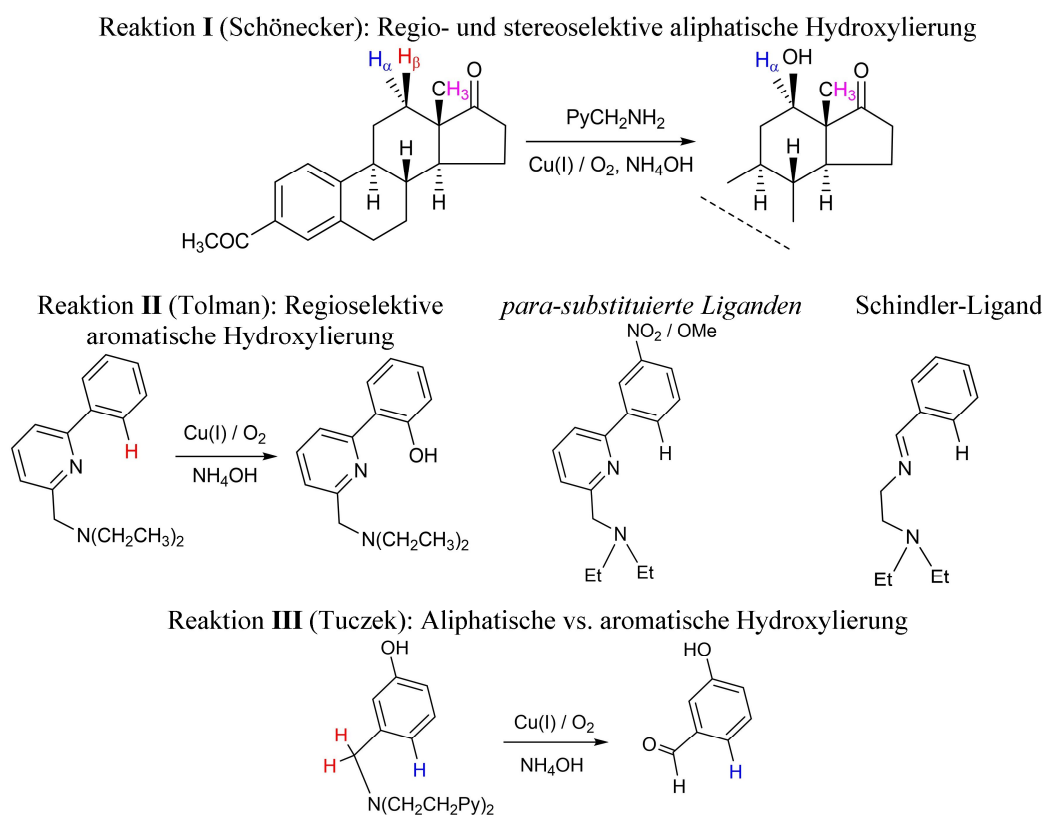
Einfluss des Anteils an Fock-Austausch der Dichtefunktionale, der Dispersionskorrektur, sowie von relativistischen Effekten. Im Falle des $\text{Cu}_2\text{P}^{\text{S}}/\text{Cu}_2\text{O}_2$ -Isomerisierungsgleichgewichts wird das Cu_2O_2 -Isomer im Vergleich zum $\text{Cu}_2\text{P}^{\text{S}}$ -Isomer mit zunehmendem Fock-Austausch destabilisiert, wohingegen dispersive und relativistische korrekturen das Cu_2O_2 -Isomer stabilisieren. Gleichsam führt in der C–H-Aktivierungsreaktion ein zunehmender Fock-Austausch zur Destabilisierung des Cu_2O_2 -Isomers; dispersive und relativistische korrekturen hingegen stabilisieren das Cu_2O_2 -Isomer relativ zum Übergangszustand. Weiterhin wurde der Effekt der Triflat-Gegenionen untersucht: während Koordination des Gegenions das Cu_2O_2 -Isomer destabilisiert, ist kein signifikanter Einfluss auf die Höhe der Aktivierungsbarriere zu erkennen.



Scheme 2. (a) $\text{Cu}_2\text{P}^{\text{S}}/\text{Cu}_2\text{O}_2$ -Isomerisierung, (b) Cu_2O_2 -vermittelte Aktivierung der C–H-Bindung.

Die zuvor etablierte DFT-Methode wurde darüber hinaus zur Untersuchung der Reaktionsmechanismen dreier Kupferdisauerstoff-vermittelter Hydroxylierungen von aliphatischen und aromatischen C–H-Bindungen angewandt (Schema 3). Die von Schönecker und Mitarbeitern experimentell etablierte Reaktion (**I**) zeichnet sich durch eine bemerkenswert regio- und stereoselektive aliphatische C–H-Hydroxylierung aus, deren Ursache in dieser Arbeit erörtert wird. Die zweite Reaktion (**II**) aus der Gruppe von Tolman zeigt einen ausgeprägten Einfluss der *para*-Substituenten wie etwa NO_2 und OCH_3 bei der regioselektiven Aktivierung aromatischer C–H-Bindungen. Im Falle der *p*- NO_2 -Gruppe beobachteten die Autoren keinerlei hydroxyliertes Produkt. Im Rahmen dieser Arbeit wurde

der Grund für die Regioselektivität und der Effekt des *para*-Substituenten (OCH₃, OH, CH₃, CH=CH₂, H, CHO, NO₂ und CF₃) näher beleuchtet. In diesem Kontext wurde auch die jüngste Arbeit von Schindler und Mitarbeitern untersucht, in der Tolmans Reaktionsbedingungen genutzt wurden, um Salicylaldehyd mittels eines „einfachen“ Kupfer-Imin-Systems darzustellen. In der dritten Reaktion (III) beobachteten Tuczek und Mitarbeiter anstelle der erwarteten Tyrosinase-ähnlichen aromatischen Hydroxylierung eine aliphatische Hydroxylierung. Im Rahmen dieser Arbeit wurde eruiert, weshalb in diesem Fall die aliphatische gegenüber der aromatischen C–H-Hydroxylierung bevorzugt ist.



Schema 3. Übersicht der in dieser Arbeit untersuchten Reaktionen

Für Reaktion I zeigten unsere Rechnungen, dass das **Cu₂O₂**-Isomer stabiler ist als das **Cu₂P^S**-Isomer, was sich mit experimentellen Befunden deckt. Die Aktivierung der C–H-Bindung wurde nachfolgend als geschwindigkeitsbestimmender Schritt der Hydroxylierungsreaktion identifiziert. Von den drei untersuchten Positionen für eine C–H-Aktivierung (Schema 3, Reaktion I), zeigte die C–H_β-Position die niedrigste Aktivierungsbarriere, in sehr guter Übereinstimmung mit experimentellen Ergebnissen.

In Reaktion **II** (Tolman und Mitarbeiter) erwies sich das Cu_2O_2 -Isomer gegenüber dem $\text{Cu}_2\text{P}^{\text{S}}$ -Isomer, wieder in Übereinstimmung mit dem Experiment, als stabiler. Auf den nachfolgenden elektrophilen Angriff des Cu_2O_2 -Zentrums in der bevorzugten *ortho*-Position der Phenylgruppe folgt in einem geschwindigkeitsbestimmenden Schritt die Bildung eines Dienon-Intermediates. Weiterhin wurde der Einfluss von *para*-Substituenten auf den geschwindigkeitsbestimmenden Schritt untersucht: elektronenschiebende Substituenten an dieser Position setzen die Barriere herab, während elektronenziehende Substituenten die Barriere des geschwindigkeitsbestimmenden Schritts erhöhen. Beispiel: Die Barriere für den *p*- NO_2 -substituierten Liganden beträgt 20 kcal/mol, während die für das *p*- OCH_3 -substituierte System bei 10 kcal/mol liegt. Eine Barriere von 20 kcal/mol ist für den Ablauf einer Reaktion bei 203K zu hoch. Dies erklärt, warum Tolman und Mitarbeiter in diesem Fall kein hydroxyliertes Produkt fanden. Unsere mechanistischen Erkenntnisse aus Reaktion **II** konnten in Zusammenarbeit mit der Gruppe um Prof. Schindler erfolgreich auf die Untersuchung einer verwandten Reaktion übertragen werden.

Für die Reaktion von Tuzek und Mitarbeitern (**III**) wurden sowohl der aliphatische als auch der aromatische Pfad zur C–H-Hydroxylierung untersucht. Die geschwindigkeitsbestimmende Barriere für den aliphatischen Pfad wurde zu 12 kcal/mol berechnet, die des aromatischen Pfades liegt bei 17 kcal/mol. Das Produkt des aromatischen Pfades ist aus thermodynamischer Sicht jedoch das stabilere. Die aliphatische C–H-Hydroxylierung sollte folglich unter kinetischer Kontrolle bevorzugt sein, während der aromatische Pfad unter thermodynamischer Kontrolle günstiger ist. Dies deckt sich mit den experimentellen Befunden.

In der vorliegenden Arbeit wurde gezeigt, dass die Anwendung der DFT-Methode BLYP-D/def2-TZVP unter Einbeziehung eines Solvensmodells und relativistischer Effekte für die Untersuchung der Kupferdisauerstoff-vermittelten aliphatischen bzw. aromatischen Hydroxylierung besonders leistungsfähig ist. Diesem Reaktionstyp geht gegebenenfalls eine $\text{Cu}_2\text{P}^{\text{S}}/\text{Cu}_2\text{O}_2$ -Isomerisierung voraus. Im Gegensatz zur $\text{Cu}_2\text{P}^{\text{S}}$ -induzierten Tyrosinase-Hydroxylierung konnte für vergleichbare synthetische Komplexe gezeigt werden, dass die Cu_2O_2 -Isomere sowohl aliphatische wie auch aromatische C–H-Bindungen aktivieren können. Diese Reaktion ist elektrophiler Natur.

Abbreviations

Ad	adamantyl
BS	broken symmetry
<i>t</i> -Bu	<i>tert</i> -butyl
CF ₃ SO ₃ ⁻	triflate counteranion
COSMO	conductor-like screening model
DFT	density functional theory
DFT-D2/D3	dispersion corrected density functional theory
ECP	effective core potential
EPR	electron paramagnetic resonance
EXAFS	extended X-ray absorption fine structure analyses
GGA	generalized gradient approximation
Glu	glutamine
His	histidine
Met	methionine
NIH	national institute of health
OPT ^{BS}	open-shell singlet optimization
OPT ^{CS}	closed-shell singlet optimization
OPT ^T	triplet optimization
<i>i</i> -Pr	isopropyl
Pz	pyrazolyl
SDD	Stuttgart-Dresden pseudopotential
SP1 ^{BS}	ECP-based broken symmetry single point
SP2 ^{BS}	ZORA-based broken symmetry single point
SP3 ^{BS}	DKH-based broken symmetry single point
SP1 ^{CS}	ECP-based closed-shell single point
SP2 ^{CS}	ZORA-based closed-shell single point
SP3 ^{CS}	DKH-based closed-shell single point
THF	tetrahydrofurane

TZVP	triple- ζ valence polarized basis set
UV-vis	ultraviolet and visible (light)
ZORA	zeroth-order regular approximation

References

- [1] E. I. Solomon, D. E. Heppner, E. M. Johnston, J. W. Ginsbach, J. Cirera, M. Qayyum, M. T. Kieber-Emmons, C. H. Kjaergaard, R. G. Hadt, L. Tian, *Chem. Rev.* **2014**.
- [2] E. I. Solomon, R. K. Szilagy, S. DeBeer George, L. Basumallick, *Chem. Rev.* **2004**, *104*, 419-458.
- [3] P. M. Colman, H. C. Freeman, J. M. Guss, M. Murata, V. A. Norris, J. A. M. Ramshaw, M. P. Venkatappa, *Nature* **1978**, *272*, 319-324.
- [4] H. B. Gray, B. G. Malmström, R. J. P. Williams, *J. Biolog. Inorg. Chem.* **2000**, *5*, 551-559.
- [5] a) J. A. Tainer, E. D. Getzoff, J. S. Richardson, D. C. Richardson, *Nature* **1983**, *306*, 284-287; b) J. A. Tainer, E. D. Getzoff, K. M. Beem, J. S. Richardson, D. C. Richardson, *J. Mol. Biol.* **1982**, *160*, 181-217.
- [6] S. T. Prigge, A. S. Kolhekar, B. A. Eipper, R. E. Mains, L. M. Amzel, *Science* **1997**, *278*, 1300-1305.
- [7] a) A. Volbeda, W. G. J. Hol, *J. Mol. Biol.* **1989**, *209*, 249-279; b) A. Volbeda, W. G. J. Hol, *J. Mol. Biol.* **1989**, *206*, 531-546.
- [8] A. Messerschmidt, A. Rossi, R. Ladenstein, R. Huber, M. Bolognesi, G. Gatti, A. Marchesini, R. Petruzzelli, A. Finazzi-Agró, *J. Mol. Biol.* **1989**, *206*, 513-529.
- [9] a) E. I. Solomon, U. M. Sundaram, T. E. Machonkin, *Chem. Rev.* **1996**, *96*, 2563-2606; b) E. I. Solomon, M. J. Baldwin, M. D. Lowery, *Chem. Rev.* **1992**, *92*, 521-542.
- [10] B. J. Brazeau, B. J. Johnson, C. M. Wilmot, *Arch. Biochem. Biophys.* **2004**, *428*, 22-31.
- [11] a) N. Ito, S. E. V. Phillips, C. Stevens, Z. B. Ogel, M. J. McPherson, J. N. Keen, K. D. S. Yadav, P. F. Knowles, *Nature* **1991**, *350*, 87-90; b) N. Ito, S. E. V. Phillips, K. D. S. Yadav, P. F. Knowles, *J. Mol. Biol.* **1994**, *238*, 704-814.
- [12] a) J. P. Klinman, *Chem. Rev.* **1996**, *96*, 2541-2562; b) J. P. Evans, K. Ahn, J. P. Klinman, *J. Biol. Chem.* **2003**, *278*, 49691-49698.
- [13] T. Klabunde, C. Eicken, J. C. Sacchettini, B. Krebs, *Nature Struct. Biol.* **1998**, *5*, 1084-1090.
- [14] Y. Matoba, T. Kumagai, A. Yamamoto, H. Yoshitsu, M. Sugiyama, *J. Biol. Chem.* **2006**, *281*, 8981-8990.
- [15] a) K. Piontek, M. Antorini, T. Choinowski, *J. Biol. Chem.* **2002**, *277*, 37663-37669; b) H. Claus, *Micron* **2004**, *35*, 93-96.
- [16] G. Musci, *Protein Pept. Lett.* **2001**, *8*, 159-169.
- [17] T. Funabiki, in *Oxygenases and Model Systems* (Ed.: T. Funabiki), Kluwer Academic Publishers, Dordrecht, The Netherlands, **1997**, pp. 1-89.
- [18] a) J. P. Klinman, *J. Biol. Chem.* **2006**, *281*, 3013-3016; b) J. P. Klinman, *Chem. Rev.* **1996**, *96*, 2541-2562.
- [19] a) H. Timmers, J. Deinum, R. A. Wevers, J. W. M. Lenders, in *Stress: Current Neuroendocrine and Genetic Approaches, Vol. 1018* (Eds.: K. Pacak, B. Aguilera, E. Saban, R. Kvetnansky), New York Acad. Sciences, New York, **2004**, pp. 520-523; b) J. F. Cubells, C. P. Zabetian, *Psychopharmacology* **2004**, *174*, 463-476.

- [20] a) B. A. Eipper, A. S. W. Quon, R. E. Mains, J. S. Boswell, N. J. Blackburn, *Biochemistry* **1995**, *34*, 2857-2865; b) S. T. Prigge, R. E. Mains, B. A. Eipper, L. M. Amzel, *Cell. Mol. Life Sci.* **2000**, *57*, 1236-1259.
- [21] R. L. Lieberman, A. C. Rosenzweig, *Nature* **2005**, *434*, 177-182.
- [22] J. Schottenheim, C. Gernert, B. Herzigkeit, J. Krahmer, F. Tuczek, *Eur. J. Inorg. Chem.* **2015**, *2015*, 3501-3511.
- [23] E. I. Solomon, P. Chen, M. Metz, S.-K. Lee, A. E. Palmer, *Angew. Chem. Int. Ed.* **2001**, *40*, 4570-4590.
- [24] H. Decker, T. Schweikardt, F. Tuczek, *Angew. Chem. Int. Ed.* **2006**, *45*, 4546-4550.
- [25] a) S. Itoh, *Curr. Opin. Chem. Biol.* **2006**, *10*, 115-122; b) J. L. Que, W. B. Tolman, *Angew. Chem. Int. Ed.* **2002**, *41*, 1114-1137; c) T. D. P. Stack, *Dalton Trans.* **2003**, 1881-1889; d) R. A. Himes, K. D. Karlin, *Curr. Opin. Chem. Biol.* **2009**, *13*, 119-131; e) N. Kitajima, Y. Moro-oka, *Chem. Rev.* **1994**, *94*, 737-757; f) A. G. Blackman, W. B. Tolman, in *Metal-Oxo and Metal-Peroxo Species in Catalytic Oxidations*, Vol. 97 (Ed.: B. Meunier), Springer-Verlag, Berlin, **2000**, pp. 179-211; g) L. M. Mirica, X. Ottenwaelder, T. D. P. Stack, *Chem. Rev.* **2004**, *104*, 1013-1046; h) E. A. Lewis, W. B. Tolman, *Chem. Rev.* **2004**, *104*, 1047-1076; i) L. Q. Hatcher, K. D. Karlin, *J. Biol. Inorg. Chem.* **2004**, *9*, 669-683; j) L. Q. Hatcher, K. D. Karlin, in *Adv. Inorg. Chem.*, Vol. Volume 58 (Eds.: R. v. Eldik, J. Reedijk), Academic Press, **2006**, pp. 131-184; k) I. A. Koval, P. Gamez, C. Belle, K. Selmecezi, J. Reedijk, *Chem. Soc. Rev.* **2006**, *35*, 814-840; l) P. L. Holland, W. B. Tolman, *Coord. Chem. Rev.* **1999**, *190-192*, 855-869; m) K. D. Karlin, S. Kaderli, A. D. Zuberbühler, *Acc. Chem. Res.* **1997**, *30*, 139-147; n) K. D. Karlin, A. D. Zuberbühler, in *Bioinorganic Catalysis* (Eds.: J. Reedijk, E. Bouwman), Marcel Dekker, New York, **1999**, pp. 469-534; o) M. Rolff, J. Schottenheim, H. Decker, F. Tuczek, *Chem. Soc. Rev.* **2011**, *40*, 4077-4098; p) S. Fukuzumi, K. D. Karlin, *Coord. Chem. Rev.* **2013**, *257*, 187-195; q) S. Itoh, in *Copper Oxygen Chemistry* (Eds.: K. D. Karlin, S. Itoh), John Wiley & Sons, Inc., New Jersey, **2011**, pp. 225-282; r) S. Schindler, *Eur. J. Inorg. Chem.* **2000**, 2311-2326; s) V. Mahadevan, R. J. M. K. Gebbink, T. D. P. Stack, *Curr. Opin. Chem. Biol.* **2000**, *4*, 228-234; t) G. Battaini, A. Granata, E. Monzani, M. Gullotti, L. Casella, in *Adv. Inorg. Chem.*, Vol. Volume 58 (Eds.: R. v. Eldik, J. Reedijk), Academic Press, **2006**, pp. 185-233; u) C. J. Cramer, W. B. Tolman, *Acc. Chem. Res.* **2007**, *40*, 601-608; v) A. De, S. Mandal, R. Mukherjee, *J. Inorg. Biochem.* **2008**, *102*, 1170-1189; w) L. Que, W. B. Tolman, *Nature* **2008**, *455*, 333-340; x) A. Company, in *Ideas in Chemistry and Molecular Sciences*, Wiley-VCH Verlag GmbH & Co. KGaA, **2010**, pp. 265-289; y) W. N. Oloo, L. Que Jr., in *Comprehensive Inorganic Chemistry II (Second Edition)* (Eds.: R. Jan, P. Kenneth), Elsevier, Amsterdam, **2013**, pp. 763-778.
- [26] A. de la Lande, H. Gérard, V. Moliner, G. Izzet, O. Reinaud, O. Parisel, *J. Biolog. Inorg. Chem.* **2006**, *11*, 593-608.
- [27] a) J. S. Thompson, *J. Am. Chem. Soc.* **1984**, *106*, 8308-8309; b) K. D. Karlin, N. Wei, B. Jung, S. Kaderli, A. D. Zuberbuehler, *J. Am. Chem. Soc.* **1991**, *113*, 5868-5870; c) M. Mahroof-Tahir, K. D. Karlin, *J. Am. Chem. Soc.* **1992**, *114*, 7599-7601; d) K. D. Karlin, N. Wei, B. Jung, S. Kaderli, P. Niklaus, A. D. Zuberbuehler, *J. Am. Chem. Soc.* **1993**, *115*, 9506-9514; e) K. Fujisawa, M. Tanaka, Y. Moro-oka, N. Kitajima, *J. Am. Chem. Soc.* **1994**, *116*, 12079-12080; f) M. Becker, F. W. Heinemann, S. Schindler, *Chem. Eur. J.* **1999**, *5*, 3124-3129; g) P. Chaudhuri, M. Hess, T.

- Weyhermuller, K. Wieghardt, *Angew. Chem. Int. Ed.* **1999**, *38*, 1095-1098; h) P. Chen, D. E. Root, C. Campochiaro, K. Fujisawa, E. I. Solomon, *J. Am. Chem. Soc.* **2003**, *125*, 466-474; i) B. A. Jazdzewski, A. M. Reynolds, P. L. Holland, V. G. Young, S. Kaderli, A. D. Zuberbühler, W. B. Tolman, *J. Biol. Inorg. Chem.* **2003**, *8*, 381-393; j) M. Weitzer, S. Schindler, G. Brehm, S. Schneider, E. Hörmann, B. Jung, S. Kaderli, A. D. Zuberbühler, *Inorg. Chem.* **2003**, *42*, 1800-1806; k) C. X. Zhang, S. Kaderli, M. Costas, E.-i. Kim, Y.-M. Neuhold, K. D. Karlin, A. D. Zuberbühler, *Inorg. Chem.* **2003**, *42*, 1807-1824; l) K. Komiyama, H. Furutachi, S. Nagatomo, A. Hashimoto, H. Hayashi, S. Fujinami, M. Suzuki, T. Kitagawa, *Bull. Chem. Soc. Jpn.* **2004**, *77*, 59-72; m) M. Schatz, V. Raab, S. P. Foxon, G. Brehm, S. Schneider, M. Reiher, M. C. Holthausen, J. Sundermeyer, S. Schindler, *Angew. Chem. Int. Ed.* **2004**, *43*, 4360-4363; n) V. V. Smirnov, J. P. Roth, *J. Am. Chem. Soc.* **2006**, *128*, 3683-3695; o) M. P. Lanci, V. V. Smirnov, C. J. Cramer, E. V. Gauchenova, J. Sundermeyer, J. P. Roth, *J. Am. Chem. Soc.* **2007**, *129*, 14697-14709; p) D. Maiti, H. C. Fry, J. S. Woertink, M. A. Vance, E. I. Solomon, K. D. Karlin, *J. Am. Chem. Soc.* **2007**, *129*, 264-265; q) A. Kunishita, M. Kubo, H. Sugimoto, T. Ogura, K. Sato, T. Takui, S. Itoh, *J. Am. Chem. Soc.* **2009**, *131*, 2788-2789; r) N. W. Aboeella, E. A. Lewis, A. M. Reynolds, W. W. Brennessel, C. J. Cramer, W. B. Tolman, *J. Am. Chem. Soc.* **2002**, *124*, 10660-10661; s) N. W. Aboeella, S. V. Kryatov, B. F. Gherman, W. W. Brennessel, V. G. Young, R. Sarangi, E. V. Rybak-Akimova, K. O. Hodgson, B. Hedman, E. I. Solomon, C. J. Cramer, W. B. Tolman, *J. Am. Chem. Soc.* **2004**, *126*, 16896-16911; t) A. M. Reynolds, B. F. Gherman, C. J. Cramer, W. B. Tolman, *Inorg. Chem.* **2005**, *44*, 6989-6997; u) C. Würtele, E. Gaoutchenova, K. Harms, M. C. Holthausen, J. Sundermeyer, S. Schindler, *Angew. Chem. Int. Ed.* **2006**, *45*, 3867-3869; v) N. W. Aboeella, B. F. Gherman, L. M. R. Hill, J. T. York, N. Holm, V. G. Young, C. J. Cramer, W. B. Tolman, *J. Am. Chem. Soc.* **2006**, *128*, 3445-3458.
- [28] A. Wada, M. Harata, K. Hasegawa, K. Jitsukawa, H. Masuda, M. Mukai, T. Kitagawa, H. Einaga, *Angew. Chem. Int. Ed.* **1998**, *37*, 798-799.
- [29] a) R. R. Smardzewski, L. Andrews, *J. Chem. Phys.* **1972**, *57*, 1327-1333; b) L. Andrews, R. R. Smardzewski, *J. Chem. Phys.* **1973**, *58*, 2258-2261.
- [30] D. J. E. Spencer, N. W. Aboeella, A. M. Reynolds, P. L. Holland, W. B. Tolman, *J. Am. Chem. Soc.* **2002**, *124*, 2108-2109.
- [31] A. M. Reynolds, E. A. Lewis, N. W. Aboeella, W. B. Tolman, *Chem. Commun.* **2005**, 2014-2016.
- [32] D. Maiti, D.-H. Lee, K. Gaoutchenova, C. Würtele, M. C. Holthausen, A. A. Narducci Sarjeant, J. Sundermeyer, S. Schindler, K. D. Karlin, *Angew. Chem. Int. Ed.* **2008**, *47*, 82-85.
- [33] a) T. Ohta, T. Tachiyama, K. Yoshizawa, T. Yamabe, T. Uchida, T. Kitagawa, *Inorg. Chem.* **2000**, *39*, 4358-4369; b) H. Ohtsu, S. Itoh, S. Nagatomo, T. Kitagawa, S. Ogo, Y. Watanabe, S. Fukuzumi, *Chem. Commun.* **2000**, 1051-1052; c) M. Kodera, T. Kita, I. Miura, N. Nakayama, T. Kawata, K. Kano, S. Hirota, *J. Am. Chem. Soc.* **2001**, *123*, 7715-7716; d) H. Ohtsu, S. Itoh, S. Nagatomo, T. Kitagawa, S. Ogo, Y. Watanabe, S. Fukuzumi, *Inorg. Chem.* **2001**, *40*, 3200-3207; e) T. Osako, S. Nagatomo, Y. Tachi, T. Kitagawa, S. Itoh, *Angew. Chem. Int. Ed.* **2002**, *41*, 4325-4328; f) T. Fujii, A. Naito, S. Yamaguchi, A. Wada, Y. Funahashi, K. Jitsukawa, S.

- Nagatomo, T. Kitagawa, H. Masuda, *Chem. Commun.* **2003**, 2700-2701; g) S. Yamaguchi, S. Nagatomo, T. Kitagawa, Y. Funahashi, T. Ozawa, K. Jitsukawa, H. Masuda, *Inorg. Chem.* **2003**, *42*, 6968-6970; h) S. Yamaguchi, A. Wada, S. Nagatomo, T. Kitagawa, K. Jitsukawa, H. Masuda, *Chem. Lett.* **2004**, *33*, 1556-1557; i) K. Itoh, H. Hayashi, H. Furutachi, T. Matsumoto, S. Nagatomo, T. Tosha, S. Terada, S. Fujinami, M. Suzuki, T. Kitagawa, *J. Am. Chem. Soc.* **2005**, *127*, 5212-5223; j) T. Osako, S. Nagatomo, T. Kitagawa, C. Cramer, S. Itoh, *J. Biolog. Inorg. Chem.* **2005**, *10*, 581-590; k) S. Yamaguchi, A. Kumagai, S. Nagatomo, T. Kitagawa, Y. Funahashi, T. Ozawa, K. Jitsukawa, H. Masuda, *Bull. Chem. Soc. Jpn.* **2005**, *78*, 116-124; l) L. E. Cheruzel, M. R. Cecil, S. E. Edison, M. S. Mashuta, M. J. Baldwin, R. M. Buchanan, *Inorg. Chem.* **2006**, *45*, 3191-3202; m) D. Maiti, H. R. Lucas, A. A. N. Sarjeant, K. D. Karlin, *J. Am. Chem. Soc.* **2007**, *129*, 6998-6999; n) D. Maiti, A. A. Narducci Sarjeant, K. D. Karlin, *J. Am. Chem. Soc.* **2007**, *129*, 6720-6721; o) D. Maiti, A. A. Narducci Sarjeant, K. D. Karlin, *Inorg. Chem.* **2008**, *47*, 8736-8747; p) T. Kamachi, Y.-M. Lee, T. Nishimi, J. Cho, K. Yoshizawa, W. Nam, *J. Phys. Chem. A* **2008**, *112*, 13102-13108.
- [34] a) P. Capdevielle, M. Maumy, *Tetrahedron Lett.* **1982**, *23*, 1573-1576; b) M. Reglier, E. Amadei, R. Tadayoni, B. Waegell, *J. Chem. Soc., Chem. Commun.* **1989**, 447-450; c) P. Capdevielle, D. Sparfel, J. Baranne-Lafont, N. K. Cuong, M. Maumy, *J. Chem. Soc., Chem. Commun.* **1990**, 565-566; d) O. Renaud, P. Capdevielle, M. Maumy, *J. Chem. Soc., Chem. Commun.* **1990**, 566-568; e) O. Renaud, P. Capdevielle, M. Maumy, *J. Mol. Catal.* **1991**, *68*, L13-L15; f) G. Rousselet, P. Capdevielle, M. Maumy, *Tetrahedron Lett.* **1995**, *36*, 4999-5002; g) W. Buijs, P. Comba, D. Corneli, H. Pritzkow, *J. Organomet. Chem.* **2002**, *641*, 71-80; h) P. Comba, S. Knoppe, B. Martin, G. Rajaraman, C. Rolli, B. Shapiro, T. Stork, *Chem. Eur. J.* **2008**, *14*, 344-357; i) S. Hong, S. M. Huber, L. Gagliardi, C. C. Cramer, W. B. Tolman, *J. Am. Chem. Soc.* **2007**, *129*, 14190-14192; j) S. Hong, A. K. Gupta, W. B. Tolman, *Inorg. Chem.* **2009**, *48*, 6323-6325.
- [35] D. Schröder, M. C. Holthausen, H. Schwarz, *J. Phys. Chem. B* **2004**, *108*, 14407-14416.
- [36] a) N. Kitajima, T. Katayama, K. Fujisawa, Y. Iwata, Y. Morooka, *J. Am. Chem. Soc.* **1993**, *115*, 7872-7873; b) A. Kunishita, H. Ishimaru, S. Nakashima, T. Ogura, S. Itoh, *J. Am. Chem. Soc.* **2008**, *130*, 4244-4245.
- [37] a) A. Kunishita, J. Teraoka, J. D. Scanlon, T. Matsumoto, M. Suzuki, C. J. Cramer, S. Itoh, *J. Am. Chem. Soc.* **2007**, *129*, 7248-7249; b) A. Kunishita, J. D. Scanlon, H. Ishimaru, K. Honda, T. Ogura, M. Suzuki, C. J. Cramer, S. Itoh, *Inorg. Chem.* **2008**, *47*, 8222-8232.
- [38] a) S. Itoh, S. Fukuzumi, *Bull. Chem. Soc. Jpn.* **2002**, *75*, 2081-2095; b) W. B. Tolman, *Acc. Chem. Res.* **1997**, *30*, 227-237; c) T. N. Sorrell, *Tetrahedron* **1989**, *45*, 3-68; d) Z. Tyeklar, K. D. Karlin, *Acc. Chem. Res.* **1989**, *22*, 241-248; e) E. I. Solomon, F. Tuczek, D. E. Root, C. A. Brown, *Chem. Rev.* **1994**, *94*, 827-856; f) H.-C. Liang, M. Dahan, K. D. Karlin, *Curr. Opin. Chem. Biol.* **1999**, *3*, 168-175; g) C. Zhang, H.-C. Liang, K. Humphreys, K. Karlin, in *Advances in Catalytic Activation of Dioxygen by Metal Complexes, Vol. 26* (Ed.: L. Simándi), Springer US, **2002**, pp. 79-121; h) S. Itoh, in *Comprehensive Coordination Chemistry II* (Eds.: L. Que, W. B. Tolman), Elsevier, Amsterdam, **2004**, pp. 369-393; i) S. Itoh, Y. Tachi, *Dalton Trans.*

- 2006, 4531-4538; j) S. Itoh, S. Fukuzumi, *Acc. Chem. Res.* **2007**, *40*, 592-600; k) M. Kodera, K. Kano, *Bull. Chem. Soc. Jpn.* **2007**, *80*, 662-676; l) M. Suzuki, *Acc. Chem. Res.* **2007**, *40*, 609-617.
- [39] R. R. Jacobson, Z. Tyeklar, A. Farooq, K. D. Karlin, S. Liu, J. Zubieta, *J. Am. Chem. Soc.* **1988**, *110*, 3690-3692.
- [40] M. J. Baldwin, P. K. Ross, J. E. Pate, Z. Tyeklar, K. D. Karlin, E. I. Solomon, *J. Am. Chem. Soc.* **1991**, *113*, 8671-8679.
- [41] a) L. Q. Hatcher, D.-H. Lee, M. A. Vance, A. E. Milligan, R. Sarangi, K. O. Hodgson, B. Hedman, E. I. Solomon, K. D. Karlin, *Inorg. Chem.* **2006**, *45*, 10055-10057; b) D.-H. Lee, L. Q. Hatcher, M. A. Vance, R. Sarangi, A. E. Milligan, A. A. Narducci Sarjeant, C. D. Incarvito, A. L. Rheingold, K. O. Hodgson, B. Hedman, E. I. Solomon, K. D. Karlin, *Inorg. Chem.* **2007**, *46*, 6056-6068; c) S. Yamaguchi, A. Wada, Y. Funahashi, S. Nagatomo, T. Kitagawa, K. Jitsukawa, H. Masuda, *Eur. J. Inorg. Chem.* **2003**, *2003*, 4378-4386; d) I. Koval, C. Belle, K. Selmeczi, C. Philouze, E. Saint-Aman, A. Schuitema, P. Gamez, J.-L. Pierre, J. Reedijk, *J. Biolog. Inorg. Chem.* **2005**, *10*, 739-750; e) D. Maiti, J. S. Woertink, A. A. Narducci Sarjeant, E. I. Solomon, K. D. Karlin, *Inorg. Chem.* **2008**, *47*, 3787-3800; f) Y. Lee, G. Y. Park, H. R. Lucas, P. L. Vajda, K. Kamaraj, M. A. Vance, A. E. Milligan, J. S. Woertink, M. A. Siegler, A. A. Narducci Sarjeant, L. N. Zakharov, A. L. Rheingold, E. I. Solomon, K. D. Karlin, *Inorg. Chem.* **2009**, *48*, 11297-11309.
- [42] C. Wurtele, O. Sander, V. Lutz, T. Waitz, F. Tuzcek, S. Schindler, *J. Am. Chem. Soc.* **2009**, *131*, 7544-7545.
- [43] I. Garcia-Bosch, A. Company, J. R. Frisch, M. Torrent-Sucarrat, M. Cardellach, I. Gamba, M. Güell, L. Casella, L. Que, X. Ribas, J. M. Luis, M. Costas, *Angew. Chem. Int. Ed.* **2010**, *49*, 2406-2409.
- [44] N. Kitajima, K. Fujisawa, Y. Morooka, K. Toriumi, *J. Am. Chem. Soc.* **1989**, *111*, 8975-8976.
- [45] a) M. Kodera, K. Katayama, Y. Tachi, K. Kano, S. Hirota, S. Fujinami, M. Suzuki, *J. Am. Chem. Soc.* **1999**, *121*, 11006-11007; b) Z. Hu, G. N. George, S. M. Gorun, *Inorg. Chem.* **2001**, *40*, 4812-4813; c) M. Kodera, Y. Kajita, Y. Tachi, K. Katayama, K. Kano, S. Hirota, S. Fujinami, M. Suzuki, *Angew. Chem.* **2004**, *116*, 338-341; d) Y. Funahashi, T. Nishikawa, Y. Wasada-Tsutsui, Y. Kajita, S. Yamaguchi, H. Arii, T. Ozawa, K. Jitsukawa, T. Tosha, S. Hirota, T. Kitagawa, H. Masuda, *J. Am. Chem. Soc.* **2008**, *130*, 16444-16445; e) B. M. T. Lam, J. A. Halfen, V. G. Young, J. R. Hagadorn, P. L. Holland, A. Lledo's, L. Cucurull-Sa'nchez, J. J. Novoa, S. Alvarez, W. B. Tolman, *Inorg. Chem.* **2000**, *39*, 4059-4072.
- [46] a) K. D. Karlin, P. L. Dahlstrom, S. N. Cozzette, P. M. Scensny, J. Zubieta, *J. Chem. Soc. Chem. Commun.* **1981**, *0*, 881-882; b) K. D. Karlin, Y. Gultneh, J. P. Hutchinson, J. Zubieta, *J. Am. Chem. Soc.* **1982**, *104*, 5240-5242; c) K. D. Karlin, J. C. Hayes, Y. Gultneh, R. W. Cruse, J. W. McKown, J. P. Hutchinson, J. Zubieta, *J. Am. Chem. Soc.* **1984**, *106*, 2121-2128.
- [47] K. D. Karlin, M. S. Nasir, B. I. Cohen, R. W. Cruse, S. Kaderli, A. D. Zuberbuehler, *J. Am. Chem. Soc.* **1994**, *116*, 1324-1336.
- [48] E. Pidcock, H. V. Obias, C. X. Zhang, K. D. Karlin, E. I. Solomon, *J. Am. Chem. Soc.* **1998**, *120*, 7841-7847.
- [49] M. S. Nasir, B. I. Cohen, K. D. Karlin, *J. Am. Chem. Soc.* **1992**, *114*, 2482-2494.

- [50] R. A. Sheldon, J. K. Kochi, *Metal-catalyzed oxidations of organic compounds*, Academic Press, New York, **1981**.
- [51] a) L. Casella, E. Monzani, M. Gullotti, D. Cavagnino, G. Cerina, L. Santagostini, R. Ugo, *Inorg. Chem.* **1996**, *35*, 7516-7525; b) L. Santagostini, M. Gullotti, E. Monzani, L. Casella, R. Dillinger, F. Tucek, *Chem. Eur. J.* **2000**, *6*, 519-522.
- [52] E. Monzani, L. Quinti, A. Perotti, L. Casella, M. Gullotti, L. Randaccio, S. Geremia, G. Nardin, P. Faleschini, G. Tabbi, *Inorg. Chem.* **1998**, *37*, 553-562.
- [53] a) K. D. Karlin, B. I. Cohen, R. R. Jacobson, J. Zubietta, *J. Am. Chem. Soc.* **1987**, *109*, 6194-6196; b) J. E. Pate, R. W. Cruse, K. D. Karlin, E. I. Solomon, *J. Am. Chem. Soc.* **1987**, *109*, 2624-2630; c) R. W. Cruse, S. Kaderli, C. J. Meyer, A. D. Zuberbühler, K. D. Karlin, *J. Am. Chem. Soc.* **1988**, *110*, 5020-5024.
- [54] S. Itoh, H. Kumei, M. Taki, S. Nagatomo, T. Kitagawa, S. Fukuzumi, *J. Am. Chem. Soc.* **2001**, *123*, 6708-6709.
- [55] G. Battaini, M. D. Carolis, E. Monzani, F. Tucek, L. Casella, *Chem. Commun.* **2003**, 726-727.
- [56] J. A. Halfen, S. Mahapatra, E. C. Wilkinson, S. Kaderli, V. G. Young, L. Que, A. D. Zuberbühler, W. B. Tolman, *Science* **1996**, *271*, 1397-1400.
- [57] a) S. Mahapatra, J. A. Halfen, E. C. Wilkinson, G. Pan, X. Wang, V. G. Young, C. J. Cramer, L. Que, W. B. Tolman, *J. Am. Chem. Soc.* **1996**, *118*, 11555-11574; b) V. Mahadevan, Z. Hou, A. P. Cole, D. E. Root, T. K. Lal, E. I. Solomon, T. D. P. Stack, *J. Am. Chem. Soc.* **1997**, *119*, 11996-11997; c) S. Mahapatra, V. G. Young, S. Kaderli, A. D. Zuberbühler, W. B. Tolman, *Angew. Chem. Int. Ed.* **1997**, *36*, 130-133; d) H. Hayashi, S. Fujinami, S. Nagatomo, S. Ogo, M. Suzuki, A. Uehara, Y. Watanabe, T. Kitagawa, *J. Am. Chem. Soc.* **2000**, *122*, 2124-2125; e) B. F. Straub, F. Rominger, P. Hofmann, *Chem. Commun.* **2000**, 1611-1612; f) M. Mizuno, H. Hayashi, S. Fujinami, H. Furutachi, S. Nagatomo, S. Otake, K. Uozumi, M. Suzuki, T. Kitagawa, *Inorg. Chem.* **2003**, *42*, 8534-8544.
- [58] X. Ottenwaelder, D. J. Rudd, M. C. Corbett, K. O. Hodgson, B. Hedman, T. D. P. Stack, *J. Am. Chem. Soc.* **2006**, *128*, 9268-9269.
- [59] P. L. Holland, K. R. Rodgers, W. B. Tolman, *Angew. Chem. Int. Ed.* **1999**, *38*, 1139-1142.
- [60] L. M. Mirica, M. Vance, D. J. Rudd, B. Hedman, K. O. Hodgson, E. I. Solomon, T. D. P. Stack, *Science* **2005**, *308*, 1890-1892.
- [61] S. Herres-Pawlis, P. Verma, R. Haase, P. Kang, C. T. Lyons, E. C. Wasinger, U. Flörke, G. Henkel, T. D. P. Stack, *J. Am. Chem. Soc.* **2009**, *131*, 1154-1169.
- [62] a) M. Rolff, J. Schottenheim, G. Peters, F. Tucek, *Angew. Chem. Int. Ed.* **2010**, *49*, 6438-6442; b) J. Schottenheim, N. Fateeva, W. Thimm, J. Krahmer, F. Tucek, *Z. Anorg. Allg. Chem.* **2013**, *639*, 1491-1497; c) J. N. Hamann, F. Tucek, *Chem. Commun.* **2014**, *50*, 2298-2300.
- [63] S. Mahapatra, J. A. Halfen, W. B. Tolman, *J. Am. Chem. Soc.* **1996**, *118*, 11575-11586.
- [64] a) S. Itoh, M. Taki, H. Nakao, P. L. Holland, W. B. Tolman, L. Que, S. Fukuzumi, *Angew. Chem. Int. Ed.* **2000**, *39*, 398-400; b) S. Itoh, T. Kondo, M. Komatsu, Y. Ohshiro, C. Li, N. Kanehisa, Y. Kai, S. Fukuzumi, *J. Am. Chem. Soc.* **1995**, *117*, 4714-4715; c) S. Itoh, H. Nakao, L. M. Berreau, T. Kondo, M. Komatsu, S. Fukuzumi, *J. Am. Chem. Soc.* **1998**, *120*, 2890-2899.

- [65] I. Blain, M. Giorgi, I. De Riggi, M. Réglie, *Eur. J. Inorg. Chem.* **2001**, 205-211.
- [66] I. Blain, M. Giorgi, I. De Riggi, M. Réglie, *Eur. J. Inorg. Chem.* **2000**, 393-398.
- [67] a) A. Magyar, B. Schönecker, J. Wölfling, G. Schneider, W. Günther, H. Görls, *Tetrahedron: Asymmetry* **2003**, *14*, 1925-1934; b) H. Arii, Y. Saito, S. Nagatomo, T. Kitagawa, Y. Funahashi, K. Jitsukawa, H. Masuda, *Chem. Lett.* **2003**, *32*, 156-157.
- [68] a) B. Schönecker, T. Zheldakova, Y. Liu, M. Kötteritzsch, W. Günther, H. Görls, *Angew. Chem. Int. Ed.* **2003**, *42*, 3240-3244; b) B. Schönecker, T. Zheldakova, C. Lange, W. Günther, H. Görls, M. Bohl, *Chem. Eur. J.* **2004**, *10*, 6029-6042; c) B. Schönecker, C. Lange, T. Zheldakova, W. Günther, H. Görls, G. Vaughan, *Tetrahedron* **2005**, *61*, 103-114; d) B. Schönecker, C. Lange, *J. Organomet. Chem.* **2006**, *691*, 2107-2124.
- [69] a) K. C. Fortner, D. Kato, Y. Tanaka, M. D. Shair, *J. Am. Chem. Soc.* **2009**, *132*, 275-280; b) A. Giannis, P. Heretsch, V. Sarli, A. Stöbel, *Angew. Chem. Int. Ed.* **2009**, *48*, 7911-7914.
- [70] Y. Y. See, A. T. Herrmann, Y. Aihara, P. S. Baran, *J. Am. Chem. Soc.* **2015**, *137*, 13776-13779.
- [71] a) I. N. Levine, *Quantum Chemistry*, 5th ed., Prentice Hall New Jersey, **1999**; b) C. J. Cramer, *Essentials of Computational Chemistry*, 2nd ed., John Wiley & Sons Ltd, West Sussex, England, **2002**; c) W. Koch, M. C. Holthausen, *A Chemist's Guide to Density Functional Theory*, 2nd ed., Wiley-VCH Verlag GmbH, Weinheim, Germany, **2001**; d) K. Burke, *J. Chem. Phys.* **2012**, *136*, 150901-150909; e) C. J. Cramer, D. G. Truhlar, *Phys. Chem. Chem. Phys.* **2009**, *11*, 10757-10816; f) A. C. Tsipis, *Coord. Chem. Rev.* **2014**, *272*, 1-29; g) P. Politzer, J. M. Seminario, *Modern Density Theory: A Tool for Chemistry*, Elsevier Science B.V., Amsterdam, The Netherlands, **1995**; h) F. Nogueira, A. Castro, M. L. Marques, in *A Primer in Density Functional Theory*, Vol. 620 (Eds.: C. Fiolhais, F. Nogueira, M. L. Marques), Springer Berlin Heidelberg, **2003**, pp. 218-256; i) P. Geerlings, F. De Proft, W. Langenaeker, *Chem. Rev.* **2003**, *103*, 1793-1874.
- [72] O. Sander, A. Henß, C. Näther, C. Würtele, M. C. Holthausen, S. Schindler, F. Tuczek, *Chem. Eur. J.* **2008**, *14*, 9714-9729.
- [73] Y. F. Liu, J. G. Yu, P. E. M. Siegbahn, M. R. A. Blomberg, *Chem. Eur. J.* **2013**, *19*, 1942-1954.
- [74] P. Spuhler, M. C. Holthausen, *Angew. Chem. Int. Ed.* **2003**, *42*, 5961-5965.
- [75] a) L. M. Mirica, M. Vance, D. J. Rudd, B. Hedman, K. O. Hodgson, E. I. Solomon, T. D. P. Stack, *J. Am. Chem. Soc.* **2002**, *124*, 9332-9333; b) M. Becker, S. Schindler, K. D. Karlin, T. A. Kaden, S. Kaderli, T. Palanché, A. D. Zuberbühler, *Inorg. Chem.* **1999**, *38*, 1989-1995.
- [76] a) M. Rolff, J. N. Hamann, F. Tuczek, *Angew. Chem. Int. Ed.* **2011**, *50*, 6924-6927; b) P. Kang, E. Bobyr, J. Dustman, K. O. Hodgson, B. Hedman, E. I. Solomon, T. D. P. Stack, *Inorg. Chem.* **2010**, *49*, 11030-11038; c) I. Blain, P. Bruno, M. Giorgi, E. Lojou, D. Lexa, M. Réglie, *Eur. J. Inorg. Chem.* **1998**, 1297-1304; d) I. Blain, M. Pierrot, M. Giorgi, M. Réglie, *C. R. Acad. Sci. Paris Sér. IIC, Chimie* **2001**, *4*, 1-10; e) S. Herres, A. J. Heuwing, U. Flörke, J. Schneider, G. Henkel, *Inorg. Chim. Acta* **2005**, *358*, 1089-1095; f) A. P. Cole, V. Mahadevan, L. M. Mirica, X. Ottenwaelder, T. D. P. Stack, *Inorg. Chem.* **2005**, *44*, 7345-7364; g) T. Matsumoto, K. Ohkubo, K. Honda, A. Yazawa, H. Furutachi, S. Fujinami, S. Fukuzumi, M. Suzuki, *J. Am. Chem.*

- Soc.* **2009**, *131*, 9258-9267; h) J. Shearer, C. X. Zhang, L. Q. Hatcher, K. D. Karlin, *J. Am. Chem. Soc.* **2003**, *125*, 12670-12671; i) R. Haase, T. Beschnitt, U. Flörke, S. Herres-Pawlis, *Inorg. Chim. Acta* **2011**, *374*, 546-557.
- [77] a) J. Cahoy, P. L. Holland, W. B. Tolman, *Inorg. Chem.* **1999**, *38*, 2161-2168; b) H.-C. Liang, M. J. Henson, L. Q. Hatcher, M. A. Vance, C. X. Zhang, D. Lahti, S. Kaderli, R. D. Sommer, A. L. Rheingold, A. D. Zuberbühler, E. I. Solomon, K. D. Karlin, *Inorg. Chem.* **2004**, *43*, 4115-4117.
- [78] L. M. Mirica, D. J. Rudd, M. A. Vance, E. I. Solomon, K. O. Hodgson, B. Hedman, T. D. P. Stack, *J. Am. Chem. Soc.* **2006**, *128*, 2654-2665.
- [79] C. J. Cramer, M. Wloch, P. Piecuch, C. Puzzarini, L. Gagliardi, *J. Phys. Chem. A* **2006**, *110*, 1991-2004.
- [80] P. E. M. Siegbahn, M. R. A. Blomberg, S.-L. Chen, *J. Chem. Theory Comput.* **2010**, *6*, 2040-2044.
- [81] D. G. Liakos, F. Neese, *J. Chem. Theory Comput.* **2011**, *7*, 1511-1523.
- [82] B. F. Gherman, C. J. Cramer, *Coord. Chem. Rev.* **2009**, *253*, 723-753.
- [83] a) T. Ziegler, A. Rauk, E. J. Baerends, *Theor. Chim. Acta* **1977**, *43*, 261-271; b) L. Noodleman, J. Joe G. Norman, *J. Chem. Phys.* **1979**, *70*, 4903-4906; c) L. Noodleman, *J. Chem. Phys.* **1981**, *74*, 5737-5743; d) L. Noodleman, E. R. Davidson, *Chem. Phys.* **1986**, *109*, 131-143; e) K. Yamaguchi, F. Jensen, A. Dorigo, K. N. Houk, *Chem. Phys. Lett.* **1988**, *149*, 537-542; f) L. Noodleman, D. A. Case, C. Richard, in *Adv. Inorg. Chem., Vol. Volume 38*, Academic Press, **1992**, pp. 423-470.
- [84] a) H.-J. Werner, P. J. Knowles, *J. Chem. Phys.* **1988**, *89*, 5803-5814; b) P. J. Knowles, H. J. Werner, *Chem. Phys. Lett.* **1988**, *145*, 514-522.
- [85] a) K. Kowalski, P. Piecuch, *J. Chem. Phys.* **2000**, *113*, 18-35; b) P. Piecuch, K. Kowalski, I. S. O. Pimienta, P. D. Fan, M. Lodriguito, M. J. McGuire, S. A. Kucharski, T. Kuś, M. Musiał, *Theor. Chem. Acc.* **2004**, *112*, 349-393; c) P. Piecuch, M. Wloch, J. R. Gour, A. Kinal, *Chem. Phys. Lett.* **2006**, *418*, 467-474.
- [86] a) F. Neese, A. Hansen, D. G. Liakos, *J. Chem. Phys.* **2009**, *131*; b) D. G. Liakos, A. Hansen, F. Neese, *J. Chem. Theory Comput.* **2010**, *7*, 76-87.
- [87] M. Reiher, O. Salomon, B. Artur Hess, *Theor. Chem. Acc.* **2001**, *107*, 48-55.
- [88] A. Hoffmann, S. Herres-Pawlis, *Chem. Commun.* **2014**, *50*, 403-405.
- [89] a) C. Lee, W. Yang, R. G. Parr, *Phys. Rev. B* **1988**, *37*, 785-789; b) A. D. Becke, *Phys. Rev. A* **1988**, *38*, 3098-3100; c) P. J. Stephens, F. J. Devlin, C. F. Chabalowski, M. J. Frisch, *J. Phys. Chem.* **1994**, *98*, 11623-11627; d) A. D. Becke, *J. Chem. Phys.* **1993**, *98*, 5648-5652; e) S. Grimme, *J. Comput. Chem.* **2006**, *27*, 1787-1799.
- [90] P. J. Hay, W. R. Wadt, *J. Chem. Phys.* **1985**, *82*, 270-283.
- [91] T. H. Dunning Jr., P. J. Hay, in *Modern Theoretical Chemistry* (Ed.: H. F. Schaefer III), Plenum, New York, **1976**, pp. 1-28.
- [92] M. J. Frisch, G. W. Trucks, H. B. Schlegel, G. E. Scuseria, M. A. Robb, J. R. Cheeseman, G. Scalmani, V. Barone, B. Mennucci, G. A. Petersson, H. Nakatsuji, M. Caricato, X. Li, H. P. Hratchian, A. F. Izmaylov, J. Bloino, G. Zheng, J. L. Sonnenberg, M. Hada, M. Ehara, K. Toyota, R. Fukuda, J. Hasegawa, M. Ishida, T. Nakajima, Y. Honda, O. Kitao, H. Nakai, T. Vreven, J. A. Montgomery Jr., J. E. Peralta, F. Ogliaro, M. Bearpark, J. J. Heyd, E. Brothers, K. N. Kudin, V. N. Staroverov, T. Keith, R. Kobayashi, J. Normand, K. Raghavachari, A. Rendell, J. C. Burant, S. S. Iyengar, J. Tomasi, M. Cossi, N. Rega, J. M. Millam, M. Klene, J. E.

- Knox, J. B. Cross, V. Bakken, C. Adamo, J. Jaramillo, R. Gomperts, R. E. Stratmann, O. Yazyev, A. J. Austin, R. Cammi, C. Pomelli, J. W. Ochterski, R. L. Martin, K. Morokuma, V. G. Zakrzewski, G. A. Voth, P. Salvador, J. J. Dannenberg, S. Dapprich, A. D. Daniels, O. Farkas, J. B. Foresman, J. V. Ortiz, J. Cioslowski, D. J. Fox, *Gaussian 09, Revision A.02*, Gaussian, Inc., Wallingford, CT, **2009**.
- [93] F. Neese, U. Becker, D. Bykov, D. Ganyushin, A. Hansen, R. Izsak, D. G. Liakos, C. Kollmar, S. Kossmann, D. A. Pantazis, T. Petrenko, C. Reimann, C. Riplinger, M. Roemelt, B. Sandhöfer, I. Schapiro, K. Sivalingam, B. Wezislá, *ORCA - An ab initio, DFT and semiempirical SCF-MO package, Version 2.9*, MPI for Chemical Energy Conversion, Mülheim, Germany, **2012**.
- [94] S. Grimme, J. Antony, S. Ehrlich, H. Krieg, *J. Chem. Phys.* **2010**, *132*, 154104-154119.
- [95] B. Miehlich, A. Savin, H. Stoll, H. Preuss, *Chem. Phys. Lett.* **1989**, *157*, 200-206.
- [96] J. P. Perdew, K. Burke, M. Ernzerhof, *Phys. Rev. Lett.* **1996**, *77*, 3865-3868.
- [97] Y. Zhang, W. Yang, *Phys. Rev. Lett.* **1998**, *80*, 890-890.
- [98] J. Tao, J. P. Perdew, V. N. Staroverov, G. E. Scuseria, *Phys. Rev. Lett.* **2003**, *91*, 146401.
- [99] a) C. Adamo, M. Ernzerhof, G. E. Scuseria, *J. Chem. Phys.* **2000**, *112*, 2643-2649; b) M. Ernzerhof, G. E. Scuseria, *J. Chem. Phys.* **1999**, *110*, 5029-5036.
- [100] L. Goerigk, S. Grimme, *Phys. Chem. Chem. Phys.* **2011**, *13*, 6670-6688.
- [101] V. N. Staroverov, G. E. Scuseria, J. Tao, J. P. Perdew, *J. Chem. Phys.* **2003**, *119*, 12129-12137.
- [102] S. Grimme, *J. Phys. Chem. A* **2005**, *109*, 3067-3077.
- [103] M. Dolg, U. Wedig, H. Stoll, H. Preuss, *J. Chem. Phys.* **1987**, *86*, 866-872.
- [104] a) E. v. Lenthe, E. J. Baerends, J. G. Snijders, *J. Chem. Phys.* **1993**, *99*, 4597-4610; b) E. v. Lenthe, J. G. Snijders, E. J. Baerends, *J. Chem. Phys.* **1996**, *105*, 6505-6516; c) C. v. Wüllen, *J. Chem. Phys.* **1998**, *109*, 392-399.
- [105] a) B. A. Hess, *Phys. Rev. A* **1986**, *33*, 3742-3748; b) G. Jansen, B. A. Hess, *Phys. Rev. A* **1989**, *39*, 6016-6017; c) B. A. Hess, C. M. Marian, in *Computational Molecular Spectroscopy* (Eds.: P. Jensen, P. R. Bunker), Wiley, New York, **2000**, p. 169; d) A. Wolf, M. Reiher, B. A. Hess, in *Relativistic Quantum Chemistry, Theoretical and Computational Chemistry, Vol. 1* (Ed.: P. Schwerdtfeger), Elsevier, Amsterdam, **2002**, p. 622; e) A. Wolf, M. Reiher, B. A. Hess, in *Recent Advances in Relativistic Molecular Theory* (Eds.: K. Hirao, Y. Ishikawa), World Scientific, Singapore, **2004**, p. 137.
- [106] a) K. Yamaguchi, Y. Takahara, T. Fueno, in *Applied Quantum Chemistry* (Ed.: V. H. Smith), Reidel, Dordrecht, **1986**, p. 155; b) T. Soda, Y. Kitagawa, T. Onishi, Y. Takano, Y. Shigeta, H. Nagao, Y. Yoshioka, K. Yamaguchi, *Chem. Phys. Lett.* **2000**, *319*, 223-230.
- [107] a) A. Schäfer, H. Horn, R. Ahlrichs, *J. Chem. Phys.* **1992**, *97*, 2571-2577; b) F. Weigend, R. Ahlrichs, *Phys. Chem. Chem. Phys.* **2005**, *7*, 3297-3305.
- [108] D. A. Pantazis, X.-Y. Chen, C. R. Landis, F. Neese, *J. Chem. Theoy Comput.* **2008**, *4*, 908-919.
- [109] a) R. A. Kendall, H. A. Früchtl, *Theor. Chem. Acc.* **1997**, *97*, 158-163; b) K. Eichkorn, O. Treutler, H. Öhm, M. Häser, R. Ahlrichs, *Chem. Phys. Lett.* **1995**, *240*,

- 283-290; c) K. Eichkorn, F. Weigend, O. Treutler, R. Ahlrichs, *Theor. Chem. Acc.* **1997**, *97*, 119-124.
- [110] F. Neese, F. Wennmohs, A. Hansen, U. Becker, *Chem. Phys.* **2009**, *356*, 98-109.
- [111] F. Weigend, *Phys. Chem. Chem. Phys.* **2006**, *8*, 1057-1065.
- [112] A. Klamt, G. Schüürmann, *J. Chem. Soc. Perkin Trans.* **1993**, *2*, 799-805.
- [113] C. Y. Legault, *CYLview, version 1.0b*, Universitède Sherbrooke, Sherbrooke, QC **2009**, <http://www.cylview.org>.
- [114] a) B. I. Dunlap, *J. Chem. Phys.* **1983**, *78*, 3140-3142; b) B. I. Dunlap, *Theochem-J. Mol. Struct.* **2000**, *529*, 37-40.
- [115] J. I. Seeman, *Chem. Rev.* **1983**, *83*, 83-134.
- [116] J. Becker, P. Gupta, F. Angersbach, F. Tuzek, C. Näther, M. C. Holthausen, S. Schindler, *Chem. Eur. J.* **2015**, *21*, 11735-11744.
- [117] P. L. Holland, K. R. Rodgers, W. B. Tolman, *Angew. Chem.* **1999**, *111*, 1210-1213.

Appendices

Appendix 1: Selective Aromatic Hydroxylation with Dioxygen and Simple Copper Imine Complexes.....	99
Appendix 2: Efficient Access to Substituted Silafluorenes by Nickel-Catalyzed Reactions of Biphenylenes with Et ₂ SiH ₂	109
Appendix 3: Determination of the Conformation of the 2'OH Group in RNA by NMR Spectroscopy and DFT Calculations.....	120

Peer-reviewed research articles on three different topics published during PhD are enclosed in this section. The research carried out in Appendix 1 has been presented in Chapter 3, Section 3.3. The theoretical part of Appendix 1 was done by Puneet Gupta. In Appendix 2, the theoretical study was accomplished by Puneet Gupta, Dr. Samat Tussupbayev and Dr. Martin Diefenbach. The theoretical work in Appendix 3 was done by Puneet Gupta and Sandor Tüllmann.

Hydroxylation | Hot Paper |

Selective Aromatic Hydroxylation with Dioxygen and Simple Copper Imine Complexes

 Jonathan Becker,^[a] Puneet Gupta,^[b, e] Friedrich Angersbach,^[c] Felix Tuczek,^{*,[d]}
 Christian Näther,^[d] Max C. Holthausen,^{*,[b]} and Siegfried Schindler^{*,[a]}

Dedicated to Professor Manfred Scheer on the occasion of his 60th birthday

Abstract: The formation of a bis(μ -oxido)dicopper complex with the ligand 2-(diethylaminoethyl)-6-phenylpyridine (PPN) and its subsequent hydroxylation of the pendant phenyl group (studied earlier by Holland et al., *Angew. Chem. Int. Ed.* **1999**, *38*, 1139–1142) has been reinvestigated to gain a better understanding of such systems in view of the development of new synthetic applications. To this end, we prepared a simple copper imine complex system that also affords selective *o*-hydroxylation of aromatic aldehydes by using dioxygen as the oxidant: Applying the ligand *N*-ben-

zylidene-*N,N*-diethylethylenediamine (BDED), salicylaldehyde was prepared in good yields and we show that this reaction also occurs through an intermediate bis- μ -oxido copper complex. The underlying reaction mechanism for the PPN-supported complex was studied at the BLYP-D/TZVP level of density functional theory and the results for representative stationary points along reaction paths of the BDED-supported complex reveal a closely related mechanistic scenario. The results demonstrate a new facile synthetic way to introduce OH groups into aromatic aldehydes.

Introduction

Tyrosinase, a copper enzyme, is an important monooxygenase responsible for the *o*-hydroxylation of the amino acid tyrosine.^[1] Aiming at the transfer of its function to synthetic applications, enormous research efforts over the past decades have led to the development of a vast number of bioinorganic

model systems (for selected references see refs. [1f], [2]). So far, however, only a few copper complexes have been identified that are actually able to hydroxylate organic substrates in a catalytic fashion, similar to the enzyme.^[3] In mechanistic considerations, a bimetallic, side-on peroxido dicopper complex has been accepted as the catalytically active species for a long time, until later findings in a bioinorganic model system provided evidence for a rapid peroxido/bis- μ -oxido equilibrium in solution, with a subtle influence of the particular supporting ligand environment, the solvent, and counterions on the relative thermodynamic stabilities of the individual isomers.^[4] With this equilibrium representing a low-barrier initial O–O bond-breaking step along the hydroxylation pathway, Tolman and co-workers suggested the involvement of a bis(μ -oxido) intermediate as the effective hydroxylating species in the course of aromatic C–H bond-activation processes taking place in enzymes or synthetic models. To investigate this question further, Holland et al. devised a bioinorganic model based on the ligand 2-(diethylaminoethyl)-6-phenylpyridine (PPN, Figure 1).^[5] Treating the PPN copper(I) complex with O₂ at low temperatures they observed initial formation of a bis(μ -oxido)dicopper complex followed by the subsequent hydroxylation of the pendant phenyl group even at low temperatures.

[a] J. Becker, Prof. Dr. S. Schindler
 Institut für Anorganische und Analytische Chemie
 Justus-Liebig-Universität Gießen
 Heinrich-Buff-Ring 58, 35392 Gießen (Germany)
 E-mail: siegfried.schindler@anorg.chemie.uni-giessen.de

[b] P. Gupta, Prof. Dr. M. C. Holthausen
 Institut für Anorganische und Analytische Chemie
 Johann Wolfgang Goethe-Universität Frankfurt
 Max-von-Laue-Strasse 7
 60438 Frankfurt am Main (Germany)
 E-mail: max.holthausen@chemie.uni-frankfurt.de

[c] Dr. F. Angersbach
 Universität Hamburg, Fachbereich Chemie
 Martin-Luther-King-Platz 6
 20146 Hamburg (Germany)

[d] Prof. Dr. F. Tuczek, Prof. Dr. C. Näther
 Institut für Anorganische Chemie
 Christian-Albrechts-Universität zu Kiel
 Max-Eyth-Strasse 2, 24118 Kiel (Germany)

[e] P. Gupta
 Current address:
 Max-Planck-Institute für Kohlenforschung
 Kaiser-Wilhelm-Platz 1
 45470 Mülheim an der Ruhr (Germany)

Supporting information for this article is available on the WWW under <http://dx.doi.org/10.1002/chem.201501003>.

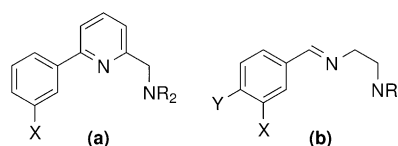
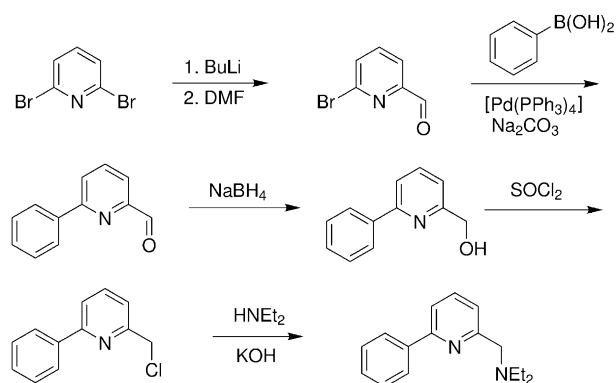


Figure 1. The ligands PPN ((a) R = Et, X = H) and BDED ((b) R = Et, X = Y = H).

We reinvestigated this system by means of fast stopped-flow techniques at low temperatures to establish a clearer picture of the formation of the bis(μ -oxido)dicopper intermediate and its reactivity. Although this system is interesting in terms of mechanistic insight, the prospects of its use for synthetic applications appear very limited. To further investigate the transferability of the structure–reactivity relationship, we devised a related system based on the supporting ligand *N*-benzylidene-*N,N*-diethylethylenediamine (BDED, Figure 1), which exhibits the same basic structural features but is synthetically more readily accessible. The reactivity of the copper complex formed with this ligand against dioxygen is studied and possible synthetic application in stoichiometric selective oxidations is reported herein. Furthermore, we unveiled the underlying mechanistic scenario for both systems by quantum chemical means.

Results and Discussion

Because 2-(chloromethyl)-6-phenylpyridine, the starting material used by Holland et al. for the synthesis of the PPN ligand, was no longer commercially available we developed a slightly different synthetic route to this ligand according to literature procedures (Scheme 1).^[5,6]



Scheme 1. Synthesis of PPN.

The structure of the complex $[\text{Cu}(\text{PPN})\text{CH}_3\text{CN}]\text{SbF}_6$ was previously characterized by Holland et al. and exhibits an unusual T-shaped coordination geometry about a three-coordinate copper ion in the solid state.^[5] For reasons detailed below, we prepared this complex in situ in acetone by mixing a solution of $[\text{Cu}(\text{CH}_3\text{CN})_4]\text{CF}_3\text{SO}_3$ under argon with a PPN solution saturated with dioxygen. Figure 2 displays the evolving time-resolved UV/Vis spectra recorded in a stopped-flow measurement at -91°C , which indicates that the Cu^{I} complex reacts quite slowly, over a period of 900 seconds, to a bis(μ -oxido)dicopper complex. Except for an initial lagging period associated with complex formation, the spectral changes are identical to those reported previously by Holland et al.^[5] After about 30 seconds, the features of complex formation visible at the beginning of the reaction disappear and an exponential increase in absorbance sets in. No indications for other inter-

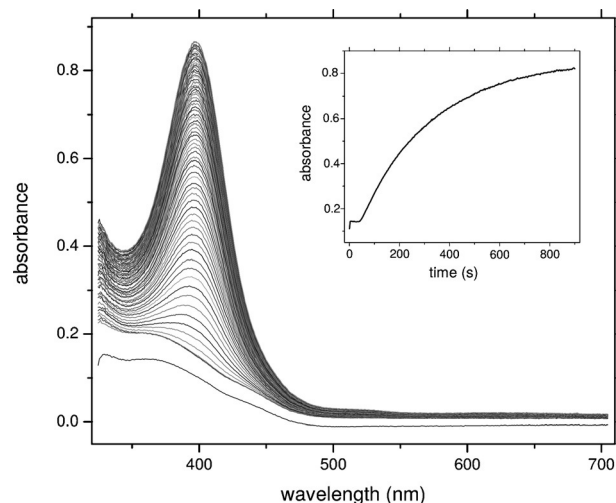
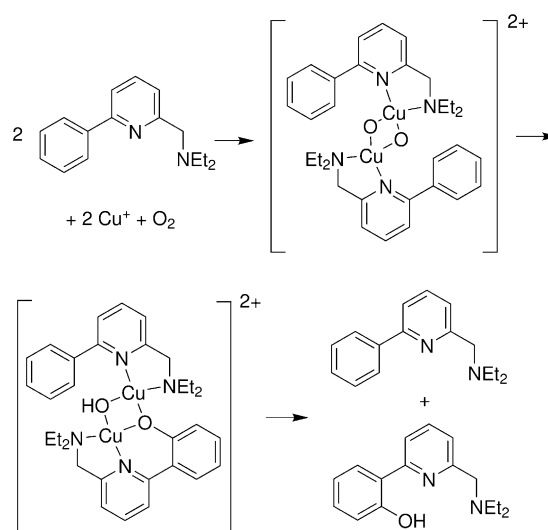


Figure 2. Time-resolved UV/Vis spectra of the reaction of $[\text{Cu}(\text{PPN})]\text{CF}_3\text{SO}_3$ ($2.5 \times 10^{-4} \text{ M}$) with dioxygen ($5.1 \times 10^{-3} \text{ M}$) in acetone at -91°C over 900 s. The inset shows the increase of absorbance at 400 nm over time (first order rate constant $k_{\text{obs}} = 2.6 \times 10^{-3} \text{ s}^{-1}$; fit after the initial lag time).

mediates such as, for example, superoxido or peroxido complexes were observed.

Clouding of the solutions over time precluded further detailed kinetic analysis. Due to the quite fast consecutive hydroxylation reaction, even at low temperatures, it was not possible to isolate and structurally characterize the bis(μ -oxido)dicopper intermediate complex. The first-order “decomposition” reaction (formation of the phenolate-bridged complex, Scheme 2) had been investigated by Holland et al.,^[5] who reported a rate constant of $k = 6 \times 10^{-4} \text{ s}^{-1}$ in acetone, at -70°C . ^1H NMR spectroscopy and GC/MS revealed partial hydroxylation of the ligand after decomposition of the product complex. The postulated mechanism is presented in Scheme 2.^[5]

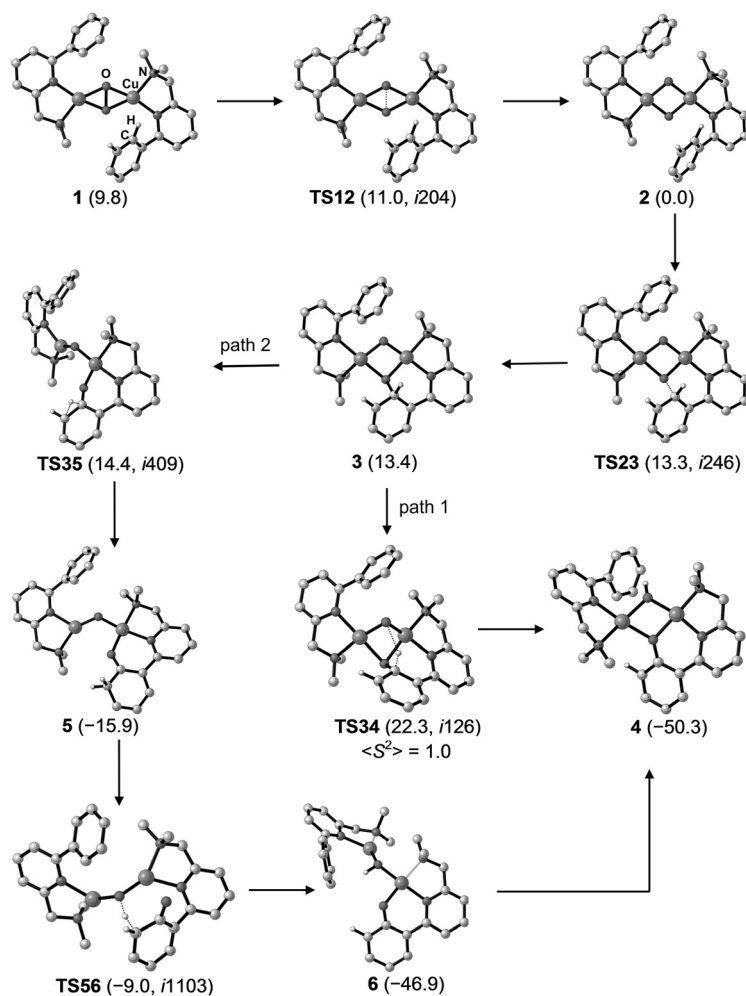
We studied the underlying reaction mechanism at the BLYP-D/TZVP(COSMO) level of density functional theory (DFT; see



Scheme 2. Oxidation of $[\text{Cu}(\text{PPN})\text{CH}_3\text{CN}]\text{SbF}_6$ with dioxygen (Scheme redrawn from ref. [5]).

the Computational Details section below), employing a slightly truncated PPN model ligand **L1** (Figure 1a: R=Me, X=H). All energies reported below refer to Gibbs energies in kcal mol⁻¹ relative to the bis(μ-oxido)dicopper(III) complex (**2** in Scheme 3) at -70 °C. Akin to earlier mechanistic studies on aromatic hydroxylation reactions,^[2c,4a,7] we assume initial formation of the (μ-η²:η²-peroxido)dicopper(II) complex and we chose **1** as starting point for the exploration of reaction pathways (Scheme 3). We find that **1** is less stable than the bis(μ-oxido) isomer **2** by 10 kcal mol⁻¹ and the core-isomerization process through **TS12** is connected with a minute activation barrier of merely 1 kcal mol⁻¹. Thus, fully in line with the experimental observation, we conclude that isomer **2** represents the dominant species in the initial phase of the reaction. One of the μ-O atoms in the dicopper core of **2** is already located in close proximity (2.86 Å) to one of the *ortho*-carbon atoms of the phenyl group, which predetermines the position of the subsequent regioselective ligand hydroxylation commencing

with the C–O bond formation via **TS23** ($\Delta G^\ddagger = 13 \text{ kcal mol}^{-1}$). The resulting σ -complex **3** is thermodynamically unstable and two pathways branch off at this point. Along path 1, complex **3** directly transforms into complex **4** through proton transfer onto the second μ-O atom. This highly exergonic step results in the formation of a (μ-OH)(μ-O)-dicopper complex, which represents the final product of the reaction sequence studied here (in our experiments, liberation of the hydroxylated ligand is accomplished by warming the reaction mixture to RT and aqueous workup, in line with the reported procedure of Holland et al.^[5]). However, with **TS34** giving rise to an effective activation barrier of $\Delta G^\ddagger = 22 \text{ kcal mol}^{-1}$ for the process leading from **2** to **4**, path 1 cannot kinetically compete with path 2: The latter involves exergonic decay of **3** to the intermediate dienone **5** and subsequent proton abstraction via **TS56** followed by a conformational transition leads to **4**. With an effective activation barrier of $\Delta G^\ddagger = 14 \text{ kcal mol}^{-1}$ associated with **TS35**, the sequence **2**→**5**→**4** represents the preferred route to product formation and the emergence of a dienone intermediate is coherent with the mechanistic picture suggested in earlier work.^[2c] However, the low barrier of merely 6 kcal mol⁻¹ computed for the strongly exergonic decay of the dienone intermediate to form **6**, and subsequently **4**, implies that this species will most likely escape any attempts for an experimental characterization.

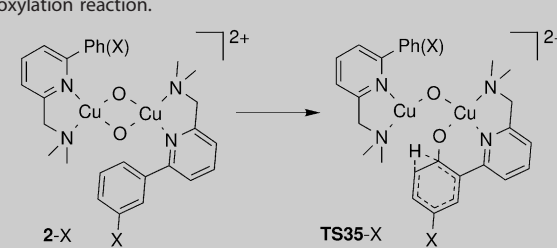


Scheme 3. Computed reaction pathways for the intramolecular aromatic hydroxylation reaction of the PPN ligand starting from **1**. Gibbs energies relative to **2** in kcal mol⁻¹ (BLYP-D/TZVP(COSMO) results, -70 °C, solvent acetone) are given in parentheses together with the characteristic imaginary wavenumbers of transition states. For all stationary points reported, closed-shell singlet wave functions resulted in the computations, except **TS34**, for which a broken-symmetry wave function was obtained. Irrelevant H atoms not shown.

For further comparison with the experimental results of Holland et al., we also investigated the influence of activating and deactivating substituents X introduced *para* to the activation position in the phenyl ring.^[5] The activation barriers resulting for the substituted systems compiled in Table 1 were computed as the Gibbs energy difference at -70 °C between **2-X** and **TS35-X** assuming that the nature of the overall rate-limiting step in the course of the hydroxylation reaction (i.e., the 1,2-H shift for the dienone formation) remains unaltered upon substitution. The resulting differences in computed barrier heights clearly follow the expected trend for substituent effects in electrophilic aromatic substitution reactions, which validates the view that the bis(μ-oxido)dicopper core acts as an electrophile.^[5] The high activation barrier obtained for the complex with the strongly deactivating NO₂ substituent (20 kcal mol⁻¹) is in line with the fact that Holland et al. did not observe formation of the hydroxylated PPN(NO₂) product in their low-temperature experiments.^[5]

Our efforts to isolate the supposed primary product of this reaction, the (μ-phenoxido)(μ-OH)dicopper complex (see Scheme 2) remained unsuccessful. Yet, during workup of one reaction batch we were able to isolate the copper(II) complex with PPN, in which the two copper(II) ions are bridged by two hydroxide groups. According to the reaction mechanism detailed above (Scheme 2) only one of the two ligands constituting the dinuclear complex is hydroxylated, that is, the maximum product yield is 50%. The re-

Table 1. Substituent effects on the overall rate-limiting step of the hydroxylation reaction.



X	ΔG^\ddagger [kcal mol ⁻¹]	Effect of X
OCH ₃	9.8	Strongly activating
OH	11.2	
CH ₃	12.7	Weakly activating
CH=CH ₂	13.6	
H	14.4	Reference
F	15.5	Weakly deactivating
CHO	18.7	
NO ₂	20.0	
CF ₃	20.5	Strongly deactivating

maining unreacted ligand equivalents form the bis(μ -hydroxo) complex $[\text{Cu}_2(\text{PPN})_2(\text{OH})_2](\text{CF}_3\text{SO}_3)_2$, which crystallized when the solution was left on the bench after oxidation. A similar observation and crystal structure for a steroid system had been described by Schönecker et al. previously and by Herres et al. for a related bisguanidine copper complex system.^[2m,8] The molecular structure of the cation of this binuclear complex is shown in Figure 3. Crystallographic data are provided in the Supporting Information.

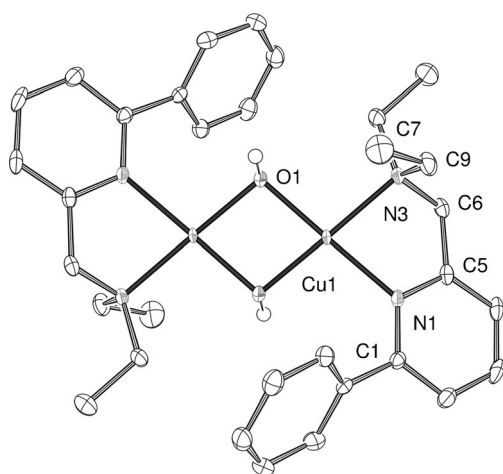


Figure 3. Molecular structure of the cation of $[\text{Cu}_2(\text{PPN})_2(\text{OH})_2](\text{CF}_3\text{SO}_3)_2$.

In contrast to the preparatively rather demanding synthesis of PPN, efficient synthetic access to the BDED ligand is readily achieved in a simple Schiff-base reaction from benzaldehyde and *N,N*-diethylethylenediamine according to the literature.^[9] To the best of our knowledge, BDED has not been used as a supporting ligand for metal ions thus far. We were able to crystallize the Cu^I complex $[\text{Cu}(\text{BDED})_2]\text{CF}_3\text{SO}_3$ and its molecu-

lar structure as derived by using X-ray crystallography is shown in Figure 4. Crystallographic data for this and the corresponding complex with the SbF_6^- anion are provided as Supporting Information.

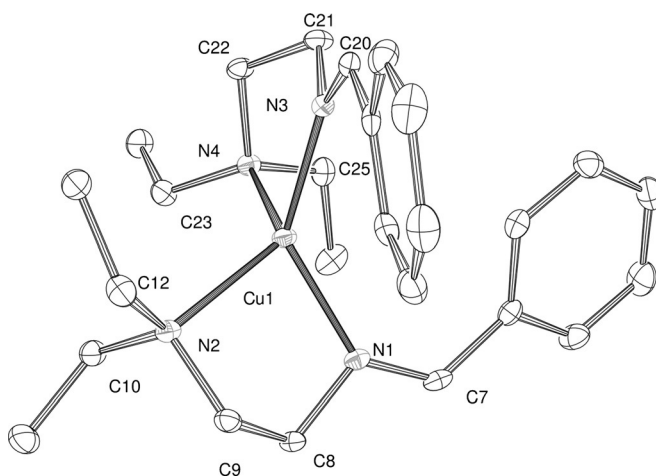


Figure 4. ORTEP plot of the molecular structure of $[\text{Cu}(\text{BDED})_2]^+$. Anion and hydrogen atoms are omitted for clarity; ellipsoids are drawn at 50% probability.

It is interesting to note that the PPN-supported copper(I) complex forms with a 1:1 ligand to Cu^I ratio (together with a coordinated acetonitrile molecule)^[5] whereas we find a 2:1 stoichiometry in the crystal structure reported above. To avoid potential problems in our kinetic studies with the formation of this complex, we decided to devise an in situ formation of the Cu^I/BDED complex in a 1:1 stoichiometry by mixing the acetone solution of the copper(I) salt under argon and the O₂-saturated acetone solution of the ligand within the stopped-flow unit. The same procedure was used in our mechanistic study on the Cu^I/PPN system described above and thus equivalent reaction conditions were established in both experiments.

Figure 5 shows time-resolved UV/Vis spectra obtained from a stopped-flow measurement at -90.0°C . The optical feature evolving at $\lambda_{\text{max}} = 400 \text{ nm}$ is consistent with the formation of a bis(μ -oxido) complex for the Cu^I/BDED system as well. As before facile kinetic fitting was not possible, however, the Cu^I/BDED complex clearly reacted faster than the Cu^I/PPN complex.

We performed the same reaction also in a bench-top experiment. After workup of the product solution according to Scheme 4 we identified the product salicylaldehyde by NMR spectroscopy and GC/MS. It is formed in high yields (approaching the optimum yield of 50%), which clearly demonstrates that selective aromatic hydroxylation can be achieved efficiently also by application of simple imine ligands (Scheme 4). This opens encouraging perspectives for synthetic applications of related ligands. The importance of *ortho*-hydroxylation of arenes has been discussed previously.^[10] For copper chemistry on biomimetic hydroxylation reactions, early work by Réglier and co-workers should be pointed out.^[11] More recently, Schö-

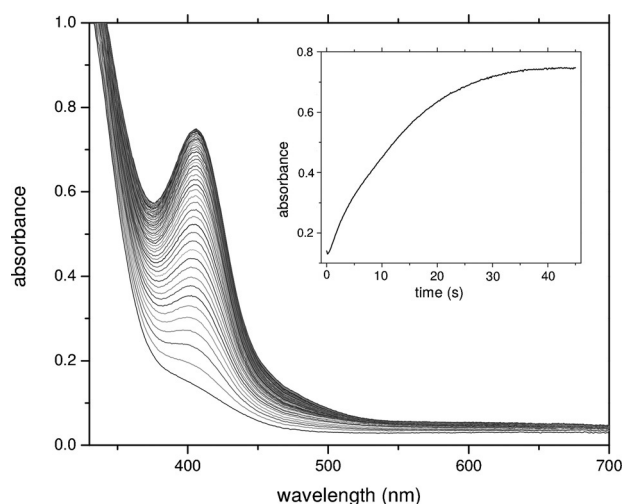
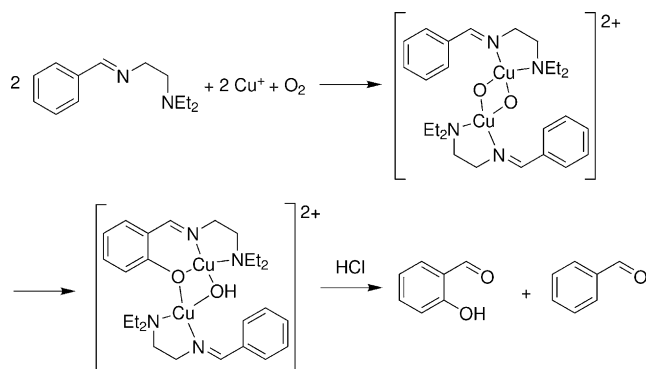


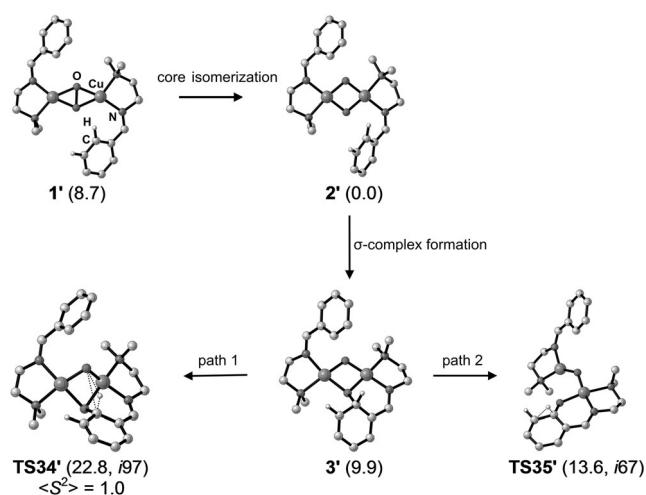
Figure 5. Time-resolved UV/Vis spectra of the reaction of $[\text{Cu}(\text{BDED})]\text{CF}_3\text{SO}_3$ (5.0×10^{-4} M) with dioxygen (5.1×10^{-3} M) in acetone at -89°C over 200 seconds. The inset shows increase of absorbance at 400 nm over time (first order rate constant $k_{\text{obs}} = 5.65 \times 10^{-2} \text{ s}^{-1}$).



Scheme 4. Oxidation of the Cu^{I} BDED complex with dioxygen.

necker et al. in particular have demonstrated the potential of such reactions in steroid synthesis.^[2m, 12]

To evaluate the influence of the supporting ligand environment on the energetics of the hydroxylation reaction, we performed additional DFT calculations for the BDED-supported complexes. As before, we employed a slightly truncated molecular model in these calculations, in which we replaced the ethyl groups at the amine donor by methyl groups. We optimized a number of minima as well as two transition structures (Scheme 5) that characterize the hydroxylation pathways identified for the PPN-based system. Comparison of the results for both systems reveals largely identical structural features and we found no indication of variations as to the reaction pathways and the nature of the rate-limiting steps. Based on these results we estimate a slightly lower overall activation barrier for the hydroxylation (via **TS34'**: $13.6 \text{ kcal mol}^{-1}$ vs. **TS34**: $14.4 \text{ kcal mol}^{-1}$), which is perfectly in line with the observation that hydroxylation in the BDED system occurs at higher rates in the experiments.



Scheme 5. Selected reaction steps computed for the intramolecular aromatic hydroxylation reaction for the BDED ligand starting from **1'**. Gibbs energies relative to **2'** in kcal mol^{-1} (BLYP-D/TZVP(COSMO) results, -70°C , solvent acetone) are given in parentheses together with the characteristic imaginary wave numbers of transition states. For all stationary points reported, closed-shell singlet wave functions resulted in the computations, except **TS34'**, for which a broken-symmetry wave function was obtained. Irrelevant H atoms not shown.

To assess substituent effects, we synthesized a series of BDED derivatives (Figure 1 b: $\text{R}=\text{Et}$ with Y ($\text{X}=\text{H}$)= Me , OMe , Cl , NO_2 and X ($\text{Y}=\text{H}$)= Me , NO_2). We prepared the corresponding copper(II) complexes and treated them with dioxygen in the same way as described before for the parent BDED system. Only negligible effects were observed for ligands with a methyl or a methoxy group. The hydroxylated product still forms in high yields and for the methyl-substituted BDED ligand (Figure 1 b, $\text{R}=\text{Et}$, $\text{Y}=\text{H}$, $\text{X}=\text{Me}$) hydroxylation occurs in *ortho* and *para* position of the methyl group, as expected. In contrast, hydroxylation yields were low for the chloro-substituted ligand ($\text{Y}=\text{Cl}$) and hydroxylation did not occur for nitro-substituted ligands. The latter finding is in accord with the report of Holland et al. for the nitro analogue of PPN^[5] and with the results of our model calculations on substituent effects on the effective barrier heights presented above. We also tested a BDED derivative, in which we replaced the ethyl groups at the amine donor by methyl groups (Figure 1 b: $\text{R}=\text{Me}$, $\text{X}=\text{Y}=\text{H}$) and we observed only insignificant differences in terms of reactivity, but a slightly smaller yield of the hydroxylated product was obtained.

Furthermore, although obviously less attractive in terms of potential synthetic applications, we tested whether the reduced form of the BDED ligand would also support ligand hydroxylation reaction. The corresponding H_2BDED ligand was obtained by the treatment of BDED with sodium borohydride (Figure 6).

However, because of problems with disproportionation reactions it was impossible to obtain and characterize the copper(II) complex of this ligand in the solid state. Oxidation experiments conducted in the same way as described for

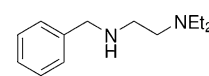


Figure 6. The ligand H_2BDED .

the imine complex did not lead to ligand hydroxylation. Even so, a copper(II) complex with this ligand was obtained by treating CuCl_2 with H_2BDED . The molecular structure of $[\text{Cu}(\text{H}_2\text{BDEDCl}_2)]$ and crystallographic data are presented in the Supporting Information.

Finally, it is important to note that the BDED system can be quite sensitive with respect to particular conditions employed in the synthetic procedures. For example, when a solution of $[\text{Cu}(\text{CH}_3\text{CN})_4]\text{CF}_3\text{SO}_3$ with BDED in dichloromethane was treated at -80°C with dioxygen, and kept at this temperature for more than half an hour, no hydroxylation was observed. Instead, after evaporation of the solvent, crystals of a dinuclear bis-hydroxido bridged copper(II) complex with a *N,N*-diethylethylenediamine ligand was obtained. The molecular structure of this complex (Figure 7; see the Supporting Information for the crystallographic data) reveals that the imine bond in the BDED ligand was cleaved: One could even smell the free benzaldehyde from the solution (a crystal structure of this complex with a different anion has been reported previously).^[113]

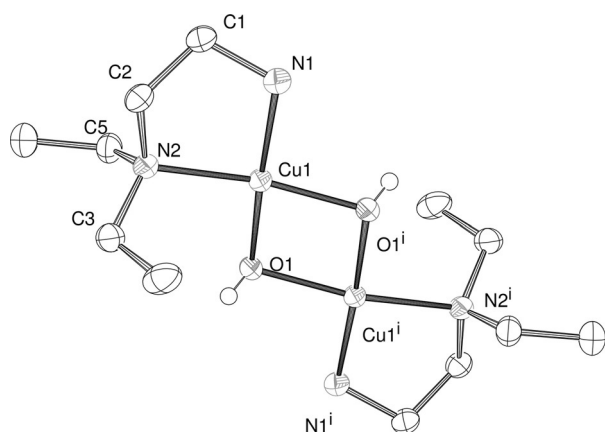


Figure 7. Molecular structure of the cation of $[\text{Cu}_2(\text{Et}_2\text{en})(\text{OH})_2](\text{CF}_3\text{SO}_3)_2$.

Conclusion

In the present contribution we have reinvestigated the aromatic hydroxylation effected by a dinuclear Cu_2O_2 complex supported by PPN ligands, which was studied earlier by Holland et al.^[5] Stopped-flow measurements at low temperatures revealed the relatively fast formation of a bis(μ -oxido)dicopper complex; however, no further intermediates such as a superoxido complex could be detected. We have elucidated the underlying reaction mechanism by DFT calculations. Fully in line with the interpretation of experimentally observed UV/Vis signatures, the quantum chemical results reveal the bis(μ -oxido) dinuclear complex as the dominant intermediate present in the initial phase of the reaction; the corresponding side-on peroxido complex is less stable by 10 kcal mol^{-1} . The hydroxylation sequence commences with an attack of one of the μ -O atoms of the bis(μ -oxido) complex on the phenyl group of the PPN ligand, which results in the formation of a thermodynamically and kinetically unstable σ -complex. Along the favored reaction path, this complex decays through a 1,2-H shift to form a dien-

one species, from which the product species is formed in subsequent steps. The bis(μ -oxido) complex and the 1,2-H shift transition state represent the rate-determining states^[14] of the reaction sequence studied here, which is characterized by the effective largest barrier of 14 kcal mol^{-1} . Substituent effects on this barrier height are consistent with the characterization of the bis(μ -oxido) complex as an electrophile in this reaction.

We have further demonstrated experimentally, as well as theoretically, that the same facile selective hydroxylation of aromatic aldehydes can also be achieved by using the related supporting imine ligand BDED, which is synthetically much easier to access than the PPN ligand. It is interesting to note at this point that intermediacy of a peroxido complex can be excluded here, which is in contrast to a related binuclear copper complex that some of us investigated previously.^[2c] Although an intramolecular *o*-hydroxylation was also observed, the active complex was characterized as a peroxido complex and no bis(μ -oxido) complex could be detected. Complexes of this type have already been used in synthesis,^[15] although synthetic applications are limited for this kind of system.

We could clearly demonstrate that the possibility of preparing complexes of this type in situ and using dioxygen as an oxidant makes the whole setup promising for a number of preparative applications in the future. Herein we have provided a new synthetic approach in regard to the importance of *ortho*-hydroxylation of arenes^[10] discussed above.

Experimental Section

Materials and methods

Solvents and reagents used were of commercially available reagent quality. $[\text{Cu}(\text{CH}_3\text{CN})_4]\text{CF}_3\text{SO}_3$ and $[\text{Cu}(\text{CH}_3\text{CN})_4]\text{SbF}_6$ were synthesized according to literature procedures.^[16] ^1H NMR and ^{13}C NMR spectra were measured on a Bruker AV 400 and Bruker AV 200 spectrometer. GC/MS spectra were recorded on a HP GL 6890 chromatograph with a HP 5973 mass detector.

Low-temperature stopped-flow measurements

Low-temperature stopped-flow experiments were performed by using a commercial HI-TECH SF-615X2 instrument (TgK Scientific, Bratford-on-Avon, UK). Solvents used for stopped-flow measurements and experiments under inert conditions were obtained as already pure chemicals and distilled under argon atmosphere prior to transferring them into a glovebox (MBraun, Garching, Germany). For the reaction of $[\text{Cu}(\text{PPN})]^+$ with dioxygen, a $5 \times 10^{-4} \text{ M}$ solution of PPN and a $5 \times 10^{-4} \text{ M}$ solution of $[\text{Cu}(\text{CH}_3\text{CN})_4]\text{CF}_3\text{SO}_3$ in acetone were prepared under inert conditions within the glovebox. For the corresponding reaction of $[\text{Cu}(\text{BDED})]^+$ with dioxygen, a $1 \times 10^{-3} \text{ M}$ solution of BDED and a $1 \times 10^{-3} \text{ M}$ solution of $[\text{Cu}(\text{CH}_3\text{CN})_4]\text{CF}_3\text{SO}_3$ in acetone were prepared under the same conditions. The solutions were transferred separately with gastight syringes to the stopped-flow instrument. The ligand solution was saturated with dioxygen (5.0) by bubbling a gas stream through the liquid for 10 min ($10.2 \times 10^{-3} \text{ M}$).^[17]

Single-crystal X-ray structure determinations

The X-ray crystallographic data for $[\text{Cu}_2(\text{N,N}(\text{Et})_2\text{en})_2(\text{OH})_2](\text{CF}_3\text{SO}_3)_2$ were collected using a BRUKER/NONIUS KappaCCD detector with a BRUKER/NONIUS FR591 rotating anode radiation source and an OXFORD CRYOSYSTEMS 600 low temperature system. $\text{MoK}\alpha$ radiation with wavelength 0.71073 Å and a graphite monochromator were used. The PLATON MULABS semi-empirical absorption correction using multiple scanned reflection was applied on the data and the structure was solved by intrinsic phasing using SHELXT2014^[18] and refined with SHELXL2014/6.^[19] All non-hydrogen atoms were refined anisotropically, C–H and N–H hydrogen atoms were positioned geometrically and O–H hydrogen atoms were located in difference map and refined isotropically.

For $[\text{Cu}(\text{BDED})_2]\text{CF}_3\text{SO}_3$ data collection, a BRUKER D8 Venture system equipped with dual μS microfocus sources, a PHOTON100 detector and an OXFORD CRYOSYSTEMS 700 low-temperature system was used. Data collection was performed using $\text{MoK}\alpha$ radiation with wavelength 0.71073 Å and a collimating Quazar multilayer mirror. Semi-empirical absorption correction from equivalents was applied using SADABS-2014/4 and the structure was solved by intrinsic phasing using SHELXT2014.^[18] Refinement was performed against F^2 using SHELXL-2014/7.^[19] All non-hydrogen atoms were refined anisotropically and hydrogen atoms were positioned geometrically.

For $[\text{Cu}_2(\text{PPN})_2(\text{OH})_2](\text{CF}_3\text{SO}_3)_2$, data collection was performed by using a STOE Imaging Plate Diffraction System (IPDS-1) with $\text{MoK}\alpha$ radiation. The structure was solved with direct methods using SHELXS-97 and refinement was performed against F^2 using SHELXL-97.^[19] All non-hydrogen atoms were refined anisotropic. The C–H atoms were positioned with idealized geometry and refined isotropic with $U_{\text{iso}}(\text{H}) = 1.2 U_{\text{eq}}(\text{C})$ using a riding model. The O–H atom was located in difference map, its bond lengths set to ideal values and finally it was refined isotropic using a riding model.

CCDC-1047585 ($[\text{Cu}_2(\text{N,N}(\text{Et})_2\text{en})_2(\text{OH})_2](\text{CF}_3\text{SO}_3)_2$), CCDC-1047583 ($[\text{Cu}(\text{BDED})_2]\text{CF}_3\text{SO}_3$), and CCDC-1032911 ($[\text{Cu}_2(\text{PPN})_2(\text{OH})_2](\text{CF}_3\text{SO}_3)_2$) contain the supplementary crystallographic data for this paper. These data can be obtained free of charge from The Cambridge Crystallographic Data Centre via www.ccdc.cam.ac.uk/data_request/cif.

Computational details

Geometry optimizations and harmonic frequency calculations were performed with the Gaussian 09 program^[20] employing the dispersion corrected^[21] BLYP-D2 density functional in combination with a triple- ζ basis-set/effective core potential (ECP) one-particle description (the def2-TZVP^[22] basis set was used for C, H, N, and O atoms, and the quasi-relativistic SDD-type^[23] ECP together with the corresponding triple- ζ basis set^[23] was used for Cu; this combination is denoted def2-TZVP(SDD)). For improved computational efficiency the density-fitting approximation was used and the corresponding density-fitting basis set was generated automatically by routines implemented in the Gaussian09 program (“auto” keyword).^[24] Default integration grids and convergence criteria have been used throughout. All structure optimizations were initially performed employing restricted Kohn–Sham (RKS) singlet wave functions. Subsequently we searched for energetically low lying unrestricted Kohn–Sham (UKS) wave functions with broken spin and spatial symmetry (“broken-symmetry” wave functions) using the “guess=mix” keyword. In all cases but two, the UKS wave functions collapsed during the self-consistent field optimization and closed-shell singlet wave functions resulted. For the two tran-

sition states **TS34** and **TS34'**, broken-symmetry wave functions were obtained with lower energies than the RKS singlet wave functions; the former were used for geometry optimizations and harmonic frequency calculations on these two species. All stationary points have been characterized as minima or first order saddle points by eigenvalue analysis of the diagonalized Hessians. The connection of transition states and related minima was established by employing small geometry displacements along both directions of the imaginary vibrational mode resulting from the vibrational frequency calculations on the transition structures, followed by unconstrained geometry optimizations. XYZ coordinates of optimized minima and transition states are provided in the Supporting Information.

Based on these optimized geometries, subsequent single-point energy calculations were performed at the BLYP-D3^[21,25]/def2-TZVP(SDD) level including the COSMO continuum solvation model^[26] implemented in the ORCA 2.9 program (solvent acetone).^[27] The resolution-of-identity (RI)^[28] approximation for the BLYP functional was used employing the auxiliary def2-TZVP/J basis set.^[29] For **TS34** and **TS34'**, broken-symmetry singlet energies (E_{BS}) were obtained by applying the formalism of Yamaguchi^[30] as implemented in the ORCA program. All energies obtained were corrected to obtain Gibbs energies at 203 K by adding the corresponding thermal and entropic increments derived from the Hessian calculations with the Gaussian program (the “freqchk” utility program of Gaussian 09 was used for this purpose). Total electronic energies and Gibbs energies at 203 K for all stationary points reported are provided in the Supporting Information. Figure of the molecular structures were produced by means of the CYLview program.^[31]

Syntheses

2-(Diethylaminomethyl)-6-phenylpyridine (PPN): The ligand was synthesized following slightly modified literature procedures^[6] and only the last step was performed according to the publication by Holland et al.^[5] because the starting material was no longer commercially available.

2-Bromo-6-formylpyridine: Following the literature procedure,^[6a] 2,6-dibromopyridine (11.8 g, 50.0 mmol) was dissolved in dry diethyl ether (150 mL) under argon atmosphere and cooled to -80°C . With vigorous stirring a solution of BuLi in hexane (2.50 M, 20.0 mL, 50.0 mmol) was added slowly. After 30 min dimethylformamide (4.5 mL, 60.0 mmol) was added dropwise and the temperature was held for another 20 min. Then the solution was slowly heated to 0°C . Hydrochloric acid (1 M) was added until an acid pH was reached and the mixture was neutralized with an aqueous solution of NaHCO_3 . After workup with ethyl acetate and water the combined organic layers were dried over Na_2SO_4 and kept in a refrigerator overnight. White-yellow crystals precipitated and were washed with pentane (3.72 g, 20.0 mmol, 40.0% yield). ^1H NMR (400 MHz, CDCl_3): $\delta = 10.01$ (s, 1H), 7.93 (d, 1H, $J = 6.6$ Hz), 7.75 ppm (m, 2H, $J = 7.8$ Hz); ^{13}C NMR (100 MHz, CDCl_3): $\delta = 191.7$, 153.5, 142.6, 139.4, 132.7, 120.4 ppm.

6-Phenyl-2-pyridinecarboxaldehyde: This reaction was performed according to the procedure described by Lin Chuang et al.^[6b] Under inert conditions, $[\text{Pd}(\text{PPh}_3)_4]$ (0.37 g, 0.30 mmol) was dispersed in dry toluene and then added to a solution of 2-bromo-6-formylpyridine (2.0 g, 11 mmol) in toluene. A solution of Na_2CO_3 (2 M) was degassed with argon for two hours and 11 mL were added to the reaction mixture. The solution was heated for 16 h to 90°C . After cooling to room temperature CH_2Cl_2 (80 mL) and an aqueous solution of Na_2SO_4 (2 M, 40 mL) was added. The organic

layer was washed with brine and dried over Na_2SO_4 . It was concentrated under reduced pressure and kept in the refrigerator. Grey crystals precipitated and were washed with pentane (1.4 g, 7.6 mmol, 69.9%). ^1H NMR (400 MHz, CDCl_3): $\delta = 10.03$ (s, 1H), 7.95 (d, 2H, $J = 8.0$ Hz), 7.75 (m, 3H, $J = 2.9$ Hz), 7.36 ppm (m, 3H, $J = 7.5$ Hz); ^{13}C NMR (100 MHz, CDCl_3): $\delta = 194.0, 157.9, 152.8, 137.78, 129.7, 129.1, 129.0, 128.3, 127.1, 125.4, 124.5$ ppm.

6-Phenyl-2-pyridinemethanol: A solution of NaBH_4 (0.380 g, 10.0 mmol) in water (10 mL) was added to a solution of 6-phenyl-2-pyridinecarboxaldehyde (1.38 g, 7.57 mmol) in methanol (30 mL). After stirring at room temperature for 30 min, the mixture was heated to boiling point and was then heated at reflux for 50 min. When the mixture was cooled to room temperature, the methanol was removed under reduced pressure and to the remaining solution hydrochloric acid (1 M) was added to reach an acid pH. Then the pH was raised to 12 with sodium hydroxide (1 M). The solution was washed three times with CH_2Cl_2 and the combined organic layers were dried over Na_2SO_4 . The solvent was removed under reduced pressure. A yellow, partly crystallized oil was obtained (1.0 g, 4.16 mmol, 72.3%). ^1H NMR (400 MHz, CDCl_3): $\delta = 7.98$ (d, 2H, $J = 7.1$ Hz), 7.67 (t, 1H, $J = 7.4$ Hz), 7.57 (d, 1H, $J = 7.4$ Hz), 7.41 (m, 3H, $J = 7.8$ Hz), 7.13 (d, 1H, $J = 8.0$ Hz), 4.78 (s, 2H), 4.34 ppm (s, 1H); ^{13}C NMR (100 MHz, CDCl_3): $\delta = 137.5, 129.2, 128.8, 127.0, 127.0, 119.0, 118.8, 64.0$ ppm.

2-(Chloromethyl)-6-phenylpyridine hydrochloride: Following the literature procedure of Makowska-Grzyska et al.^[6c] thionyl chloride (6 mL) was added dropwise to 6-phenyl-2-pyridinemethanol (1.00 g, 5.40 mmol) under inert conditions while being cooled with an ice bath. At the end of the reaction, the mixture was heated under reflux for two hours. The remaining thionyl chloride was removed under reduced pressure and the residue was washed several times with CH_2Cl_2 . A white solid was obtained (1.06 g, 5.16 mmol, 95.6%). ^1H NMR (400 MHz, CDCl_3): $\delta = 8.31$ (t, 2H, $J = 8.2$ Hz), 8.18 (d, 1H, $J = 7.3$ Hz), 7.92 (dd, 2H, 4.3 Hz), 7.61 (m, 2H, $J = 3.9$ Hz), 7.27 (s, 1H), 5.49 ppm (s, 2H); ^{13}C NMR (100 MHz, CDCl_3): $\delta = 155.0, 154.3, 144.1, 132.3, 129.5, 129.1, 124.0, 41.3$ ppm.

2-(Diethylaminomethyl)-6-phenylpyridine: The ligand was synthesized according to the literature.^[5] A mixture of 2-(chloromethyl)-6-phenylpyridine hydrochloride (0.60 g, 3.0 mmol) and diethylamine (4.5 mL, 43 mmol) in dry THF (40 mL) with powdered KOH (1.5 g, 27 mmol) was heated to reflux under inert conditions for 22 h. The solvent was removed under reduced pressure and water (5 mL) and brine (5 mL) were added to the residue. The mixture was washed with diethyl ether several times and the combined organic layers were dried over Na_2SO_4 . After removing the solvent under reduced pressure the remaining oil was purified using a Kugelrohr distillation. A yellow oil was obtained (0.44 g, 1.8 mmol, 61.4%). ^1H NMR (400 MHz, CDCl_3): $\delta = 7.92$ (d, 2H, $J = 7.1$ Hz), 7.62 (t, 1H, $J = 7.6$ Hz), 7.49 (d, 1H, $J = 8.0$ Hz), 7.36 (m, 4H, $J = 3.9$ Hz), 3.76 (s, 2H), 2.55 (q, 4H, $J = 7.0$ Hz), 1.02 ppm (t, 6H, $J = 7.3$ Hz); ^{13}C NMR (100 MHz, CDCl_3): $\delta = 139.7, 136.9, 128.7, 127.0, 121.1, 118.4, 59.5, 47.4, 12.1$ ppm.

***N'*-Benzylidene-*N,N*-diethyl-ethylendiamine (BDED):** A solution of benzaldehyde (7.96 g, 75.0 mmol) in diethyl ether (200 mL) was stirred for one hour over MgSO_4 at room temperature. Then the mixture was heated for another hour under reflux. The solvent was removed under reduced pressure after filtration. A yellow oil was obtained (13.2 g, 64.9 mmol, 86.5%). ^1H NMR (400 MHz, CDCl_3): $\delta = 8.21$ (s, 1H), 7.64 (m, 2H, $J = 2.4$ Hz), 7.31 (t, 2H, $J = 2.8$ Hz), 3.64 (t, 2H, $J = 7.1$ Hz), 2.70 (t, 2H, $J = 7.5$ Hz), 2.53 (q, 4H, $J = 7.3$ Hz), 0.97 ppm (t, 6H, $J = 7.2$ Hz); ^{13}C NMR (100 MHz, CDCl_3): $\delta = 161.7, 136.3, 130.5, 128.6, 128.0, 60.0, 53.5, 47.6, 12.0$ ppm.

$[\text{Cu}^{\text{I}}(\text{BDED})_2]\text{CF}_3\text{SO}_3$: BDED (82 mg, 0.4 mmol) and $[\text{Cu}(\text{CH}_3\text{CN})_4]\text{CF}_3\text{SO}_3$ (38 mg, 0.1 mmol) were dissolved in dry acetone (2 mL) in a glovebox under argon atmosphere. Orange crystals were obtained by slow ether diffusion over four weeks at -40°C .

$[\text{Cu}^{\text{I}}(\text{BDED})_2]\text{SbF}_6$: BDED (41 mg, 0.20 mmol) and $[\text{Cu}(\text{CH}_3\text{CN})_4]\text{SbF}_6$ (93 mg, 0.20 mmol) were dissolved in dry THF (1 mL) under inert conditions. Orange crystals were obtained with ether diffusion at -40°C over one week.

***N'*-Benzyl-*N,N*-diethyl-ethane-1,2-diamine (H_2BDED):** A solution of sodium borohydride (0.80 g, 21.1 mmol) in about methanol (50 mL) was added slowly to a solution of BDED (5.55 g, 27.0 mmol) in methanol (50 mL). After stirring for 30 min, the reaction mixture was heated under reflux for another 2 h. The mixture was washed three times with diethyl ether after aqueous workup. It was dried over Na_2SO_4 and the solvent was removed under vacuum. A yellow oil was obtained (4.88 g, 23.7 mmol, 87.6%). ^1H NMR (400 MHz, CDCl_3): $\delta = 7.30$ (m, 2H), 7.22 (m, 3H), 3.78 (s, 2H), 2.67 (t, 2H, $J = 5.6$ Hz), 2.56 (t, 2H, $J = 5.6$ Hz), 2.49 (q, 4H, $J = 7.1$ Hz), 1.94 (s, 1H), 0.99 ppm (t, 6H, $J = 7.1$ Hz); ^{13}C NMR (100 MHz, CDCl_3): $\delta = 140.6, 128.3, 128.1, 126.8, 54.1, 52.7, 47.0, 46.9, 11.8$ ppm.

$[\text{Cu}^{\text{II}}(\text{H}_2\text{BDED})\text{Cl}_2]$: Copper(II) chloride (0.83 g, 4.88 mmol) was dried with heating under vacuum and dissolved in a few mL of acetone. H_2BDED (1.00 g, 4.85 mmol) was added dropwise and the complex solution was divided in several samples and crystallized at -30°C . Green crystals were obtained.

Synthetic hydroxylation reactions: A solution of $[\text{Cu}(\text{CH}_3\text{CN})_4]\text{CF}_3\text{SO}_3$ (9.4 g, 25 mmol) in acetone (70 mL) was prepared under inert condition and a solution of BDED (5.1 g, 25 mmol) in acetone (20 mL) was added at room temperature. Dioxygen was passed through the mixture for 45 min. After one hour, 1 M HCl (40 mL) was added. The mixture was stirred for one hour and then heated to its boiling point. Most of the acetone was then removed under reduced pressure, CuCl_2 (2 g, 12 mmol) was added, and the mixture was washed with CH_2Cl_2 . The combined organic phases were stirred over Na_2SO_4 and the solvent was removed under reduced pressure. The remaining oil was purified with flash chromatography over aluminium oxide with CH_2Cl_2 . Pure salicylic aldehyde was obtained (0.24 g, 2.0 mmol, 8%).

Variation of the BDED ligand: 2-(Diethylamino)ethyl(4-methoxyphenyl)methylideneamine ($\text{X} = \text{H}$, $\text{Y} = \text{OMe}$): 4-Methoxybenzaldehyde (1.36 g, 10.0 mmol) was dissolved in methanol (300 mL). While stirring over Na_2SO_4 , *N,N*-diethylethylendiamine (1.16 g, 10.0 mmol) was added. After heating at reflux for 24 h the solvent was removed under reduced pressure and a slightly yellow oil was obtained (2.14 g, 9.5 mmol, 95%). ^1H NMR (400 MHz, CDCl_3): $\delta = 8.23$ (s, 1H), 7.66 (d, 2H, $J = 8.7$ Hz), 6.91 (d, 2H, $J = 8.7$ Hz), 3.83 (s, 3H), 3.69 (t, 2H, $J = 7.5$ Hz), 2.77 (t, 2H, $J = 7.5$ Hz), 2.61 (q, 4H, $J = 7.2$ Hz), 1.06 ppm (t, 6H, $J = 7.2$ Hz); ^{13}C NMR (100 MHz, CDCl_3): $\delta = 161.5, 161.1, 129.6, 129.3, 113.9, 59.8, 55.3, 53.6, 47.6, 11.9$ ppm.

2-(Diethylamino)ethyl(4-nitrophenyl)methylideneamine ($\text{X} = \text{H}$, $\text{Y} = \text{NO}_2$): *N,N*-Diethylethylendiamine (1.16 g, 10.0 mmol) was added to a solution of *p*-nitrobenzaldehyde (1.51 g, 10.0 mmol) in methanol (300 mL) stirred over Na_2SO_4 . After 24 h the solvent was removed under reduced pressure and a viscous, red oil was obtained (2.07 g, 8.3 mmol, 83%). ^1H NMR (400 MHz, CDCl_3): $\delta = 8.39$ (s, 1H), 8.26 (d, 2H, $J = 8.7$ Hz), 7.90 (d, 2H, $J = 8.7$ Hz), 3.79 (t, 2H, $J = 6.9$ Hz), 2.81 (t, 2H, $J = 6.9$ Hz), 2.61 (q, 4H, $J = 7.1$ Hz) 1.05 ppm (t, 6H, $J = 7.1$ Hz); ^{13}C NMR (100 MHz, CDCl_3): $\delta = 159.4, 148.9, 141.8, 128.7, 123.8, 60.1, 53.2, 47.6, 11.9$ ppm.

2-(Diethylamino)ethyl(4-methyl-phenyl)methylideneamine (X = H, Y = Me): 4-Methylbenzaldehyde (0.60 g, 5.0 mmol) and *N,N*-diethylethylenediamine (0.58 g, 5.0 mmol) were dissolved in about 50 mL diethyl ether and stirred for one hour over Na_2SO_4 and then heated under reflux for another hour. After filtration the solvent and remaining starting material were removed under reduced pressure and a yellow oil was obtained (0.79 g, 3.7 mmol, 73%). ^1H NMR (400 MHz, CDCl_3): δ = 8.26 (s, 1H), 7.60 (m, 2H), 7.22 (m, 2H), 3.71 (t, 2H, J = 7.2 Hz), 2.78 (t, 2H, J = 7.2 Hz), 2.61 (q, 4H, J = 7.2 Hz), 2.38 (s, 3H), 1.06 ppm (t, 6H, J = 7.2 Hz); ^{13}C NMR (100 MHz, CDCl_3): δ = 161.7, 140.8, 133.7, 129.3, 128.0, 59.9, 53.5, 47.6, 21.5, 12.0 ppm.

2-(Diethylamino)ethyl(4-chloro-phenyl)methylideneamine (X = H, Y = Cl): *N,N*-Diethylethylenediamine (1.16 g, 10.0 mmol) was added to a solution of 4-chlorobenzaldehyde (1.41 g, 10.0 mmol) in diethyl ether (60 mL). The solution was stirred over Na_2SO_4 for one hour and heated under reflux for one hour. The solvent and remaining starting material were removed under reduced pressure after filtration and a slightly yellow oil was obtained (2.04 g, 8.6 mmol, 86%). ^1H NMR (200 MHz, CDCl_3): δ = 8.25 (s, 1H), 7.63 (m, 2H), 7.39 (m, 2H), 3.71 (t, 2H, J = 7.2 Hz), 2.78 (t, 2H, J = 7.2 Hz), 2.59 (q, 4H, J = 7.2 Hz) 1.05 ppm (t, 6H, J = 7.2 Hz); ^{13}C NMR (50 MHz, CDCl_3): δ = 160.3, 136.4, 134.7, 129.2, 128.8, 59.9, 53.4, 47.6, 11.9 ppm.

2-(Diethylamino)ethyl(3-nitrophenyl)methylideneamine (X = NO_2 , Y = H): *m*-Nitrobenzaldehyde (7.56 g, 50.0 mmol) was solved in diethyl ether (150 mL) and *N,N*-diethylethylenediamine (5.81 g, 50.0 mmol) was added. It was stirred over Na_2SO_4 and heated under reflux for 16 h. The mixture was filtrated and the solvent was removed under reduced pressure; a yellow oil was obtained (12.02 g, 48.0 mmol, 96%). ^1H NMR (400 MHz, CDCl_3): δ = 8.56 (s, 1H), 8.37 (s, 1H), 8.24 (d, 1H, J = 7.9 Hz), 8.07 (d, 1H, J = 7.9 Hz), 7.59 (t, 1H, J = 7.9 Hz), 3.77 (t, 2H, J = 7.0 Hz), 2.81 (t, 2H, J = 7.0 Hz), 2.62 (q, 4H, J = 7.1 Hz), 1.05 ppm (t, 6H, J = 7.1 Hz); ^{13}C NMR (100 MHz, CDCl_3): δ = 159.0, 148.5, 138.0, 133.5, 129.5, 124.8, 122.5, 59.8, 53.3, 47.6, 12.0 ppm.

2-(Diethylamino)ethyl(3-methyl-phenyl)methylideneamine (X = Me, Y = H): *N,N*-Diethylethylenediamine (0.59 g, 5.0 mmol) was added to a solution of 3-methylbenzaldehyde (0.60 g, 5.0 mmol) in diethyl ether (50 mL). The solution was stirred for one hour over Na_2SO_4 and heated under reflux for another hour. After filtration and removing the solvent under reduced pressure, a slightly yellow oil was obtained (1.00 g, 4.6 mmol, 92%). ^1H NMR (400 MHz, CDCl_3): δ = 8.28 (s, 1H), 7.46 (m, 2H), 7.23 (m, 2H), 3.72 (t, 2H, J = 7.2 Hz), 2.78 (t, 2H, J = 7.2 Hz), 2.61 (q, 4H, J = 7.2 Hz), 2.38 (s, 3H), 1.06 ppm (t, 6H, J = 7.2 Hz); ^{13}C NMR (100 MHz, CDCl_3): δ = 162.0, 138.3, 136.3, 131.4, 128.9, 128.5, 125.6, 59.9, 53.6, 47.6, 21.3, 12.0 ppm.

***N'*-Benzylidene-*N,N*-dimethyl-ethylenediamine (R = Me):** Benzaldehyde (5.31 g, 50.0 mmol) and *N,N*-dimethylethylenediamine (4.41 g, 50.0 mmol) were dissolved in diethyl ether (200 mL). The reaction mixture was stirred over Na_2SO_4 for one hour and heated under reflux for one hour. It was filtrated, the solvent was removed under reduced pressure and a slightly yellow oil was obtained (7.87 g, 44.5 mmol, 89%). ^1H NMR (400 MHz, CDCl_3): δ = 8.31 (s, 1H), 7.73 (m, 2H), 7.40 (m, 3H), 3.75 (t, 2H, J = 7.1 Hz), 2.66 (t, 2H, J = 7.1 Hz), 2.32 ppm (s, 6H); ^{13}C NMR (100 MHz, CDCl_3): δ = 161.8, 136.2, 130.6, 128.5, 128.1, 60.1, 59.9, 45.9 ppm.

Aromatic hydroxylation with BDED variations: For each of the modified BDED-ligands 2-(diethylamino)ethyl(4-methoxy-phenyl)-methylideneamine, 2-(diethylamino)ethyl(4-nitrophenyl)methylideneamine, and 2-(diethylamino)ethyl(3-nitrophenyl)methylideneamine, 5 mmol were dissolved in acetone (10 mL) under inert conditions. A 0.6 M solution of $[\text{Cu}(\text{CH}_3\text{CN})_4]\text{CF}_3\text{SO}_3$ in acetone (8.3 mL)

was added and dioxygen was passed through the solution for 30 min. For the other derivatives, 2-(diethylamino)ethyl(4-methyl-phenyl)methylideneamine, 2-(diethylamino)ethyl(4-chloro-phenyl)-methylideneamine, and 2-(diethylamino)ethyl(3-methyl-phenyl)methylideneamine, 1 mmol was dissolved in dry acetone (10 mL) and a solution of $[\text{Cu}(\text{CH}_3\text{CN})_4]\text{CF}_3\text{SO}_3$ (377 mg, 1 mmol) in dry acetone (10 mL) was added. Dioxygen was also passed through these complex solutions. For *N'*-Benzylidene-*N,N*-dimethyl-ethylenediamine (1.76 g, 10 mmol) ligand and $[\text{Cu}(\text{CH}_3\text{CN})_4]\text{CF}_3\text{SO}_3$ (3.76 g, 10 mmol) in dry acetone (40 mL) were used in similar way. The mixture was left overnight in the refrigerator. Hydrochloric acid (20 mL 1 M) was added and the solution was heated up to 70 °C for 30 min. Most of the acetone was removed under reduced pressure and the remaining solution was washed with CH_2Cl_2 several times. The combined organic phases were dried over Na_2SO_4 , the solvent was removed and a "pre"-purification was performed over silica. The remaining oil was analyzed by using GC/MS.

Acknowledgements

Pascal Specht is acknowledged for his assistance with some of the experiments performed during his Bachelor research project (JLU, Gießen). P.G. gratefully acknowledges a Ph.D. grant provided by the Beilstein-Institut, Frankfurt am Main (Germany) within the research collaboration NanoBiC. Quantum chemical calculations have been performed at the Center for Scientific Computing (CSC) Frankfurt on the Fuchs and LOEWE-CSC high-performance computer clusters.

Keywords: aldehydes · copper · density functional calculations · hydroxylation · transition states

- [1] a) E. I. Solomon, U. M. Sundaram, T. E. Machonkin, *Chem. Rev.* **1996**, *96*, 2563–2605; b) H. Decker, R. Dillinger, F. Tuzcek, *Angew. Chem. Int. Ed.* **2000**, *39*, 1591–1595; *Angew. Chem.* **2000**, *112*, 1656–1660; c) Á. Sánchez-Ferrer, J. N. Rodríguez-López, F. García-Cánovas, F. García-Carmona, *Biochim. Biophys. Acta Protein Struct. Mol. Enzymol.* **1995**, *1247*, 1–11; d) Y. Matoba, T. Kumagai, A. Yamamoto, H. Yoshitsu, M. Sugiyama, *J. Biol. Chem.* **2006**, *281*, 8981–8990; e) H. Decker, T. Schweikhardt, F. Tuzcek, *Angew. Chem. Int. Ed.* **2006**, *45*, 4546–4550; *Angew. Chem.* **2006**, *118*, 4658–4663; f) L. Que, Jr., W. B. Tolman, *Nature* **2008**, *455*, 333–340.
- [2] a) A. L. Lewis, W. B. Tolman, *Chem. Rev.* **2004**, *104*, 1047–1076; b) L. M. Mirica, X. Ottenwaelder, T. D. P. Stack, *Chem. Rev.* **2004**, *104*, 1013–1045; c) O. Sander, A. Henß, C. Näther, C. Würtele, M. C. Holthausen, S. Schindler, F. Tuzcek, *Chem. Eur. J.* **2008**, *14*, 9714–9729; d) L. Q. Hatcher, K. D. Karlin, *J. Biol. Inorg. Chem.* **2004**, *9*, 669–683; e) M. Becker, S. Schindler, K. D. Karlin, T. A. Kaden, S. Kaderli, T. Palanché, A. D. Zuberbühler, *Inorg. Chem.* **1999**, *38*, 1989–1995; f) K. D. Karlin, S. Kaderli, A. D. Zuberbühler, *Acc. Chem. Res.* **1997**, *30*, 139–147; g) K. D. Karlin, J. C. Hayes, Y. Gultneh, R. W. Cruse, J. W. Mckown, J. P. Hutchinson, J. Zubieta, *J. Am. Chem. Soc.* **1984**, *106*, 2121–2128; h) S. Itoh, H. Kumei, M. Taki, S. Nagatomo, T. Kitagawa, S. Fukuzumi, *J. Am. Chem. Soc.* **2001**, *123*, 6708–6709; i) M. Réglie, C. Jorand, B. Waegell, *J. Chem. Soc. Chem. Commun.* **1990**, 1752–1755; j) A. Company, S. Palavicini, I. Garcia-Bosch, R. Mas-Ballesté, L. Que Jr., E. V. Rybak-Akimova, L. Casella, X. Ribas, M. Costas, *Chem. Eur. J.* **2008**, *14*, 3535–3538; k) T. Osako, K. Ohkubo, M. Taki, Y. Tachi, S. Fukuzumi, S. Itoh, *J. Am. Chem. Soc.* **2003**, *125*, 11027–11033; l) S. Itoh, S. Fukuzumi, *Acc. Chem. Res.* **2007**, *40*, 592–600; m) B. Schönecker, T. Zheldakova, Y. Liu, M. Köttritzsch, W. Günther, H. Görls, *Angew. Chem. Int. Ed.* **2003**, *42*, 3240–3244; *Angew. Chem.* **2003**, *115*, 3361–3365; n) S. Palavicini, A. Granata, E. Monzani, L. Casella, *J. Am. Chem. Soc.* **2005**, *127*, 18031–18036; o) K. D. Karlin, C. X. Zhang, A. L. Rheingold, B. Galliker, S. Kaderli, A. D. Zuberbühler, *Inorg. Chim. Acta* **2012**, *389*, 138–150;

- p) M. S. Nasir, B. I. Cohen, K. D. Karlin, *J. Am. Chem. Soc.* **1992**, *114*, 2482–2494; q) K. D. Karlin, M. S. Nasir, B. I. Cohen, R. W. Cruse, S. Kaderli, A. D. Zuberbühler, *J. Am. Chem. Soc.* **1994**, *116*, 1324–1336.
- [3] a) L. Casella, M. Gullotti, R. Radaelli, P. Di Gennaro, *J. Chem. Soc. Chem. Commun.* **1991**, 1611–1612; b) M. Rolff, J. Schottenheim, G. Peters, F. Tuzcek, *Angew. Chem. Int. Ed.* **2010**, *49*, 6438–6442; *Angew. Chem.* **2010**, *122*, 6583–6587; c) A. Hoffmann, C. Citek, S. Binder, A. Goos, M. Rübhausen, O. Troepfner, I. Ivanović-Burmazović, E. C. Wasinger, D. P. Stack, S. Herres-Pawlis, *Angew. Chem. Int. Ed.* **2013**, *52*, 5398–5401; *Angew. Chem.* **2013**, *125*, 5508–5512; d) J. Schottenheim, N. Fateeva, W. Thimm, J. Krahmer, F. Tuzcek, *Z. Anorg. Allg. Chem.* **2013**, *639*, 1491–1497; e) M. Rolff, J. Schottenheim, H. Decker, F. Tuzcek, *Chem. Soc. Rev.* **2011**, *40*, 4077–4098; f) L. Santagostini, M. Gullotti, E. Monzani, L. Casella, R. Dillinger, F. Tuzcek, *Chem. Eur. J.* **2000**, *6*, 519–522; g) B. T. Op't Holt, M. A. Vance, L. M. Mirica, D. E. Heppner, T. D. P. Stack, E. I. Solomon, *J. Am. Chem. Soc.* **2009**, *131*, 6421–6438.
- [4] a) L. M. Mirica, M. A. Vance, D. J. Rudd, B. Hedman, K. O. Hodgson, E. I. Solomon, T. D. P. Stack, *Science* **2005**, *308*, 1890–1892; b) S. Herres-Pawlis, P. Verma, R. Haase, P. Kang, C. T. Lyons, E. C. Wasinger, U. Flörke, G. Henkel, T. D. P. Stack, *J. Am. Chem. Soc.* **2009**, *131*, 1154–1169; c) J. A. Halfen, S. Mahapatra, E. C. Wilkinson, S. Kaderli, V. G. Young, Jr., L. Que Jr., A. D. Zuberbühler, W. B. Tolman, *Science* **1996**, *271*, 1397–1400; d) L. Que, Jr., W. B. Tolman, *Angew. Chem. Int. Ed.* **2002**, *41*, 1114–1137; *Angew. Chem.* **2002**, *114*, 1160–1185; e) K. V. N. Esguerra, Y. Fall, J.-P. Lumb, *Angew. Chem. Int. Ed.* **2014**, *53*, 5877–5981; *Angew. Chem.* **2014**, *126*, 5987–5991; f) K. V. N. Esguerra, Y. Fall, L. Peitjean, J.-P. Lumb, *J. Am. Chem. Soc.* **2014**, *136*, 7662–7668.
- [5] P. L. Holland, K. R. Rodgers, W. B. Tolman, *Angew. Chem. Int. Ed.* **1999**, *38*, 1139–1142; *Angew. Chem.* **1999**, *111*, 1210–1213.
- [6] a) A. Orita, H. Taniguchi, J. Otera, *Chem. Asian J.* **2006**, *1*, 430–437; b) C. L. Chuang, K. Lim, Q. Chen, J. Zubieta, J. W. Canary, *Inorg. Chem.* **1995**, *34*, 2562–2568; c) M. M. Makowska-Grzyska, E. Szajna, C. Shipley, A. M. Arif, M. H. Mitchell, J. A. Halfen, L. M. Berreau, *Inorg. Chem.* **2003**, *42*, 7472–7488.
- [7] a) Y. F. Liu, J. G. Yu, P. E. M. Siegbahn, M. R. A. Blomberg, *Chem. Eur. J.* **2013**, *19*, 1942–1954; b) M. Güell, J. M. Luis, P. E. M. Siegbahn, M. Solà, *J. Biol. Inorg. Chem.* **2009**, *14*, 273–285; c) A. Poater, M. Solà, *Beilstein J. Org. Chem.* **2013**, *9*, 585–593; d) A. Poater, X. Ribas, A. Llobet, L. Cavallo, M. Solà, *J. Am. Chem. Soc.* **2008**, *130*, 17710–17717.
- [8] S. Herres, A. J. Heuwing, U. Flörke, J. Schneider, G. Henkel, *Inorg. Chim. Acta* **2005**, *358*, 1089–1095.
- [9] A. R. Surrey, *J. Am. Chem. Soc.* **1949**, *71*, 2941–2942.
- [10] a) X. Li, Y.-H. Liu, W.-J. Gu, B. Li, F.-J. Chen, B.-F. Shi, *Org. Lett.* **2014**, *16*, 3904–3907; b) F. Mo, L. J. Trzepakowski, G. Dong, *Angew. Chem. Int. Ed.* **2012**, *51*, 13075–13079; *Angew. Chem.* **2012**, *124*, 13252–13256.
- [11] a) E. Amadéi, E. H. Alilou, F. Eydoux, M. Pierrot, M. Réglie, B. Waegell, *J. Chem. Soc. Chem. Commun.* **1992**, 1782–1784; b) I. Blain, P. Bruno, M. Giorgi, E. Lojou, D. Lexa, M. Réglie, *Eur. J. Inorg. Chem.* **1998**, 1297–1304; c) I. Blain, M. Giorgi, I. De Riggi, M. Réglie, *Eur. J. Inorg. Chem.* **2000**, 393–398.
- [12] a) B. Schönecker, C. Lange, *J. Organomet. Chem.* **2006**, *691*, 2107–2124; b) B. Schönecker, C. Lange, T. Zheldakova, W. Günther, H. Görls, G. Vaughan, *Tetrahedron* **2005**, *61*, 103–114; c) B. Schönecker, T. Zheldakova, C. Lange, W. Günther, H. Görls, M. Bohl, *Chem. Eur. J.* **2004**, *10*, 6029–6042.
- [13] P. Naumov, S. W. Ng, *J. Coord. Chem.* **2006**, *59*, 1307–1309.
- [14] S. Kozuch, J. M. L. Martin, *ChemPhysChem* **2011**, *12*, 1413–1418.
- [15] C. Zondervan, E. K. van den Beuken, H. Kooijman, A. L. Spek, B. L. Ferin-ga, *Tetrahedron Lett.* **1997**, *38*, 3111–3114.
- [16] G. J. Kubas in *Inorganic Syntheses* (Ed.: D. F. Shriver), Vol. 19, John Wiley & Sons, New York, **1979**, p. 1990.
- [17] P. Luehring, A. Schumpe, *J. Chem. Eng. Data* **1989**, *34*, 250–252.
- [18] G. M. Sheldrick, *Acta Crystallogr. A* **2015**, *71*, 3–8.
- [19] G. M. Sheldrick, *Acta Crystallogr. A* **2008**, *64*, 112–122.
- [20] Gaussian 09, Revision A.02, M. J. Frisch, G. W. Trucks, H. B. Schlegel, G. E. Scuseria, M. A. Robb, J. R. Cheeseman, G. Scalmani, V. Barone, B. Men-nucci, G. A. Petersson, H. Nakatsuji, M. Caricato, X. Li, H. P. Hratchian, A. F. Izmaylov, J. Bloino, G. Zheng, J. L. Sonnenberg, M. Hada, M. Ehara, K. Toyota, R. Fukuda, J. Hasegawa, M. Ishida, T. Nakajima, Y. Honda, O. Kitao, H. Nakai, T. Vreven, J. A. Montgomery Jr., J. E. Peralta, F. Ogliaro, M. Bearpark, J. J. Heyd, E. Brothers, K. N. Kudin, V. N. Staroverov, T. Keith, R. Kobayashi, J. Normand, K. Raghavachari, A. Rendell, J. C. Burant, S. S. Iyengar, J. Tomasi, M. Cossi, N. Rega, J. M. Millam, M. Klene, J. E. Knox, J. B. Cross, V. Bakken, C. Adamo, J. Jaramillo, R. Gomperts, R. E. Strat-mann, O. Yazyev, A. J. Austin, R. Cammi, C. Pomelli, J. W. Ochterski, R. L. Martin, K. Morokuma, V. G. Zakrzewski, G. A. Voth, P. Salvador, J. J. Dan-nenberg, S. Dapprich, A. D. Daniels, O. Farkas, J. B. Foresman, J. V. Ortiz, J. Cioslowski, D. J. Fox, Gaussian, Inc., Wallingford, CT, **2009**.
- [21] a) A. D. Becke, *Phys. Rev. A* **1988**, *38*, 3098–3100; b) C. Lee, W. Yang, R. G. Parr, *Phys. Rev. B* **1988**, *37*, 785–789; c) B. Miehlich, A. Savin, H. Stoll, H. Preuss, *Chem. Phys. Lett.* **1989**, *157*, 200–206; d) S. Grimme, *J. Comput. Chem.* **2006**, *27*, 1787–1799.
- [22] a) A. Schäfer, H. Horn, R. Ahlrichs, *J. Chem. Phys.* **1992**, *97*, 2571–2577; b) F. Weigend, R. Ahlrichs, *Phys. Chem. Chem. Phys.* **2005**, *7*, 3297–3305.
- [23] M. Dolg, U. Wedig, H. Stoll, H. Preuss, *J. Chem. Phys.* **1987**, *86*, 866–872.
- [24] a) B. I. Dunlap, *J. Chem. Phys.* **1983**, *78*, 3140–3142; b) B. I. Dunlap, *J. Mol. Struct.* **2000**, *529*, 37–40.
- [25] S. Grimme, J. Antony, S. Ehrlich, H. Krieg, *J. Chem. Phys.* **2010**, *132*, 154104–154119.
- [26] A. Klamt, G. Schüürmann, *J. Chem. Soc. Perkin Trans. 2* **1993**, 799–805.
- [27] F. Neese, U. Becker, D. Bykov, D. Ganyushin, A. Hansen, R. Izsak, D. G. Liakos, C. Kollmar, S. Kossmann, D. A. Pantazis, T. Petrenko, C. Reimann, C. Riplinger, M. Roemelt, B. Sandhöfer, I. Schapiro, K. Sivalingam, B. Wez-sla, ORCA - An ab initio, DFT and semiempirical SCF-MO package, Ver-sion 2.9, MPI for Chemical Energy Conversion, Mülheim, Germany, **2012**.
- [28] a) R. A. Kendall, A. Früchtl, *Theor. Chem. Acc.* **1997**, *97*, 158–163; b) K. Eichkorn, O. Treutler, H. Öhm, M. Häser, R. Ahlrichs, *Chem. Phys. Lett.* **1995**, *240*, 283–290; c) K. Eichkorn, F. Weigand, O. Treutler, R. Ahlrichs, *Theor. Chem. Acc.* **1997**, *97*, 119–124.
- [29] F. Weigend, *Phys. Chem. Chem. Phys.* **2006**, *8*, 1057–1065.
- [30] a) K. Yamaguchi, Y. Takahara, T. Fueno in *Applied Quantum Chemistry* (Ed.: V. H. Smith), Reidel, Dordrecht, **1986**, p. 155; b) T. Soda, Y. Kitaga-wa, T. Onishi, Y. Takano, Y. Shigeta, H. Nagao, Y. Yoshioka, K. Yamaguchi, *Chem. Phys. Lett.* **2000**, *319*, 223–230.
- [31] C. Y. Legault, CYLview, version 1.0b ed., Université de Sherbrooke, Sher-brooke, QC, **2009**, <http://www.cylview.org>.

Received: March 13, 2015
Published online on June 18, 2015

Efficient Access to Substituted Silafluorenes by Nickel-Catalyzed Reactions of Biphenylenes with Et₂SiH₂

Jens Michael Breunig, Puneet Gupta, Animesh Das, Samat Tussupbayev, Martin Diefenbach, Michael Bolte, Matthias Wagner, Max C. Holthausen,* and Hans-Wolfram Lerner*[^a]

Abstract: The reaction of biphenylene (**1**) with Et₂SiH₂ in the presence of [Ni(PPhMe₂)₄] results in the formation of a mixture of 2-diethylhydrosilylbiphenyl [**2**(Et₂HSi)] and 9,9-diethyl-9-silafluorene (**3**). Silafluorene **3** was isolated in 37.5% and **2**(Et₂HSi) in 36.9% yield. The underlying reaction mechanism was elucidated by DFT calculations. 4-Methyl-9,9-diethyl-9-silafluorene (**7**) was obtained selectively from the [Ni(PPhMe₂)₄]-catalyzed reaction

of Et₂SiH₂ and 1-methylbiphenylene. By contrast, no selectivity could be found in the Ni-catalyzed reaction between Et₂SiH₂ and the biphenylene derivative that bears *t*Bu substituents in the 2- and 7-positions. Therefore, two pairs of isomers of *t*Bu-substituted sila-

fluorenes and of the related diethylhydrosilylbiphenyls were formed in this reaction. However, a subsequent dehydrogenation of the diethylhydrosilylbiphenyls with Wilkinson's catalyst yielded a mixture of 2,7-di-*tert*-butyl-9,9-diethyl-9-silafluorene (**8**) and 3,6-di-*tert*-butyl-9,9-diethyl-9-silafluorene (**9**). Silafluorenes **8** and **9** were separated by column chromatography.

Keywords: C–C activation • density functional calculations • nickel • Si–H activation • silanes

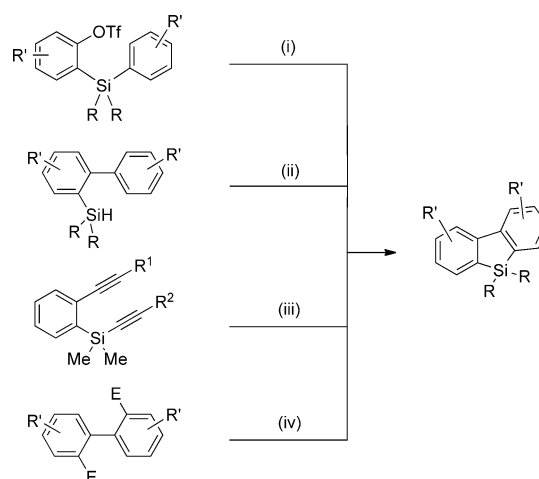
Introduction

Silafluorenes are being increasingly recognized as π -conjugated materials with promising potential for device applications, and important contributions have been made in the areas of electro- and photoluminescence.^[1–5] With their typically low lying LUMO energy level originating from interference of the exocyclic Si–C σ^* orbital and the π^* orbital of the biphenyl fragment,^[6–9] this class of compounds can be used as electron-transporting material for emitters in organic light-emitting diodes.^[10] In this context, the ability to control the electronic nature of these chromophores by variation of the functional groups is critical to optimize and fine-tune their properties.

We have a long-standing interest in boron-doped aromatics^[11–15] and have developed inter alia a protocol for the synthesis of 9-borafluorenes by treatment of the corresponding 9-silafluorene derivatives with BBr₃.^[12,13] However, conven-

ient access to silafluorenes with an asymmetric substitution pattern in the 4-positions is lacking as of yet.

A number of synthetic routes towards 9-silafluorenes have been reported earlier (cf. Scheme 1): Silafluorenes were prepared i) by Pd-catalyzed C–C coupling reactions of diaryl silanes ArAr'SiR₂ carrying a triflate group in the 2-position of the aryl substituent Ar, whereby bond formation occurs with the corresponding unsubstituted 2-position of the aryl substituent Ar',^[16,17] ii) by ring closure via a silylium



Scheme 1. Known preparation routes of 9-silafluorenes. i) [Pd], Et₂NH, dimethylacetamide, 100°C, 24 h; ii) Ph₃CB(C₆F₅)₄, 1,6-lutidine, CH₂Cl₂, RT, 1 h or [Rh], 1,4-dioxane, 135°C, 15 min; iii) [Ir], +R³CCR³, Bu₂O, 110°C, 24 h; iv) E = Li, Mg; +R₂SiCl₂.

[a] J. M. Breunig, P. Gupta, Dr. A. Das, Dr. S. Tussupbayev, Dr. M. Diefenbach, Dr. M. Bolte, Prof. Dr. M. Wagner, Prof. Dr. M. C. Holthausen, Dr. H.-W. Lerner
Institut für Anorganische Chemie
Goethe-Universität Frankfurt
Max-von-Laue-Strasse 7, 60438 Frankfurt (Germany)
Fax: (+49) 69-79829260
E-mail: lerner@chemie.uni-frankfurt.de
max.holthausen@chemie.uni-frankfurt.de

Supporting information for this article is available on the WWW under <http://dx.doi.org/10.1002/asia.201402599>.

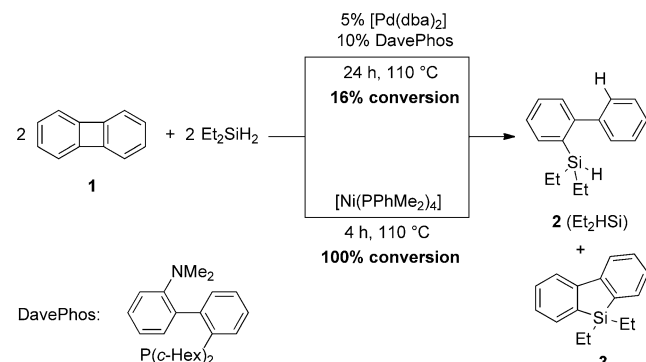
ion formed in the reaction of HSi-functionalized 2-silylbiphenyl derivatives **2**(R₂HSi) and the trityl cation^[18] or by Rh-catalyzed H₂ elimination from **2**(R₂HSi) and subsequent C–C coupling;^[19–21] iii) by Ir-catalyzed [2+2+2] cycloaddition of silicon-bridged 1,6-diyne with alkynes;^[22] and iv) by metathesis reactions of 2,2'-dimetalated biphenyls and R₂SiX₂^[8,23–26] or triorganyl silanes R₃SiX.^[27–29] Furthermore, a Pd-catalyzed reaction starting from 2,2-dihalogenated biphenyls and Et₂SiH₂ has also been reported.^[30] However, each of these protocols has specific disadvantages.^[31]

In search of alternative synthetic concepts we asked ourselves whether it is possible to gain access to 9-silafluorenes via transition metal catalyzed routes from biphenylenes and diethylsilane through C–C and Si–H bond-activation reactions with concomitant dehydrogenation. For biphenylenes bearing bulky substituents in the 1,8- or 2,7-positions, oxidative addition of the metal should occur selectively into the sterically less hindered C–C bond of the four-membered ring of biphenylenes.^[32] In this way, the selective preparation of 9-silafluorene derivatives with sophisticated substitution patterns should be possible.

As relevant precedent, we noticed a recent report of Matsuda et al. on the Pd-catalyzed hydrosilylation of biphenylenes with triorganyl silanes to give 2-silylbiphenyls.^[33] Hence, without doubt, such products were formed in C–C and Si–H activation reactions, but unfortunately the use of dialkyl silanes was not considered by these authors. Here we report an efficient approach for the synthesis of substituted 9-silafluorenes based on the nickel-catalyzed reaction of biphenylenes with Et₂SiH₂.

Results and Discussion

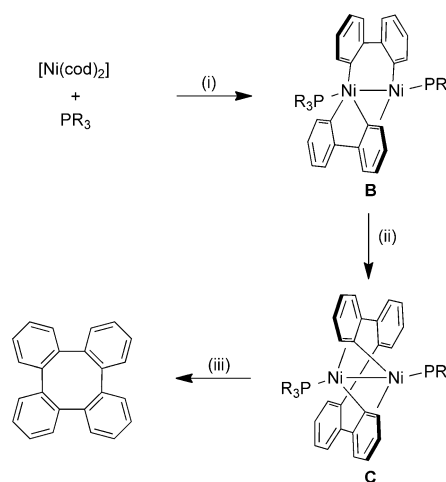
Following the approach of Matsuda et al., we first investigated the Pd-catalyzed hydrosilylation of biphenylene with Et₂SiH₂, but after heating the reaction mixture to 110 °C for 24 h we found only 16% conversion of biphenylene (20% after 6 d at 110 °C), and the 2-silylbiphenyl **2**(Et₂HSi) was formed in a mixture with the desired 9-silafluorene **3** (Scheme 2).^[34] Isolation of **3** from this reaction mixture would further lower the yield drastically.



Scheme 2. Pd- and Ni-catalyzed reaction of biphenylene with Et₂SiH₂.

In our search for alternative, more efficient catalysts, we identified nickel complexes that were reported previously to activate both C–C^[35–42] and Si–H bonds,^[43–45] and we chose to continue our efforts by employing the well-defined nickel catalyst [Ni(PPhMe₂)₄].^[46] Treatment of **1** with Et₂SiH₂ and 5 mol % [Ni(PPhMe₂)₄] in toluene at 110 °C resulted in a fast reaction with concomitant release of H₂. The ¹H NMR spectrum of the reaction solution revealed complete consumption of biphenylene after 4 h at 110 °C and formation of silylated biphenyl **2**(Et₂HSi) and silafluorene **3** in a ratio of 40:60 (Scheme 2). We were able to separate the two products by column chromatography and isolated **2**(Et₂HSi) and **3** in 36.9 and 37.5% yield, respectively. The outcome of this reaction is independent of the solvent (e.g., THF, toluene, benzene, or 1,4-dioxane).

To assess mechanistic aspects of this reaction, we conducted a series of further experiments. Firstly, the [Ni(PPhMe₂)₄] catalyst was mixed with Et₂SiH₂ in the absence of biphenylene, but no reaction was observed up to 110 °C. Secondly, the [Ni(PPhMe₂)₄] catalyst was mixed with biphenylene in the absence of Et₂SiH₂, and biphenylene dimerization to tetraphenylene was observed at 110 °C with no reaction at lower temperatures. In this context we note that Johnson and Beck^[35] obtained tetraphenylene in a similar reaction at 90 °C by employing the nickel catalyst [Ni(cod)₂]/P*i*Pr₃ (cod=1,5-cyclooctadiene). In contrast, when the reaction was conducted at room temperature, the dinuclear species **B** and **C** (Scheme 3) were isolated, but no tetraphenylene was



Scheme 3. Ni-catalyzed synthesis of tetraphenylene. i) R = *i*Pr, + biphenylene, toluene, 30 min, 25 °C; ii) R = *i*Pr, 6 h, 25 °C, toluene; iii) R = *i*Pr, 90 °C, toluene.^[35]

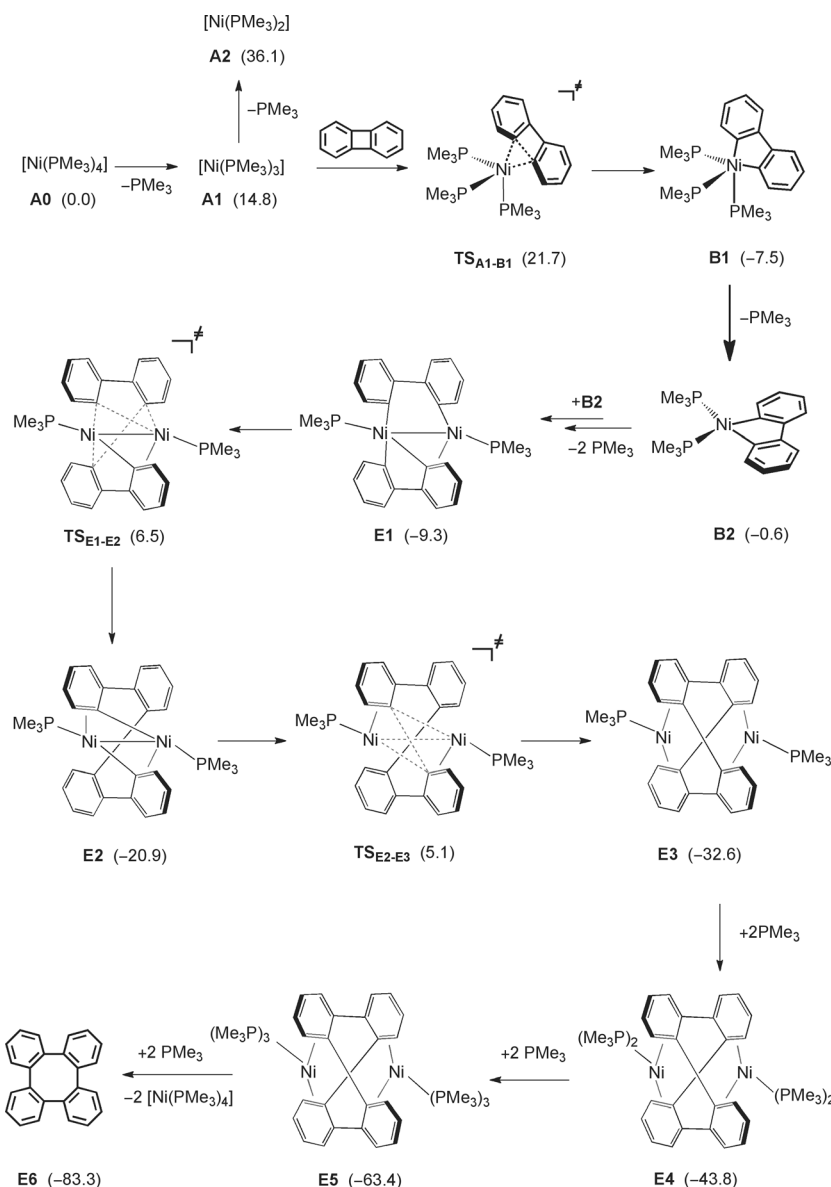
formed under these conditions. On the basis of these findings, it was concluded that tetraphenylene formation at 90 °C occurs via dinuclear intermediates **B** and **C**, while the mononuclear pathway was proposed to be less favorable.^[35]

We further investigated the possibility of interconversion between the products **2**(Et₂HSi) and **3** by dihydrogen elimination/addition in the presence of the [Ni(PPhMe₂)₄] cata-

lyst. In a reaction of $[\text{Ni}(\text{PPhMe}_2)_4]$ with $2(\text{Et}_2\text{HSi})$ carried out at 110°C , no **3** was formed by dehydrogenation even in the presence of a hydrogen scavenger (3,3-dimethyl-1-butene). We then examined the reactivity of **3** towards dihydrogen (1 or 130 bar) at 110°C in the presence of $[\text{Ni}(\text{PPhMe}_2)_4]$, but no $2(\text{Et}_2\text{HSi})$ was formed. Thus, we conclude that **2** (Et_2HSi) and **3** are not interconvertible under any reaction conditions relevant to their formation.

To elucidate the mechanistic details underlying the experimental observations, we carried out a computational study on $[\text{Ni}(\text{PMe}_3)_4]$ and Me_2SiH_2 as smaller molecular models. For selected pathways we performed additional calculations using the realistic catalyst $[\text{Ni}(\text{PPhMe}_2)_4]$. The dispersion-corrected BP86-D2 functional was chosen in combination with the def2-TZVP basis set; the performance of this level of density functional theory (DFT) was favorably tested in a careful benchmark study against high-level coupled-cluster results for a set of model reactions relevant to the present study (see the Supporting Information for details). All relative energies reported in this work are based on Gibbs free energies in kcal mol^{-1} at 298.15 K . In the following, we report our results for the $\text{Ni}(\text{PMe}_3)_4$ -catalyzed dimerization of biphenylene and for the reaction between biphenylene and Me_2SiH_2 .

The computed reaction paths commence with activation of the coordinatively saturated complex $[\text{Ni}(\text{PMe}_3)_4]$ (**A0**) by liberation of PMe_3 to create a vacant coordination site (Scheme 4). Dissociation of the first PMe_3 ligand to give $[\text{Ni}(\text{PMe}_3)_3]$ (**A1**) can readily occur under the reaction conditions ($\Delta_r G_{298}^\circ = 15\text{ kcal mol}^{-1}$), whereas detachment of a second phosphine ligand would be a substantially more endergonic step ($\Delta_r G_{298}^\circ = 36\text{ kcal mol}^{-1}$ relative to **A0**). Energetically favored, in fact, is the activation of one of the strained central C–C bonds in biphenylene by oxidative addition to **A1**, which leads to exergonic formation of metallacycle **B1** with an overall activation barrier of 22 kcal mol^{-1}



Scheme 4. Activation of Ni catalyst **A0** and its insertion into the C–C bond of biphenylene. Gibbs free energies $\Delta_r G_{298}^\circ$ [kcal mol^{-1}] are relative to **A0**.

(referenced to **A0**). Subsequent liberation of a second PMe_3 ligand from **B1** leads to the 16-electron complex **B2** ($\Delta_r G_{298}^\circ = 7\text{ kcal mol}^{-1}$). We investigated an obvious mononuclear pathway, that is, oxidative addition of another biphenylene molecule to **B2** followed by reductive elimination of tetraphenylene, but we regarded such a process as irrelevant because of its unreasonably high activation barrier (see Supporting Information, Section 5 and Scheme 2S). Instead, we identified a dinuclear route that nicely explains tetraphenylene formation, including all pertinent experimental findings reported by Johnson and Beck^[35] (Scheme 3).

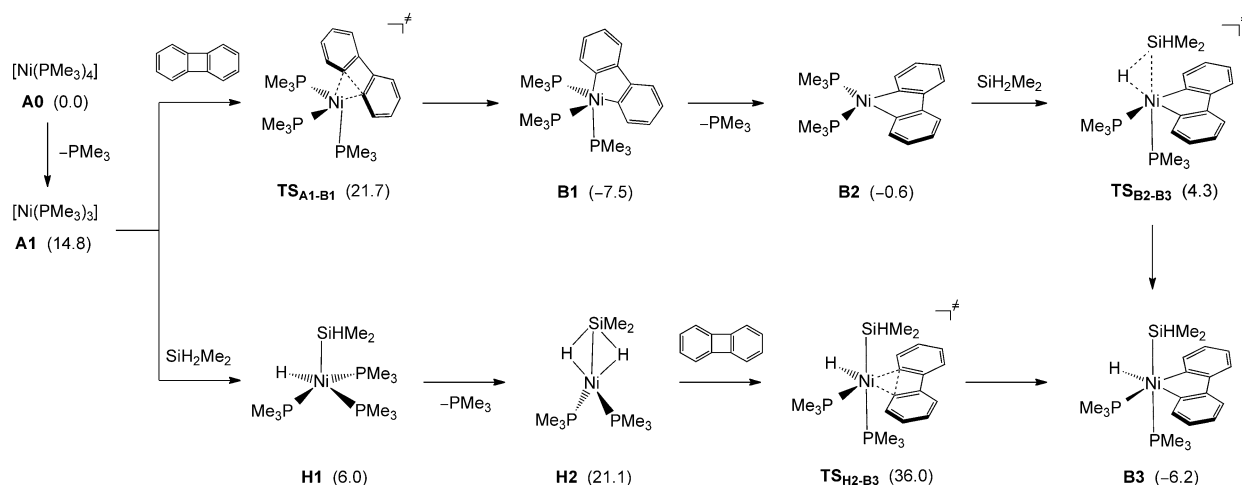
In our computational evaluation of the dinuclear route we adopted **E1**, the structural analogue of the experimentally characterized species **B** (Scheme 3), as starting point. We

relate its formation to dimerization of two molecules of **B2** on release of another phosphine ligand per unit to give **E1** ($\Delta_r G_{298}^\circ = -9 \text{ kcal mol}^{-1}$ for this step). This dimerization occurs asymmetrically, and **E1** features, apart from an Ni–Ni σ bond, one formal Ni^{III} ion engaged in three Ni–C σ bonds and a formal Ni^I ion involved in one Ni–C σ bond and η^2 coordination with one of the phenyl rings. This formal mixed-valence description is moderately pronounced, as indicated by CM5 charges^[47] of +0.393 and +0.288 calculated for the Ni^{III} and Ni^I ions, respectively. The two nickel centers in **E1** cooperatively promote the first C–C coupling step through transition state **TS_{E1-E2}** to yield metallacycle **E2**, which formally contains two Ni^I ions, in an exergonic step ($\Delta_r G_{298}^\circ = -12 \text{ kcal mol}^{-1}$). This reductive elimination proceeds with a moderate energy barrier of 16 kcal mol⁻¹, which indicates that it is kinetically feasible and irreversible at room temperature (reverse barrier: 27 kcal mol⁻¹).

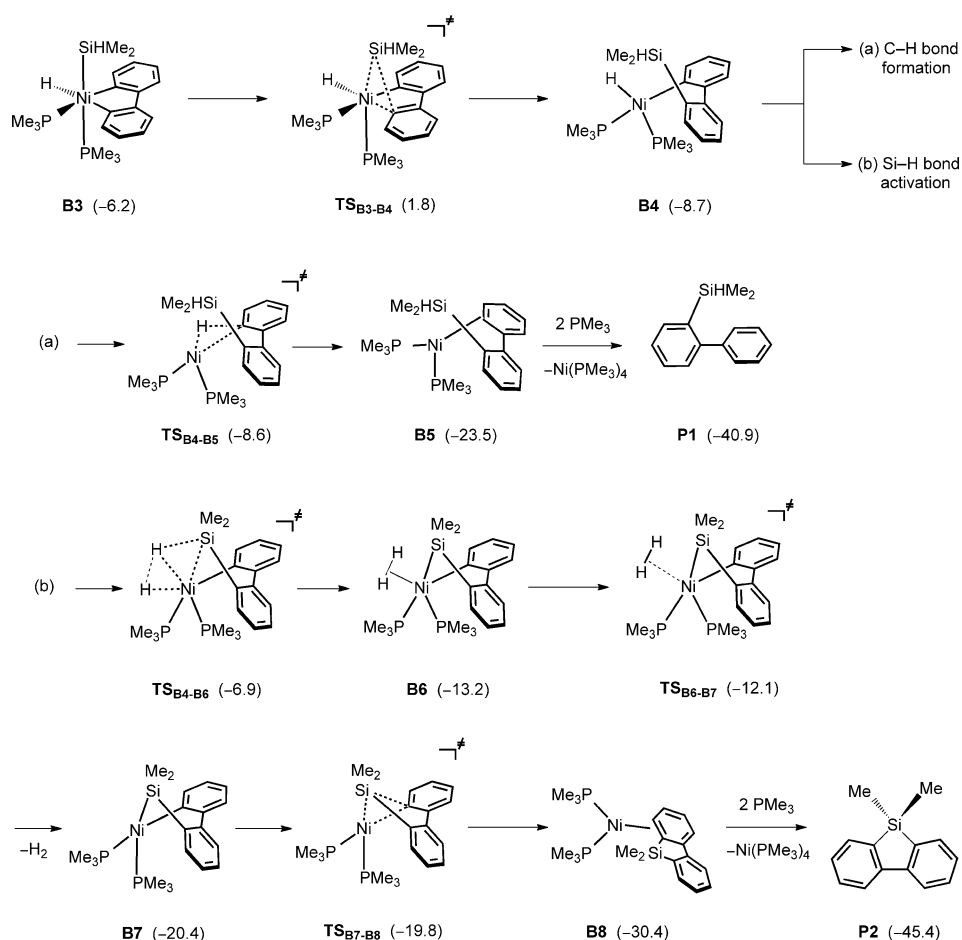
The second C–C coupling step resulting in **E3**, in which tetraphenylene is coordinatively bound to two Ni⁰ centers, is also exergonic ($\Delta_r G_{298}^\circ = -12 \text{ kcal mol}^{-1}$). However, it has a significantly higher energy barrier of 26 kcal mol⁻¹, which is most probably related to the loss of Ni–Ni interaction via **TS_{E2-E3}**. The Ni atoms readily coordinate free phosphine ligands in the next steps to liberate tetraphenylene (**E6**) with reformation of the initial catalyst **A0** in a highly exergonic reaction sequence ($\Delta_r G_{298}^\circ = -83 \text{ kcal mol}^{-1}$). These results are nicely in line with the findings of Johnson and Beck, who reported the first C–C coupling to proceed at room temperature and the second, yielding tetraphenylene, to occur only on heating. With an overall activation barrier of 26 kcal mol⁻¹, the dinuclear pathway is clearly more favorable than the mononuclear route (31 kcal mol⁻¹, see the Supporting Information). Nevertheless, DFT predicts a rather moderate barrier of 22 kcal mol⁻¹ for the initial C–C bond activation of biphenylene, in contrast to our experimental results, in which no reaction was observed at room temperature.

We hence investigated the influence that our choice of PMe₃ ligands as molecular model has on the computed reaction paths compared to the PPhMe₂ ligands used in our experiments. In the realistic catalyst model, liberation of one of the phosphine ligands from the [Ni(PPhMe₂)₄] complex is significantly endergonic by 23 kcal mol⁻¹, and the activation barrier for subsequent insertion into the C–C bond of biphenylene is 9 kcal mol⁻¹ (see Supporting Information, Section 5 and Scheme 3S). The overall activation barrier of this insertion step is 32 kcal mol⁻¹, which is clearly efficiently surmountable only at elevated temperatures. The main contribution to the increase in the total barrier to insertion stems from the energy needed for the detachment of PPhMe₂, and we attribute the stronger binding of PPhMe₂ to additional stabilizing π -stacking interactions among the phenyl rings in the reactant complex [Ni(PPhMe₂)₄].

We studied two pathways for the initial phase of the reaction, which commence with oxidative addition of the silane or biphenylene to the nickel catalyst. Initial Si–H bond activation by **A1** leads to silyl hydride complex **H1** and, after decooordination of another phosphine ligand, to **H2** in a substantially endergonic sequence (Scheme 5). Subsequent oxidative addition of biphenylene to **H2** via **TS_{H2-B3}** yields **B3** with an overall reaction barrier of 36 kcal mol⁻¹ relative to **A0**.^[48] With its high barrier, this process is kinetically not competitive with the alternative route commencing with the oxidative addition of the C–C bond in biphenylene to form complex **B1** in an exergonic step. In view of the expected substantial entropic penalty, we did not investigate pathways involving dinuclear species.^[49] After loss of PMe₃ from **B1**, **B3** is formed by oxidative addition of the silane with only a small activation barrier, so that the initial C–C bond activation barrier of 22 kcal mol⁻¹ (with respect to **A0**) represents the overall kinetic bottleneck for this route. Hence, fully in line with our experimental observations detailed above, initial Si–H bond activation is clearly disfavored and biphenylene C–C bond activation is the initial step in the



Scheme 5. Two alternative pathways for the formation of **B3**. Gibbs free energies $\Delta_r G_{298}^\circ$ [kcal mol⁻¹] are relative to **A0**.



Scheme 6. Pathways leading to the products 2-dimethylhydrosilylbiphenyl (**P1**) and 9-silafluorene (**P2**). Gibbs free energies ΔG_{298}^\ddagger [kcal mol^{−1}] are relative to **A0**.

overall course of the reaction, also in the presence of dimethylsilane.

From **B3**, a silyl shift from the Ni ion onto the carbon framework leads to the formation of **B4**, in which one of the phenyl rings has been silylated in *ortho* position (Scheme 6). At this point two pathways branch off: a) a low-barrier hydrogen atom transfer via **TS_{B4-B5}** leads to the π -coordinated complex **B5** and coordination of PMe_3 ligands finalizes the reaction sequence leading to product **P1**; b) Si–H bond activation with concomitant H–H bond formation through multicenter transition state^[51] **TS_{B4-B6}** leads to the formation of dihydrogen complex **B6**, which readily eliminates H_2 to give **B7**. The second Si–C bond is formed on reductive elimination of silafluorene **P2**, which involves intermediate π -bonded complex **B8** and ligand substitution by PMe_3 .

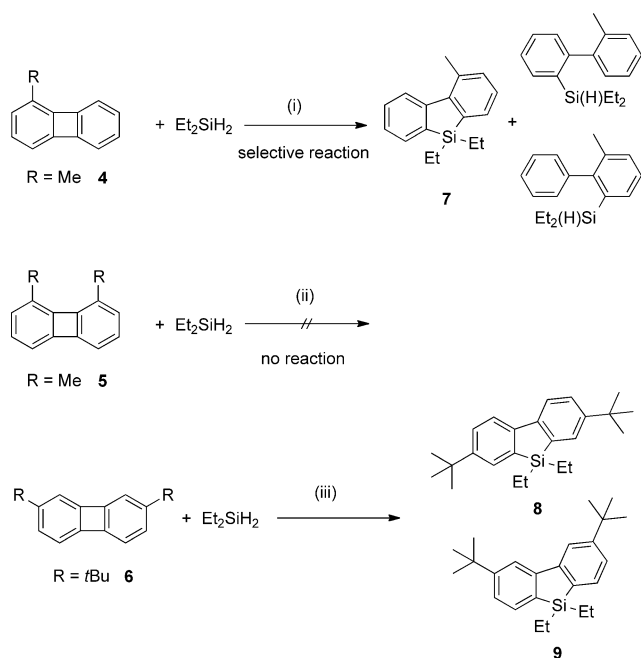
As illustrated in Scheme 6, both pathways starting from **B4** have moderately low energy barriers and most of the steps are exergonic. With prohibitively high reverse activation barriers of 34 and 39 kcal mol^{−1}, respectively, products **P1** and **P2** are not readily interconvertible under the reaction conditions. Hence, the resulting product mixture is not thermodynamically controlled and, independent of the relative stability of **P1** and **P2**, the product distribution is deter-

mined by the relative barrier heights associated with the two routes leading to **P1** and **P2** (i.e., **TS_{B4-B5}** and **TS_{B4-B6}**, respectively). With nearly barrierless formation of **P1** and a barrier of 2 kcal mol^{−1} associated with the formation of **P2**, the computational results do not quantitatively account for the experimental observation that the two products are formed in approximately equal yield, but this small difference in barrier heights falls within the accuracy limitations of the computational method chosen (2 kcal mol^{−1}, cf. the benchmark section provided in the Supporting Information). However, only minute barriers occur along reaction paths (a) and (b), and we find that the initial C–C bond activation step via **TS_{A1-B1}** is rate-limiting. Subsequent to formation of **B1**, oxidative addition of the silane occurs with an effective barrier of only 12 kcal mol^{−1} (**B1** → **TS_{B2-B3}**, Scheme 5). We find this route to be favored over the first kinetically relevant steps of the oxidative addition of a second biphenylene unit, which occurs with an effective

barrier of 16 kcal mol^{−1} (**E1** → **TS_{E1-E2}**, Scheme 4). Hence, nicely in line with the experimental observations, dimerization of biphenylene to form tetraphenylene does not occur in the presence of dimethylsilane.

The computed reaction mechanism indicates no obvious way to improve silafluorene yields in the product distribution. This can be accomplished, however, by adopting the known dehydrogenation of 2-hydrosilylbiphenyls with Wilkinson's catalyst.^[21] However, $[\text{Rh}(\text{PPh}_3)_3\text{Cl}]$ cannot just be added to the reaction mixture, because this catalyst is poisoned by PPhMe_2 and/or Et_2SiH_2 . Consequently, we conducted a brief aqueous workup and flash column chromatography prior to the conversion of silylbiphenyl **2** (Et_2HSi) to the silafluorene **3** (yield of **3**: 49%).

To gain access to silafluorene derivatives, our approach relies on the steric hindrance of one of the two C–C single bonds in the four-membered rings of biphenylenes. Substituents in the 1- and 8-positions of biphenylenes should prevent oxidative addition of the catalyst. Accordingly, we examined the $[\text{Ni}(\text{PPhMe}_2)_4]$ -catalyzed reaction of 1-methylbiphenylene (**4**) and 1,8-dimethylbiphenylene (**5**) with Et_2SiH_2 with regard to their reactivity and selectivity (Scheme 7). Whereas **4** reacted nicely with Et_2SiH_2 in the presence of $[\text{Ni}$ -



(PPhMe_2) $_4$], biphenylene **5** showed no reactivity at all. Clearly, steric repulsion of the two methyl groups prevents C–C bond activation during fluorene formation. Surprisingly, the steric hindrance introduced by a single methyl group suffices to obtain selectivity in the $[\text{Ni}(\text{PPhMe}_2)_4]$ -catalyzed reaction of **4** with Et_2SiH_2 (Scheme 7). 4-Methyl-9,9-diethyl-9-silafluorene (**7**) is a colorless liquid, the constitution of which was determined by 2D NMR experiments. Concomitant with the formation of **7** also the two isomeric biphenyl species 2-diethylsilyl-6-methylbiphenyl and 2-diethylsilyl-2'-methylbiphenyl were produced in this reaction. Takai et al. showed that treatment of 2-dimethylsilyl-2'-methylbiphenyl with Wilkinson's catalyst gave a silaphenanthrene derivative by C–H activation of the arylmethyl group of the silylated methylbiphenyl.^[21]

For the nickel-mediated reaction of biphenylene carrying bulky *tert*-butyl groups in the 2- and 7-positions, no selectivity was observed. However, by means of our protocol established before to improve the yield of the parent silafluorene, we converted the product mixture to an isomeric mixture of 2,7-di-*tert*-butyl-9,9-diethyl-9-silafluorene (**8**) and 3,6-di-*tert*-butyl-9,9-diethyl-9-silafluorene (**9**; Scheme 7).

The isomeric silafluorenes **8** and **9** were separated by column chromatography and crystallized by slow evaporation of CHCl_3 solutions (see Figure 1 and the Supporting Information for more details). Silafluorene **8** crystallizes in the orthorhombic space group $Pbca$ with one molecule in the asymmetric unit. Compound **9** crystallizes in the monoclinic space group $P2_1/n$ with one molecule in the asymmetric unit. X-ray quality crystals of **3** (monoclinic, Pc , two mole-

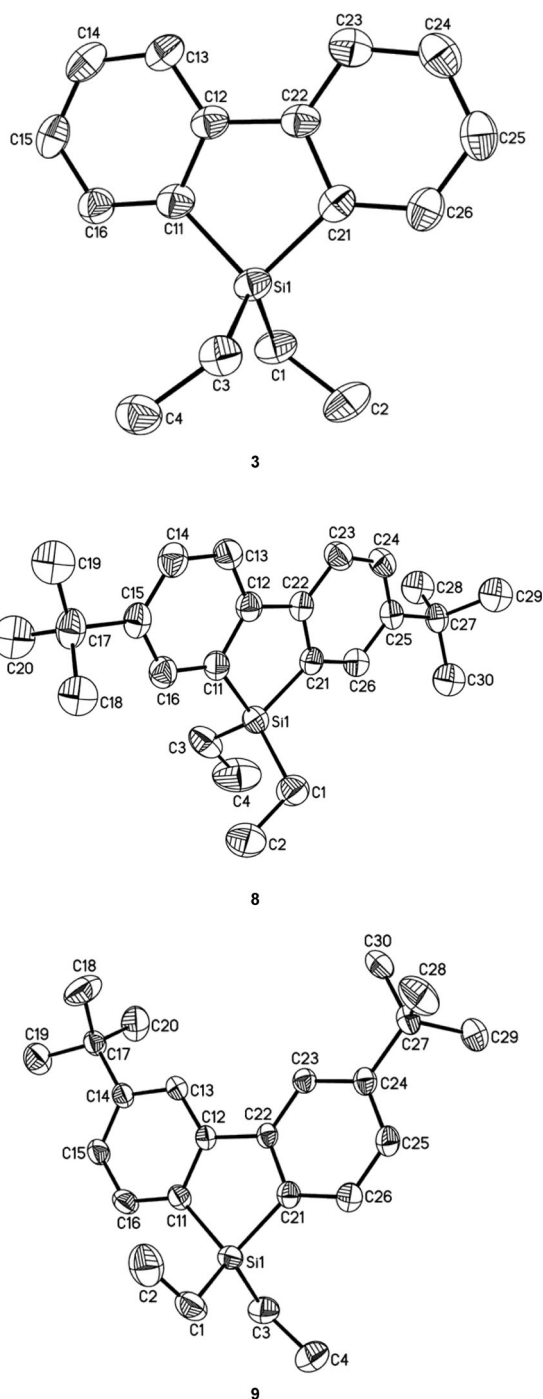


Figure 1. Molecular structures of **3**, **8**, and **9**.

cules in the asymmetric unit) were obtained by storing a concentrated hexane solution at -40°C (see Figure 1 and the Supporting Information for more details).

By cooling a concentrated diethyl ether solution of $[\text{Ni}(\text{PPhMe}_2)_4]$ to -78°C single crystals of the catalyst were obtained (see Supporting Information). $[\text{Ni}(\text{PPhMe}_2)_4]$ crystallized in the triclinic space group $P\bar{1}$ with one molecule in the asymmetric unit. The structure of $[\text{Ni}(\text{PPhMe}_2)_4]$ exhibits its perpendicular edge-to-face (T-shaped) configurations of

two phenyl rings of the phosphine ligands.^[52,53] One interaction of the phenyl rings of PPhMe₂ ligands is intramolecular and is located between H12 and the center of gravity of phenyl ring C41–C46 with a distance of 2.582 Å. The second interaction of the phenyl rings of the PPhMe₂ ligands is intermolecular (Figure 2) with a distance of 2.857 Å.

In addition we also investigated the [Ni(PPhMe₂)₄]-catalyzed reaction of biphenylene with R₃SiH (Table 1; R₃Si=

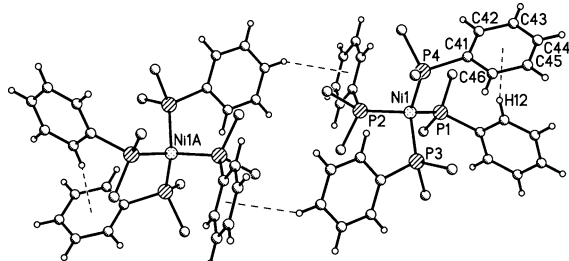
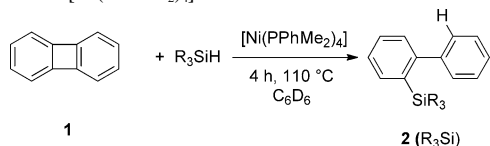


Figure 2. Packing diagram of [Ni(PPhMe₂)₄] (triclinic, *P* $\bar{1}$). H atoms on the methyl groups are omitted for clarity. Dashed lines indicate intra- and intermolecular T-shaped CH– π interactions.

Table 1. Yields of the reactions of biphenylene with triorganyl silanes in the presence of [Ni(PPhMe₂)₄].

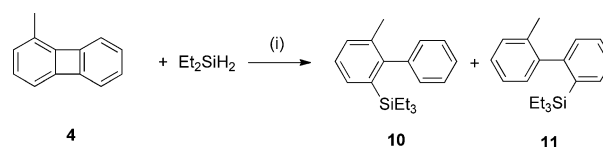


R ₃ SiH	2	Yield [%]
Et ₃ SiH	2 (Et ₃ Si)	93
<i>n</i> Pr ₃ SiH	2 (<i>n</i> Pr ₃ Si)	90
Me ₂ PhSiH	2 (Me ₂ PhSi)	85
Ph ₃ SiH	2 (Ph ₃ Si)	72

Et₃Si, *n*Pr₃Si, *i*Pr₃Si, *t*Bu₃Si, Me₂PhSi, Ph₃Si). In these reactions the corresponding 2-silylbiphenyls **2**(R₃Si) were formed in good yields when the mixtures were heated to 110 °C for 4 h (cf. Table 1).

Surprisingly, the Ni-catalyzed reaction with triisopropylsilane and tri-*tert*-butylsilane resulted only in conversion of biphenylene to tetraphenylene, just as found in the reaction of **1** with [Ni(PPhMe₂)₄] in the absence of silanes. Apparently, the steric bulk introduced by bulky alkyl groups in these two silanes makes their Si–H bonds inaccessible for oxidative addition to the nickel biphenylene metallacycle **B2**, such that its dimerization and thus tetraphenylene formation becomes favored.

Finally we found that the [Ni(PPhMe₂)₄]-catalyzed reaction of **4** with Et₃SiH (Scheme 8) yielded an inseparable mixture of the isomeric 2-triethylsilyl-6-methylbiphenyl (**10**) and 2-triethylsilyl-2'-methylbiphenyl (**11**).



Scheme 8. Reaction of **4** with Et₃SiH in the presence of [Ni(PPhMe₂)₄] yielding an isomeric mixture of **10** and **11**. i) [Ni(PPhMe₂)₄], C₆D₆, 120 °C, 2 h.

Summary and Conclusions

Convenient access to silafluorenes with sophisticated substitution patterns was established. Reaction of biphenylene with Et₂SiH₂ in the presence of [Ni(PPhMe₂)₄] resulted in the formation of a mixture of **2**(Et₂HSi) and **3**, which were separable by column chromatography in decent yields. Under the same conditions, **7** was obtained selectively by employing 1-methylbiphenylene as reactant. In contrast, no selectivity was found in the Ni-catalyzed reaction between Et₂SiH₂ and the 2,7-*t*Bu₂-substituted biphenylene derivative, and two *t*Bu-substituted silafluorene isomers **8** and **9** were obtained in a mixture with the related diethylhydrosilylbiphenyls. However, by subsequent dehydrogenation of the diethylhydrosilylbiphenyls with Wilkinson's catalyst, a mixture of isomeric silafluorenes **8** and **9** was obtained and separated by column chromatography. Further, we investigated the [Ni(PPhMe₂)₄]-catalyzed reaction of biphenylene with R₃SiH (R₃Si = Et₃Si, *n*Pr₃Si, *i*Pr₃Si, *t*Bu₃Si, Me₂PhSi, Ph₃Si), and the corresponding 2-silylbiphenyls **2**(R₃Si) (R₃Si = Et₃Si, *n*Pr₃Si, Me₂PhSi, Ph₃Si) were obtained in good yields when the mixtures were heated to 110 °C for 4 h. The constitutions of these 2-silylbiphenyls were confirmed by NMR spectroscopy. Surprisingly, no hydrosilylation of biphenylene was observed with the silanes *i*Pr₃SiH and *t*Bu₃SiH, and only tetraphenylene was obtained.

The underlying reaction mechanism was elucidated by means of DFT calculations. In keeping with earlier experimental findings, we identified a dinuclear pathway for tetraphenylene formation, which is observed for the reaction of the nickel catalyst with biphenylene in the absence of silanes. This route starts with the activation of the nickel catalyst by detachment of a phosphine ligand and subsequent insertion into the strained C–C bond of biphenylene to give nickel biphenylene intermediate **B2**. This intermediate dimerizes with concomitant detachment of two more phosphine ligands and two C–C coupling steps, cooperatively mediated by the two nickel ions, leading to tetraphenylene formation.

In the presence of silane, oxidative addition of the Si–H bond to the nickel ion in **B2** is kinetically favored over tetraphenylene formation. The resulting hexacoordinate nickel species readily undergoes reductive elimination to form a silylated phenyl ring in intermediate **B4**. Two competing pathways branch off at this point and lead to the formation of the two products observed experimentally with low activation barriers: 2-dimethylhydrosilylbiphenyl (**P1**) is formed by C–H bond formation through reductive elimination,

whereas Si–H bond activation and subsequent elimination of dihydrogen leads to the 9,9-dimethyl-9-silafluorene (**P2**). The two products are formed with high exergonicity and are not interconvertible under the reaction conditions.

Experimental Section

Computational Details

Geometry optimizations and Hessian calculations were carried out with Gaussian 09 (Revision D.01)^[54] by employing the BP86^[55,56] density functional including Grimme's D2 empirical dispersion correction^[57] in combination with the def2-TZVP^[58] basis set obtained from the EMSL basis set exchange library.^[59–61] To accelerate calculations we made use of the resolution-of-identity^[62–64] approximation, and automatically generated auxiliary basis sets were employed as provided by the *auto*^[65,66] keyword implemented in Gaussian09. This functional was selected after a careful benchmark study (see Supporting Information). All stationary points were characterized as minima or first-order saddle points by eigenvalue analysis of the computed Hessians. The connectivities of transition states and the respective minima implied in the presentation were validated by means of energy minimizations following small geometry displacements along the reaction coordinate obtained from the vibrational frequency analyses of transition-state structures. XYZ coordinates of optimized minima and transition states are provided in the Supporting Information. Unscaled zero-point vibrational energies as well as thermal and entropic correction terms were added to total energies to obtain Gibbs free energies (298 K) by using the standard procedures implemented in the Gaussian program.

General Remarks

All manipulations were carried out under a nitrogen atmosphere by using standard Schlenk techniques or in an argon-filled glovebox. NMR spectra were recorded on Bruker DPX-250, Avance 300, Avance 400, or Avance 500 spectrometers. Chemical shifts are referenced to (residual) solvent signals (¹H, ¹³C) or to external 85% H₃PO₄ (³¹P) and tetramethylsilane (²⁹Si). [Ni(cod)₂], PPhMe₂, Et₃SiH, *n*Pr₃SiH, *i*Pr₃SiH, Ph₃SiH, Me₂PhSiH, and Et₂SiH₂ are commercially available and were used as received. *t*Bu₃SiH was prepared according to the published procedure.^[67–69] For syntheses of biphenylene and its derivatives, see the Supporting Information. HPLC was either performed with reversed phase (Reposil-Pur C18-AQ, 10 μm, 250 × 20 mm) or normal phase (Nucleosil 100 Si, 10 μm, 250 × 20 mm).

Synthesis

Synthesis of [Ni(PPhMe₂)₄]: [Ni(PPhMe₂)₄] was prepared by a modified literature procedure.^[46] [Ni(cod)₂] (1.05 g, 3.82 mmol) and PPhMe₂ (2.19 g, 15.9 mmol) were mixed in a Schlenk tube, whereupon the mixture turned intensely red and warmed up. Et₂O (15 mL) was added and the resulting orange solution was stirred for 2 d at room temperature. The solution was concentrated to about 2 mL and cooled to –78 °C. Orange X-ray-quality crystals formed. The supernatant was removed by cannula and the orange solid was dried to constant mass in vacuo. Yield: 1.964 g (84%). ¹H NMR (300.0 MHz, C₆D₆): δ = 7.41–7.35 (m, 8H, ArH), 7.15–7.04 (m, 12H, ArH), 1.30 ppm (s, 24H, Me); ³¹P{¹H} NMR (121.5 MHz, C₆D₆): δ = –9.7 ppm (cf. ref. [70]); ¹³C{¹H} NMR (75.4 MHz, C₆D₆): δ = 148.0 (m, ArC), 129.9 (m, ArC), 128.0 (m, ArC), 126.8 (s, ArC), 22.2 ppm (m, Me).

Reaction of biphenylene (1**) with Et₂SiH₂ and [Pd(dba)₂]/DavePhos:** An NMR tube was charged with **1** (40 mg, 0.26 mmol), Et₂SiH₂ (35 mg, 0.40 mmol), [Pd(dba)₂] (dba = *trans,trans*-dibenzylideneacetone, 11 mg, 0.019 mmol), and DavePhos (10 mg, 0.025 mmol). C₆D₆ (0.5 mL) was added and the tube was sealed. After heating to 110 °C for 24 h the reaction mixture was investigated by NMR spectroscopy.

Reaction of Et₂SiH₂ with [Ni(PPhMe₂)₄]: An NMR tube was charged with Et₂SiH₂ (20 mg, 0.23 mmol) and [Ni(PPhMe₂)₄] (40 mg, 0.065 mmol).

C₆D₆ (0.5 mL) was added and the tube was sealed. After heating to 110 °C for 2 h the reaction mixture was investigated by NMR spectroscopy, and only the starting materials Et₂SiH₂ and [Ni(PPhMe₂)₄] were observable.

Reaction of biphenylene (1**) with [Ni(PPhMe₂)₄]:** An NMR tube was charged with **1** (20 mg, 0.13 mmol) and [Ni(PPhMe₂)₄] (80 mg, 0.13 mmol). C₆D₆ (0.5 mL) was added and the tube was sealed. After heating to 110 °C for 2 h the reaction mixture was investigated by NMR spectroscopy.

Reaction of 2(Et₂HSi) with [Ni(PPhMe₂)₄] and 3,3-dimethyl-1-butene: An NMR tube was charged with **2**(Et₂HSi) (52 mg, 0.22 mmol), [Ni(PPhMe₂)₄] (6 mg, 0.01 mmol), and 3,3-dimethyl-1-butene (0.14 mL). C₆D₆ (0.5 mL) was added and the tube was sealed. After heating to 110 °C for 13 h the reaction mixture was investigated by NMR spectroscopy.

Reaction of 3 with [Ni(PPhMe₂)₄] in an H₂ atmosphere: Compound **3** (120 mg, 0.503 mmol) and [Ni(PPhMe₂)₄] (31 mg, 0.051 mmol) were dissolved in toluene (20 mL). This mixture was heated in an autoclave under an H₂ atmosphere (130 bar) to 110 °C for 16 h. An aliquot of this mixture was investigated by NMR spectroscopy.

Reaction of biphenylene (1**) with Et₂SiH₂ and [Ni(PPhMe₂)₄] in an H₂ atmosphere:** Compound **1** (100 mg, 0.657 mmol), Et₂SiH₂ (87 mg, 0.99 mmol), and [Ni(PPhMe₂)₄] (20 mg, 0.033 mmol) were dissolved in toluene (20 mL). This mixture was heated to 110 °C for 3 h in an autoclave under an H₂ atmosphere (130 bar). An aliquot of this mixture was investigated by NMR spectroscopy. The product ratio of **2**(Et₂HSi):**3** was still 4:6, but the major product of the reaction was biphenyl.

Reaction of 1 with *i*Pr₃SiH: An NMR tube was charged with **1** (50 mg, 0.33 mmol), [Ni(PPhMe₂)₄] (10 mg, 0.016 mmol), and *i*Pr₃SiH (62 mg, 0.39 mmol). C₆D₆ (0.5 mL) was added and the NMR tube was sealed. After heating to 110 °C for 4 h the reaction mixture was investigated by NMR spectroscopy.

Reaction of 1 with *t*Bu₃SiH: An NMR tube was charged with **1** (40 mg, 0.26 mmol), [Ni(PPhMe₂)₄] (8 mg, 0.01 mmol), and *t*Bu₃SiH (80 mg, 0.40 mmol). C₆D₆ (0.5 mL) was added and the NMR tube was sealed. After heating to 110 °C for 4 h the reaction mixture was investigated by NMR spectroscopy.

Synthesis of 2-triethylsilylbiphenyl [2(Et₃Si)]: Compound **1** (50 mg, 0.33 mmol) and [Ni(PPhMe₂)₄] (10 mg, 0.016 mmol) were charged in an NMR tube. Et₃SiH (115 mg, 0.989 mmol) and C₆D₆ (1.5 mL) were added and the tube was sealed. After 2 h at 110 °C the ¹H NMR spectrum showed quantitative formation of **2**(Et₃Si). The reaction mixture was quenched with water and extracted into ethyl acetate (twice). The combined organic layers were dried (Na₂SO₄) and filtered. All volatile substances were removed in vacuo. The crude product was purified by flash column chromatography (silica gel/hexane). Yield: 93%. The NMR data were in accordance with those found in the literature.^[33] ²⁹Si INEPT NMR (59.6 MHz, C₆D₆): δ = 3.5 ppm.

Synthesis of 2-tripropylsilylbiphenyl [2(*n*Pr₃Si)]: An NMR tube was charged with **1** (50 mg, 0.33 mmol), [Ni(PPhMe₂)₄] (12 mg, 0.020 mmol), *n*Pr₃SiH (55 mg, 0.35 mmol), and C₆D₆ (1.5 mL). The tube was sealed and kept at 110 °C. After 4 h the reaction mixture was quenched with water and the organic compounds in the aqueous layer were extracted into ethyl acetate. The combined organic layers were dried over Na₂SO₄ and filtered. The solvent was removed in vacuo. Purification by flash column (silica gel/hexane) yielded **2**(*n*Pr₃Si) (92 mg, 90%) as a colorless oil. ¹H NMR (400.1 MHz, CDCl₃): δ = 7.56 (dd, ³J(H,H) = 7.2 Hz, ⁴J(H,H) = 1.6 Hz, 1H, ArH), 7.40–7.32 (m, 5H, ArH), 7.31–7.27 (m, 2H, ArH), 7.21 (dd, ³J(H,H) = 7.2 Hz, ⁴J(H,H) = 1.6 Hz, 1H, ArH), 1.24–1.14 (m, 6H, CH₂), 0.85 (t, ³J(H,H) = 7.2 Hz, 9H, CH₃), 0.47–0.43 ppm (m, 6H, CH₂); ¹³C{¹H} NMR (100.6 MHz, CDCl₃): δ = 149.7, 144.7, 136.0, 135.8, 129.8, 129.4, 128.4, 127.7, 127.2, 126.2 (ArC), 18.6, 17.6, 16.3 ppm (CH₂CH₂CH₃); ²⁹Si INEPT NMR (59.6 MHz, C₆D₆): δ = –1.6 ppm; elemental analysis calcd (%) for C₂₁H₃₀Si: C 81.22, H 9.74; found: C 81.01, H 9.53.

Synthesis of 2-dimethylphenylsilylbiphenyl [2(Me₂PhSi)]: Compound **1** (50 mg, 0.33 mmol), Me₂PhSiH (45 mg, 0.33 mmol), and [Ni(PPhMe₂)₄]

(12 mg, 0.020 mmol) were dissolved in C_6D_6 (1.5 mL). The NMR tube was sealed and the mixture was heated to 110 °C for 4 h. After quenching with water and extraction of the product into ethyl acetate, the crude product was purified by column chromatography (silica gel/hexane) to afford **2**(Me₂PhSi) (81 mg, 85 %). The ¹H and ¹³C{¹H} NMR data were in accordance those reported by Matsuda et al.^[33] ²⁹Si HMBC (250.1 MHz, 49.7 MHz, CDCl₃): δ = -8.0 ppm.

Synthesis of 2-triphenylsilylbiphenyl [2(Ph₃Si)]: A sealable NMR tube was charged with **1** (50 mg, 0.33 mmol), Ph₃SiH (86 mg, 0.33 mmol), and [Ni(PPhMe₂)₄] (12 mg, 0.020 mmol). After adding C_6D_6 (1.5 mL), the tube was sealed and kept at 110 °C for 4 h. The reaction mixture was quenched with water and the product in the aqueous layer was extracted into ethyl acetate. The combined organic layers were dried over Na₂SO₄ and filtered. All volatile substances were removed in vacuo. Flash column chromatography (silica gel/hexane) yielded **2**(Ph₃Si) (98 mg, 72 %) as a colorless solid. ¹H NMR (400.1 MHz, CD₂Cl₂): δ = 7.58 (ddd, ³J(H,H) = 7.5 Hz, ⁴J(H,H) = 1.5 Hz, ⁵J(H,H) = 0.6 Hz, 1H, ArH), 7.50 (dvt, ³J(H,H) = 7.5 Hz, ⁴J(H,H) = 1.4 Hz, 1H, ArH), 7.44–7.41 (m, 6H, ArH), 7.35–7.23 (m, 11H, ArH), 6.95–6.88 (m, 3H, ArH), 6.83–6.79 ppm (m, 2H, ArH); ¹³C{¹H} NMR (100.6 MHz, CD₂Cl₂): δ = 151.2, 143.7, 138.9, 136.5, 135.8, 132.8, 131.1, 130.0, 129.8, 129.4, 128.0, 127.6, 126.9, 126.5 ppm (ArC); ²⁹Si HMBC (400.1 MHz, 79.5 MHz, CD₂Cl₂): δ = -15.2 ppm; elemental analysis calcd (%) for C₃₀H₂₄Si: C 87.33, H 5.86; found: C 85.25, H 5.93.

Synthesis of 2-diethylsilylbiphenyl [2(Et₂HSi)] and 9,9-diethylsilafuorene (3): A Schlenk flask was charged with **1** (1.087 g, 7.142 mmol), Et₂SiH₂ (1.00 g, 11.3 mmol), and [Ni(PPhMe₂)₄] (0.22 g, 0.36 mmol). Toluene (60 mL) was added and the resulting yellow solution was heated to reflux for 4 h. Within 10 min after starting heating, the solution turned red. After an additional hour the color of the mixture turned to black with a yellow hue. After quenching of the mixture with water (40 mL), the product in the aqueous layer was extracted into ethyl acetate (3 × 40 mL). The combined organic phases were dried over MgSO₄ and filtered. All volatile substances were removed in vacuo to give the crude product as a yellow oil. Column chromatography (silica gel/hexane) yielded **2**(Et₂HSi) as a colorless oil (*R*_f = 0.66, 634 mg, 36.9 %) and **3** as a colorless solid (*R*_f = 0.57, 639 mg, 37.5 %). X-ray-quality crystals of **3** were grown from a concentrated hexane solution at -40 °C. The ¹H and ¹³C{¹H} NMR of **2**(Et₂HSi) and **3** are in accord with the data reported by Takai et al.^[21] ²⁹Si INEPT (59.6 MHz, C₆D₆): δ = -4.8 [2(Et₂HSi)], 5.5 ppm (**3**).

Optimized synthesis of 9,9-diethylsilafuorene (3): Compound **1** (393 mg, 2.58 mmol), [Ni(PPhMe₂)₄] (80 mg, 0.13 mmol), and Et₂SiH₂ (0.38 g, 4.3 mmol) in toluene (25 mL) were heated to reflux for 4 h. The color of the solution turned from yellow to black with a yellow hue. H₂O (20 mL) was added and the two layers were separated. The product in the aqueous layer was extracted into ethyl acetate (3 × 20 mL). The combined organic layers were dried over MgSO₄ and filtered. All volatile substances were removed in vacuo to give crude **3** as a yellow oily residue (681 mg). Flash column chromatography (silica gel/hexane) yielded a colorless oil (458 mg). This oil was dissolved in toluene (30 mL), and [Rh(PPh₃)₃Cl] (83 mg, 0.09 mmol) and 3,3-dimethyl-1-butene (1.3 mL, 10 mmol) were added. After heating this mixture to reflux for 1 d, H₂O (20 mL) was added and the two layers were separated. The organic compounds in the aqueous layer were extracted into toluene (2 × 30 mL). Drying the combined organic layers over MgSO₄, removal of all volatile substances in vacuo, and flash column chromatography (silica gel/hexane) yielded **3** (300 mg, 49 %).

Synthesis of 4-methyl-9,9-diethyl-9-silafuorene (7): 1-Methylbiphenylene (**4**; 30 mg, 0.18 mmol), Et₂SiH₂ (24 mg, 0.27 mmol), and [Ni(PPhMe₂)₄] (5 mg, 0.008 mmol) in C_6D_6 (0.5 mL) were heated to 120 °C for 2 h in a sealed vial. The reaction mixture was quenched with water and the product was extracted into ethyl acetate (three times). Drying over MgSO₄, filtering, and removing all volatile substances in vacuo gave crude **7** as a yellow oil. Reversed-phase HPLC (MeOH, flow rate: 3 mL min⁻¹, retention time: 33.3 min) yielded **7** as a colorless oil (22 mg, 48 %). ¹H NMR (400.1 MHz, CDCl₃): δ = 8.07 (d, ³J(H,H) = 8 Hz, 1H, H⁵), 7.66 (ddd, ³J(H,H) = 7 Hz, ⁴J(H,H) = 1.5 Hz, ⁵J(H,H) = 0.7 Hz, 1H, H⁸), 7.49 (ddd, ³J(H,H) = 7 Hz, ⁴J(H,H) = 1.5 Hz, ⁵J(H,H) = 0.6 Hz, 1H,

H¹), 7.45 (dvt, ³J(H,H) = 7.5 Hz, ⁴J(H,H) = 1.5 Hz, 1H, H⁶), 7.27 (dvt, ³J(H,H) = 7 Hz, ⁴J(H,H) = 1 Hz, 1H, H⁷), 7.24 (dm, ³J(H,H) = 7.7 Hz, 1H, H²), 7.18 (vt, ³J(H,H) = 7 Hz, 1H, H³), 2.76 (s, 3H, ArMe), 1.01–0.83 ppm (m, 10H, CH₂CH₃); ¹³C{¹H} NMR (100.6 MHz, CDCl₃): δ = 150.6 (C^{5A}), 147.0 (C^{4A}), 139.0, 138.9 (C^{1A,8A}), 134.4 (C³), 134.3 (C⁴), 133.3 (C⁶), 131.0 (C¹), 130.0 (C⁶), 126.8 (C²), 126.4 (C⁷), 125.8 (C⁵), 24.5 (ArMe), 7.7, 4.0 ppm (CH₂CH₃); ²⁹Si HMBC (400.1 MHz, 79.5 MHz, CDCl₃): δ = 4.2 ppm; elemental analysis calcd (%) for C₁₇H₂₀Si: C 80.89, H 7.99; found: C 80.59, H 8.09.

Synthesis of 2,7-di-tert-butyl-9,9-diethyl-9-silafuorene (8) and 3,6-di-tert-butyl-9,9-diethyl-9-silafuorene (9): 2,7-Di-tert-butylbiphenylene (**6**; 350 mg, 1.32 mmol), Et₂SiH₂ (263 mg, 2.98 mmol), and [Ni(PPhMe₂)₄] (53 mg, 0.087 mmol) in toluene (20 mL) were heated to 110 °C for 5.5 h, whereupon the color of the mixture changed from yellow to dark red with a yellow hue. H₂O (20 mL) was added, the two phases were separated, and the product in the aqueous layer was extracted into ethyl acetate (3 × 30 mL). The combined organic layers were dried over MgSO₄ and filtered. All volatile substances were removed in vacuo. Flash column chromatography yielded a mixture of **8** and **9** (442 mg). A vial was charged with 310 mg of this product mixture, [Rh(PPh₃)₃Cl] (65 mg, 0.070 mmol), 3,3-dimethyl-1-butene (0.60 mL), and toluene (22 mL). The vial was sealed and the mixture was heated to 135 °C for 3 d, whereupon the color of the mixture changed to black. After aqueous workup (20 mL) and extraction of the H₂O phase with toluene (3 × 20 mL), all volatile substances were removed in vacuo to yield the products as a dark red oil. Column chromatography (silica gel/hexane) yielded analytically pure **8** (*R*_f = 0.36, 98 mg, 30 %) and crude **9** (*R*_f = 0.44, 82 mg, 25 %). Analytically pure **9** was obtained by normal-phase HPLC (*n*-heptane, flow rate: 3 mL min⁻¹, retention time: 20.5 min). Analytical data of **8**: ¹H NMR (300.0 MHz, CDCl₃): δ = 7.70 (d, ³J(H,H) = 8.1 Hz, 2H, ArH), 7.60 (d, ⁴J(H,H) = 2 Hz, 2H, ArH), 7.43 (dd, ³J(H,H) = 8.1 Hz, ⁴J(H,H) = 2 Hz, 2H, ArH), 1.36 (s, 18H, *t*Bu), 1.06–1.01 (m, 6H, CH₃), 0.97–0.89 ppm (m, 4H, CH₂); ¹³C{¹H} NMR (75.4 MHz, CDCl₃): δ = 149.5, 146.0, 137.2, 130.0, 127.2, 120.2 (ArC), 34.8, 31.6 (Ar*t*Bu), 7.9, 4.1 ppm (CH₂CH₃); ²⁹Si INEPT (59.6 MHz, CDCl₃): δ = 4.8 ppm; elemental analysis calcd (%) for C₂₄H₃₄Si: C 82.22, H 9.77; found: C 82.46, H 9.89. Analytical data of **9**: ¹H NMR (500.2 MHz, CDCl₃): δ = 7.87 (d, ⁴J(H,H) = 1.6 Hz, 2H, ArH), 7.54 (d, ³J(H,H) = 7.5 Hz, 2H, ArH), 7.29 (dd, ³J(H,H) = 7.5 Hz, ⁴J(H,H) = 1.6 Hz, 2H, ArH), 1.40 (s, 18H, *t*Bu), 1.03–1.00 (m, 6H, CH₃), 0.92–0.87 ppm (m, 4H, CH₂); ¹³C{¹H} NMR (125.8 MHz, CDCl₃): δ = 153.1, 148.8, 134.6, 133.1, 124.4, 117.5 (ArC), 35.1, 31.5 (Ar*t*Bu), 7.8, 4.0 ppm (CH₂CH₃); ²⁹Si{¹H} NMR (99.4 MHz, CDCl₃): δ = 3.9 ppm; HRMS (MALDI): *m/z* calcd for C₂₄H₃₄Si⁺: 350.2430 [*M*⁺]; found: 350.2422.

Reaction of 1-methylbiphenylene (4) with triethylsilane: A sealable NMR tube was charged with **4** (30 mg, 0.18 mmol), Et₃SiH (32 mg, 0.28 mmol), and [Ni(PPhMe₂)₄] (5 mg, 0.008 mmol). C_6D_6 (0.5 mL) was added and the NMR tube was sealed. After heating to 120 °C for 2 h, the orange-yellow solution was treated with water. The product in the aqueous layer was extracted into ethyl acetate (twice). All volatile substances were removed in vacuo to yield 58 mg of a yellow oil. Reversed-phase HPLC (MeOH, flow rate: 3 mL min⁻¹, retention time: 38 min) yielded a mixture of isomeric products 2-triethylsilyl-6-methylbiphenyl (**10**) and 2-triethylsilyl-2'-methylbiphenyl (**11**) (40 mg, 78 %). ¹H NMR (300.0 MHz, CDCl₃): δ = 7.61–7.58 (m, 1H, ArH, **10** or **11**), 7.43–7.28 (m, 7H, ArH, **10** or **11**), 7.24–7.09 (m, 8H, ArH, **10** and **11**), 2.07 (s, 3H, ArMe, **10** or **11**), 1.99 (s, 3H, ArMe **10** or **11**), 0.83–0.77 (m, 18H, CH₂CH₃, **10** and **11**), 0.47–0.34 ppm (m, 12H, CH₂CH₃, **10** and **11**); ¹³C{¹H} NMR (75.4 MHz, CDCl₃): δ = 148.8, 148.7, 143.8, 143.0, 136.2, 135.9, 135.8, 135.7, 135.6, 133.3, 130.6, 130.1, 129.9, 129.8, 129.7, 128.3, 127.9, 127.5, 127.1, 126.6, 126.0, 124.9 (ArC, **10** and **11**), 21.2, 20.6 (ArMe, **10** and **11**), 7.7, 7.6, 4.1, 3.8 ppm (CH₂CH₃, **10** and **11**); ²⁹Si INEPT (59.6 MHz, CDCl₃): δ = 3.6, 3.4 ppm (**10** and **11**); elemental analysis calcd (%) for C₁₉H₂₆Si: C 80.78, H 9.28; found: C 80.39, H 9.11. The ¹H and ¹³C NMR spectra of **10** and **11** are similar to those reported for the trimethylsilyl analogues.^[71,72]

Single-crystal X-ray diffraction: The data for **3** were measured on a STOE IPDS-II diffractometer equipped with a sealed tube with MoK_α

radiation. An empirical absorption correction with the program PLATON^[73] was performed. The data for remaining structures ([Ni(PPhMe₂)₄], **8**, and **9**) were measured on a STOE IPDS-II diffractometer using a Genix Microfocus X-ray source with mirror optics and Mo_{K α} radiation. The data were corrected for absorption with the frame-scaling procedure contained in the X-Area package.^[74] The structures were solved by direct methods by using the program SHELXS and refined against F^2 with full-matrix least-squares techniques by using the program SHELXL.^[75] The crystal of **3** was a nonmerohedral twin with a fractional contribution of 0.228(5) for the minor domain. The absolute structure could not be determined reliably, Flack x parameter: $-0.3(2)$. In **8**, both *tert*-butyl groups are disordered over two sites with a site occupation factor of 0.582(16) and 0.642(7) for the major occupied site, respectively. The disordered atoms were refined isotropically. CCDC 1006499 (**3**), 1006496 (**5**), 1006495 (**6**), 1006503 (**8**), 1006502 (**9**), 1006501 (**12**), 1006497 (**13**), 1006498 (**14**) and 1006500 ([Ni(PPhMe₂)₄]) contain the supplementary crystallographic data for this paper. These data can be obtained free of charge from The Cambridge Crystallographic Data Centre via www.ccdc.cam.ac.uk/data_request/cif.

Acknowledgements

This work was supported by the Beilstein-Institut, Frankfurt/Main (Germany), within the research collaboration NanoBiC (projects eNet and π Oligo). Quantum-chemical calculations were performed at the Center for Scientific Computing (CSC) Frankfurt on the Fuchs and LOEWE-CSC high-performance computer clusters.

- [1] a) J. Y. Corey, *Adv. Organomet. Chem.* **2011**, *59*, 1–180; b) J. Y. Corey, *Adv. Organomet. Chem.* **2011**, *59*, 181–328.
- [2] Y.-Q. Mo, X.-Y. Deng, X. Jiang, Q.-H. Cui, *J. Polym. Sci. Part A* **2009**, *47*, 3286–3295.
- [3] J. C. Sanchez, A. G. DiPasquale, A. L. Rheingold, W. C. Troglor, *Chem. Mater.* **2007**, *19*, 6459–6470.
- [4] J. C. Sanchez, W. C. Troglor, *J. Mater. Chem.* **2008**, *18*, 3143–3156.
- [5] E. Wang, C. Li, W. Zhuang, J. Peng, Y. Cao, *J. Mater. Chem.* **2008**, *18*, 797–801.
- [6] K. Tamao, M. Uchida, T. Izumizawa, K. Furukawa, S. Yamaguchi, *J. Am. Chem. Soc.* **1996**, *118*, 11974–11975.
- [7] J. H. Hong, P. Boudjouk, I. Stoescu, *Organometallics* **1996**, *15*, 2179–2181.
- [8] Y. Liu, T. C. Stringfellow, D. Ballweg, I. A. Guzei, R. West, *J. Am. Chem. Soc.* **2002**, *124*, 49–57.
- [9] A. V. Zabula, A. Y. Rogachev, I. A. Guzei, R. West, *Organometallics* **2013**, *32*, 3760–3768.
- [10] S. Zhang, R. Chen, J. Yin, F. Liu, H. Jiang, N. Shi, Z. An, C. Ma, B. Liu, W. Huang, *Org. Lett.* **2010**, *12*, 3438–3441.
- [11] J. M. Breunig, A. Hübner, M. Bolte, M. Wagner, H.-W. Lerner, *Organometallics* **2013**, *32*, 6792–6799.
- [12] A. Hübner, M. Diefenbach, M. Bolte, H.-W. Lerner, M. C. Holthausen, M. Wagner, *Angew. Chem. Int. Ed.* **2012**, *51*, 12514–12518; *Angew. Chem.* **2012**, *124*, 12682–12686.
- [13] A. Hübner, Z.-W. Qu, U. Englert, M. Bolte, H.-W. Lerner, M. C. Holthausen, M. Wagner, *J. Am. Chem. Soc.* **2011**, *133*, 4596–4609.
- [14] A. Lorbach, M. Bolte, H. Li, H.-W. Lerner, M. C. Holthausen, F. Jäkle, M. Wagner, *Angew. Chem. Int. Ed.* **2009**, *48*, 4584–4588; *Angew. Chem.* **2009**, *121*, 4654–4658.
- [15] C. Reus, S. Weidlich, M. Bolte, H.-W. Lerner, M. Wagner, *J. Am. Chem. Soc.* **2013**, *135*, 12892–12907.
- [16] M. Shimizu, K. Mochida, T. Hiyama, *Angew. Chem. Int. Ed.* **2008**, *47*, 9760–9764; *Angew. Chem.* **2008**, *120*, 9906–9910.
- [17] R. Shintani, H. Otomo, K. Ota, T. Hayashi, *J. Am. Chem. Soc.* **2012**, *134*, 7305–7308.
- [18] A. S. Dudnik, N. Chernyak, C. Huang, V. Gevorgyan, *Angew. Chem. Int. Ed.* **2010**, *49*, 8729–8732; *Angew. Chem.* **2010**, *122*, 8911–8914.
- [19] Y. Kuninobu, K. Yamauchi, N. Tamura, T. Seiki, K. Takai, *Angew. Chem. Int. Ed.* **2013**, *52*, 1520–1522; *Angew. Chem.* **2013**, *125*, 1560–1562.
- [20] M. Onoe, K. Baba, Y. Kim, Y. Kita, M. Tobisu, N. Chatani, *J. Am. Chem. Soc.* **2012**, *134*, 19477–19488.
- [21] T. Ureshino, T. Yoshida, Y. Kuninobu, K. Takai, *J. Am. Chem. Soc.* **2010**, *132*, 14324–14326.
- [22] T. Matsuda, S. Kadowaki, T. Goya, M. Murakami, *Org. Lett.* **2007**, *9*, 133–136.
- [23] K. L. Chan, S. E. Watkins, C. S. K. Mak, M. J. McKiernan, C. R. Towns, S. I. Pascu, A. B. Holmes, *Chem. Commun.* **2005**, 5766–5768.
- [24] J. Y. Corey, L. S. Chang, *J. Organomet. Chem.* **1986**, *307*, 7–14.
- [25] H. Gilman, R. D. Gorsich, *J. Am. Chem. Soc.* **1958**, *80*, 1883–1886.
- [26] J. Song, C. Du, C. Li, Z. Bo, *J. Polym. Sci. Part A* **2011**, *49*, 4267–4274.
- [27] J. P. M. van Klink, H. J. R. de Boer, G. Schat, O. S. Akkerman, F. Bickelhaupt, A. L. Spek, *Organometallics* **2002**, *21*, 2119–2135.
- [28] P. F. Hudrlik, D. Dai, A. M. Hudrlik, *J. Organomet. Chem.* **2006**, *691*, 1257–1264.
- [29] Z. Wang, H. Fang, Z. Xi, *Tetrahedron Lett.* **2005**, *46*, 499–501.
- [30] Y. Yabusaki, N. Ohshima, H. Kondo, T. Kusamoto, Y. Yamanoi, H. Nishihara, *Chem. Eur. J.* **2010**, *16*, 5581–5585.
- [31] Good yields of silafluorenes were reported for route (i) only for bulky groups such as isopropyl. Furthermore, for the synthesis of unsymmetrically substituted silafluorenes the Pd-catalyzed C–C coupling reactions between C(Tf) and C(H) of diaryl silanes ArAr'SiR₂ have poor selectivity when Ar' bears an additional substituent in the 3-position (e.g., OMe or F). The trityl-cation-induced silafluorene synthesis yielding an unsymmetrically 2,7-substituted silafluorene (reaction (ii) in Scheme 1) has so far only been described for one example in the literature. An Rh-catalyzed coupling of the 2'-methyl-2-silylbiphenyl derivative leads to a product mixture. The major product of this reaction is a silaphenanthrene derivative, which is formed by dehydrogenative coupling of the hydrosilyl moiety with the methyl group. Route (iii) is limited to substitution patterns in the 2,3-positions. In the end, the reaction of type (iv) (Scheme 1) runs into selectivity problems if substituents are introduced in inappropriate positions of biphenyls.
- [32] Normally, C–C activation reactions have succeeded on using strained ring systems such as the four-membered rings of biphenylenes.^[76,77] In contrast, Si–H bond activation reactions are often described in the literature.^[78,79] As we wanted to perform both reactions simultaneously, the activation of the Si–H and C–C bonds represent competitive reactions.
- [33] T. Matsuda, H. Kirikae, *Organometallics* **2011**, *30*, 3923–3925.
- [34] For comparison, the Pd-catalyzed hydrosilylation of biphenylene with trialkyl silanes was completed after 2–3 h under the same reaction conditions.^[33]
- [35] R. Beck, S. A. Johnson, *Chem. Commun.* **2011**, *47*, 9233–9235.
- [36] B. L. Edlbach, R. J. Lachicotte, W. D. Jones, *Organometallics* **1999**, *18*, 4040–4049.
- [37] B. L. Edlbach, R. J. Lachicotte, W. D. Jones, *Organometallics* **1999**, *18*, 4660–4668.
- [38] J. J. Eisch, A. M. Piotrowski, K. I. Han, C. Krüger, Y. H. Tsay, *Organometallics* **1985**, *4*, 224–231.
- [39] C. Müller, R. J. Lachicotte, W. D. Jones, *Organometallics* **2002**, *21*, 1975–1981.
- [40] S. Saito, T. Yoshizawa, S. Ishigami, R. Yamasaki, *Tetrahedron Lett.* **2010**, *51*, 6028–6030.
- [41] T. Schaub, U. Radius, *Chem. Eur. J.* **2005**, *11*, 5024–5030.
- [42] H. Schwager, S. Spyroudis, K. P. C. Vollhardt, *J. Organomet. Chem.* **1990**, *382*, 191–200.
- [43] W. Chen, S. Shimada, M. Tanaka, Y. Kobayashi, K. Saigo, *J. Am. Chem. Soc.* **2004**, *126*, 8072–8073.
- [44] M. Tanabe, R. Yumoto, K. Osakada, *Chem. Commun.* **2012**, *48*, 2125–2127.
- [45] T. Zell, T. Schaub, K. Radacki, U. Radius, *Dalton Trans.* **2011**, *40*, 1852–1854.

- [46] C. A. Tolman, D. W. Reutter, W. C. Seidel, *J. Organomet. Chem.* **1976**, *117*, C30–C33.
- [47] A. V. Marenich, S. V. Jerome, C. J. Cramer, D. G. Truhlar, *J. Chem. Theory Comput.* **2012**, *8*, 527–541.
- [48] The optimized structures of **H1**, **H2**, and **TS_{H2-B3}** exhibit features in line with the earlier notion of a structural continuum between hydrido silyl and η^2 -SiH silane σ complexes;^[49,50] the Lewis structures in Scheme 5 illustrate the respective limiting case considered most relevant for the individual species based on the Ni–H and Si–H bond lengths found in the optimized geometries.
- [49] R. Beck, S. A. Johnson, *Organometallics* **2012**, *31*, 3599–3609.
- [50] V. M. Iluc, G. L. Hillhouse, *Tetrahedron* **2006**, *62*, 7577–7582.
- [51] S. S. Yi, E. L. Reichert, M. C. Holthausen, W. Koch, J. C. Weisshaar, *Chem. Eur. J.* **2000**, *6*, 2232–2245.
- [52] C. A. Hunter, J. K. M. Sanders, *J. Am. Chem. Soc.* **1990**, *112*, 5525–5534.
- [53] F. Meyer-Wegner, H.-W. Lerner, M. Bolte, *Acta. Cryst. Sect. C* **2010**, *66*, o182–o184.
- [54] Gaussian 09 (Revision D.01), M. J. Frisch, G. W. Trucks, H. B. Schlegel, G. E. Scuseria, M. A. Robb, J. R. Cheeseman, G. Scalmani, V. Barone, B. Mennucci, G. A. Petersson, H. Nakatsuji, M. Caricato, X. Li, H. P. Hratchian, A. F. Izmaylov, J. Bloino, J. Zheng, J. L. Sonnenberg, M. Hada, M. Ehara, K. Toyota, R. Fukuda, J. Hasegawa, M. Ishida, T. Nakajima, Y. Honda, O. Kitao, H. Nakai, T. Vreven, J. A. Montgomery Jr., J. E. Peralta, F. Ogliaro, M. Bearpark, J. J. Heyd, E. Brothers, K. N. Kudin, V. N. Staroverov, T. Keith, R. Kobayashi, J. Normand, K. Raghavachari, A. Rendell, J. C. Burant, S. S. Iyengar, J. Tomasi, M. Cossi, N. Rega, J. M. Millam, M. Klene, J. E. Knox, J. B. Cross, V. Bakken, C. Adamo, J. Jaramillo, R. Gomperts, R. E. Stratmann, O. Yazyev, A. J. Austin, R. Cammi, C. Pomelli, J. W. Ochterski, R. L. Martin, K. Morokuma, V. G. Zakrzewski, G. A. Voth, P. Salvador, J. J. Dannenberg, S. Dapprich, A. D. Daniels, O. Farkas, J. B. Foresman, J. V. Ortiz, J. Cioslowski, D. J. Fox, Gaussian, Inc., Wallingford, CT, **2013**.
- [55] J. P. Perdew, *Phys. Rev. B* **1986**, *33*, 8822–8824.
- [56] A. D. Becke, *Phys. Rev. A* **1988**, *38*, 3098–3100.
- [57] S. Grimme, *J. Comput. Chem.* **2006**, *27*, 1787–1799.
- [58] F. Weigend, R. Ahlrichs, *Phys. Chem. Chem. Phys.* **2005**, *7*, 3297–3305.
- [59] D. Feller, *J. Comput. Chem.* **1996**, *17*, 1571–1586.
- [60] K. L. Schuchardt, B. T. Didier, T. Elsethagen, L. Sun, V. Gurumoorathi, J. Chase, J. Li, T. L. Windus, *J. Chem. Inf. Model.* **2007**, *47*, 1045–1052.
- [61] EMSL basis set exchange. <https://bse.pnl.gov/bse/portal>.
- [62] R. A. Kendall, H. A. Früchtl, *Theor. Chem. Acc.* **1997**, *97*, 158–163.
- [63] K. Eichkorn, O. Treutler, H. Öhm, M. Häser, R. Ahlrichs, *Chem. Phys. Lett.* **1995**, *240*, 283–290.
- [64] K. Eichkorn, F. Weigend, O. Treutler, R. Ahlrichs, *Theor. Chem. Acc.* **1997**, *97*, 119–124.
- [65] B. I. Dunlap, *J. Chem. Phys.* **1983**, *78*, 3140–3142.
- [66] B. I. Dunlap, *Theochem-J. Mol. Struct.* **2000**, *529*, 37–40.
- [67] H.-W. Lerner, *Coord. Chem. Rev.* **2005**, *249*, 781–798.
- [68] N. Wiberg, *Coord. Chem. Rev.* **1997**, *163*, 217–252.
- [69] N. Wiberg, K. Amelunxen, H.-W. Lerner, H. Schuster, H. Nöth, I. Krossing, M. Schmidt-Amelunxen, T. Seifert, *J. Organomet. Chem.* **1997**, *542*, 1–18.
- [70] V. Miluykov, A. Kataev, O. Sinyashin, P. Lönnecke, E. Hey-Hawkins, *Organometallics* **2005**, *24*, 2233–2236.
- [71] A. Nagaki, N. Takabayashi, Y. Tomida, J.-i. Yoshida, *Beilstein J. Org. Chem.* **2009**, *5*, 16.
- [72] R. Klein, P. Sedmera, J. Cejka, K. Mach, *J. Organomet. Chem.* **1992**, *436*, 143–153.
- [73] A. L. Spek, *Acta Crystallogr. Sect. D* **2009**, *65*, 148–155.
- [74] Stoe & Cie, X-AREA. Diffractometer control program system **2002**.
- [75] G. M. Sheldrick, *Acta. Cryst. Sect. A* **2008**, *64*, 112–122.
- [76] C. Perthusot, B. L. Edelbach, D. L. Zubris, N. Simhai, C. N. Iverson, C. Müller, T. Satoh, W. D. Jones, *J. Mol. Catal. A* **2002**, *189*, 157–168.
- [77] A. Steffen, R. M. Ward, W. D. Jones, T. B. Marder, *Coord. Chem. Rev.* **2010**, *254*, 1950–1976.
- [78] J. Y. Corey, *Chem. Rev.* **2011**, *111*, 863–1071.
- [79] J. Y. Corey, J. Braddock-Wilking, *Chem. Rev.* **1999**, *99*, 175–292.

Received: June 3, 2014
Published online: September 9, 2014

RNA Conformations

Determination of the Conformation of the 2'OH Group in RNA by NMR Spectroscopy and DFT Calculations**

Senada Nozinovic, Puneet Gupta, Boris Fürtig, Christian Richter, Sandor Tüllmann, Elke Duchardt-Ferner, Max C. Holthausen,* and Harald Schwalbe*

In contrast to DNA, RNA exhibits pronounced functional, structural, and chemical diversity, which has been considered essential for the evolution of the RNA world.^[1] The presence of the 2'OH group induces a change in the predominant sugar conformation and provides catalytic activity, but at the same time it reduces the chemical stability of RNA. 2'OH groups are involved in hydrogen-bonding interactions in noncanonical regions and are responsible for the formation of a well-ordered water network spanning the minor groove of the RNA helix.^[2] It is therefore of considerable interest to determine experimentally the conformation of the 2'OH group.

Molecular dynamics (MD) simulations suggest three preferred orientations for the 2'OH group in the C3'-endo sugar conformation (Figure 1), while for the C2'-endo sugar conformation exclusively O3'-domain orientations are predicted.^[3] Experimental determinations of this exocyclic torsion angle pose a serious challenge in RNA structure analyses, because the hydrogen atoms of 2'OH groups are only visible in electron density maps derived by X-ray crystallography at resolutions < 1 Å and therefore their positions generally remain undetectable. Neutron diffraction is an alternative method for proton detection but reports are sparse, especially for large RNAs. Recent low-temperature NMR spectroscopic studies enabled conformational analyses involving the 2'OH

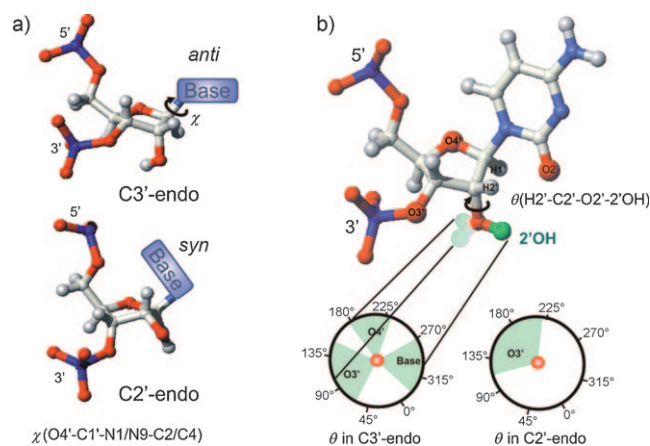


Figure 1. a) Representation of the sugar and nucleobase conformations by two exemplary structures with C3'-endo/anti and C2'-endo/syn conformations. b) The 2'OH orientation. The structure represents the three favored orientations of the 2'OH group (highlighted in green) in which it points towards O3', O4', or the nucleobase domain. Conformational wheels represent the distribution of the torsion angles $\theta(\text{H2}'\text{-C2}'\text{-O2}'\text{-2'OH})$ for sugars identified in MD simulations.^[3]

proton.^[4] Such studies rely on limited chemical exchange of the hydroxy group with the solvent. 2'OH groups of nucleotides in noncanonical regions of RNA are, however, in rapid exchange with hydrogen atoms of the solvent and the corresponding signals cannot be detected. Therefore the direct measurement of structural parameters restraining the exocyclic torsion angle remains impossible.

Based on the interpretation of $^1J(\text{C,H})$ coupling constants we suggest here a general method for the conformational analysis of sugar pucker modes and nucleobase orientations as well as for the determination of 2'OH group conformations in large RNAs. In contrast to $^3J(\text{H,H})$ coupling constants, which are typically well approximated by a conformational dependence on a single torsion angle (Karplus relationship), $^1J(\text{C,H})$ coupling constants are sensitive to C–H bond lengths,^[5] which in turn are influenced by local conformations and thus depend on multiple torsion angles.^[5b,6] As a consequence, 1J couplings are generally difficult to translate into conformational information.

The present work was inspired by reports from several groups, in which the influence of hyperconjugative effects ($n \rightarrow \sigma^*/\sigma \rightarrow \sigma^*$ donation) on $^1J(\text{C,H})$ coupling constants in ethanol and methylamine was demonstrated.^[7] Based on these findings we anticipated that the lone electron pairs of the 2'OH group in RNA should exert a corresponding influence on the $^1J(\text{C,H})$ coupling constants of the adjacent bonds at C1' and C2' ring positions in a systematic and

[*] Dipl.-Chem. S. Nozinovic, Dr. B. Fürtig, Dr. C. Richter, Prof. Dr. H. Schwalbe
Johann Wolfgang Goethe-Universität
Zentrum für biomolekulare magnetische Resonanzspektroskopie
Max-von-Laue Strasse 7, 60439 Frankfurt (Germany)
Fax: (+49) 69-7982-9515
E-mail: schwalbe@nmr.uni-frankfurt.de

Dr. E. Duchardt-Ferner
Johann Wolfgang Goethe-Universität, Institut für Biochemie
Max-von-Laue-Strasse 7, 60438 Frankfurt (Germany)
M. Sc. P. Gupta, Dipl.-Chem. S. Tüllmann, Prof. Dr. M. C. Holthausen
Johann Wolfgang Goethe-Universität
Institut für anorganische und analytische Chemie
Max-von-Laue-Strasse 7, 60438 Frankfurt (Germany)
Fax: (+49) 69-798-29417
E-mail: max.holthausen@chemie.uni-frankfurt.de

[**] We thank Beatrix Suess and Julia E. Weigand for providing the 27-mer riboswitch RNA and Jens Wöhnert for helpful discussions. This work was supported by the state of Hesse (BMRZ), the DFG (SFB579: "RNA-Ligand-Interaction"), the Studienstiftung des Deutschen Volkes (grants to S.N. and B.F.), and CitySolar AG (grant to P.G.). H.S. is member of the DFG-funded Cluster of Excellence: Macromolecular Complexes.

Supporting information for this article is available on the WWW under <http://dx.doi.org/10.1002/anie.201007844>.

predictable way. By mapping this dependence it should be possible to determine the conformation of the 2'OH group.

In order to dissect the multiple conformational dependencies of $^1J(\text{C,H})$ in RNA, we compared experimental NMR data with predictions from DFT calculations. Firstly, DFT calculations of $^1J(\text{C,H})$ scalar coupling constants in nucleotide-like model structures were performed to confirm their dependence on different sugar and nucleobase conformations. Secondly, the influence of 2'OH group orientations for fixed sugar and nucleobase conformations was investigated by systematic scans of the 2'OH group orientation. The results revealed in fact that the sugar pucker and the nucleobase conformations, as well as the 2'OH group orientations all have an appreciable influence on $^1J(\text{C,H})$ coupling constants. However, for known sugar and nucleobase conformations, 2'OH group orientations can be determined precisely solely by interpretation of $^1J(\text{C,H})$ coupling constants. This is possible even for residues whose 2'OH proton cannot be detected by NMR spectroscopy owing to exchange with solvent H_2O or D_2O . $^1J(\text{C,H})$ coupling constants can generally be measured at high resolution with high sensitivity so that the procedure suggested here is applicable also to large RNAs.

For DFT calculations the B3LYP/TZVP(+PCM:water) level of theory was chosen after a careful series of benchmark calculations of the NMR spin-spin coupling constants for relevant model systems (see Tables S1 and S2 in the Supporting Information). Then, for each nucleotide type, four representative molecular models with the main conformations characteristic for RNA (C3'-endo/*anti* or *syn*, C2'-endo/*anti* or *syn*) were constructed from the ribosome crystal structure (pdb code: 2ffk)^[8] and the previously solved high-resolution 14-mer RNA solution structure (pdb code: 2koc)^[4e] for calculations of the $^1J(\text{C,H})$ coupling constants (see Table S6 in the Supporting Information). Orientations of the individual 2'OH groups were constrained in these calculations to the O3' domain with torsion angles θ fixed at 100° for the C3'-endo and 160° for the C2'-endo conformation, respectively. The construction of the molecular models and the constraints introduced for partial geometry optimizations are described in detail in the Supporting Information.

Figure 2a shows a map of the resulting $^1J(\text{C,H})$ coupling constants predicted for the four nucleobases assuming either a *syn* or an *anti* orientation for both sugar conformations (C3'-endo or C2'-endo), respectively. The calculated data show clearly that the sugar conformation has a significant effect on both coupling constants, while the nucleobase conformation (*syn* or *anti*) mainly influences $^1J(\text{C1',H1'})$. With computed coupling constants spanning a range of 14 Hz, a reliable differentiation of the four conformations is possible by comparison to measured $^1J(\text{C,H})$ coupling constants. We therefore suggest the chart in Figure 2a as a simple means for determining RNA conformation and we tested it by analysis of a 27-mer riboswitch RNA, the structure and dynamic features of which were recently reported in an NMR study.^[9a,b] The detailed results of this cross-validation are presented in the Supporting Information (Figure S8). The conformations of a total of 21 residues can be assigned unambiguously by comparison with Figure 2a. The remaining

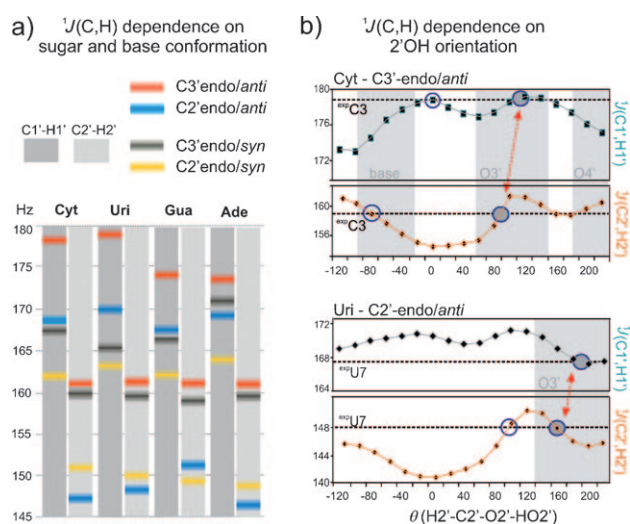


Figure 2. a) DFT-based $^1J(\text{C1',H1'})$ and $^1J(\text{C2',H2'})$ coupling constants calculated for each nucleotide (cytosine, uridine, guanosine, adenosine) adopting four mainly populated conformations defined by the individual sugar pucker (C3'- and C2'-endo) and nucleobase orientations (*anti* and *syn*). b) Computed $^1J(\text{C,H})$ coupling constants for residues C3 and U7 as a function of the torsion angle $\theta(\text{H2'-C2'-O2'-2'OH})$. Experimental values for C3 and U7 of the 14-mer RNA are indicated by dashed lines. Best fit between experimental and calculated values is indicated by the colored circles. 2'OH orientations most populated according to MD simulations are shadowed in gray.

five residues are characterized experimentally by averaged coupling constants (Figure S9 in the Supporting Information), which cannot be assigned to a single conformation. Indeed, those residues are placed within the bulge region and at the 3'-terminus of the RNA, and it is known from the original NMR study that these residues exhibit higher flexibility.^[9b]

In a second set of DFT calculations, the dihedral angle $\theta(\text{H2'-C2'-O2'-2'OH})$, which describes the orientation of the exocyclic 2'OH group, was varied from 0° to 340° in steps of 20°. Figure 2b shows the results obtained for a cytosine and for a uridine model constructed from C3 and U7 in the 14-mer solution structure (Figure 3a), with the sugar in C3'- and C2'-endo conformation, respectively, while the bases adopt *anti* conformations. We observed that the orientation of the 2'OH group exerts considerable influence on the $^1J(\text{C,H})$ coupling constants: $^1J(\text{C1',H1'})$ couplings vary by 6 Hz (Cyt) and 3 Hz (Uri); $^1J(\text{C2',H2'})$ couplings, with differences of up to 7 Hz (Cyt) and 9 Hz (Uri), are even more sensitive. Agreement between the experimental and computed $^1J(\text{C,H})$ couplings for these residues in the 14-mer is found only for one respective 2'OH group orientation (Figure 2b); for both nucleotides the same orientations had been derived from MD simulations.^[4e]

Previously, comprehensive NMR measurements allowed us to determine the high-resolution solution structure (0.3 Å) of a 14-mer UUCG hairpin RNA.^[4e] Analysis of homonuclear couplings and cross-correlated relaxation rates revealed that the sugar moieties of the stem nucleotides and of the hydrogen-bonded loop nucleotides U6 and G9 adopt C3'-endo conformations. The two loop nucleotides U7 and C8 adopt C2'-endo conformations and do not undergo conformational averaging on the NMR time scale (Figure 3a).^[4e] The

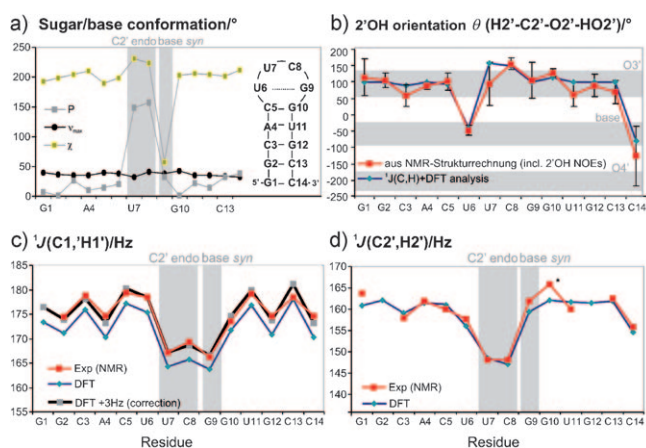


Figure 3. a, b) Secondary structure and conformation of the 14-mer RNA: nucleobase orientations described by the torsion angle χ , sugar puckers described by P and ν_{\max} ,^[14] and 2'OH group orientations described by the torsion angle θ were extracted from 20 lowest-energy structures. Loop residues with the unusual *syn* nucleobase orientation for G9 and C2'-endo sugar conformation for U7 and C8 are highlighted with gray shadows in (a), (c), and (d). Orientations toward O3', nucleobase, and O4' domains as predicted by MD simulations (Figure 1) are shadowed in gray (b). c, d) Experimental (NMR) and DFT computed $^1J(\text{H1}',\text{C1}')$ / $^1J(\text{H2}',\text{C2}')$ coupling constants. DFT computed data for $^1J(\text{C1}',\text{H1}')$ are shown with and without a linear shift of +3 Hz. The experimental $^1J(\text{C2}',\text{H2}')$ coupling of G10 is marked by an asterisk (see text).

nucleobase of residue G9 adopts an unusual *syn* conformation.^[10] In our previous work, NOE contacts of the 2'OH group were analyzed to determine the preferred orientation of the ribose moiety. The final structure bundle, which is consistent with the NOE analysis, indicates that the 2'OH groups of the stem mainly adopt the O3' domain orientation and that the 2'OH group of U6, which is located in the loop region, is oriented towards the nucleobase domain (Figure 3b). For loop residues U7, C8, and G9 and the terminal residues G1 and C14, NOE analysis could not be performed since no NMR signals of the 2'OH protons could be recorded owing to fast exchange with water. Hence, the 2'OH group orientations suggested for these residues in previous work resulted solely from the ARIA force field refinement^[11] without experimental constraints and are thus only weakly defined.

The experimentally derived $^1J(\text{C,H})$ coupling constants of the 14-mer RNA structure measured in H₂O are depicted in Figure 3c,d (Measurements in D₂O resulted in identical values; Figure S1 in the Supporting Information). $^1J(\text{C,H})$ coupling constants cluster systematically around larger values for C3'-endo and lower values for C2'-endo conformations. As a notable exception, $^1J(\text{C1}',\text{H1}')$ for residue G9 does not follow the trend for C3'-endo conformations. This deviation is caused by the *syn* orientation of the nucleobase for G9.

We computed all coupling constants of the 14-mer RNA by DFT employing molecular models for the individual residues constructed from the high-resolution solution structure, constraining the 2'OH groups to the experimentally derived orientations (Figure 3; see the Supporting Information for details). Figure 3c and d show that the computed

$^1J(\text{C,H})$ coupling constants reproduce the experimental data very well, both in terms of the absolute values and in terms of conformational dependence, with the only exception of G10 (marked with an asterisk in Figure 3d). We note, however, that other data hint at the presence of additional conformational exchange phenomena of G10.^[12] In the observed range of coupling constants (140–180 Hz), the average deviations from experimental data amount to 4 Hz and 1.7 Hz for $^1J(\text{C1}',\text{H1}')$ and $^1J(\text{C2}',\text{H2}')$ couplings, respectively. A reduced average error of only 1 Hz in $^1J(\text{C1}',\text{H1}')$ couplings is obtained by application of an empirical constant linear shift of +3 Hz, such that the maximum error for all coupling constants is 2.9 (G10 excluded).^[13] The combined DFT and NMR analysis provides accurate information on 2'OH orientations of the 14-mer RNA and makes it possible to determine the conformation of the 2'OH protons that remain undetectable experimentally. The results presented above (Figure 2b) demonstrate that $^1J(\text{C,H})$ calculations based on systematic scans of the torsion angle θ in appropriately constructed molecular models permit the unambiguous characterization of the 2'OH group.

In summary, we have investigated the conformational dependence of $^1J(\text{C,H})$ coupling constants in RNAs as readily measurable NMR parameters, and we have demonstrated a marked dependence of $^1J(\text{C1}',\text{H1}')$ and $^1J(\text{C2}',\text{H2}')$ on the conformation of the sugar and the nucleobase, and the 2'OH group orientation. Experimental and theoretical results are in very good agreement, which confirms the high accuracy of the structure as well as the quantum chemical approach chosen. We have shown that $^1J(\text{C1}',\text{H1}')$ and $^1J(\text{C2}',\text{H2}')$ coupling constants can serve as valuable probes for ribose and nucleobase conformations in RNA molecules, and suggest their use as a new tool for conformational analysis. For the majority of nucleotides within an RNA molecule, the sugars assume either a C3'-endo or a C2'-endo conformation, while nucleobases can adopt *anti* and *syn* orientations.^[15] The qualitative interpretation of the $^1J(\text{C,H})$ couplings constitutes a reliable method to discriminate between the four conformational extremes with an accuracy sufficient for structure calculation. Our procedure is particularly useful for the structure determination of larger RNAs, since $^1J(\text{C,H})$ coupling constants can be measured readily even without the use of isotope-labeling techniques. The utility of this approach is further demonstrated for the 27-mer riboswitch RNA in an unambiguous conformational analysis of rigid parts of the structure and identification of flexible regions. So far, the conformational characterization of 2'OH groups—which determine the unique conformational properties of RNA compared to DNA—was possible only in rare cases. The marked dependence of $^1J(\text{C,H})$ coupling constants on 2'OH group orientations demonstrated here facilitates reliable indirect determination of this elusive structural parameter even under rapid-exchange conditions.

Received: December 13, 2010

Published online: April 20, 2011

Keywords: conformation analysis · density functional calculations · NMR spectroscopy · RNA

- [1] W. Gilbert, *Nature* **1986**, *319*, 618.
- [2] M. Egli, S. Portmann, N. Usman, *Biochemistry* **1996**, *35*, 8489.
- [3] P. Auffinger, E. Westhof, *J. Mol. Biol.* **1997**, *274*, 54.
- [4] a) M. Hennig, J. Fohrer, T. Carlomagno, *J. Am. Chem. Soc.* **2005**, *127*, 2028; b) J. Ying, A. Bax, *J. Am. Chem. Soc.* **2006**, *128*, 8372; c) J. Fohrer, M. Hennig, T. Carlomagno, *J. Mol. Biol.* **2006**, *356*, 280; d) J. Fohrer, U. Reinscheid, M. Hennig, T. Carlomagno, *Angew. Chem.* **2006**, *118*, 7191; *Angew. Chem. Int. Ed.* **2006**, *45*, 7033; e) S. Nozinovic, B. Fürtig, H. R. A. Jonker, C. Richter, H. Schwalbe, *Nucleic Acids Res.* **2010**, *38*, 683.
- [5] a) C. Thibaudeau, R. Stenutz, B. Hertz, T. Klepach, S. Zhao, Q. Wu, I. Carmichael, A. S. Serianni, *J. Am. Chem. Soc.* **2004**, *126*, 15668; b) F. Cloran, I. Carmichael, A. S. Serianni, *J. Phys. Chem. A* **1999**, *103*, 3783.
- [6] a) D. B. Davies, P. Rajani, M. MacCoss, S. S. Danyluk, *Magn. Reson. Chem.* **1985**, *23*, 72; b) M. L. Munzarová, V. Sklenar, *J. Am. Chem. Soc.* **2003**, *125*, 3649; c) J. T. Fischer, U. M. Reinscheid, *Eur. J. Org. Chem.* **2006**, 2074; d) Z. Vokáčová, F. M. Bickelhaupt, J. Šponer, V. r. Sychrovský, *J. Phys. Chem. A* **2009**, *113*, 8379; e) P. C. Kline, A. S. Serianni, *J. Org. Chem.* **1992**, *57*, 1772; f) C. A. Podlasek, W. A. Stripe, I. Carmichael, M. Shang, B. Basu, A. S. Serianni, *J. Am. Chem. Soc.* **1996**, *118*, 1413; g) A. S. Serianni, J. Wu, I. Carmichael, *J. Am. Chem. Soc.* **1995**, *117*, 8645; h) J. M. Duker, A. S. Serianni, *Carbohydr. Res.* **1993**, *249*, 281; i) J. H. Ippel, S. S. Wijmenga, R. de Jong, H. A. Heus, C. W. Hilbers, E. de Vroom, G. A. van der Marel, J. H. van Boom, *Magn. Reson. Chem.* **1996**, *34*, S156.
- [7] a) S. Watanabe, I. Ando, Y. Sakamoto, *J. Mol. Struct.* **1982**, *82*, 237; b) R. H. Contreras, J. E. Peralta, *Prog. Nucl. Magn. Reson. Spectrosc.* **2000**, *37*, 321; c) N. C. Maiti, Y. Zhu, I. Carmichael, A. S. Serianni, V. E. Anderson, *J. Org. Chem.* **2006**, *71*, 2878.
- [8] N. Ban, P. Nissen, J. Hansen, P. B. Moore, T. A. Steitz, *Science* **2000**, *289*, 905.
- [9] a) J. E. Weigand, M. Sanchez, E.-B. Gunnesch, S. Zeiher, R. Schroeder, B. Suess, *RNA* **2008**, *14*, 89; b) E. Duchardt-Ferner, J. Weigand, O. Ohlenschläger, S. Schmidtke, B. Suess, J. Wöhnert, *Angew. Chem.* **2010**, *122*, 6352; *Angew. Chem. Int. Ed.* **2010**, *49*, 6216.
- [10] a) E. Duchardt, C. Richter, O. Ohlenschläger, M. Görlach, J. Wöhnert, H. Schwalbe, *J. Am. Chem. Soc.* **2004**, *126*, 1962; b) J. Rinnenthal, C. Richter, J. Ferner, E. Duchardt, H. Schwalbe, *J. Biomol. NMR* **2007**, *39*, 17.
- [11] a) M. Nilges, M. J. Macias, S. I. O'Donoghue, H. Oschkinat, *J. Mol. Biol.* **1997**, *269*, 408; b) J. P. Linge, S. I. O'Donoghue, M. Nilges, *Methods Enzymol.* **2001**, *339*, 71.
- [12] A. Cherepanov, C. Glaubitz, H. Schwalbe, *Angew. Chem.* **2010**, *122*, 4855; *Angew. Chem. Int. Ed.* **2010**, *49*, 4747.
- [13] A. Bagno, F. Rastrelli, G. Saielli, *Magn. Reson. Chem.* **2008**, *46*, 518.
- [14] C. Altona, M. Sundaralingam, *J. Am. Chem. Soc.* **1972**, *94*, 8205.
- [15] B. Schneider, Z. Moravek, H. M. Berman, *Nucleic Acids Res.* **2004**, *32*, 1666.

Curriculum Vitae

PERSONAL DETAILS

Full Name Puneet Gupta
Date and Place of Birth 30th March 1984 in Kanpur, India
Nationality Indian
Marital Status Married



EDUCATION

07/2003 – 05/2008 Master of Science (5 Years Integrated) in Chemistry at Indian Institute of Technology (IIT) Kanpur, India.
Supervisor: Prof. Dr. Rabindranath Mukherjee
05/2009 – 12/2014 PhD Student at Goethe University Frankfurt, Germany.
Supervisor: Prof. Dr. Max C. Holthausen

EMPLOYMENT

05/2006 – 07/2006 Summer Internship at University of Massachusetts, Amherst, USA. Supervisor: Prof. Dr. Patricia Bianconi
Since 01/2015 Research Assistant at Max-Planck Institute for Coal Research, Mülheim (Ruhr), Germany. Supervisor: Prof. Dr. Walter Thiel

PUBLICATIONS

- S. Nozinovic, **P. Gupta**, B. Fürtig, C. Richter, S. Tüllmann, E. Duchardt-Ferner, M. C. Holthausen, H. Schwalbe, "Determination of the Conformation of the 2'OH Group in RNA by NMR Spectroscopy and DFT Calculations", *Angew. Chem. Int. Ed.* **2011**, *50*, 5397-5400.
- J. M. Breunig, **P. Gupta**, A. Das, S. Tussupbayev, M. Diefenbach, M. Bolte, M. Wagner, M. C. Holthausen, H-W Lerner, "Efficient Access to Substituted Silafluorenes by Nickel-Catalyzed Reactions of Biphenylenes with Et₂SiH₂", *Asian J. Chem.* **2014**, *9*, 3163-3173.
- J. Becker, **P. Gupta**, F. Angersbach, F. Tuzcek, C. Näther, M. C. Holthausen, S. Schindler, "Selective Aromatic Hydroxylation with Dioxygen and Simple Copper Imine Complexes", *Chem. Eur. J.* **2015**, *21*, 11735-11744. (Appeared at Journal's Cover Page)
- M. Leutzsch, L. M. Wolf, **P. Gupta**, M. Fuchs, W. Thiel, C. Farès, A. Fürstner, "Formation of Ruthenium Carbenes by *gem*-Hydrogen Transfer to Internal Alkynes: Implications for Alkyne *trans*-Hydrogenation", *Angew. Chem. Int. Ed.* **2015**, *54*, 12431-12436. (Appeared at Journal's Cover Page)